

國立台灣大學理學院地質科學系

博士論文

Department of Geosciences

College of Science


National Taiwan University

Doctoral Dissertation

台北都會區山腳活斷層之地震地質研究

Earthquake Geology of the Active Shanchiao Fault in the

Taipei Metropolis, Taiwan



陳致同

Chih-Tung Chen

指導教授：盧佳遇 博士

詹瑜璋 博士

Advisors: Chia-Yu Lu, Ph.D.

Yu-Chang Chan, Ph.D.

中華民國 101 年 1 月

January, 2012

國立台灣大學博士學位論文
口試委員會審定書

台北都會區山腳活斷層之地震地質研究
Earthquake geology of the active Shanchiao Fault
in the Taipei Metropolis, northern Taiwan

本論文係陳致同君 (F94224120) 在國立台灣大學地質
科學所完成之博士學位論文，於民國一百零一年一月九日承
下列考試委員審查通過及口試及格，特此證明

口試委員：

<u>鄧屬予</u>	<u>張中白</u>
<u>李建成</u>	<u>詹瑜璋</u>
<u>朱傲祖</u>	<u>盧佳遇</u>
<u>林正瑛</u>	<u>李正雲</u>
<u>傅子高</u>	

誌謝

進入台大已接近十年，就讀研究所更已整整六年，能夠走到今日、在這裡思索從何下筆致謝，皆仰賴師長、同窗、家人，與學校社會環境的栽培、照顧與支持，實在是萬分幸運。幸好論文裡有這個章節，讓學生能仔細咀嚼這些年來的歷程軌跡，找出論文成形的背後支柱與動力，在此略表謝忱！

首先要感謝我的導師－盧佳遇老師，這麼多年來無私的教導所學所知，從方方面面啟發學生，主動提供或為學生爭取機會與各種補助，在此同時給予最大的空間讓學生學習發展；不論在專業研究上，抑或是工作事務，與人生價值態度，盧老師都展現了最珍貴的身教與言教。同為導師的詹瑜璋老師在研究學業之路上不斷的引導學生，長年的循循善誘讓學生能在學術的十里霧中逐步摸索出自己的路，在一次次的討論中學生獲得的不只是科學上的新視野與觀念糾正，更有做人處世的歷練與原則。李建成老師是這份論文關鍵的指導老師，從學生在中研院暑期生的研究初體驗至今，不間斷的指導與討論，尤其是台北盆地相關文章的投稿過程老師辛勤的教導改正，為學生的成長付出非常多心血。老師辛苦了，真是謝謝！

除了導師以外我還有許多老師長期指導引領我：鄧屬予老師自大二開啟了我的地質生涯，學生不論在台北盆地、台灣板岩帶、甚至遠到四川，老師都毫不吝嗇的將所知所得指導分享給學生，討論中老師所給予的鼓勵與肯定真是學生學海茫茫中的定心丸；陳于高敬愛的歪老師，感謝您從大二起就一路照看學生，給予學生眾多的發展學習機會以及諸多關鍵的建議，讓學生能不斷的向前進展；胡植慶老師自大三一直很看重學生，在 meeting 與野外時的討論，課務上的信任，特別是重要科學資料的分享，讓學生在學術上能跨出第一步(07 年的文章)並持續前進；賈儀平老師從學生進入地質系以來就很關照學生，不時給予寶貴意見與鼓勵，口試當天更慷慨借出教室解救了學生！羅清華老師雖然日理萬機卻持續關心學生，力挺學生拿回院長獎，更在研究與文章上給了非常多關鍵的意見與肯定；鍾孫霖老師從大學的指導到學生板岩帶的研究討論幫助甚多；黃武良老師是我大學時的導師，老師的關懷讓學生能平穩發展；江博明老師、劉平妹老師、劉聰桂老師、魏國彥老師、楊燦堯老師、宋聖榮老師、陳文山老師、鄧茂華老師、洪淑惠老師、吳逸民老師、沈川洲老師、林立虹老師、徐濬德老師、林忠成老師、郭本垣老師、李德貴老師、饒瑞鈞老師、林殿順老師、李元希老師、胡賢能老師，您們在研討會、書報討論、野外、實驗等等的場合機會曾經給予學生建議鼓勵與指導，在此一並致謝！

感謝口試委員們仔細檢閱學生的論文、排除萬難前來為學生考試提出珍貴的建議與關鍵的問題。朱傲祖朱爺不知已帶領學生野外教學多少次，學生每有一些學術上的想法與新結果朱爺總是不厭其煩的聽學生報告然後跟學生熱切討論，對學生的文章更是幫助甚多；張中白老師也是多年來一直關心學生，不論是台灣還是四川的工作老師既建議又鼓勵，跟老師談天喝小酒超開心的；李通藝老師多年

前就關心過學生的學業，口試更是提出重要的問題非常感激；林正洪老師在口試時提出許多問題與建議，以及地震相關的意見很是要緊。謝謝老師們~

自從大三加入盧爺實驗室，同門的師兄弟姊妹實是惠我良多：葉恩筆葉教授多年來熱忱的討論與建議；張國楨學長與陳柔妃學姐在各項工作特別是西進四川的引領照顧與資源的慷慨分享；焦中輝學長長年業界經驗分享，和您一同奮鬥真是榮幸；吳方義旺旺學長(與陳怡吟小啾同學)是我的領門人，讓我順利融入研究室生活；王芳琳學姐我們長年相互打氣，你要繼續加油；林義凱學長多年指引一同出任務；大總管王釋賢學長這些年實在是多虧有你，幫了太多忙，不知該如何言謝；陳麗雯學姐感謝你的諸多幫忙與討論，祝你順利！徐乙君小可愛同學還有潘昌志阿樹同學，回想當年太麻里看日出颯吉普車切薄片推砂箱，一起打拼還要謝謝你們對我的包涵；陳建宏與黃欽煌，同窗與共事辛苦你們了；謝謝你們！

在地質系行走多年我仰賴許多系上學長姐、同學與學弟妹的支持、陪伴與鼓勵。一定要寫在前面的是黃鐘學長，感謝你的幫忙讓我入行，一路至今八年有餘不管是學業、研究、野外、還是學生生活的方方面面多謝你的帶引與作伴！特別要感謝的是歪老師大軍中的賴光胤蛋哥，你現在可是我們詹門的老大請您多多指教；鍾令和阿和感謝你多年來的討論與鼓勵，等著參加你的口試啦；郭昱廷鴉哥、姜宏偉菇哥、黃韶怡韶子姐、林殷田帥學長、張瀨之學姐、李珀儂學長、林蔭學長、巫姿萱烏茲，不論是去中橫暑地當助教同時自我鍛鍊、或是去舊金山 AGU 出國打天下，感謝你們讓我加入也幫我許多忙。同樣在野外與 AGU 幫忙與作伴的景國恩學長、李政益 Sep、莊勻睿 Ray、黃信樺信業哥等等，謝謝！一同書報討論以及常常一同野外、出任務的老胡實驗室同胞們，何宛芸 kukuli、黃孟涵學長、曾佳漢學長、唐昭榮學長、吳育雅老師、吳秋雅學姐、謝有忠學長、陳致言學長、楊宜蓉學姐、邱俊穎蚯蚓、李易叡小猛、黃筱婷、邱詠恬、童忻、彭葦、Maple、冠翔、宣維、宛君、喬茵，謝謝你們的討論、幫忙、支持與作伴，你們都是最好的夥伴！感謝奎含與鄭小雅在研究最初期時的共同打拼與長期支持，慶怡一路以來諸多幫忙還有多年來的 NASA 月曆，還有我的大學同學們黃琳、聖元、曉明、洪小四、陳大吟、賢元、吳阿笨，以及語涵 Kitty、胖達，感謝有你們一起努力互相砥礪！楊欣穎火星娘娘、張英如仙女學姊、郭力維學長、周祐民學長、賴昱銘學長、李曉芬學姐、傅慶洲學長、張佳菱學姐、洪瑋立學長、莊佩娟學姊、許緯豪學長、施國偉、阿刀、皇伶、韻如、心怡會長、嘉俞、淵淑、乙嘉、張冕、勁璿、致展...看來沒法齊列，但我們都曾一同野外工作或是深入討論給我很多啟發，請容我說：謝謝你！

除了台大我也在中研院地球所受到好多照應，羅秋月學姊我真是太感謝你了，你越來越漂亮可愛小 baby 也會很快來報到啦~周素卿學姊如果沒有您的開示開導大家應該都已經 hold 不住崩潰了...虎兒學姊在中研院看著我長大，這一切都多虧學姊照顧！淑貞感謝你好多的幫忙與關心！王興桂學長跟小紅雖然已經被油公司挖角去發財，還是要感謝你們許多的幫忙照應~感謝葉致翔學長的好多討論，學長加油！牟鍾香牟牟學姐也是！以及楊天南學長、張書豪學長、已經高

就中央大學的黃文正學長，與姜彥麟山豬學長~還要感謝李家慶學長在拉曼光譜儀使用上的協助。我的許多高中與社團同學也在我的這段求學過程給我很多鼓勵、增廣見聞視野與紓發牢騷，特別是馬丘(子軒)與猴哥(國臻)，真是謝謝了。

一路上還有很多台灣以外老師與友人指導與幫助過我，特別是法國蒙波利埃的 Jacques Malavieille, Serge Lallemand 與 Alain Chauvet，在天國的安爺爺 Jacques Angelier，巴黎的 Olivier Beyssac 及 Martine Simoes，在 Grenoble 的 Anne-Marie Boullier，還有我的 Montpellier 朋友們(Marie, Marianne, Maryse, Audrey, Angélique, Christopher, Theo, Clément, Remi, Vincent)。美國則有紐約的吳大銘老師，康州的 Timothy Byrne，賓州的 Donald Fisher，

加州理工的 Steven Kidder，印地安納的 Robert Wintsch。大陸四川地礦部的潘桂棠老師，丁俊所長，王劍副所長，尹福光主任，劉宇平研究員與李建忠研究員。還有日本的岡本和明(Kazuaki Okamoto)，瑞士的 Sean Willett 等人，在此一並致謝！Thank you! Merci beaucoup!

寫在最後卻是最重要最根本的，感謝我的家庭給了我這麼好的根基讓我能追求我的夢想，父母給我完整全人的教育以及全力的支持，使我不斷的改進自我，還有彥文的陪伴。謹獻上最真摯的謝意。



摘要

擁有近千萬居民的台北都會區面臨多樣的地震災害潛在來源，包括臺灣島周圍造山與隱沒系統相關震源，以及都會區內的活斷層「山腳斷層」。山腳斷層為一東傾之正斷層，斷層線位於台北盆地西緣，其活動主控了台北盆地的生成以及盆地內四十萬年來七百餘公尺厚河相為主沉積物的堆積。潛在的地震可能造成台北都會區大規模的災害，特別是沿著地表斷層線附近地帶、斷層上盤位移量較大地區、以及震央附近地區。為了增進對此活動斷層基本性質的了解，本研究分析了台北盆地地區的水準資料、地形資料與鑽井資料，並更清楚解析斷層實際所在位置、斷層的活動情形、斷層帶構造與斷層幾何。近三十年來(1975-2003)的水準資料顯示，台北盆地的地表垂直變形主要受控於受壓含水層孔隙水壓變化造成的含水層與阻水層變形；考慮自現地實驗觀察所估計的沉積物壓密速率，以及含水層孔隙水壓回覆造成的彈性回彈，盆地西緣五股至新莊地區有較高的下陷速率，指示山腳斷層目前正在潛移。台北盆地西緣山腳斷層帶的數值高程地形模型分析以及現地實測結果可以追蹤描繪出一系列右階雁行排列的斷層相關地形崖，與斷層的左移性質有關。為了探討較長時間尺度斷層的活動情形，首先選取了斷層中段五股地區岩性紀錄與定年資料相當完備三口鑽井的沖積物進行沉積相與年代的整理分析，對比全球海水面變化曲線，以構造剖面回復方式重建了山腳斷層帶自末次冰期以來的生長斷層演育。由生長斷層的同構造沉積物堆疊架構顯示山腳斷層自末次冰期以來持續活動，斷層帶是由一高角度的主斷層以及西側一較低角度的分支斷層所組成，因斷層含有左移的分量而呈現負花狀構造。兩萬三千年來主斷層的平均垂直向構造滑移速率約為 2 mm/yr 而分支斷層約為 1 mm/yr，而九千至八千四百年前的六百年區間內我們紀錄到特別高量的構造沉陷(主斷層 7.4 米，分支斷層 3.3 米)，與前人提出該時段內曾發生古地震的觀察相吻合。在山腳斷層帶中北段的蘆洲剖面亦觀察到了相似的負花狀構造並且可判釋出多條分支斷層的存在，斷層上盤末次冰期以來之構造沉陷速率約為 3 mm/yr 與五股剖面估算所得相當接近，顯示如此之負花狀生長斷層是山腳斷層帶的共同特徵。將地表地形與地下構造對比顯示地形崖多對比至較西側/外側之分支斷層，主斷層的斷層跡則已被快速的侵蝕與堆積作用完全抹除，因此山腳斷層在地表上的分布並非一單獨的線形，而是一個可達數百公尺寬的斷層帶。在生長斷層分析中，末次冰期末期因大漢溪襲奪事件而在台北盆地形成的景美沖積扇礫石層因其形成迅

速、分布廣泛、頂面形貌較規則平整、井下辨認容易，成為同構造生長沉積物中紀錄與估計山腳斷層長期、綜合同震與間震期完整地震循環的垂直位移相當可靠的指準層。整合盆地內超過五百口鑽井資料可見此指準層-景美礫石層頂部-已被山腳斷層明顯強烈變形，並呈現 roll-over 的單斜褶皺形態；末次冰期以來斷層最大位移位於斷層中段的蘆洲至五股地區，並迅速向南減少，向西也快速減少但至盆地中心後減少速度變緩。斷層造成指準層位移的量值與分布為斷層的幾何形貌所控制，本研究選取垂直斷層線的五股-三重-台北區域的景美礫石層頂部深度變化進行模擬，以簡單的彈性半空間邊界元素數值模擬法嘗試解析山腳斷層在上部地殼的幾何形貌；模擬結果顯示山腳斷層在淺部傾角約 75 至 85 度接近垂直，然而在三至五公里深處急遽轉折至近水平 15 至 5 度，呈現強烈的匙狀幾何，指示山腳斷層在地下三至五公里深處與造山時期的逆衝斷層結合並構造反轉重新滑動。考量山腳斷層為一可能發震的斷層，而全球至今尚未紀錄到低角度正斷層所產生的中大型地震，低角度正斷層的發震機制亦缺乏適當的力學解釋，同時進入台灣造山帶的中國大陸邊緣在造山運動之前發育有許多地塹相關的正斷層為先存弱面，故此研究在上述幾何組合下又在深部加上一 60 度的高角度斷面；模擬結果顯示若在地下八公里深處斷層面由近水平角度轉折為 60 度可獲得較前述相當甚至更好的擬合結果，隱示山腳斷層可能不僅重新活化了造山時期的逆衝(底脫)斷層也同時活化了前造山時期正斷層系統。在全球許多後造山伸張環境的地震研究指出活動斷層斷面傾角急遽轉折處常為中大型地震的孕震發震位置，而 2004 年發生於台北盆地以東四獸山地區的中型地震其震源機制解與上述雙斷坡斷層幾何模型的深部斷坡相吻合，震源深度接近斷坪-斷坡轉折處，進一步支持此幾何的可靠性，並對大台北都會區的地震災害、以及台灣北部山脈垮塌轉型伸張的大地構造運動有重大意義。

Abstract

The Taipei Metropolis, home to some 10 million people, is subject to seismic hazard from not only ground shaking in thick alluvial deposits due to distant faults or sources scattered throughout the Taiwan region, but also active faulting directly underneath. Northern Taiwan including the Taipei region is currently affected by post-orogenic (Plio-Pleistocene arc-continent collision) processes related to backarc extension of the Ryukyu subduction system. The Shanchiao Fault, an active normal fault outcropping along the western boundary of the Taipei Basin and dipping to the east, is investigated here for the areal extent and magnitude of its recent activity. Based on growth faulting analysis in the Wuku profile in the central portion of the fault, the Shanchiao Fault is found to be incessantly active since about 23 ka with an averaged tectonic subsidence rate about 3 mm/yr. A geologic profile across the north-central portion of the fault zone in the Luzhou area reveals similar main-branch fault half-negative flower structural pattern and slip rates observed in the Wuku profile, a phenomenon we interpret to originate from the geometry of the basin basement and the strong rheological contrast between unconsolidated basin sediments and basement rocks. One key horizon within the growth sediments – the top of the Jingmei Formation which was an alluvial fan formed rapidly when a major drainage reorganization occurred during the Last Glacial Maximum – is noted to serve as the marker of tectonic subsidence since its inception around 23 ka. A determination and compilation of the depths of the Jingmei Formation top horizon from nearly 500 borehole records within the Taipei Basin demonstrates that the hanging-wall of the Shanchiao Fault is deformed in a roll-over fashion with up to three branch faults sub-parallel to the main fault in the several-hundred-meter wide fault zone, and the offset is largest in the Wuku-Luzhou area in the central portion of the fault and decreases toward the southern tip of the fault. Along traces of the branch faults subtle fault-related geomorphic scarps can be mapped which exhibit a right-stepping en-echelon pattern, indicating recent sinistral transtensional faulting. Contemporary tectonic subsidence revealed by leveling data across the Taipei Basin during 1975 to 2003 was concentrated again in the Wuku-Luzhou near-fault hanging-wall area, probably representing an interseismic fault behavior. An attempt to resolve the poorly-known subsurface geometry of the Shanchiao Fault is carried out by simple elastic dislocation modeling of the surface deformation recorded by the Jingmei Formation top horizon compilation, which is representative of the latest Quaternary period as it spans probably more than 10 earthquake cycles. Preliminary results suggest that the Shanchiao Fault possesses shallow listric geometry where the low-dipping part may be inherited from the negative tectonic inversion of former thrusts, while deeper rift-related normal faults is also likely to be reactivated. Such constraints and knowledge are crucial in earthquake hazard evaluation and mitigation in the Taipei Metropolis, and in understanding the kinematics of transtensional tectonics in northern Taiwan.

Contents

口試委員會審定書.....	i
誌謝.....	ii
中文摘要.....	v
Abstract.....	vii
Contents.....	viii
List of figures.....	xii
List of tables.....	xv
Chapter 1: Introduction.....	1
Chapter 2: Thirty-Year Land Elevation Change from Subsidence to Uplift Following the Termination of Groundwater Pumping and Its Geological Implications in the Metropolitan Taipei Basin, Northern Taiwan.....	4
2.1 Introduction.....	4
2.2 Regional Setting.....	7
2.2.1 Geological Background.....	7
2.2.2 Hydrogeologic Framework and Utilization of Groundwater.....	10
2.3 Analyses and Results.....	12
2.3.1 Description of Data Analyses.....	12
2.3.2 Results of Post-Pumping Land Elevation Change.....	13
2.4 Mechanics of Land Elevation Changes during Post-Pumping.....	17
2.4.1 Near Surface Soil Compaction (the Shallow Component).....	17
2.4.2 Tectonic Load (the Deep and Crust-Scale Component).....	20
2.4.3 Deformation of Aquifers (the Intermediate Component).....	20
2.4.4 Synthesis and Discussion.....	22
2.5 Summary.....	28
Chapter 3: Growth Normal Faulting at the Western Edge of the Metropolitan Taipei Basin since the Last Glacial Maximum, Northern Taiwan.....	29
3.1 Introduction.....	29
3.2 Geological Setting.....	30
3.3 The Active Shanchiao Fault.....	33
3.4 Reconstruction of Geological Profile across the Shanchiao Fault.....	34
3.4.1 Stratigraphic Correlation between the Boreholes.....	34
3.4.2 Stratigraphic Architecture of the Shanchiao Fault Zone.....	44
3.5 Reconstruction of Growth Faulting History.....	46
3.5.1 Sea Level Fluctuation and Sedimentation in the Taipei Basin.....	46
3.5.2 Restoration by a Simple Back-Stripping Method.....	48
3.5.3 Evolution of Sedimentation vs. Growth Faulting.....	51

3.6 Discussion.....	55
3.6.1 Tectonic Loading Rates and Earthquake Events.....	55
3.6.2 Correlation between Surface Topography and Sub-Surface Geology....	58
3.7 Concluding Remarks.....	60
Chapter 4: Fault Zone Characteristics and Basin-wide Distribution of Post-Last Glacial Maximum Tectonic Subsidence of the Active Shanchiao Fault in the Metropolitan Taipei Basin, Northern Taiwan.....	61
4.1 Introduction.....	61
4.2 Regional Setting.....	62
4.2.1 Geology of the Taipei Basin.....	62
4.2.2 The Active Shanchiao Fault.....	64
4.3 Fault Zone Geomorphology.....	67
4.3.1 North of the Tanshui River (Beitou Area)	67
4.3.2 Wuku Area.....	71
4.3.3 Hsinchuang-Shulin Area.....	75
4.4 Fault Zone Structure.....	80
4.4.1 Growth Faulting at the Wuku Profile in the Central Portion of the Fault.....	80
4.4.2 Structure and Growth Faulting at the Luzhou Profile in the North-Central Portion of the Fault.....	82
4.4.3 Geological Interpretation of the Shulin Profile in the Southern End of the Fault.....	90
4.5 Distribution of Tectonic Subsidence since the Last Glacial Maximum across the Taipei Basin.....	91
4.5.1 Jingmei Formation Top Horizon as a Key Marker.....	91
4.5.2 Data and Result.....	91
4.5.3 Factors Affecting the Depth Distribution of the Jingmei Formation Top Horizon.....	93
4.6 Discussions.....	96
4.6.1 Delineating the Shanchiao Fault Zone.....	96
4.6.2 Characteristics of the Fault Zone Structure.....	98
4.6.3 Extent of the Magnitude and Rate of Fault-Related Vertical Deformation since the Last Glacial Maximum.....	101
4.7 Summary.....	103
Chapter 5: Active Post-Collisional Normal Fault Reactivating Syn-Convergence Thrust Detachment and Involvement of Deep-Seated Pre-Orogen Rift Faults: a Case Study of the Shanchiao Fault in the Taipei Metropolis, Northern Taiwan.....	104

5.1 Introduction.....	104
5.2 Regional Setting.....	107
5.2.1 The Taiwan Orogen and Post-Collisional Tectonics in Northern Taiwan.....	107
5.2.2 The Active Shanchiao Fault.....	110
5.3 Reconstruction of Late-Quaternary Post-Last Glacial Maximum Vertical Tectonic Deformation.....	111
5.3.1 The Jingmei Formation Top Horizon as a Key Marker.....	111
5.3.2 Mapping of Tectonic Subsidence across the Taipei Basin.....	112
5.4 Half-Space Elastic Dislocation Modeling.....	119
5.4.1 Model Setup.....	119
5.4.2 Fault Plane Models with Uniform Dip.....	121
5.4.3 Fault Plane Models with Listric Geometry.....	123
5.5 Discussions.....	126
5.5.1 Shallow Crust Fault Geometry and Its Relation with Syn-Convergence Thrust Detachment.....	126
5.5.2 Deeper Fault Geometry and the Low-Angle-Normal-Fault Enigma....	127
5.5.2.1 Global Debate on Seismogenesis on Low Angle Normal Faults.....	127
5.5.2.2 Half-Space Elastic Dislocation Modeling of Fault Plane Models with Double-Ramp Geometry.....	128
5.5.2.3 The Role of Pre-Orogen Rift Normal Faults on Post-Collisional Extension Tectonics.....	130
5.5.3 Seismic Hazard Implication.....	131
5.6 Concluding Remarks.....	133
Chapter 6: Conclusions and Future Scope.....	134
6.1 Mapping the Shanchiao Fault with Illumination of Fault Zone Structure....	134
6.2 Continued and Ongoing Activity of the Shanchiao Fault since 23 ka to Present Constrained by Growth Faulting Study and Leveling Data Analysis.....	134
6.3 Joint Reactivation of Syn-Convergence Thrust and Pre-Orogen rift fault by the Shanchiao Fault during Orogen Wedge Collapse.....	134
6.4 Future scope: unresolved Dilemmas and Some Directions for Further Investigations.....	135
References.....	137
Appendices.....	148
A1. Note on Chapter 2 (Chen C.-T. et al., 2007, Engineering Geology).....	148
A2. Note on Chapter 3 (Chen C.-T. et al., 2010, Terrestrial, Atmospheric, and	

Oceanic Sciences)167
A3. Note on other published manuscript (Chen C.-T. et al., 2011, Terra Nova)..188



List of Figures

Fig. 2-1. General conceptual model of ground elevation change due to short- and long-term artificial piezometric head drawdown and recovery.	5
Fig. 2-2. (a) Tectonic framework of Taiwan. (b) Geological outline of the Taipei area (c) Simplified geological cross section of the Taipei Basin.....	9
Fig. 2-3. (a) Cumulated subsidence in the Taipei Basin from 1955 to 1991. (b) Stratigraphic and aquifer architecture of late Quaternary deposits within the basin. (c) Piezometric head records since 1972 to 2003.....	11
Fig. 2-4. Distribution of the benchmarks analysed in this study.....	13
Fig. 2-5. Contour maps of observed land surface elevation change in Phase 1 (1975-1989) of post-pumping period.....	15
Fig. 2-6. Contour maps of observed land surface elevation change in Phase 2 (1989-2003) of post-pumping period.....	16
Fig. 2-7. Evolution of ground elevation change rate in post-pumping period in Wuku and central Taipei areas from 1975 to 2003.....	17
Fig. 2-8. (a) Isopach of the Holocene clayish sediments (topmost 50-m deposits) in Taipei basin. (b) Estimated soil compaction rate.....	19
Fig. 2-9. Mechanisms of three depth-related components responsible for land elevation change in Western Taipei (Wuku) and Central Taipei.	23
Fig. 2-10. Ground level changes during Phase 2 of post-pumping period. (a) Cumulated change. (b) Residual change as soil compaction removed.	25
Fig. 2-11. A schematic model for evaluating aquifer elastic rebound during the Phase 2 of the post-pumping period.	27
Fig. 3-1. (A) General tectonic framework of Taiwan. (B) Simplified geology of the Taipei area. (C) Geological cross section of the Taipei Basin.	31
Fig. 3-2. (A) Map of the Wuku area. (B) Interpreted Wuku geological profile.	35
Fig. 3-3. Stratigraphic correlation between boreholes of the Wuku profile.	39
Fig. 3-4. Thickness variations of units in the Sungshan Formation along the Wuku Profile.....	45
Fig. 3-5. Eustatic sea level changes since 30 ka.	47
Fig. 3-6. Back-stripping method and reconstruction of cumulative deformation on the Shanchiao Fault since the LGM of about 23 ka.	50
Fig. 3-7. Interpreted sedimentation and growth faulting and post-LGM development history of the Shanchiao Fault zone in the Wuku profile.	54
Fig. 3-8. (A) Sedimentation rate and tectonic subsidence rate of the C1 and C2 units at the Wuku boreholes. (B) Accumulative vertical slips for the Shanchiao fault since the LGM in the Wuku Profile.....	57
Fig. 3-9. Schematic 3-D diagram of the fault zone in the Wuku area, central	

portion of the Shanchiao Fault.	59
Fig. 4-1. (A) General tectonic framework of Taiwan. (B) Simplified geology of the Taipei area. (C) Geological cross section of the Taipei Basin.	66
Fig. 4-2. Map of the surface trace of the Shanchiao Fault in the Beitou area.	69
Fig. 4-3. Topographic profiles across the Shanchiao fault in the Beitou Area.	70
Fig. 4-4. Map of the surface trace of the Shanchiao Fault in the Wuku area.	73
Fig. 4-5. Topographic profiles in the Wuku Area.	74
Fig. 4-6. Map of the surface trace of the Shanchiao Fault in the Hsinchuang-Shulin area.	77
Fig. 4-7. Topographic profiles in the Hsinchuang-Shulin area.	78
Fig. 4-8. High-resolution topographic measurements in the northern Hsinchuang-Shulin area.	79
Fig. 4-9. (A) Map of the Luzhou area. (B) Interpreted Luzhou geological profile.	84
Fig. 4-10. Stratigraphic correlation between boreholes of the Luzhou Profile.	85
Fig. 4-11. Depth variations of the Jingmei Formation top horizon and the deduced tectonic subsidence rates since ~ 23 ka in the Luzhou Profile.	88
Fig. 4-12. (A) Sedimentation rate and tectonic subsidence rate of the C1 and C2 units at the Luzhou boreholes. (B) Accumulative vertical slips for the Shanchiao fault since the LGM in the Luzhou Profile.	89
Fig. 4-13. Basin-wide compilation of depth distribution of the Jingmei Formation top horizon.	92
Fig. 4-14. Variations of the Jingmei Formation top horizon depth, and the deduced tectonic subsidence amount and rate in the Wuku-Sanchung-Taipei profile.	94
Fig. 4-15. Variations of the Jingmei Formation top horizon depth, and the deduced tectonic subsidence rate in the Wuku-Hsinchuang-Banchiao profile.	95
Fig. 4-16. Updated mapping of the Shanchiao Fault zone.	97
Fig. 4-17. Schematic 3-D diagram of the fault zone in the Wuku-Luzhou area, central portion of the Shanchiao Fault.	100
Fig. 4-18. Cartoon exhibiting the deformation of the Jingmei Formation top horizon by the Shanchiao Fault.	102
Fig. 5-1. (a) Tectonic framework of Taiwan. (b) Simplified geology of the Taipei area. (c) Simplified geological cross section of the Taipei Basin.	106
Fig. 5-2. Lithostratigraphic log of the Taipei Basin sediments	109
Fig. 5-3. Basin-wide compilation of depth distribution of the Jingmei Formation top horizon.	113
Fig. 5-4. Basin-wide variation of post-LGM tectonic subsidence revealed by the depth distribution of the Jingmei Formation top horizon.	114

Fig. 5-5. Variations of the Jingmei Formation top horizon depth, and the deduced tectonic subsidence amount and rate in the Wuku-Sanchung-Taipei profile.115

Fig. 5-6. Settings of the uniform dip and listric models in elastic half-space dislocation modeling.....120

Fig. 5-7. (A) Normalized vertical offset values by the Shanchiao Fault recorded by the Jingmei Formation top horizon. (B) Modeling outcomes of the uniform dip models.122

Fig. 5-8. Modeling outcomes of the listric models.....124

Fig. 5-9. Settings of the double-ramp models in elastic half-space dislocation modeling.128

Fig. 5-10. Modeling outcomes of the double-ramp models.....129

Fig. 5-11: Interpretation of modeling results on the upper crust geometry of the Shanchiao Fault.132



List of Tables

Table 2-1: The in situ compaction in clayey layers of top 50 m basin sediments recorded by Lin et al. (1999).20

Table 3-1: Radiocarbon age data of the three boreholes along the Wuku Profile.....40

Table 3-2: Thermal luminescence (TL) ages. Data from Lin et al., 1999.....41

Table 3-3: Lithofacies of the Wuku Profile.....42

Table 3-4: Sedimentation rate and inferred tectonic subsidence rate of the Shanchiao Fault zone in the Wuku Profile since ~9 ka.56

Table 4-1: Radiocarbon age data incorporated in the Luzhou Profile.....86

Table 5-1: Borehole records of Jingmei Formation top horizon in the Wuku-Sanchung-Taipei profile.116



Chapter1: Introduction

The Taipei Metropolis area, the political and economical capital of Taiwan with several million inhabitants and my hometown as well, situates in a complex geologic environment with numerous imposing geological hazard (Chan et al., 2010). One recognized but poorly understood, yet probably the most devastating kind of hazard is the potential earthquakes generated by the Shanchiao Fault (e.g. Shyu et al., 2005). Through decades of devoted research this active normal fault is known to govern the development the Taipei Basin and is responsible for accommodating the extension in the northern tip of the island during post-collisional collapse of the Taiwan Orogen (Wang Lee et al., 1978; Teng et al., 2001; Rau et al., 2008). The details and recent activities of the Shanchiao Fault, in contrast, remain elusive owing to the lack of surface outcrops and related seismicity. Series of deep boreholes penetrating the entire basin deposits to reach the basement carried out by the Central Geological Survey shed light on the possible locations of the surface fault trace (Lin, 2001) and allowed ventures to investigate its paleoseismic history (Huang et al., 2007). Despite the efforts mentioned above along with other geodetic (e.g. Yu et al., 1999a), geophysical (e.g. Wang and Sun, 1999) and geochemical (e.g. Walia et al., 2005) inquiries, key parameters of this active fault including the exact location of the surface trace, geomorphic fingerprint of faulting, fault geometry in the near surface to the upper crust, and rate of deformation of contemporary to long-term time scales, went unconstrained or debated, although they bear critical clues to the seismic hazard evaluation and mitigation as well as the understanding of post-orogenic tectonics in northern Taiwan. A multi-discipline approach is therefore presented in this thesis aiming at characterizing the Shanchiao Fault, based mainly upon the extreme wealth of leveling and borehole records across the Taipei Basin thanks to the plentiful previous works and the efforts by the Central Geological Survey in collecting and making public the precious data.

The itinerary of the work generally follows the present-to-past and surface-to-deep tracks in unraveling the properties the fault. Leveling data of past four decades is first examined for signs present-day fault activities, and growth sediment accumulation from borehole correlations yield millennial to late-Quaternary fault vertical offset rates. Fault-related scarps are found to represent only part of the complex fault zone at shallow underground from borehole synthesis, which denotes a half-tulip structure inherited from the transtensional nature of fault movement. Growth faulting analysis revealed an intimate coupling between sea level rise and normal faulting since the Last Glacial Maximum (LGM) in the fault zone along much of the Shanchiao Fault, which permits fault slip rate estimations noted previously and identification of a key

tectonic subsidence marker, the Jingmei Formation top horizon. The horizon depth distribution across the basin is converted to estimates of post-LGM vertical fault offset, which demonstrate the extent and magnitude of fault-induced deformation in the Taipei Basin. Finally the tectonic subsidence variation deduced from horizon depth normal to the fault strike is modeled to resolve the upper crustal geometry of the Shanchiao Fault. These results are presented in four chapters; each of the chapters is an independent manuscript published (information listed in the Appendix section) or under preparation for submission. Briefing of these chapters is outlined below:

Chapter 2: Leveling across the Taipei Basin during 1975 to 2003 is analyzed to illuminate the modern vertical ground motion. Initially intended to elucidate and quantify contemporary tectonic subsidence rate, the subsidence and uplift of basin floor observed during the period was dominated by aquifer deformation as residual compaction caused by preceding severe groundwater pumping and elastic rebound due to pore-pressure recovery in natural recharge. Other than the intermediate depth (about 50 to 100 m deep) aquifer component, shallow soil compaction of the most recent sediments contributed significant subsidence in several areas and an attempt was made to quantify this natural subsidence. After tentative removing of soil compaction and discussion on extent of aquifer elastic rebound, enhanced subsidence was still found along the western margin of the Taipei Basin in the near-fault hanging-wall region, which serves to be a solid proof of ongoing modern fault creep although the exact amount of slip rate is not obtainable.

Chapter 3: Basin sediments of three well-documented boreholes (SCF-1, SCF-2 and WK-1) across the central Shanchiao Fault zone in Wuku area is analyzed in the light of growth faulting. The stacking pattern of sediments in the fault zone is controlled by the sea level change and modified by normal faulting. During the LGM the basin was in an eroding environment until the captured Tahan River laid down a massive alluvial fan across the basin as the Jingmei Formation which capped the entire fault zone. The hanging wall and extensional fault block within the fault zone were subsequently down thrown by the fault, and with the rising sea level growth sediments were first accumulated on the hanging wall and progressively onlapped to the extensional fault block and then the footwall. The latest Sungshan Formation as the sediments covering the Jingmei Formation contains horizons downward-displaced towards east, providing estimations on regional sedimentation rates on the footwall (SCF-1) and additional tectonic subsidence rates on the extensional fault block (SCF-2) and the hanging wall (WK-1) since 8.4 ka to present and 9 to 8.4 ka. From the offset pattern of the horizons in the Sungshan Formation and the top of the Jingmei Formation, the fault located between SCF-1 and 2 is a branch fault while the majority of slip occurred on the main

fault between SCF-2 and WK-1, together they consist of a half-tulip structure.

Chapter 4: This chapter intends to summarize the available surface and shallow underground data to give a thorough picture of the Shanchiao Fault zone and the deformation it exerted across the Taipei Basin. Fault zone topographic analysis is first presented delineating series of right-stepping en-echelon vague scarps. In examining fault zone structure a comparable but more detailed half tulip structure is revealed in the Luzhou Profile northwards of the Wuku Profile with similar growth strata stacking fashion, suggesting this kind of fault zone configuration is operating along its entire length and is probably the result of basement geometry and the strong rheological contrast between the basement rock and the loose basin sediments. The Shanchiao Fault is therefore better mapped as a several hundred-meter wide fault zone instead of a single fault line. The Jingmei Formation top horizon in the base of growth sediments deposited during the recent eustatic rise serves to be a clear and widespread tectonic subsidence marker since the LGM ~ 23 ka, and a basin-wide compilation of its depth and the calculated vertical offset demonstrates that the hanging wall is deformed into a prominent roll-over monocline with tectonic subsidence decreases systematically towards the southern tip of the fault.

Chapter 5: Deformation in the Shanchiao Fault hanging wall normal to the strike is most likely to reflect its underground fault plane geometry, which was unknown due to lack of constraints. Based on the Jingmei Formation top horizon offset data compiled in Chapter 4, different geometric configurations are tested against the geological constraints using simple half-space elastic dislocation modeling. Drastic listric geometry at shallow depth is needed to produce the pronounced roll-over folding immediately east of the fault. At further depth a steeper fault patch is likely to take over the extensional detachment inverted from the syn-convergence Hsinchuang Thrust considering the fitting of model outcomes with tectonic subsidence in the eastern half of the basin, the existence of pre-orogen normal fault underneath the fold-thrust pile, the few but well-resolved steep-dipping normal faulting focal mechanisms, and the debated seismogenic ability of extensional detachment. The Shanchiao Fault is hereby proposed to possess a ramp-flat-ramp (double-ramp) geometry reactivating both syn-convergence thrust and pre-orogen rift normal fault, and the seismic hazard this geometry may imply is discussed.

Chapter 2: Thirty-year land elevation change from subsidence to uplift following the termination of groundwater pumping and its geological implications in the Metropolitan Taipei Basin, Northern Taiwan

2.1 Introduction

Excessive groundwater utilization in agricultural and urban area is known to cause rapid human-induced land subsidence and pose severe problems including damage to building and infrastructures, exhaustion of groundwater resources, increase of risks of inundation, and inland sea water intrusion, as documented in many places around the world (e.g. Bangkok, Thailand, Phien-wej et al., 2006; Jakarta, Indonesia, Abidin et al., 2001; Ravenna, Italy, Teatini et al., 2005; Pingtung Plain, Taiwan, Hu et al., 2006). Pumping-induced subsidence is resulted primarily from irreversible compaction of aquitard material composed of fine-grained silt and clay layers during prolonged drainage process, and from minor amount of presumably elastic compaction from compression of coarse-grained conglomerate and sand deposits in aquifers (Holzer, 1984; Waltham, 2002). Ground surface change due to pumping generally reflects the response to dropping piezometric level (Fig. 2-1). Ban or controls on pumping are the actions usually taken by many authorities to mitigate the hazards, and regional groundwater table rises accordingly due to natural groundwater recharge. Ground elevation change during groundwater recovery after long-term extensive pumping should exhibit some amount of uplift. This effect is considered to be originated from relaxation of elastically compressed aquifer materials when pore-pressure regained, as illustrated by injection experiment carried out at the severely subsided Wilmington oilfield in the Long Beach harbour area of California (Allen and Mayuga, 1969), a phenomenon commonly referred as elastic rebound (Waltham, 2002). Characterization of such post-pumping behaviour, however, has not yet been studied in detail.

Typical ground response during fast artificial recharge for short-period pumping tests (e.g. Cappa et al., 2005) is well known as curve A in Fig. 2-1, indicating immediate and direct coupling of changes between ground elevation and hydraulic head. On the other hand, ground surface variations following cessation of prolonged groundwater pumping are mainly characterized by a transition of minor movements from subsidence to uplift (curve B in Fig. 2-1), as reported in Venice, Italy (e.g., Gatto

and Carbognin, 1981). It demonstrates a more complicated scheme when groundwater production is of greater spatial and temporal scales. Characteristics and mechanisms of regional land elevation change, particularly the elastic rebound after experiencing basin-wide groundwater over-extraction, remain unclear. The history of pumping and recovery of the groundwater in the Taipei basin in northern Taiwan, therefore, provides a good opportunity for better understanding of this post-pumping mechanism.

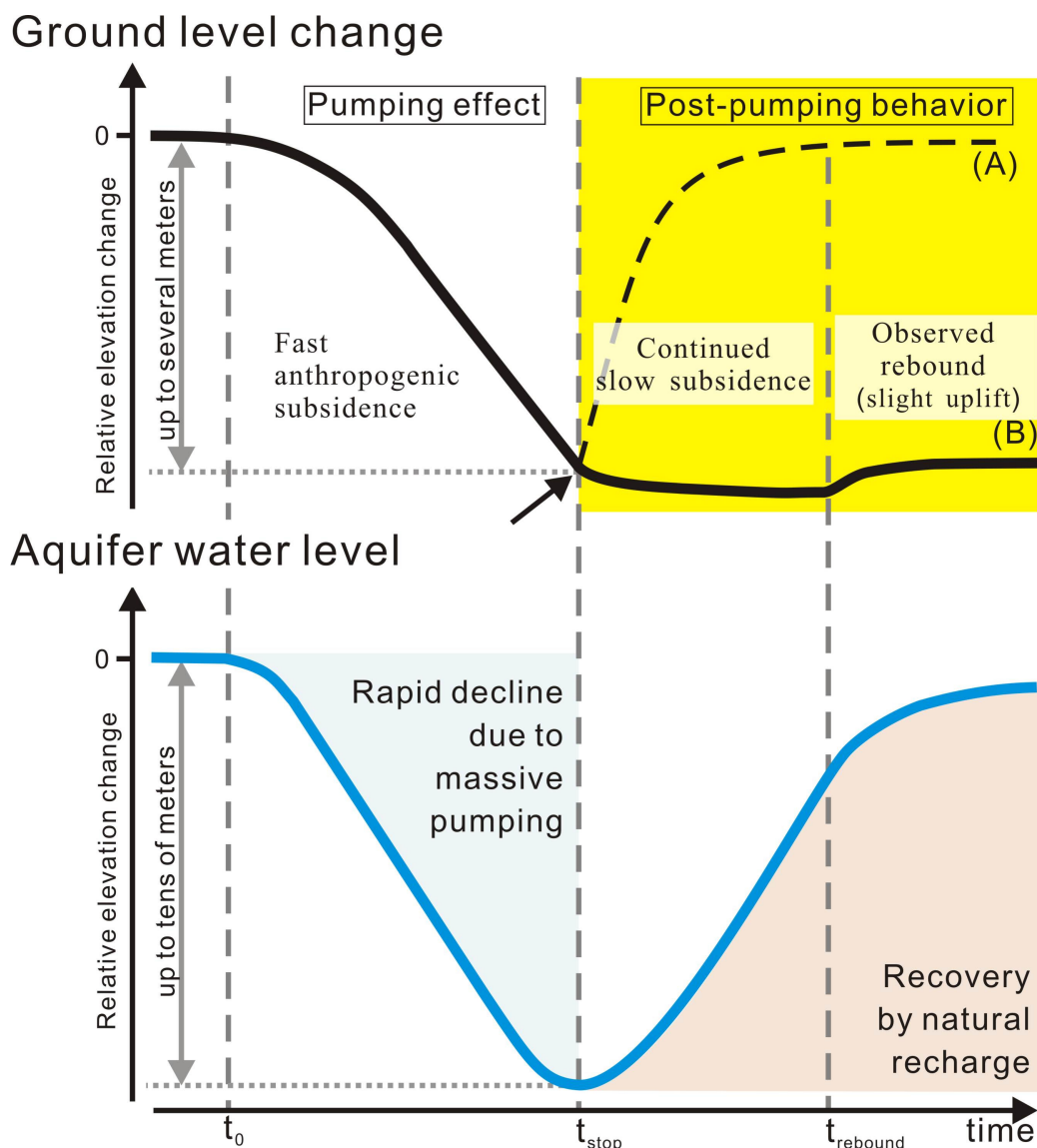


Fig. 2-1. General conceptual model of ground elevation change due to artificial piezometric head drawdown and recovery. Note that two different post-pumping behaviours of ground level change: (a) short-term pumping test and (b) long-term artificial pumping. See text for details.

The Taipei City is the political and economical centre of Taiwan (Fig. 2-2a) with dense population of about 3 million habitation and another several million inhabitants in the surrounding suburban areas. Like many big cities in the world, early development of the Taipei city was partly facilitated by its rich groundwater resources. However, unrestriction of groundwater over-pumping resulted in both dry-ups of wells and severe land subsidence, especially during 1955 – 1970 (Hwang and Wu, 1969; Wu, 1987). In order to prevent more ground subsidence and further associated damage, the government put a stop on the use of groundwater in the Taipei Basin during the early 1970s. Rapid land subsidence has therefore significantly decreased (Wu, 1987), and the groundwater table was gradually recovered and became approximately stable since late 90s (Chia et al., 1999; Fig. 2-3c). In this paper, we intend to examine recent vertical change of ground surface in response to the post-pumping ground water recharge in more details. Thanks to several annually measured levelling routes across the Taipei Basin, we are able to reconstruct the history of the land vertical change following the recharge of the aquifers.

Furthermore, while severe anthropogenic land subsidence has been stopped in the Taipei metropolitan area, concerns on potential earthquakes and related geohazards due to possible reactivation of the active Shanchiao fault continue to be discussed (e.g., Teng et al., 2001; Shyu et al., 2005; Huang et al., 2007). Taiwan is situated in a plate boundary between the actively converging Eurasian and Philippine Sea plates beginning about 5 Ma (Suppe, 1981; Teng, 1990). At present, the collision process is manifested in southern and central Taiwan as demonstrated by the intense crustal shortening, according to data from the GPS and seismic networks of Taiwan. In contrast, north-eastern Taiwan underwent post-collisional processes and has been considered to be incorporated in the opening of the southern Ryukyu back-arc system (Teng et al., 2000a), as evidenced by the presence of Quaternary extensional structures (Lee and Wang, 1988; Lu et al. 1995) and extensional earthquake focal mechanisms (Yeh et al., 1991; Kao et al., 1998). The Shanchiao Fault, which bounds the western edge of the Taipei Basin, has attracted attention in terms of earthquake hazards during the last decades. Tectonic subsidence related to this possible active fault is illuminated through recent levelling data, and should have an influence on the land elevation change in the Taipei Basin especially in the western part.

Levelling data in the Taipei area from 1975 to 2003 postdating the massive groundwater exploitation is utilized in the present study to examine the general conceptual model relating ground level response to recharge of aquifers. The various depth-related processes responsible for the observed occurrences of subsidence and uplift are discussed, including shallow soil compaction, crustal-scale tectonic

movement, and irreversible compaction and elastic rebound within aquifer. A schematic model explaining recent 30 years land elevation change in the Taipei Basin is proposed.

2.2 Regional setting

2.2.1 Geological background

The Taipei region can be divided into four geological domains (Fig. 2-2b): (1) the Foothills, hilly terrains north, east, and south of the Taipei Basin, consisting of fold-and-thrust belt of Miocene continental margin sedimentary packages; (2) the Tatun and Kuanyinshan volcanoes, north and northwest of the Taipei Basin, piled up of late Quaternary andesitic volcanic formations; (3) the Linkou Tableland, west of the Taipei Basin, covered by Quaternary thick lateritic conglomerates as an ancient fan-delta which rests above Miocene/Pliocene sedimentary rocks (Chen and Teng, 1990); (4) the Taipei Basin, a triangular-shaped half-graben filled with late-Quaternary fluvial deposits since about 0.4 Ma (Wei et al., 1998; Teng et al., 2001), which lie unconformably over the deformed Miocene sedimentary packages.

The late-Quaternary deposits of the Taipei basin form an asymmetric wedge shape in thickness: reaching a maximum depth of about 700 m in the western margin and gradually becoming thinner toward the east and south (Fig. 2-2c). These unconsolidated deposits in the Taipei basin are divided into four lithostratigraphic units (Teng et al., 1999), from bottom to top (Fig. 2-3b): (1) the lowest Banchiao formation, consisting of fluvial sand, mud and conglomerates, with minor pyroclastic debris and thick varved mud in the upper section; (2) the Wuku formation, consisting of fluvial sand and conglomerates with minor mud and lateritic conglomerates; (3) the Jingmei formation, comprising of lateritic alluvial-fan conglomerates; (4) the Sungshan formation, composed of estuary interbedded sand-mud deposits. The basin deposits are marked by prominent facies changes and most of the sedimentary layers laterally pinch out rapidly. However, the widespread lateritic gravel of the Jingmei formation and the varved layers in upper Banchiao formation serve as basin-wide marker beds (Teng et al., 1999).

Brief geological evolution of the Taipei Basin is summarized in the following, based on previous studies. In Pliocene, the Taiwan Orogeny has initiated as the Luzon Arc of the Philippine Sea plate approaching to continental margin of Eurasia (e.g. Suppe, 1981). The Miocene shallow marine sedimentary rocks of the Taipei area were deformed into imbricated fold and thrust sheets with several major faults including the Hsinchuang, Kanjiao, and Taipei Faults (Fig. 2-2b, c) as mountainous ranges (Ho, 1975; Wang-Lee et al., 1978). While the orogeny reached climax in northern Taiwan about 2 Ma, the Paleo-Tanshui River, the major river in the Taipei Basin, produced the

Linkou fan-delta around the ancient mountain front thrust (Chen and Teng, 1990), the Hsinchuang Fault which runs approximately parallel to the western margin of the Taipei basin (Teng et al., 2001). The compressive stress regime of the northernmost Taiwan appeared to cease during the middle to late Quaternary (Lee and Wang, 1988). The eruption of the Tatun volcanism to the north of the Taipei Basin might reflect the onset of regional extension which was interpreted to be related to the Okinawa trough back-arc opening and/or lateral extraction in the corner of plate convergence (Lee and Wang, 1988; Lu et al., 1995; Hu et al., 2002). Subsidence along western margin of the Taipei basin is interpreted to result from the repeated normal faulting on the Shanchiao Fault as tectonic inversion on the Hsinchuang thrust fault (Chiu, 1968; Hsieh et al., 1992). It turned the Taipei area from rugged mountains into a sediment-receiving basin. The accumulation of fluvial and lacustrine sediments was estimated to be started at about 0.4 Ma (Wei et al., 1998; Teng et al., 2001). Since then the Taipei Basin has kept expanding due to continual asymmetric subsidence along the Shanchiao fault in the western edge of the basin (Wang-Lee et al., 1978). Under the combining influences of sea level fluctuations, volcanic activities, drainage system changes, and tectonic processes, the basin was filled with various types of sediments, including alluvial, lacustrine, marine and pyroclastic deposits, as mentioned above.

As a consequence, the Shanchiao Fault, which separates the Linkou Tableland from the Taipei Basin, is considered the major active structure responsible for accommodating the extension across the Taipei region and thus for the formation of the half-graben Taipei Basin (Teng et al., 2001). Shallow seismic reflections across the Shanchiao Fault imaged an offset of Holocene sediments at shallow tens of meters depth (Wang and Sun, 1999). GPS surveys of the Taipei area showed extension with a rate of 0.08 ± 0.02 $\mu\text{strain/yr}$ in the direction of SEE - NWW across the fault (Yu et al., 1999a). Huang et al. (2007) correlated stratigraphy of three sets of boreholes across the Shanchiao Fault, and identified three paleoseismic events within the Holocene time (8400-8600, 9000-9300, and 11100 years b.p.). Geomorphology analysis also exhibits series of scarps closely related to the development of the Shanchiao Fault (Chen et al., 2006). Thus the Shanchiao Fault is considered active (as stated in reports of Central Geological Survey, Chang et al., 1998 and Lin et al., 2000).

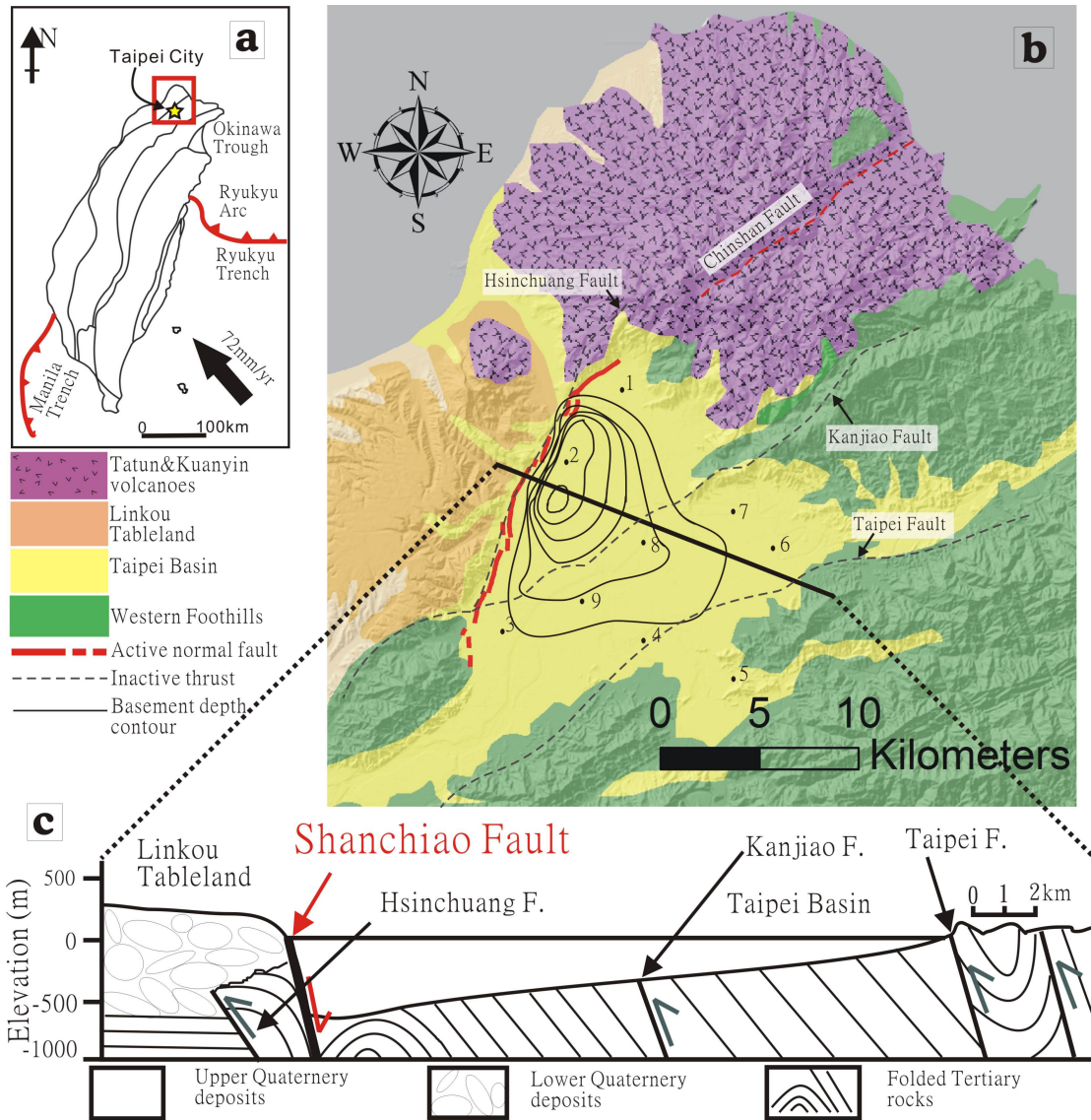


Fig. 2-2. (a) Tectonic framework of Taiwan. The converging rate and direction of Philippine Sea Plate relative to Eurasia plate is adapted from Yu et al. (1999b) and Zang et al. (2002). (b) Four geological domains of Taipei area (see text for details). The thin grey lines within the Taipei Basin are the basement depth contour of 100 m interval (after Teng et al., 2001). The red line along the western margin of the Taipei Basin is the Shanchiao Fault (after Chen et al., 2006). The black dots mark local district names in the Taipei Basin: 1. Guandu, 2. Wuku, 3. Shulin, 4. Zhonghe, 5. Jingmei, 6. Sungshan, 7. Dazhi, 8. central Taipei, 9. Banchiao. (c) Simplified geological cross section of the Taipei Basin (modified from Teng et al., 1999). The Hsinchuang, Kanjiao, and Taipei Faults are inactive thrust faults (denoted with grey arrows) which slipped during the collision phase in the Taipei area.

2.2.2 Hydrogeologic framework and utilization of groundwater

Four major aquifers, which generally correspond to the stratigraphic formations, have been defined in the late-Quaternary sediments of the Taipei Basin (Fig. 2-3b; Wu, 1987). The topmost free aquifer (Aquifer 0), which extends from ground surface to depth around 50 m (except in the western edge of the basin being deeper to about 120 m in maximum), is composed of interbedded clay, sand and pebbles. Aquifer 0 is thus considered to correspond to the Sungshan formation. The confined Aquifer 1 sits at depth between 50 to around 100 m (again except in the western edge of basin, about 115-140 m) in the conglomerate layer covered by laterite. This conglomerate layer is interpreted to correspond to the Jingmei formation, with hydraulic diffusivity around 0.12 to 0.18 m²/s and storage coefficient ranging from 0.001 to 0.004 (Chia et al., 1999). The lower aquifers (Aquifer 2, 3) are present approximately 100 to 130 m and 140 to 160 m underground (depths for the central portion of the basin), as two layers of conglomerates within the Wuku and Banchiao formations, respectively (Fig. 2-3b). Among them Aquifer 1 appeared to be the major groundwater source of the pumping wells in the Taipei Basin. The groundwater of the lower three aquifers comes mainly from two of the major rivers in the Taipei basin, the Xindian River and the Dahan River (Fig. 2-3a). On the other hand, rainfall is the major water source for Aquifer 0 (Chia et al., 1999).

First massive utilization of groundwater source in the Taipei Basin (primarily Aquifer 1) was initiated by an English engineer W. K. Bardon in 1895. Under his advisory the government set up 150 wells (Wu, 1987). Since then the number of wells was rapidly increasing and the groundwater resource drained twice in 1906 and 1960 to early 1970s. The second event was accompanied by severe land subsidence. Piezometric head of Aquifer 1 decreased more than 40 m and reached the lowest point around 1975 (Wu, 1987; Chia et al., 1999; Fig. 2-3c). The basin-wide subsidence resulted from over-pumping was particularly concentrated in the central portion of the Taipei Basin where maximum land subsidence exceeded 2 m (Fig. 2-3a), corresponding to the site of major pumping at that time. Severe restriction taken by the government on groundwater pumping in the early 1970s had successfully stopped the fast decline of groundwater table which immediately began to rise as the piezometric head having gradually recovered 30-40 m in 30 years (Chia et al., 1999; Cho, 2006; Fig. 2-3c). Water resource of the Taipei metropolitan since the 1970s has been supplied by surface water mainly from two reservoirs in upstream Dahan and Xindian Rivers.

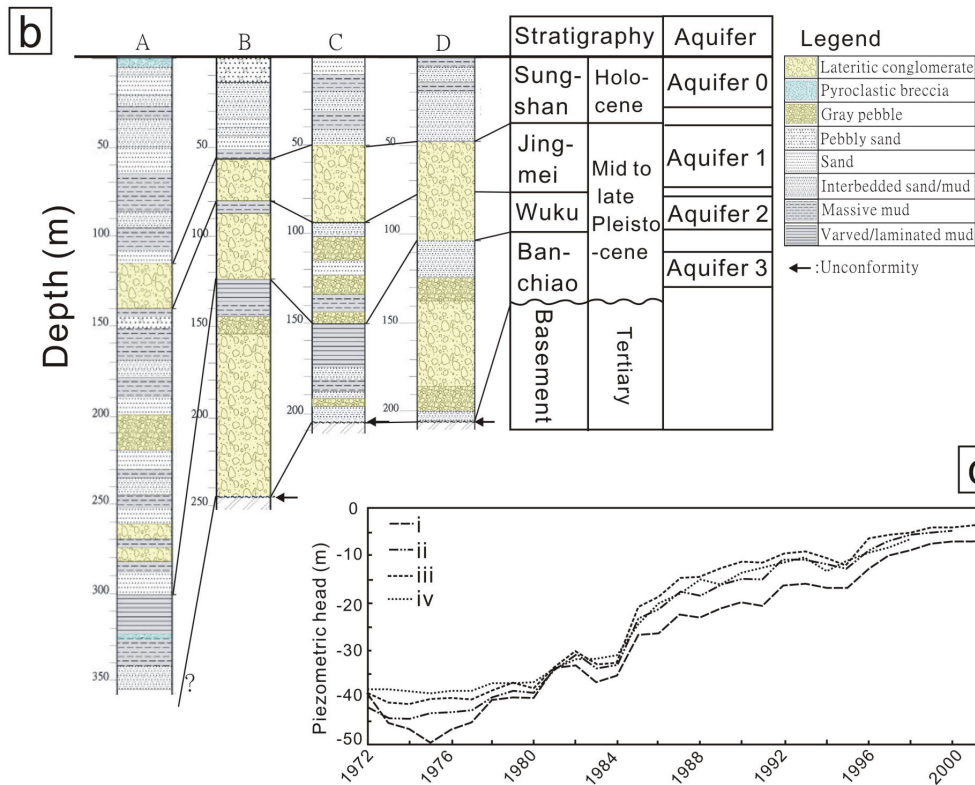
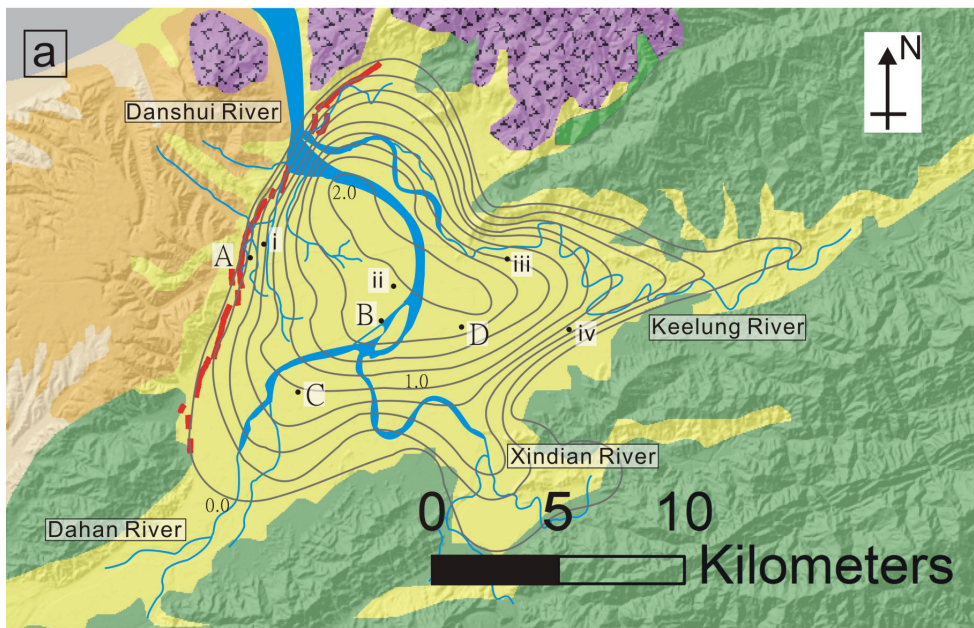


Fig. 2-3. (a) Cumulated subsidence in the Taipei Basin from 1955 to 1991 (after Lin et al., 1999). Contour interval is 0.25 m. Borehole sites: A: Wuku (WK-1), B: Sanchung (SC-1), C: Banchiao (PC-2), D: Shingongyuan (Shingongyuan No.1). Groundwater monitoring wells: i: Wuku, ii: Sanchung, iii: Shingtien Palace, iv: Sungshan. (b) Stratigraphic architecture of late Quaternary deposits within the basin, along with the four aquifers (modified from Teng et al., 1999). (c) Piezometric head records of Aquifer 1 at four monitoring wells since 1972 to 2003 (Chia et al., 1999; Cho, 2006).

2.3 Analyses and results

2.3.1 Description of data analyses

For the purpose of monitoring the land subsidence due to groundwater pumping, several levelling routes were established by government authorities since 1948 in the Taipei basin. More than 406 benchmarks were constructed in different periods of the levelling (Fig. 2-4). Most of the benchmarks were installed on concrete foundation or rock basement. In this study, we analysed the levelling data from 1975 to 2003, in order to decipher effects of post-pumping. Only benchmarks with repeated measurements were taken into account. The observed elevations from these surveys were orthometrically corrected. The more recent data (since 1989) were additionally corrected for temperature variations for rod and instrumental biases. The levelling was deployed conventionally by closing a series of double-run sections. These data sets called TWVD2001 (TaiWan Vertical Datum, the reference of absolute elevation of benchmarks, calculated from the tide data of Keelung tide station) are stored in archive centre of the Ministry of the Interior and Land Subsidence Prevention and Reclamation Corp of National Chengkung University. The survey adopted the standard procedures of the first order high precision levelling, which is of a standard error of about $2\sqrt{D}$ mm, where D is the distance of measurement (unit of km). As a result, the uncertainties of the elevations for each benchmark during surveys are usually within 1-3 mm.

For the sake of discontinuity of measurements, we divided the data into 7 periods from 1975 to 2003 (1975-1980, 1980-1985, 1985-1989, 1989-1994, 1994-1996, 1996-2000, and 2000-2003). For each period, the elevation changes of the benchmarks are transferred to elevation change rates, in order for comparison. Based on the rates of elevation change for each benchmark, we then construct contour map of land change for each period (1975-1989 for Fig. 2-5 and 1989-2003 for Fig. 2-6), adopting the commonly used extrapolation technique of kriging (Olivier and Webster, 1990). For each period, the contours were derived from data of more than 76 benchmarks. Note that ground level fluctuation shown outside the basin plain is mostly a result of extrapolation which may contain large errors and should not be taken into account.

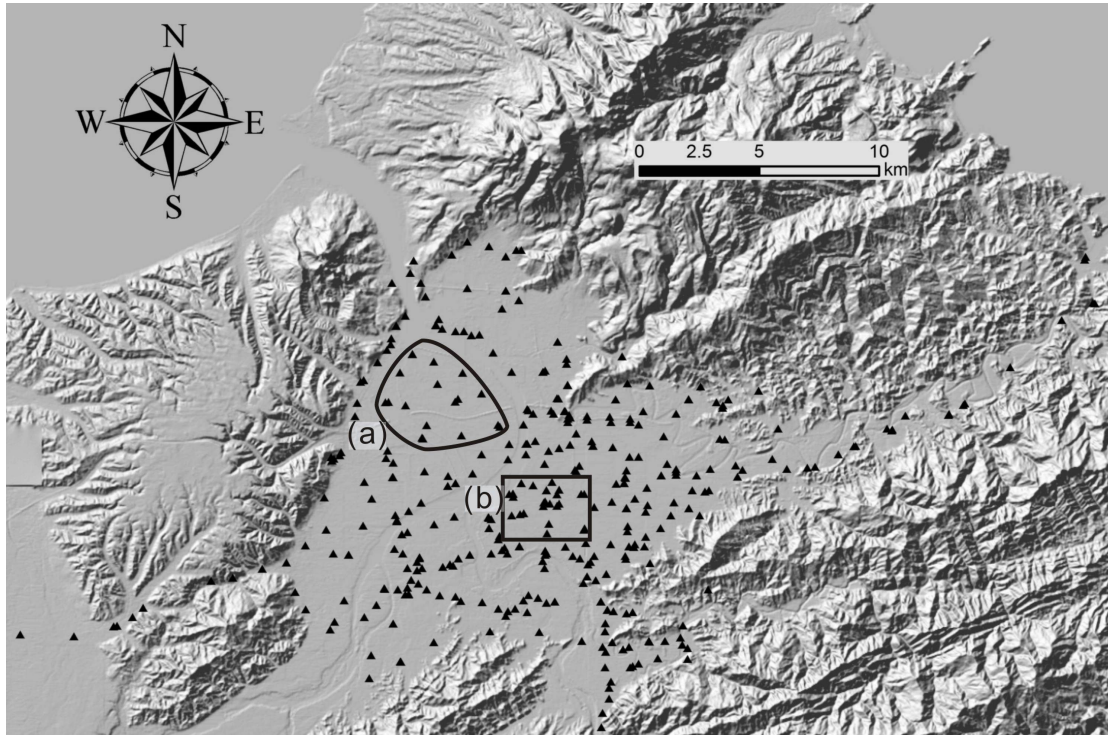


Fig. 2-4. Distribution of the 406 benchmarks of levelling routes analysed in this study. Benchmarks in groups (a) and (b) are used to represent the average movements in western Taipei Basin and Central Taipei, respectively.

2.3.2 Results of post-pumping land elevation change

Several interesting and important characteristics of the land surface level change (subsidence and uplift) in the Taipei Basin during the post-pumping time can be inferred from the contour maps. First, the whole basin still subsided after the stop of groundwater pumping, but with a decreasing trend from 40-70 mm/yr to 0-30 mm/yr, during 1975 to 1989, denoted here as Phase 1 (Fig. 2-5). Second, a large part of the land became to uplift since 1989, denoted as Phase 2 (Fig. 2-6). However, the surface elevation change was far from homogeneous. For instance, enhanced and persistent subsidence occurred in north-western margin of the basin near Guandu (for the place names mentioned, please refer to Fig. 2-2b) throughout the entire time span (1975-2003), and concentrated subsidence in western margin of the basin (Wuku, Shulin) and north-eastern basin (Dazhi-Sungshan) was also very persistent before 1996. Other locus of subsidence (e.g., Banchiao, Zhonghe, Jingmei) as well as irregular and short-lived subsidence or uplift were also observed.

A period-by-period account of land elevation change in the Taipei Basin is presented as followed. Basin-wide decreasing subsidence characterized all three periods in Phase 1. During 1975-1980 (Fig. 2-5a; 94 benchmark), subsidence was dominant and was mostly concentrated in the northwestern (Guandu, exceeded 60 mm/yr; and Wuku, maximum 75 mm/yr) and northeastern portions (Dazhi, nearly 70

mm/yr). In 1980-1985 (Fig. 2-5b; 76 benchmark), significant subsidence continuously occurred along the western margin of the basin (Guandu, reached 12 mm/yr; Wuku, over 10 mm/yr) and in the northeastern corner (Dazhi, more than 20 mm/yr), however, with smaller rates compared to the previous period. For 1985-1989 (Fig. 2-5c; 157 benchmark), a large part of areas in the basin were continuous to subside (in particular, the western margin), but some small areas began to show slight uplifting, especially in the central and southern parts, although some of the benchmark records showing extremely sharp uplift might be anomalies. In general, the subsidence rate continued to decrease, comparing to the two previous periods; nonetheless, localized subsidence was still persistent along the western margin of the basin (Guandu, attained 30 mm/yr; northern Wuku, >10 mm/yr; Shulin, 10 mm/yr) and other patches in the basin (south Dazhi, maximum 15 mm/yr; and Jingmei, around 5 mm/yr).

Starting from about 1989 (Phase 2), uplift began to appear significantly in the Taipei basin and declined in magnitude in the later half of this Phase. During 1989 to 1994 (Fig. 2-6a; 111 benchmark), we observed that the surface subsidence almost ceased and a large portion of the Taipei Basin began to slight uplift, especially in the centre of the basin (central Taipei, 10 to 15 mm/yr; Banchiao, 10 to 15 mm/yr). Nevertheless, slight subsidence still persisted in western margin of the basin (e.g., 0 to 5 mm/yr in Guandu and Wuku). In 1994-1996 (Fig. 2-6b; 146 benchmark), slight subsidence continuously occurred and was localized in western side of the basin (Guandu, as high as 14 mm/yr; Wuku, maximum 10 mm/yr; and Shulin to Banchiao, up to 6 mm/yr), and in southern Taipei (Zhonghe, reached 10 mm/yr). On the other hand, uplift seemed to begin to dominate the eastern half of the basin, but with a lesser magnitude. In 1996-2000 (Fig. 2-6c; 103 benchmark), the whole Taipei Basin was generally experiencing mild uplift, except for north-western margin of the basin (Guandu – Wuku, subsidence with a possible bull-eye reaching maximum over 20 mm/yr), and other local areas (Dazhi, Zhonghe, and Jingmei). During the most recent period, 2000-2003 (Fig. 2-6d; 94 benchmark), slight uplift prevailed in the Taipei Basin (0-5 mm/yr) with subsidence in north-western basin (Guandu, Wuku, 0 to 5 mm/yr), and other local areas along the southern and eastern edge of the basin (Sungshan, Zhonghe and Jingmei).

In summary, the subsidence rate for the Taipei Basin as a whole generally decreased from 1975 to 1989 (Phase 1), and then the elevation change of the basin gradually switched to slight uplift since about 1989 during Phase 2 (Fig. 2-7). The waning subsidence during the 1975-1989 of Phase 1 is interpreted to be mainly ascribed to the compaction of the water-depleted aquifers, resulting from the residual effect of the rapidly declined piezometric head due to over-pumping of groundwater.

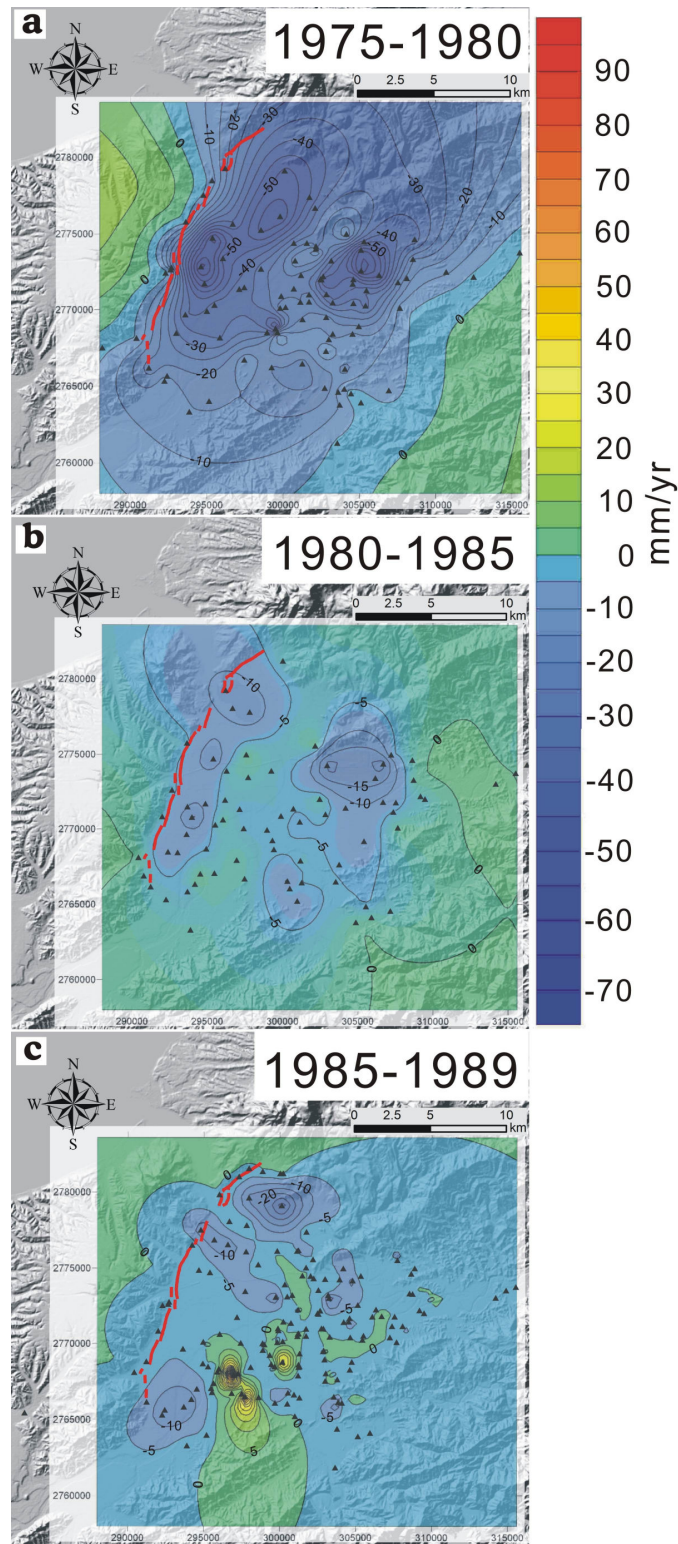


Fig. 2-5. Contour maps of observed land surface elevation change in Phase 1 (1975-1989) of post-pumping period. (a) 1975-1980. (b) 1980-1985. (c) 1985-1989. Negative rate values indicate subsidence, and vice versa. Contour interval is 5 mm/yr. Coordinates shown are of TWD 67 Transverse Mercator system. The whole basin revealed a general subsidence from 1975-1985, with some localized effects. See detailed discussion in text.

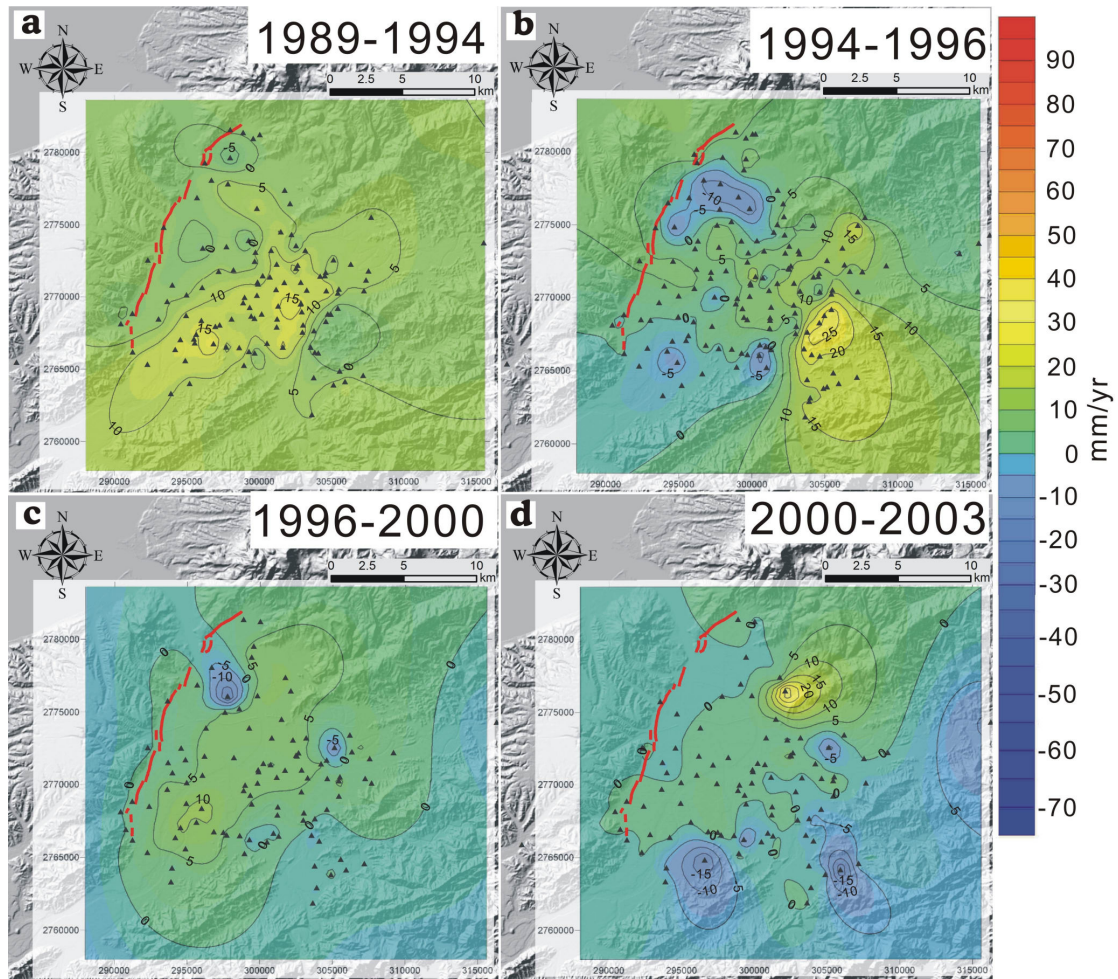
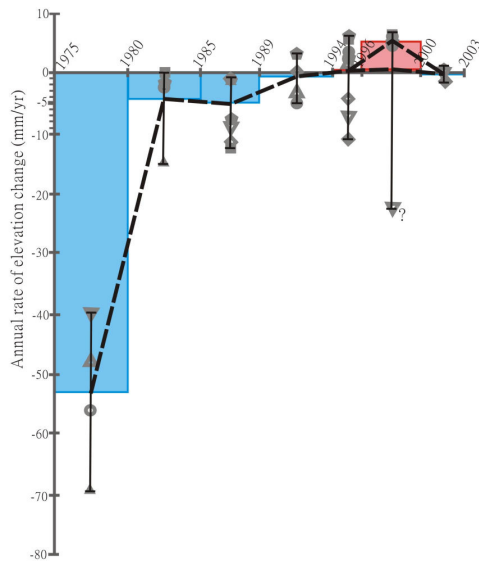


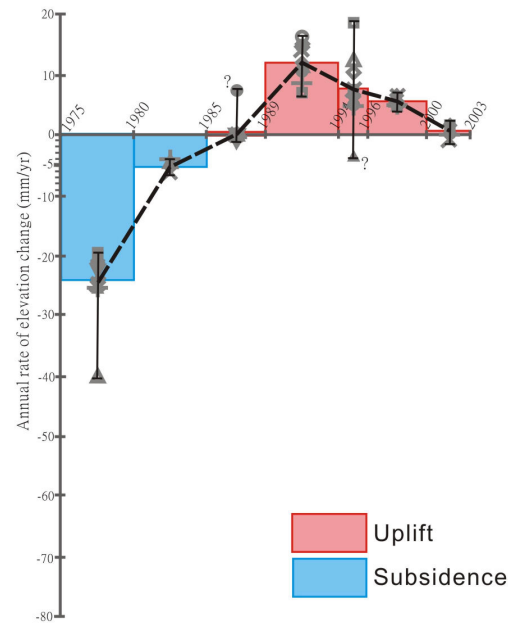
Fig. 2-6. Contour maps of observed land surface elevation change in Phase 2 (1989-2003) of post-pumping period. (a) 1989-1994. (b) 1994-1996. (c) 1996-2000. (d) 2000-2003. Annotations see Fig. 2-5. The basin showed a general uplift from 1989 to 2003; however, local subsidence occurred at several places. See details in text.

While massive pumping was ceased, recharge of groundwater from two major rivers (Xindian and Dahan Rivers) to the aquifers has raised the water table for more than 30 m from the 1970s to 2003 (Fig. 2-3c). We anticipate that the recovery of the groundwater level would produce an elastic rebound for the aquifers, thus caused basin uplift since 1989 in Phase 2. However, the concentrated and rather persistent subsidence and the reduced uplift occurred along the western margin and northern part of the Taipei Basin, compared to the central part of the basin, suggesting under impacts of other factors.

(a) Wuku area (Western Taipei)



(b) Central Taipei



Benchmarks			
▲ Wr 7	▲ Wr 27	○ Wr 28	● Wr 43
■ Wr 44	■ Wr 45	◇ Wr 46	◇ Wr 48
◇ Wr 50	◆ Wr 51	▽ Wr 75	▽ Bank 3

Benchmarks			
× Lc007	+	Lc008	
▲ 9535	▲ 9536	○ Bdng 12	● Bdng 22
■ Bdng 27	■ Bm No8	◇ BM No10	◇ CW No5
◇ CW No11	◆ Bank 1	▽ Kan 39	▽ Bm 0

Fig. 2-7. Evolution of ground elevation change rate in post-pumping period from 1975 to 2003. (a) Western Taipei as the Wuku area. (b) Central Taipei. Distribution of the benchmarks used for calculation is shown on Fig. 2-4.

2.4 Mechanisms of land elevation changes during post-pumping

The land elevation change of the Taipei basin could be a product of complexly interfering natural and artificial processes. The heterogeneous pattern of land vertical changes in the Taipei Basin certainly reflects the spatial and temporal context of different agents. In the spatial domain, these agents, according to where the processes take place, can be described and classified by their operation depth. Here we propose main mechanisms to explain the land elevation changes in the Taipei Basin, attributing effects of land elevation change of the Taipei basin to three major components: (1) surface soil compaction (the shallow component), (2) deformation of aquifers, including compaction and elastic rebound due to groundwater effect (the intermediate component), and (3) tectonic load (the deep and crustal-scale component).

2.4.1 Near surface soil compaction (the shallow component)

Local enhanced subsidence can be observed in several areas within the Taipei Basin in many periods we analysed. Subsidence caused by construction (loads of new

buildings) cannot be omitted, but such phenomenon might be extremely localized and short-lived. Otherwise, subsidence in several places, such as Dazhi, Sungshan, Jingmei, Banchiao and Shulin, occurred throughout many periods although not always present (Figs. 5 and 6). Since their close proximity to the three major river channels in the Taipei basin (i.e., Keelung, Dahan and Xindian Rivers), we intend to interpret that a large part of subsidence in these areas to be contributed by compaction of recent flood or overbank deposits (especially mud). Effect of in situ sediment compaction, often referred as natural subsidence (Waltham, 2002), therefore must be evaluated in order to further distinguish the role and intensity of natural and artificial factors played on the observed ground level change.

According to a recent in situ study in the Taipei Basin conducted by Lin et al. (1999), compaction of the loose sediments occurred mainly in the clayey layers of the uppermost 50 m Holocene deposits (generally corresponding to the Sungshan Formation) in three monitored wells in the western part of the basin at Wuku and Banchiao, in a time span of three and a half years from March, 1994 to September, 1997. For older sediments underneath, the compaction and consolidation were observed to be rather slow and was ignorable regardless of the types of the deposits. Based on their results, we estimated the averaged annual rate of compaction for 1-meter-thick clayey layers to be ranging from 0.14 to 0.28 mm/yr (Table 1) by dividing the cumulative compaction of the clay sections in the monitored wells by the monitoring interval of three and half years. Meanwhile we reconstructed an isopach map for clay thickness within the topmost deposits of the Sungshan Formation in the basin (Fig. 2-8a) based on 350 borehole records from Central Geological Survey (open source, available on <http://210.69.81.69/geo/frame/gsb88.cfm>). The proxy of present variation of shallow soil compaction rate in the Taipei Basin can be obtained by multiplying the deduced average annual compaction rate for 1-meter-thick clay (i.e., 0.2 ± 0.07 mm/yr) with the shallow clay thickness isopach. We estimate contemporary shallow soil compaction to contribute 1-8 mm/yr of subsidence in the basin with most land ranging 2 to 5 mm/yr (Fig. 2-8b).

Natural subsidence rates of surface soil documented elsewhere in similar flood plain and deltaic environments fall in the same order of magnitude (Jelgersma, 1996), such as Ravenna (4-6 mm/yr, Teatini et al., 2005), Romagna (0-5 mm/yr, Gambolati et al., 1999), Venice (0.5-1.3 mm/yr, Gatto and Carbognin, 1981), and Po River Delta (3-5 mm/yr, Gambolati and Teatini, 1998) in Italy and coastal Louisiana, USA (shallow component 1.5-2.5 mm/yr, Dokka, 2006). In addition, the modelling results of Meckel et al. (2006) based on Holocene stratigraphy of lower Mississippi River Delta in southern Louisiana, which closely resembles the compacting shallow

sediments of the Sungshan formation in the Taipei Basin, is applied to evaluate our proxy. Taking the surface soil in the Taipei Basin (50-meter thick and deposited within the Holocene) into their cumulative distribution functions of compaction rate model, the 90th percentile compaction rate (figure 2 of Meckel et al., 2006) ranges from 1.5 to 4 mm/yr. This suggests that our estimate is reasonable and not likely to underestimate present soil compaction.

Comparison between the contour maps of the observed elevation change (Figs. 5 and 6) and the estimated shallow soil compaction (Fig. 2-8b) shows that concentrated subsidence are indeed in a close relation with thicker soil/clay layers, especially along the main river courses (Fig. 2-3a). For example, ultra thick clay with resultant peak soil compaction is likely the main source of continuous subsidence in the marshy Guandu area along the Danshui River in the north-western corner of the basin. However, the Wuku area in western Taipei, on the contrary, is not subject to high soil compaction. As a consequence, persistent subsidence in the western margin of the Taipei Basin (Guandu, Wuku, and sometimes extending to Shulin) cannot be attributed totally to natural compaction especially during Phase 2, and requires other explanations to decipher its origin.

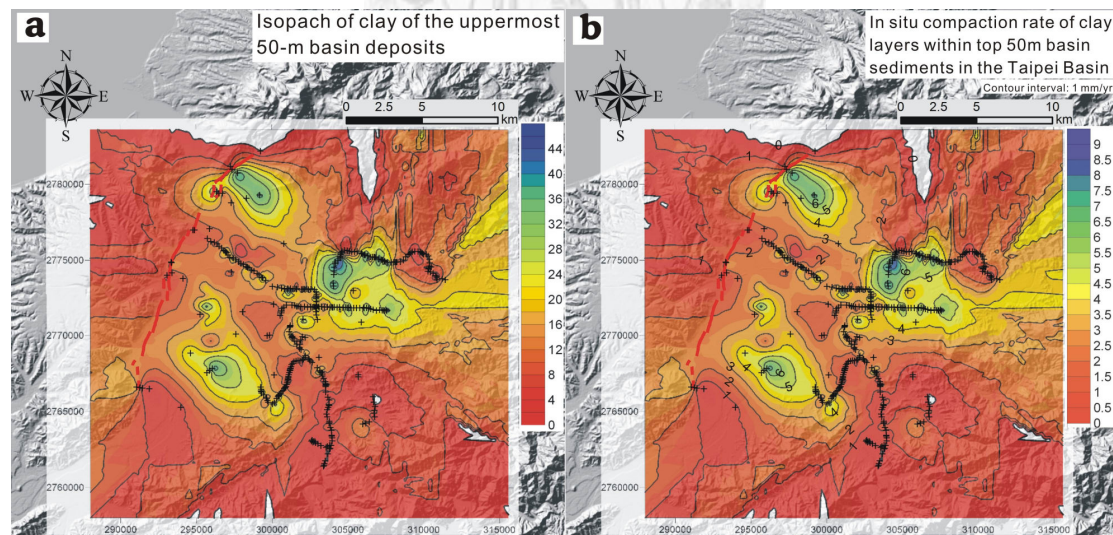


Fig. 2-8. (a) Isopach of the Holocene clayish sediments (topmost 50-m deposits) in Taipei basin, constructed from 350 borehole records from Central Geological Survey (borehole sites marked in cross). (b) Estimated compaction rate of clayey layers within the Holocene deposits (soil compaction). See text for reference.

Table 2-1. The in situ compaction in clayey layers of top 50 m basin sediments recorded by Lin et al. (1999). The averaged annual rate of compaction in 1-meter-thick clayey layers is deduced.

Well	Presence of clayey layers (meters in depth)	Cumulated compaction (mm)	Calculated annual compaction rate per meter of clayey layers (mm/yr)
Wuku	~27-35	4 (14-10)	0.1429
(Industrial Park)	~42-48	4 (6-2)	0.1905
Banchiao (Veterans Affairs Office)	~10-20	10 (18-8)	0.2857

2.4.2 Tectonic load (the deep and crust-scale component)

Tectonic subsidence from activities of the Shanchiao Fault is thought to affect ground surface elevation change since present extensional deformation across the fault was documented (Yu et al., 1999a). It's expected to be most pronounced in the near-fault hanging wall region, that is, the western margin of the basin, where the basin basement is dramatically deepened and reaches maximum depth. The long-term averaged tectonic subsidence rate in western Taipei Basin thus can be estimated by stratigraphic offset across the fault. The onset of basin sediment deposition was estimated to be around 0.4 Ma when basin basement was lowered to near sea level (Chen et al., 1995; Wei et al., 1998; Teng et al., 2001) and since then approximately 700 meters of basin sediments were accumulated. Dividing the total thickness of late-Quaternary basin deposits (700 m) by the time span of sedimentation (0.4 Myr) we obtain the late Quaternary averaged tectonic subsidence rate to be 1.75 mm/yr since 0.4 Ma. Note that it may contain contributions from co-seismic slips (Huang et al., 2007), thus representing the upper limit of value for interseismic tectonic subsidence rate. In the central part of the basin tectonic subsidence may attain half of the rate in western Taipei, approximately 0.88 mm/yr. We consider the tectonic subsidence rates to be constant over the investigated time intervals since no major earthquakes were recorded in shallow crust of the Taipei area during 1975 to 2003. More accurate assessment of the ongoing tectonic subsidence could be derived from levelling of benchmarks attached to deep boreholes (e.g. Dokka, 2006) and is in urgent need for earthquake hazard research and mitigation in the Taipei metropolis.

2.4.3 Deformation of aquifers (the intermediate component)

In the hydro-mechanical coupling scheme as illustrated by Waltham (2002), abstracting groundwater would reduce pore-water pressure in aquifers, usually as sand or conglomerate beds, which behave in a seemingly elastic manner (Karig and Hou,

1992). However, this would be followed by reduced pore-water pressure in usually intercalated clay and aquitard materials in order to regain hydraulic equilibrium. Clay compaction is largely an irreversible one-way process, and is the major source for severe pumping-induced land subsidence (Terzaghi, 1925; Holzer, 1984; Phien-wej et al., 2006). When groundwater is recharged into the starved aquifers to recover the pore pressure, expansion of aquifer sand and gravel layers occurs and contributes to uplift of ground surface as elastic rebound (Waltham, 2002). In detail of this hydro-mechanical coupling, during piezometric head rise, the recharged sections of the aquifer will release the formerly imposed compressive strain to show dilatation, producing elastic rebound. On the other hand, the starved sections of aquifer and aquitard will continue to show compression as the result of time-dependent consolidation behaviour caused by past piezometric drawdown, until groundwater table has risen to remove deficits of pore pressure in these sections. Ground level change reflected on groundwater recovery is the competition between subsidence from starved aquifer (plus aquitard) section and uplift from the recharged aquifer section. The evolution generally follows the pattern of curve B in Fig. 2-1. Similar mechanism was also invoked to explain land level fluctuation in Las Vegas controlled by seasonal water table variations (Amelung et al., 1999).

According to well monitor records in the Taipei Basin (Fig. 2-3c), groundwater table started to rise as soon as pumping ceased in 1975. Compaction of Aquifer 1 during massive groundwater extraction would arrest gradually, following the recharge of groundwater in the aquifer. Near the end of Phase 1 as piezometric head was largely recovered, deformation of aquifer would become neutral as that rebound had developed to surpass remaining compaction. The uplift due to elastic rebound of Aquifer 1 was not visible on land surface until 1989 at the beginning of Phase 2 (Fig. 2-6). We interpret that at this time the amount and rate of elastic rebound outpaced residual aquifer clay compaction and other subsidence effects including the compaction of surface soil and tectonic subsidence of normal faulting. Elastic rebound of recharged aquifer would then gradually decrease in amount and rate since the groundwater level stabilized from mid 1990s. Ground level change pattern of the Taipei Basin after cessation of massive pumping with natural groundwater recharge thus fits well with the scheme of curve B in Fig. 2-1. The evolution of the post-pumping elevation change is characterized by a relatively longer period of waning subsidence (Phase 1: 1975-1989) followed by a shorter period of slight uplift (Phase 2: 1989-2003), due to a combination of decreasing compaction and increasing refill in Aquifer 1. The time lag between the start of piezometric level rise (t_{stop} in Fig. 2-1) and the first occurrence of the observed uplift of land surface (t_{rebound} in Fig. 2-1) in Taipei basin is about 15 years, which is believed to be closely related to the

recharge rate of Aquifer 1. The contrast on amount between the non-reversible, plastic clay compaction and the elastic rebound of aquifer strata may be a viable explanation to the fact that the recent uplift (since 1989) in the Taipei basin has a much lesser magnitude than that of the severe subsidence during massive pumping as before the 1970s. Most surface uplift due to rebound was observed in the central to eastern portion of the basin, roughly corresponding to area of most intense anthropogenic subsidence during pumping (compare Fig. 2-6 and Fig. 2-3a).

Similar phenomenon following cessation of massive groundwater exploitation was documented in Venice, Italy by Gatto and Carbognin (1981) where a land rebound of 2 cm, 15% of subsidence due to groundwater withdraw, occurred about five years later than the onset of regional piezometric head recovery from natural recharge. Artificial recharge of a severely depleted hydrocarbon reservoir in Long Beach, California, induced an observed rebound of 33.5 cm where precedent subsidence due to petroleum production reached 9 meters in maxima (Allen and Maguya, 1969). Both cases demonstrated that aquifer rebound is generally about one order less in magnitude than the preceding subsidence. This is in good accordance with the situation in the Taipei Basin, whose subsidence is of two meters and rebound is of 10-20 cm in general. Recent studies of geodetic records in regions including Ravenna, Italy (Teatini et al., 2005) and Shanghai, China (Chai et al., 2004) displayed a sharp change on subsidence rates showing a switch from severe to slight subsidence while groundwater utilization was controlled or stopped; however, no uplift due to aquifer rebound was observed in these above regions yet. Differences in groundwater exploitation history, piezometric level evolution, and local hydrogeological properties (e.g. aquifer compressibility, porosity, permeability) are major factors for the discrepancies documented in the localities cited above.

As mentioned above in section 2.2.2, most groundwater extraction in the Taipei basin was from Aquifer 1, which is generally located about 50 to 100 m underground within the Jingmei Formation. We intend to call the direct resultant effects from post-pumping compaction and rebound of aquifer strata due to natural recharge of groundwater as the “intermediate” component, compared with the compaction of the surface soil above the Aquifer 1 and the possible crust-scale subsidence due to the normal faulting of the Shanchiao Fault. This component is expected to have basin-wide impact since the Aquifer 1 is distributed throughout the entire basin.

2.4.4 Synthesis and discussion

The mechanisms of land elevation change in the Taipei Basin during the past 30-year post-pumping period are summarized in Fig. 2-9, showing the effect from three major depth-related components in the central and western parts of the basin.

Soil compaction (the shallow component) is estimated with averaged rates of 3.5 mm/yr and 2 mm/yr for Central Taipei and the western margin, respectively (see Fig. 2-8, section 2.4.1.). The tectonic load from the Shanchiao Fault (the deep and crustal-scale component) contributes subsidence of approximately 1.75 mm/yr for the western margin of the basin and 0.9 mm/yr for Central Taipei (discussed in section 2.4.2.). As for aquifer deformation (the intermediate component), due to combination of compaction and rebound of natural recharge, its deformation rate is estimated by subtracting the soil compaction rate and the tectonic subsidence rate from the land elevation change rate. We thus obtain the evolution of the aquifer deformation rate in western and central Taipei basin, as the dashed curved in Fig. 2-9.

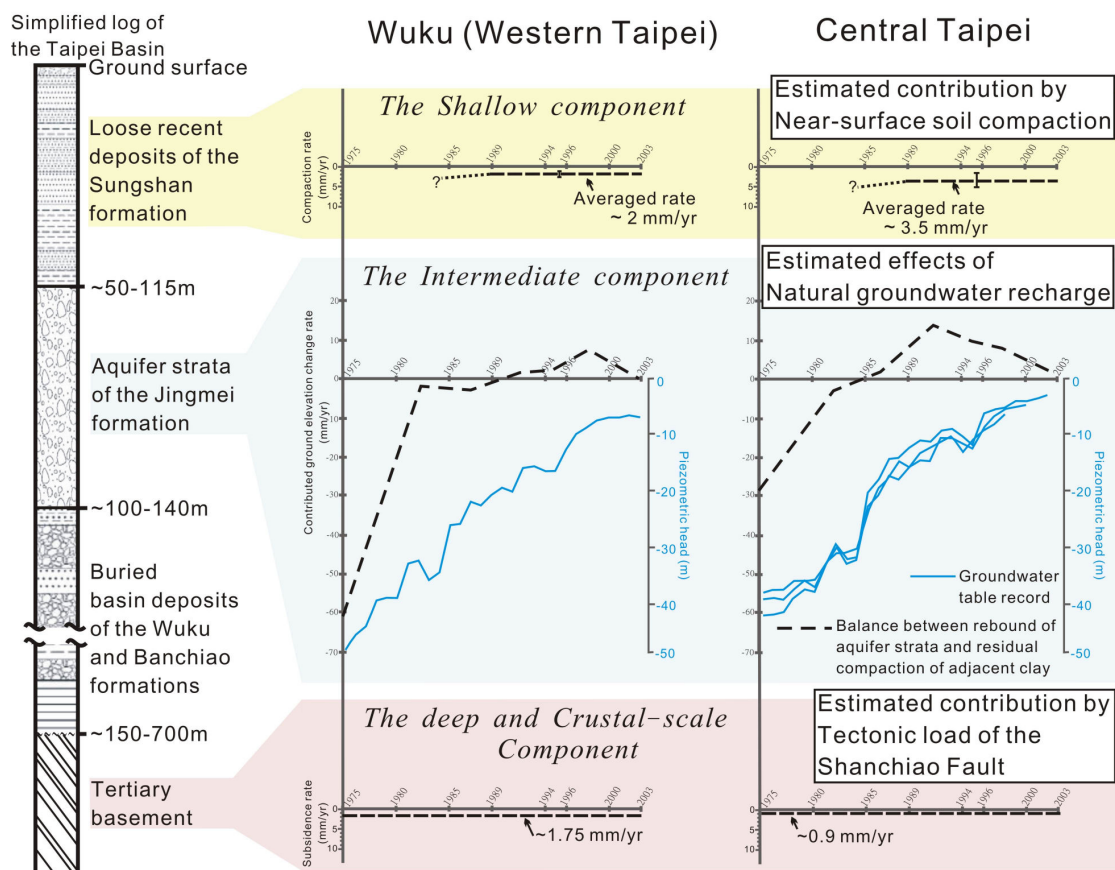


Fig. 2-9. Mechanisms of three depth-related component responsible for land elevation change in Western Taipei (Wuku) and Central Taipei. The shallow component represents the surfacial soil compaction with the average rates estimated after Lin et al. (1999). The intermediate component represents the aquifer deformation consists of compaction and elastic rebound within Aquifer 1. The deep and crustal-scale component represents asymmetric tectonic subsidence due to the activity of the Shanchiao fault in the western margin of the basin. Calculation of each component is explained in the text.

As revealed by Fig. 2-9, among the three major mechanisms, the aquifer deformation appears to be the main driving source of ground elevation changes, that is, subsidence in Phase 1 and uplift in Phase 2. Furthermore, the observed prominent land uplift in Phase 2, which is interpreted to be mainly related to the aquifer rebound, was significantly less in western margin than in Central Taipei.

In order to illuminate the actual extent of effects from aquifer deformation (compaction vs. rebound) and tectonic load, we sum up the ground level change in the Taipei area during Phase 2 (1989-2003, Fig. 2-10a) then remove estimate of shallow soil compaction to create the map of residual cumulative ground level change (Fig. 2-10b). The major remaining factors affecting land elevation fluctuation during Phase 2 are (1) elastic rebound of recharged Aquifer 1 contributing uplift and (2) tectonic subsidence. Note that the residual compaction of Aquifer 1 had declined to a neglected minimal rate as groundwater table almost fully recovered and stabilized. Most of the Taipei Basin, except the western margin, showed rather homogeneous uplift of 13-18 cm (spatial variation) during 1989-2003 (or 9-13 mm/yr in average), and is interpreted as a manifestation of elastic rebound of Aquifer 1 due to natural recharge. The western part of the basin, in contrast, exhibited less amount of uplift (1-9 cm, or 0-6 mm/yr in average throughout the area) which decreased toward the west and northwest (also exhibited in Fig. 2-7). The “differential uplift” was partially resulted from variations of elastic rebound of Aquifer 1 possibly related to changes in sedimentary facies (hence the thickness and composition of the aquifer strata) and hydrological parameters. However, the pattern of uplift diminishing toward the Shanchiao Fault also demonstrated a likely effect of tectonic load especially for the near-fault hanging-wall regions including Guandu, Wuku, and Shulin.

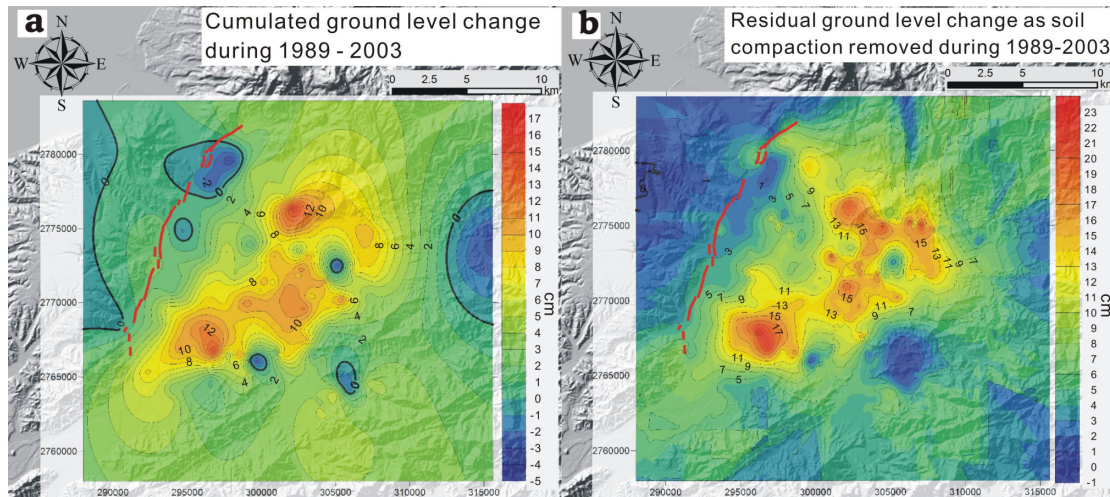


Fig. 2-10. Ground level changes during Phase 2 of post-pumping period. (a) Cumulated ground elevation change from 1989 to 2003. (b) Residual ground elevation change from 1989 to 2003 as soil compaction (shallow component) removed.

A schematic model of mechanisms for the cumulative land elevation changes of Central and Western Taipei areas during Phase 2 of post-pumping from 1989 to 2003 is presented in Fig. 2-11. For Central Taipei, adapting 3.5 mm/yr of shallow soil compaction and 0.9 mm/yr of long-term tectonic subsidence, we obtain a total aquifer rebound of 16 cm in 1989-2003 (Fig. 2-11b). For the Wuku area of western Taipei in the same manner by adopting averaged shallow soil compaction of 2 mm/yr and the long-term tectonic subsidence rate of 1.75 mm/yr, we come to an estimation of rebound in the region as 6.7 cm in 1989-2003 (Fig. 2-11a). The values of total rebound are of reasonable magnitude as the preliminary test given below. Based on injection experiments carried out in Wilmington oilfield, California, Allen and Mayuga (1969) proposed a simplified empirical equation: the amount of rebound (u) is a function of thickness of the recharged aquifer strata ($t_{aquifer}$):

$$u = a \cdot bt_{aquifer}$$

Where a is the ratio of surface uplift to actual amount of aquifer elastic rebound and was given as 0.5, b is the expansion factor per aquifer unit and was estimated to be 0.005 per unit. Taking averaged thickness of Aquifer 1 (the Jingmei formation) of 50 meters in Central Taipei into calculation, the aquifer rebound is estimated to be 12.5 cm. For Western Taipei by adapting known minimum thickness of Aquifer 1 in the region as 25 m, amount of the aquifer rebound is estimated to be 6.25 cm. Although minor amount of aquifer rebound may still in operation after 2003, fair agreement is

found between the above estimation and our results (16 cm versus 12.5 cm in Central Taipei, and 6.7 cm versus 6.25 in Western Taipei).

Improvements from these preliminary results and statements will come from more comprehensive study on geotechnical and hydrological properties of the basin deposits to contribute a realistic modelling, and further level monitoring of both ground surface and down-hole benchmarks.



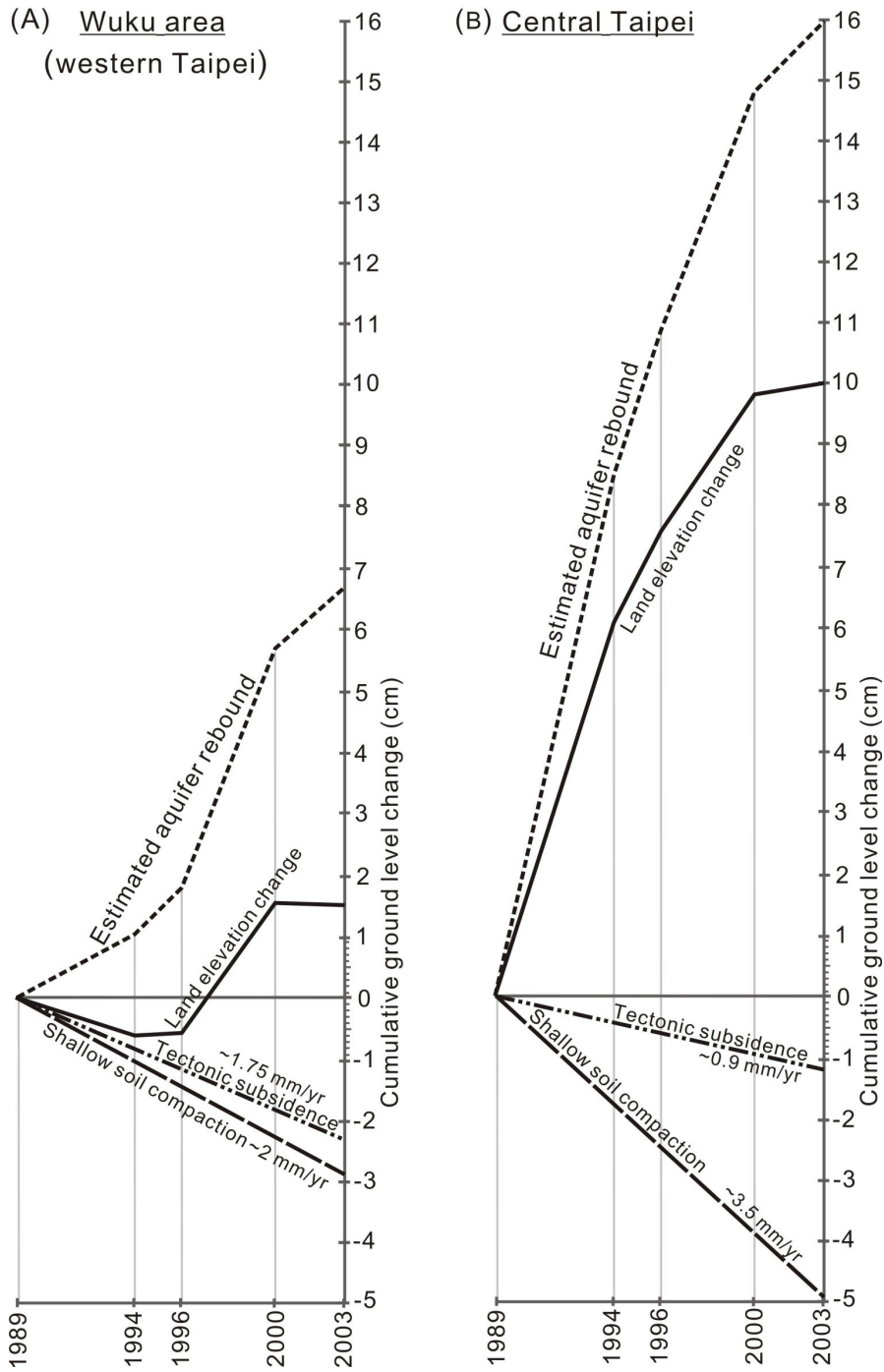
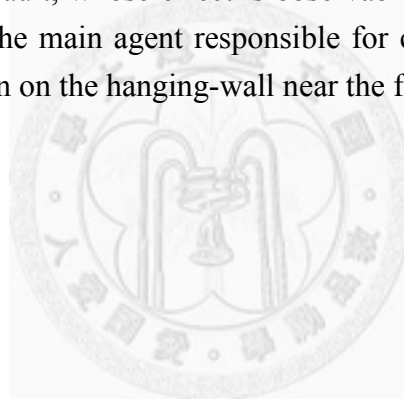


Fig. 2-11. A schematic model for evaluating aquifer elastic rebound during the Phase 2 of the post-pumping period 1989-2003, in (a) Wuku (Western Taipei) and (b) Central Taipei.

2.5 Summary

Land elevation change during post-pumping in 1975 – 2003 in the Taipei Basin illuminated by levelling data was documented in details. The post-pumping behaviour is characterized by an interval of waning subsidence followed by one of slight uplift, as Phase 1 and Phase 2, respectively. This behaviour was dominated by aquifer internal deformation in response to piezometric level changes. The aquifer is observed to exhibit substantial elastic rebound in the later stage of groundwater recharge, whose magnitude is about 10 percent of that of the former pumping-induced subsidence. This further confirms that land subsidence caused by aquifer/reservoir overdraft is largely an irreversible process and should be avoided especially in critical areas of flat low-lying topography and flood risk.

Two other major mechanisms also imposed significant effects on basin ground level change. Shallow soil compaction contributed enhanced subsidence especially near river courses and marshy areas. Regional tectonic asymmetric subsidence related to the Shanchiao normal Fault, whose effect is observable from the elevation change data, is interpreted to be the main agent responsible for continued subsidence in the western margin of the basin on the hanging-wall near the fault line.



Chapter 3: Growth normal faulting at the western edge of the Metropolitan Taipei Basin since the Last Glacial Maximum, northern Taiwan

3.1 Introduction

History of fault development is often tape-recorded in syn-tectonic sediments associated with the fault motion. Such growth faulting scheme has been invoked to interpret fault slip accumulation through time and variation of strata across and along strike, leading to models describing fault evolution and kinematics (e.g. Childs et al., 2003; Bull et al., 2006). Much attention has been paid to growth strata genesis in compressional tectonic environments, such as foreland settings in determining fault-fold kinematics (Vergés et al., 2002; Hubert-Ferrari et al., 2007). Growth faulting along with sequence analyses were successfully applied to understand basin formation and petroleum systems of northern Gulf of Mexico, where deltaic shelf sediment infills are modulated by gravity-driven normal faulting and eustatic sea level change (Brown et al., 2004). Growth faulting may form at low elevations in the vicinity influenced by recent sea level rise, and thus serve to be a potential tool for neotectonic investigations on seismogenic normal faults.

Normal fault system is one of the important sources of earthquake hazard in continental extensional provinces, where large plains, and therefore urban development and heavy populations, are often present. Examples of paleoseismology and earthquake geology studies in such setting include the Tyrnavos Basin in the Aegeon region (Caputo et al., 2004), the Wasatch Fault Zone in central Utah, United States (Machette et al., 1991; McCalpin and Nishenko, 1996), and the upper Rhine Graben near Basel, northern Switzerland (Meghraoui et al., 2001). The Taipei metropolis, the capital of Taiwan where several million people reside, is unfortunately also under seismic threat from the active Shanchiao normal fault (Fig. 3.1, Chang et al., 1998; Lin et al., 2000). Since the pioneer studies of the Shanchiao Fault (e.g. Lin, 1957; Wu, 1965), the geological characteristics of this fault have remained relatively poorly understood though they bear important information on hazard mitigation and regional geodynamics. Properties of the activity of the fault such as its long-term Quaternary slip rate are mostly inferred from geologic data in the Taipei Basin (Teng et al., 2001) and are therefore crude in nature. Recently, Huang et al. (2007) correlated the sediments of three borehole sets across the deduced fault surface trace (Lin, 2001) and proposed three paleoseismic events during the Holocene; the validity

of their analysis is doubtful as the borehole sets may have covered only part of the Shanchiao Fault zone when considering the geometry of the basin basement. In this study, we connect their borehole set in the central part of the Shanchiao Fault to form the Wuku Profile (Fig. 3.2A). Stratigraphy of the three wells in the Wuku Profile is correlated and a geologic cross-section is thus constructed.

In the present paper, a valuable example of subaerial growth faulting case is documented in the central portion of the Shanchiao Fault, where growth strata provide a clear distinction on sedimentation rate and throw rate across the fault on the thousand-year scale. Detailed growth faulting history is constructed at a time span since the Last Glacial Maximum, revealing close coupling between sedimentation, tectonic process, drainage system changes, and eustatic sea level rise. Fault zone location and its deformation structure within unconsolidated basin sediment can therefore be better defined. Vertical slip rates on main and branch faults starting from 23 ka are constrained, implying an approximately 2 mm/yr averaged tectonic subsidence rate across the Shanchiao fault zone for the last 8400 years.

3.2 Geological Setting

Taiwan is situated on the plate boundary of active convergence between the Eurasian and Philippine Sea plates since around 5 Ma (Ho, 1986; Suppe, 1981; Teng, 1990; Wu et al., 1997) with a rapid convergent rate of about 82 mm/yr in the NW direction (Seno, 1977; Yu et al., 1997; Fig. 3.1A). This oblique convergence leads to the southward-propagation of the Taiwan orogeny (Suppe, 1981). Unlike regions of central and southern Taiwan are presently in a state of full and mature collision (Angelier et al., 1986; Yu et al., 1997; Shyu et al., 2005), the northern part of the mountain belt, including the Taipei region, is now in a state of post-collision with an extensional or transtensional tectonic setting rather than a compressional one (Teng, 1996), as evidenced by the presence of Quaternary extensional structures (Lee and Wang, 1988; Lee, 1989; Lu et al., 1995), extensional earthquake focal mechanisms (Yeh et al., 1991; Kao et al., 1998), and GPS displacement fields (Yu et al., 1997; Rau et al., 2008). The Taipei half-graben of Quaternary deposits is therefore formed in a close association with down-dip slips on the Shanchiao Fault, which is considered as the major neotectonic structures responsible for the tectonic inversion from compression to extension across the Taipei region (Teng et al., 2001; Fig. 3.1).

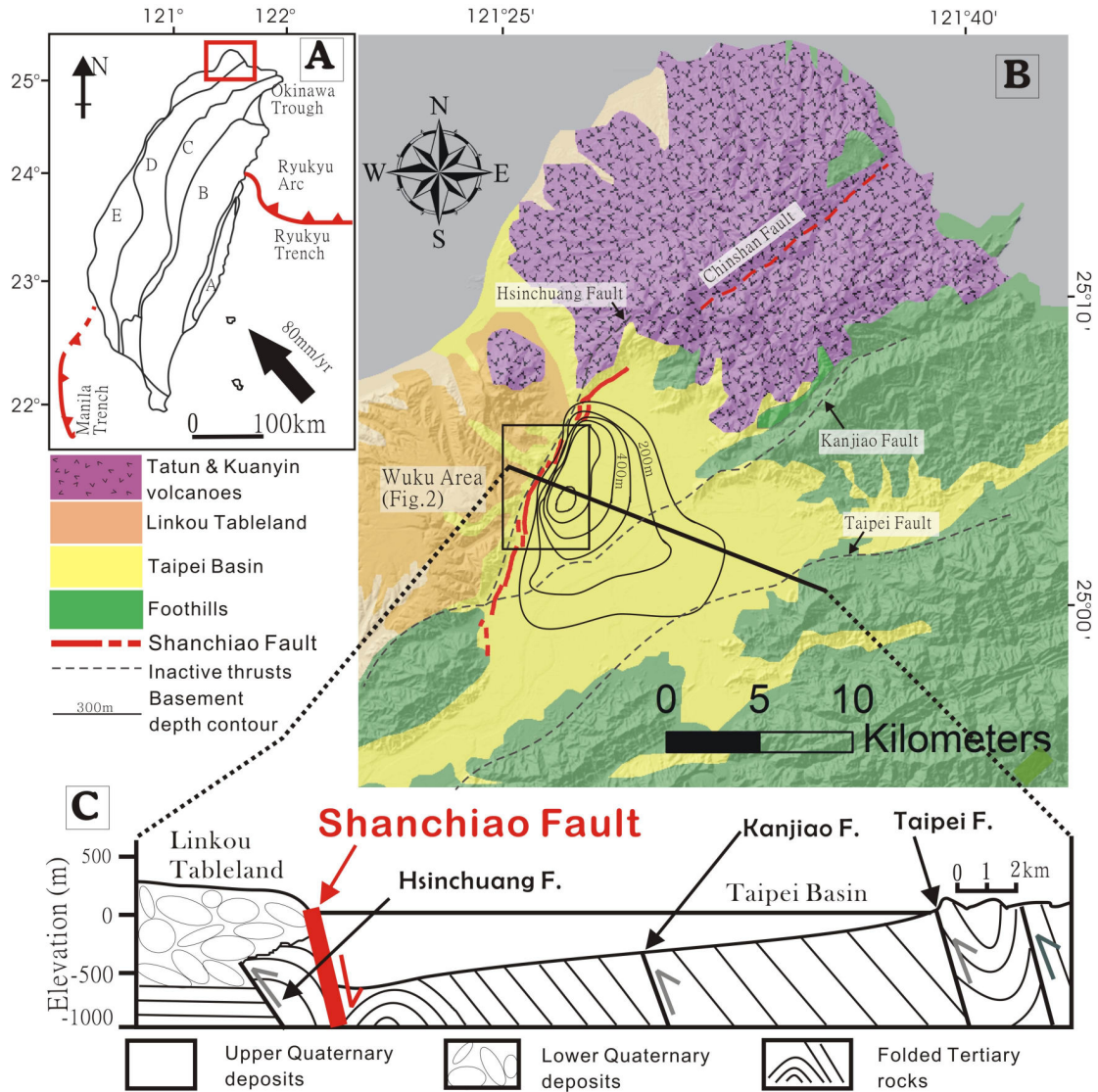


Fig. 3-1. (A) General tectonic framework of Taiwan. A: Coastal Range; B: Backbone Range; C: Hsueshan Range; D: Western Foothills; E: western Coastal Plain. (B) Simplified geology of the Taipei area. Four geological domains are defined in the Taipei area as indicated by different colors shown in the legend. The thick red lines are the Shanchiao Fault traces (Chen et al., 2006). Thin black lines within the Taipei Basin are the basement depth contour of 100 m interval (adapted from Teng et al., 2001). (C) Geological cross section of the Taipei Basin (modified from Teng et al., 1999).

The flat low-lying Taipei Basin, a triangular-shaped half-graben filled with late-Quaternary fluvial deposits since c. 400 ka (Wei et al., 1998; Teng et al., 2001), developing on top of the folded Oligo-Mio-Pliocene shallow marine strata, as a fold-and-thrust belt during earlier stage of mountain building. The late Quaternary terrestrial deposits in the Taipei basin form an asymmetric sedimentary wedge: reaching a maximum depth of about 700 m near the western margin and rather drastically becoming thinner toward the east and south (Fig. 3.1C). These unconsolidated deposits are divided into four major lithostratigraphic units (Teng et al., 1999). From bottom to top (Fig. 3.2B), they are: (1) the *Banchiao Formation*: consisting of intercalated fluvial sands, muds and conglomerates, with occasional pyroclastics and topped by thick laminated mud, with maximum thickness of 380 m with ages ranging from 250 to 400 ka; (2) the *Wuku Formation*: consisting of fluvial sands and conglomerates, with minor mud and lateritic conglomerates, reaching a maximum thickness of c. 160 m with ages ranging from 80 to 250 ka; (3) the *Jingmei Formation*: comprising lateritic fluvial (alluvial-fan) conglomerates with an utmost thickness of 50 m. These particular conglomerates layers are interpreted as products when the Tahan River was captured and flowing into the Taipei basin about 25 to 23 ka (Teng et al., 2004a); (4) the *Sungshan Formation*, composed of estuarine interbedded sand-mud deposits, with a thickness of 50-100 m. The basin deposits are marked by prominent lateral facies changes with frequent pinch-outs. However, the widespread lateritic gravels of the Jingmei Formation and the laminated muds in the upper Banchiao Formation (Teng et al., 2004b) usually serve as basin-wide marker beds (Teng et al., 1999).

Geological evolution of the Taipei Basin was proposed by Teng et al. (2001), based on interpretation of regional geology. While the Plio-Pleistocene orogeny of mountain building reached its climax in northern Taiwan in Quaternary, the Paleo-Tanshui River, the major river in the Taipei Basin, began to provide sediments to produce the Linkou fan-delta around the ancient mountain front (Chen and Teng, 1990). Accompanying the waning of compressive stress in the northernmost Taiwan island during the middle to late Quaternary (Lee and Wang, 1988) is the vigorous eruptions of the Tatun volcanoes to the north of the Taipei Basin (Wang and Chen, 1990; Song et al., 2000), probably reflecting the onset of regional extension. Subsidence along western margin of the Taipei basin, as evidenced by several hundred meters thick fluvial deposits, is interpreted to result from the repeated normal faulting (the Shanchiao Fault) as inverted from the Hsinchuang fault, an ancient frontal thrust in northern Taiwan (Chiu, 1968; Hsieh et al., 1992). The extension tectonics turned the Taipei area from rugged mountains gradually into a sediment-receiving basin. The accumulation of fluvial and lacustrine sediments

started at about 0.4 Ma (Wei et al., 1998; Teng et al., 2001). Since then the Taipei Basin has kept expanding due to erosion and continual asymmetric subsidence along the Shanchiao Fault in the western edge of the basin. Under the combining influences of sea level fluctuations, volcanic activities, drainage system changes, and tectonic processes, the basin was infilled with various types of sediments, including alluvial, lacustrine, marine and pyroclastic deposits, up to 700 m thick as mentioned above.

3.3 The active Shanchiao Fault

The Shanchiao Fault was mapped (Lin, 2001; Huang et al., 2007; Chen et al., 2004, 2006; Fig. 3.1B and Fig. 3.2A) along the topographic boundary between the Linkou Tableland and the Taipei Basin, sub-parallel to the Hsinchuang Fault (Lin, 2001; Teng et al., 2001). There are features indicate that the steeper Shanchiao normal fault may merge into the Hsinchuang thrust fault at depth (e.g. Hsieh et al., 1992). Following the late-Quaternary tectonic inversion, tectonic subsidence from down-dip slips on the Shanchiao Fault led to formation and development of the Taipei Basin. Left-lateral transcurrent motion together with clockwise block rotation is also expected to occur along the Shanchiao Fault, based on studies on regional structural geology, paleomagnetism, and GPS measurements (Lu et al., 1995; Lee et al., 1999; Rau et al., 2008).

Many efforts have been made to characterize this active fault. Shallow reflection seismic profiling across the Shanchiao Fault imaged vertical offsets of Holocene sediments at shallow depth, although the location of the main fault remains questionable (Wang and Sun, 1999; Shih et al., 2004). GPS surveys of the Taipei area showed WNW-ESE extension with a slow rate of 0.08 μ strain/yr across the fault (Yu et al., 1999a). Asymmetric tectonic subsidence related to the Shanchiao Fault across the basin was illuminated through recent study on 30-year-long levelling data (Chen et al., 2007). Huang et al. (2007) correlated stratigraphy of three sets of boreholes, and proposed three paleoseismic events during the Holocene (i.e. at 8500, 9200, and 11100 years b.p., respectively). Geomorphology analysis also reveals a series of scarps closely related to the development of the Shanchiao Fault (Chen et al., 2006; Fig. 3.2A). Radon and helium anomalies in soil-gas along the fault zone were documented (Walia et al., 2005) indicating the presence of possible active faults and deep fracture-advection system. The Shanchiao Fault is therefore considered currently active (Chang et al., 1998; Lin et al., 2000). Subsurface geology of the fault zone, by contrast, has not been fully explored.

3.4 Reconstruction of geological profile across the Shanchiao fault

In recent years, the Central Geological Survey of Taiwan has carried out a number of drillings in the Taipei Basin in order to better understand its subsurface geology and engineering environment (e.g. Lin et al., 1999). Among them three boreholes in the Wuku area, SCF-1, 2, and WK-1, have been selected for the present analysis due to their optimal locations associated with the Shanchiao fault (Fig. 3.2A) and data quality. All three wells are situated in flat marshy lowland in the Wuku area, western edge of the basin. The WK-1 reaches the deepest known depth of the basin late Quaternary basin deposits at 679 m. Many radiocarbon dates have been acquired (Lin et al., 1999) which are crucial for a successful stratigraphic correlation. At SCF-1 and SCF-2 boreholes, the Sungshan Formation of the uppermost layers was studied by Huang et al. (2007) whose classification of strata serves as a basis for this study. The main stratigraphic system of the whole basin deposits is adapted from Teng et al. (1999), as discussed above. Through stratigraphic analysis of the three boreholes by incorporating the growth faulting scheme, we reconstruct the Wuku geological profile to reveal the present configuration of fault zone stratigraphy and structure in central part of the Shanchiao Fault.

3.4.1 Stratigraphic correlation between the boreholes

First, we carried out analysis and correlation of stratigraphic units between three boreholes of SCF-1, SCF-2 and WK-1 based on lithology and radiocarbon dates. We reprocessed all available raw radiocarbon dates which were previously published (Lin et al., 1999, Huang et al., 2007) by calibrating these radiocarbon dates to calendar years before present (cal. yr BP) using the model curve of Fairbanks et al. (2005). Table 3.1 shows details of the results. Note that a few calibrated radiocarbon dates reveal a reversed stratigraphic order (i.e. older ages on top of younger ones), implying that they might be reworked samples. Thermoluminescence ages acquired in WK-1 (Lin et al., 1999) are summarized in Table 3.2. We thus reconstructed a detailed correlation of lithostratigraphic units of the three boreholes (Fig. 3.3) and the unit descriptions are listed in Table 3.3. Comparing the strata in three boreholes (SCF-1, SCF-2 and WK-1), one finds that the thickness of all the four formations increases dramatically toward the east. Hereafter we describe how we correlated the lithofacies units between these three boreholes (Fig. 3.3).

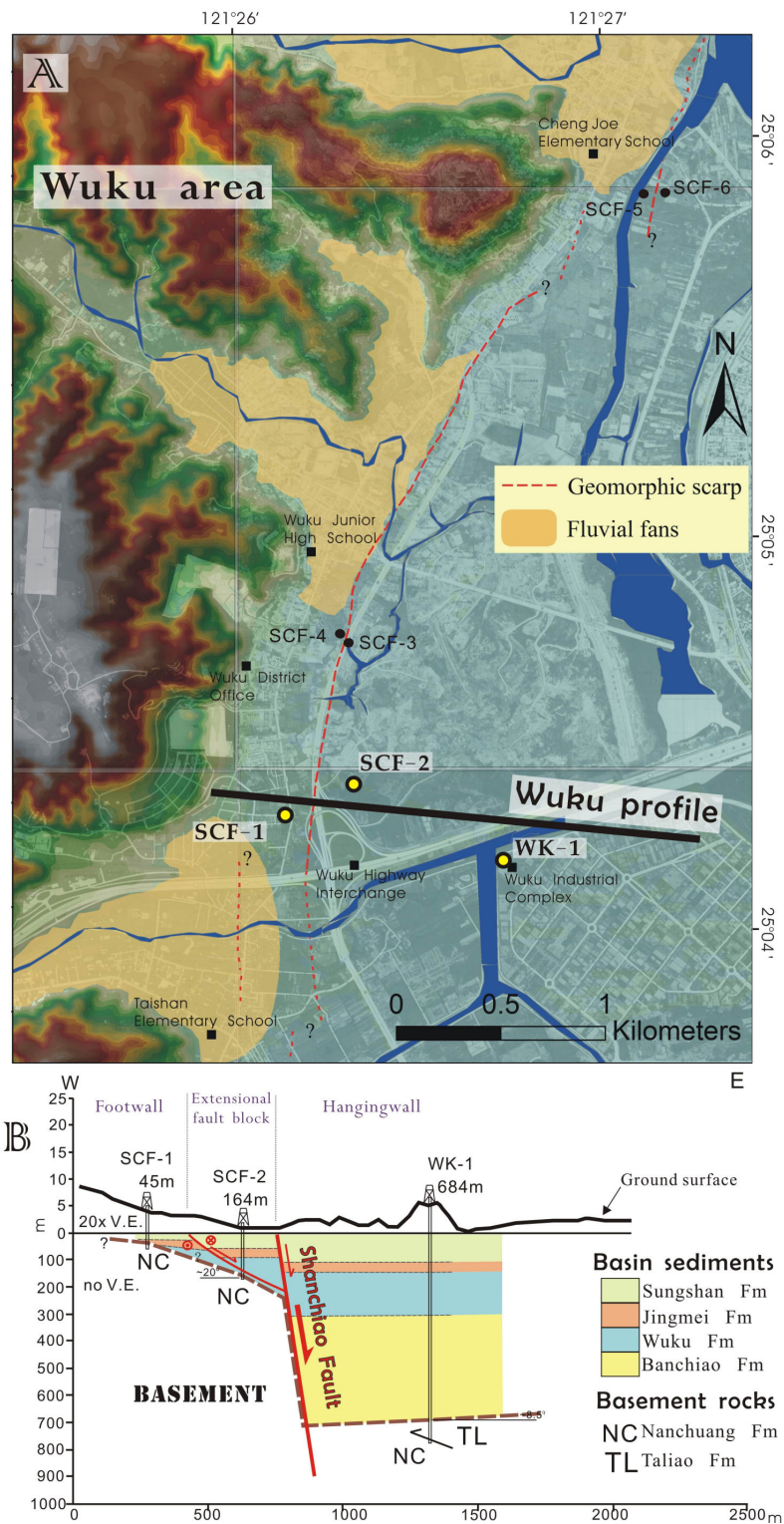


Fig. 3-2. (A) Map of the Wuku area, showing locations of the three boreholes used in this study, the Shanchiao Fault trace (dashed lines), and geomorphic features. (B) Interpreted Wuku geological profile. We interpret the Shanchiao fault as a combination of a main fault between SCF-2 and WK-1 to the east and the branch fault between the SCF-1 and SCF-2 to the west. Note that there is no vertical exaggeration beneath the sea level, and 20 times vertical exaggeration for surface topography.

For the uppermost Sungshan Formation at SCF-1 and SCF-2, Huang et al. (2007) divided this formation into three units as C1, C2, and C3. We find that such division also applies to the Sungshan Formation at WK-1 (Fig. 3.3 and Tab. 3.3). The C1 unit comprises mainly sandy layers with mollusk shells at bottom, whose onset of deposition is around 8400 years B.P. (8.4 ka) and is of alluvial facies (Huang et al., 2007). At SCF-1 this unit extends from land surface to depth of 14.5 m (where the shells occurs) and is filled with fine to medium sands with occasional thin silts at 2-3 m and 8 m depths. At SCF-2 this unit is composed of fine sands with one thin mud and silt layers, and ends at the shell lag of 22.3 m depth. Collectively, we find that the C1 unit shows a prograde depositional character in both SCF-1 and SCF-2. At WK-1 the shell layer is found at 33.6 m depth with age \sim 8.4 ka, which lies under interlayers of fine to medium sands and muddy-silts; these sediments of floodplain facies in a prograding fashion (Teng et al., 2000b) are therefore considered to be correlative to the C1 unit.

Underneath the C1 unit, the C2 unit which was deposited from \sim 9 to 8.4 ka is predominantly clayey and rich in peat and charcoal as defined at SCF-1 and SCF-2 (Huang et al., 2007). The upper part of C2 at SCF-1 is filled with muddy silts and the lower part with mud to depth 21.3 m. At SCF-2 the C2 unit consists of mud in the upper section and silts near the bottom at 32.4 m depth. At WK-1 a thick muddy-silt layer of estuarine environment (Teng et al., 2000b) extending to 51.1 m deep is found corresponding to the C2 unit with analogous sediments. In fact, the radiocarbon ages also support this correlation of stratigraphy. The sediments of the C2 unit are distinctively finer-grained than those above (C1 unit) or beneath (C3 unit), making it much easier to recognize. Abundant detrital charcoal chips and mollusk shells are present in C2 unit at all three boreholes.

The C3 unit, the lowermost member in the Sungshan Formation, is made up of sandy layers with alternating thin charcoal-rich clay layers older than 9 ka at SCF-1 and SCF-2. At SCF-1, the C3 unit consists of silts and fine sands of 13.9 m thickness, and their accumulation started at \sim 10 ka. At SCF-2 the C3 unit is 27.5 m thick composed of interbedded fine sands and silts, and began sedimentation \sim 12 ka. Between 51.1 m and 110.8 m depth at WK-1, alternating charcoal-rich layers of fine-medium sands and mud is found equivalent to the C3 unit described above, albeit of greater thickness and longer time span of deposition ranging from \sim 23 to \sim 9 ka. The C3 sediments in WK-1 exhibit an upward transition from alluvial fan to distal floodplain facies in a retrograde stacking pattern, without a break of sedimentation between C3 and underlying Jingmei Formation of C4 unit (Teng et al., 2000b). By contrast, there appears a substantial hiatus at the same stratigraphic boundary between

C3 and C4 units at SCF-1 and SCF-2, according to the radiocarbon dates.

The Jingmei Formation (lateritic clast-supported conglomerate layer, C4 unit in Table 3.3) also appears to increase its thickness towards the east. At borehole SCF-1, it rests unconformably above weathered Tertiary basement rock and is 9.9 m thick. At SCF-2 it is 33.1 m thick (between 59.9 m to 93 m), and at WK-1 it is 30 m (between 110.8 m to 140.8 m), both lying on the Wuku Formation. The Jingmei Formation, product from the diversion of the Tahan River into the Taipei Basin, was interpreted to be formed during 23 and 25 ka (Teng et al., 2004a). The only radiocarbon date of 38-40 ka in the lower part of the Jingmei Formation at SCF-2 is presumably acquired from reworked material.

The remaining lower part of SCF-2 of about 71 m thick (93 - 164 m), below the Jingmei Formation, is composed of silts in combination of sands, with three conglomeratic units, and is defined as the upper part of the Wuku Formation (C5 – C12 units), which lies unconformably upon the folded Miocene basement rocks. At borehole WK-1, below the Jingmei Formation, two late Quaternary formations lying unconformably above the Tertiary basement rocks can be observed: (a) the Wuku Formation lies in between 140.8 to 301 m (about 140 m thick) and (b) the underlying Banchiao Formation extends from 301 to 679 m (378 m thick). The uppermost Wuku Formation was dated to be far older than 50 ka, implying a large gap of sedimentation before the onset of depositing the overlying Jingmei conglomerates. The oldest dated age for the Wuku Formation is about 200 ka at WK-1 borehole. The Banchiao Formation constitutes the lower half of the WK-1 borehole. Existing thermoluminescence ages imply that the age for the Banchiao Formation is no younger than 150 ka (Table 3.2) and might be no older than 400 ka (Wei et al., 1998; Teng et al., 2001).

All three boreholes penetrated to the Tertiary basement rocks which are known exposed surrounding the Taipei Basin as the rugged foothills. Basement rocks reached at SCF-1 and 2 are probably the late-Miocene Nanchuang Formation, with weathered top basement rock in SCF-1. Rocks retrieved from WK-1 in 679 m to 741 m belongs to the early Miocene Taliao Formation, which is thrust over the Nanchuang Formation at 750-760 m depth by a shear zone containing fault breccias (Lin, 2005). Note the dramatic increase of basement depth between SCF-2 and WK-1 boreholes compared to a relatively mild one between SCF-1 and SCF-2 boreholes (Fig. 3.2B), implying the location of the main Shanchiao Fault between the SCF-2 and WK-1. We will discuss later in more details.

Through lithologic correlation in aid of radiocarbon ages, the Sungshan and Jingmei formations are present across the entire profile, while the Wuku Formation is only found at SCF-2 and WK-1, and the Banchiao Formation is restricted to WK-1. The Sungshan Formation (and units within), the Jingmei Formation, and the Wuku Formation all thicken toward the east, and the stratigraphic horizons deepen eastward. Sedimentation rate appears to vary both temporally and spatially. We found two major hiatus: one between the deposition of Wuku and Jingmei sediments, and the other one between deposition of Jingmei and Sungshan sediments at SCF-1 and 2. Sediments within the Sungshan and Jingmei formations are quite similar between the boreholes, indicating the sediment source was generally the same and was presumably basin wide, as from the Tahan - Danshui river system (sediment transporting direction normal to the profile and rather homogeneous). Tributaries drained from the Linkou Tableland to the east didn't seem to assert significant contribution to the deposits since no alluvial-fan conglomerates are found beyond deposition of the Jingmei gravels in these boreholes, suggesting little local sediment transport.



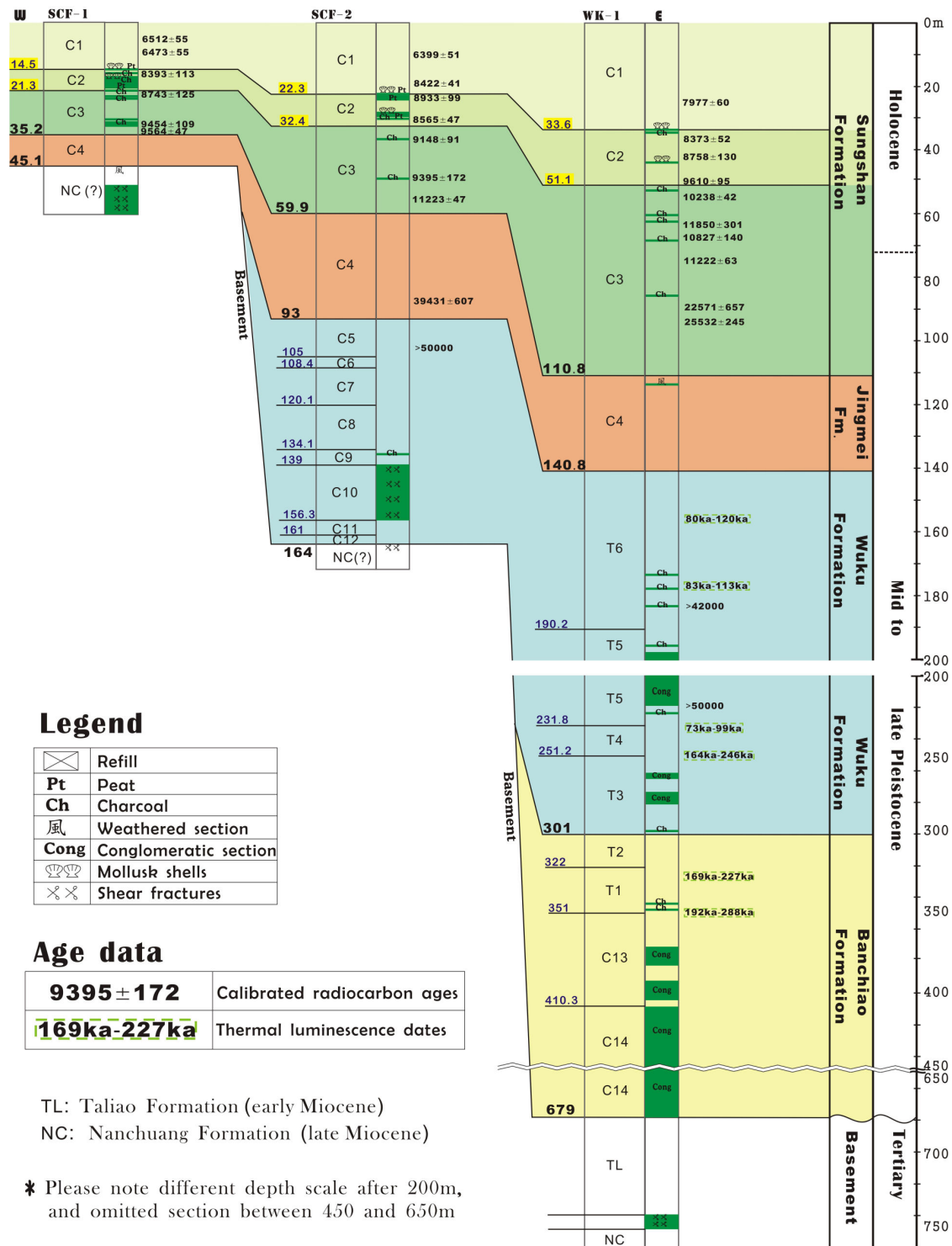


Fig. 3-3. Stratigraphic correlation between boreholes (SCF-1, SCF-2, and WK-1) of the Wuku profile. Location of the boreholes is indicated in Fig. 3-2. Four major geological formations consist of the late Quaternary deposits of the Taipei basin: from top to bottom, the Sungshan, Jingmei, Wuku, and Banchiao Formations. Each formation has been divided into several stratigraphic units. See details in the text. Please note different depth scales between 0-200 m and 200-750 m, and omitted section between 450 m and 650 m.

Table 3-1: Radiocarbon age data of the three boreholes along the Wuku Profile.

Borehole	Data source ^a	¹⁴ C age (yr B.P.±2σ)	Calendar year range ^b (cal. yr B.P.)	Depth (m)	Unit
SCF-1	(1)	5730±40	6457-6567	5.35	C1
	(1)	5697±46	6418-6528	9.40	C1
	(1)	7590±130	8280-8506	16.12	C2
	(1)	7923±58	8618-8868	22.80	C3
	(1)	8450±120	9345-9563	32.30	C3
	(1)	8620±60	9517-9611	34.99	C3
SCF-2	(1)	5625±49	6348-6450	10.40-10.50	C1
	(1)	7635±55	8381-8463	19.20-19.30	C1
	(1)	8018±54	8834-9032	22.55	C2
	(1)	7790±50	8518-8612	30.40	C2
	(1)	8200±56	9057-9239	36.70	C3
	(1)	8400±160	9223-9567	49.00	C3
	(1)	9064±67	11176-11270	55.50	C3
	(1)	34060±600	38824-40038	87.52	Jingmei
	(1)	>50000	N/A	102.20	Wuku
	(1)	>47100	N/A	138.18	Wuku
WK-1	(2)	7160±70	7917-8037	24.80	C1
	(2)	7560±70	8321-8425	36.55	C2
	(2)	7930±60	8628-8888	42.2-42.6	C2
	(2)	9010±110	10035-10301	49.4-50.2	C2
	(2)	8660±80	9515-9705	50.2-50.4	C2
	(2)	9090±60	10196-10280	54.7-55.05	C3
	(2)	10180±150	11549-12151	63.4-63.8	C3
	(2)	9530±60	10687-10967	67.6-67.7	C3
	(2)	10080±60	11493-11805	68.6-68.7	C3
	(2)	9810±80	11159-11285	74.1-74.7	C3
	(2)	18950±540	21914-23228	89.3-89.5	C3
	(2)	21300±160	25287-25777	94.0-94.1	C3
	(2)	>42000	N/A	183.6	Wuku
	(2)	>50000	N/A	219.3	Wuku

^a Raw radiocarbon ages reported in Huang et al., 2007, and in Central Geological Survey report Lin et al., 1999, are labeled with (1) and (2), respectively.

^b Calibration with Fairbanks 0107 calibration curve (Fairbanks et al., 2005).

Table 3-2: Thermal luminescence (TL) ages. Data from Lin et al., 1999

Borehole	TL age (ka B.P.)	Depth (m)	Unit
WK-1	80-120	155.9	Wuku
	83-113	177	Wuku
	73-99	234.2	Wuku
	164-264	251	Wuku
	169-227	328	Banchiao
	192-288	351.5	Banchiao



Table 3-3: Lithofacies of the Wuku Profile.

Unit	Description	Thickness (m)			Stratigraphy [#]	Reference*
		SCF-1	SCF-2	WK-1		
C1	Mainly sandy layers, parallel lamination in clayey layers, mollusk shells at bottom	14.5	22.3	33.6	Sungshan	a
C2	Mainly clay layers, occurrences of mollusk shells, peat in top section, paleosol and peat in middle section, charcoal-rich bottom section	6.8	10.1	17.5	Sungshan	a
C3	Sand within thin charcoal-rich clay layers, occurrences of paleosols	13.9	27.5	59.7	Sungshan	a
C4	Lateritic conglomerates with minor grey gravels	9.9	33.1	30	Jingmei	b
C5	Brown-grey silty sand	-	12	-	Wuku	
C6	Conglomerate with grey silt	-	3.4	-	Wuku	
C7	Brown silt	-	11.7	-	Wuku	
C8	Conglomerate with brown clay	-	14	-	Wuku	
C9	Charcoal-rich silt	-	4.9	-	Wuku	
C10	Sand-silt thin interlayers (containing several sheared sections localized in silt layers)	-	17.3	-	Wuku	
C11	(Tuffaceous?) silt	-	4.7	-	Wuku	
C12	Conglomerate with yellow-brown clay	-	3	-	Wuku	
T6	Clay within thin silt/sand	-	-	49.4	Wuku	c
T5	Conglomerate bounded by sand	-	-	41.6	Wuku	c
T4	Non-stratified clay with sand of parallel and cross	-	-	19.4	Wuku	c

lamina						
T3	Two conglomeratic layers in sands	-	-	49.8	Wuku	c
T2	Varve with rare thin silt/sand	-	-	21	Banchiao	c
T1	Non-stratified clay containing vivianite concretes, cross-laminated sand at bottom section	-	-	29	Banchiao	c
C13	Silt-clay with thin conglomerates	-	-	59.3	Banchiao	
C14	Conglomerate with rare thin sand/silt	-	-	268.7	Banchiao	



3.4.2 Stratigraphic architecture of the Shanchiao Fault zone

In active extensional settings, such as the Shanchiao fault area, rate of increase of accommodation space is enhanced on the hanging-wall due to subsidence caused by normal faulting. Hereafter we briefly describe the theory of reconstructing the growth strata across an active normal fault we apply in this study. On a relatively flat depositional surface, sediments deposited within a given time span (growth strata) will be thicker on the hanging wall than those in the footwall if the normal fault is active, and uniform if there's quiescence in tectonic activity. The top of such layers will be even when deposition smooth out the fault scarp (if there is any), mimicking the regional topography. Subsequent layers will continue to form above the newly-formed horizon and repeat the geometric pattern governed by fault activity should there be room for sedimentation. The existing growth strata will be displaced downward at the same time, and record all successive deformations. The entire package of syn-tectonic sediments may therefore yield information on fault location and structure, faulting history, and kinematics of fault-related folding (e.g. Sharp et al., 2000).

Upon the above established stratigraphic correlation, the growth normal faulting scheme within shallow sediments are illuminated. First, architecture of the latest Sungshan Formation is most useful for its completeness and synchronicity of sedimentary facies within Holocene. Between the SCF-1 and SCF-2, the units within the Sungshan Formation are indeed down-thrown and thickened eastward, representing effects of normal faulting, as Huang et al. (2007) previously proposed, at the same site of mapped fault-related scarp by Chen et al. (2004). However, these effects on growth strata appear to be much more pronounced between boreholes WK-1 and SCF-2. We thus estimate the accumulation (sedimentation) rates at each drilling hole for the Sungshan Formation, including the C1, C2, and C3 units. By adopting the dated ages and the thickness of the units in each hole with simple mathematics, we obtain variation of thickness for each unit across the three holes (Fig. 3.4). It reveals that the thickness shows an eastward increasing trend for each unit, in particular across the SCF-2 and the WK-1 holes. As a result, it indicates the presence of a likely normal fault between SCF-1 and SCF-2 and a more significant vertical offset of normal faulting between SCF-2 and WK-1. We therefore intend to map two fault zones in the shallow sediments of the Wuku profile, with the eastern one as the main fault zone (Fig. 3-2B).

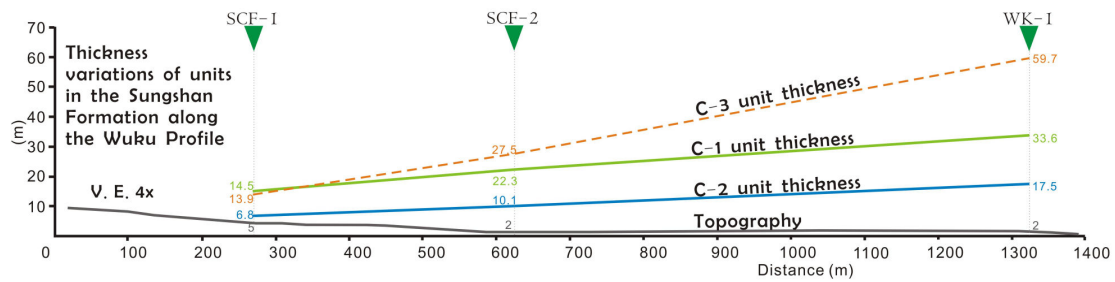


Fig. 3-4. Thickness variations of units in the Sungshan Formation along the Wuku Profile. Three units all show an increase of thickness toward the east, strongly suggesting growth faulting in-between the drilling holes. By comparing the present topography, the thickness variations clearly exceed differences of local topography and therefore advocate syn-sedimentation normal faulting.

Because that the interface between unconsolidated basin sediments and the Tertiary basement rocks dramatically deepen between boreholes SCF-2 and WK-1 to be at least 34° of dip angle (Fig. 3-2B), we tend to interpret the main fault zone in further depth to follow this interface. The secondary fault zone between SCF-1 and 2 is supported by a shear zone near the bottom of the basin sediments at SCF-2 within the C10 unit, which contains several sheared intervals with striations denoting oblique sinistral-normal faulting and frequent centimeter-scale growth normal faults (Lee et al., 1999). This secondary fault may merge with the main fault zone at where the basement floor abruptly steepened. The secondary fault is therefore regarded as a branch fault, which develops within the basin sediments. We interpret the region between the branch and main fault zones as an ‘extensional fault block’. The Wuku formation is much thinner in the extensional fault block than in the actual hanging wall east of the main fault zone, and probably a slim sheet of it remains west of the branch fault but is terminated east of SCF-1. The Banchiao formation is exclusively confined in the hanging wall in greater depth.

Figure 3-2B shows the proposed fault zone structure in the late-Quaternary basin sediments consisting of a high-angle main fault and a western lower-angle branch fault. Seismic profiling about 1.5 km south of the studied boreholes (Wang and Sun, 1999) reveals similar two-fault setting in the Shanchiao Fault zone. Minor sinistral slip component is present on the branch fault according to oblique fault striations documented by Lee et al. (1999), and such fault zone configuration may genetically bear resemblance to a negative flower structure or tulip structure (Woodcock and Schubert, 1994) as unveiled in shallow seismic survey along the fault zone in the northern corner of the Taipei Basin (Shih et al., 2004).

We can not rule out the possibility that the branch fault zone between SCF-1 and 2 may extend down into the basement other than lying entirely within loose sediments.

The extensional fault block may include the basement rock, producing staircase-shaped basement floor geometry in imbricate listric normal faulting (e.g., Wernicke and Burchfiel, 1982). It is also possible that the area between SCF-1 and WK-1 rests above an extensional fault-propagation fold (e.g. Gawthorpe and Hardy, 2002) with the two fault zones as trishear zone boundaries where shearing is concentrated. These options, though cannot be excluded, are not incorporated in the present study due to lack of evidence, and will not lead to momentous defects in the following presentation.

3.5 Reconstruction of growth faulting history

3.5.1 Sea level fluctuation and sedimentation in the Taipei Basin

Sedimentary processes in coastal areas and their vicinities are sensitive to base level changes (van Wagoner et al., 1988), so are in the Taipei Basin. Teng et al. (2000b) noted two erosion surfaces below lowstand systems tracts in the basin deposits. Sedimentary facies of the basin deposits include estuary and lake, distal to proximal floodplain, braid plain, and alluvial fan facies (Peng et al., 1999; Teng et al., 2000b). Given that the present sits at the highstand of the eustatic sea level cycle since around 20 ka of the Last Glacial Maximum (LGM) (Fig. 3-5), the youngest basin deposits of the Sungshan Formation (10-23 ka to present) are accumulated during the recent sea level rise. Before the Jingmei conglomerates deposited at about 25 ka when the Tahan River was captured, the basin (by then covered by the Wuku Formation) was in a stage of erosion with deeply-incised valleys (Teng et al., 2000b, 2004a) during the period of LGM. The restored geometry of the top of the Wuku formation represents the paleogeography of the Taipei Basin in LGM. Subsequent stacking of Jingmei and Sungshan deposits, belonging to the most recent sequence, can be comprehended by linking rates and facies of sedimentation to accommodation provided by base level rise and tectonic subsidence.

Under the basin-wide deposition scheme described above, the geological history of the sediments in association with the activity of the Shanchiao Fault since the LGM can be illuminated through sedimentary records recovered from the investigated boreholes. A series of retro-deformed cross-sections can therefore be established since LGM of about 25 ka. In the following two sections, we first present the criteria for generating the restored cross-sections by a back-stripping method and the resultant profiles, and then illustrate the geological evolution of the Shanchiao Fault zone starting from 25 ka through semi-quantitative sections under the same scheme. Compaction of loose sediments is negligible because of the young ages and shallow depths of the units (Chen et al., 2007; Taylor et al., 2008).

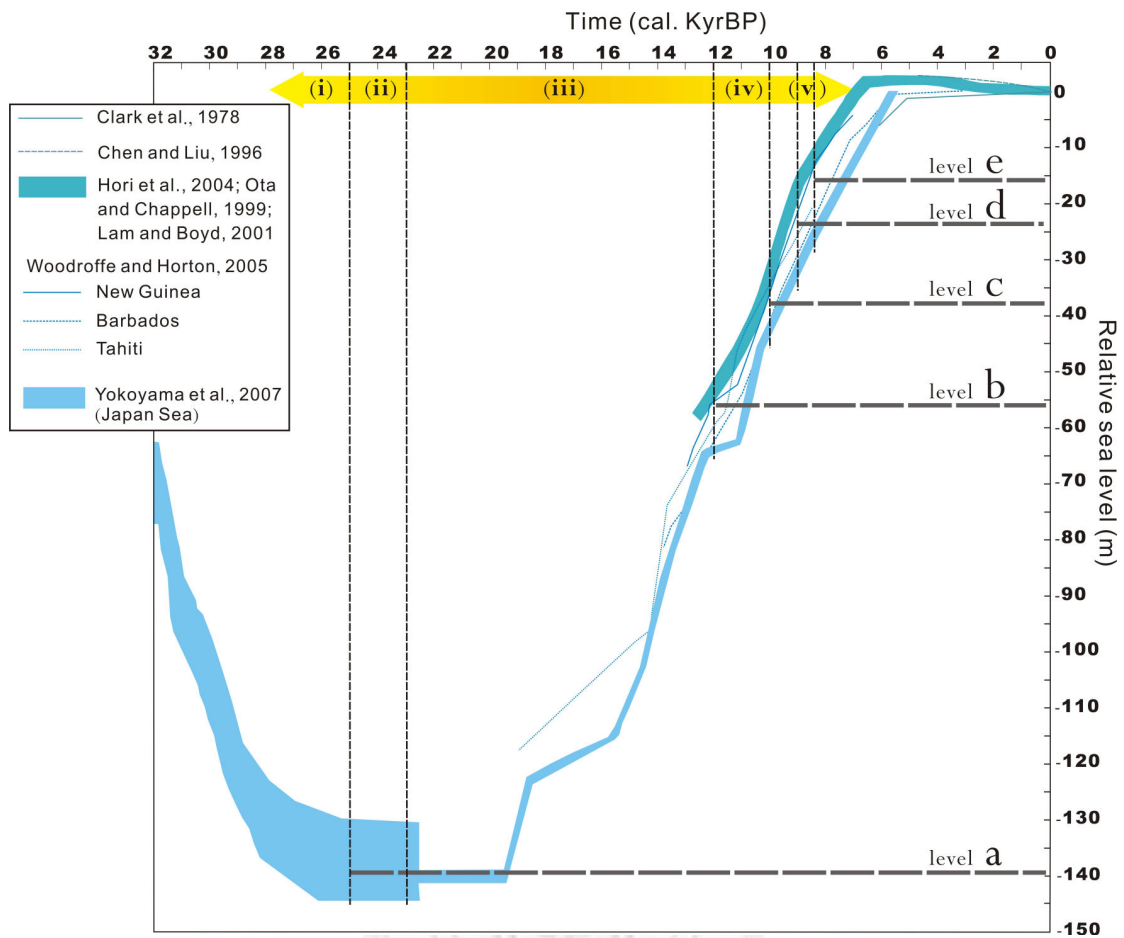


Fig. 3-5. Eustatic sea level changes since 30 ka. Levels are compiled from Clark et al., 1978; Chen and Liu, 1996; Ota and Chappell, 1999; Lam and Boyd, 2001; Hori et al., 2004; Woodroffe and Horton, 2005; and Yokoyama et al., 2007. In addition to the present-day sea level, five paleo-levels (Level a-e) were selected as the sea levels corresponding to specific ages with significant geological processes. See details in the text.

3.5.2 Restoration by a simple back-stripping method

As mentioned above, the basin-wide sedimentation process in late Quaternary was governed by sea level fluctuations along with changes of drainage system, so did the accumulation of Sungshan and Jingmei Formations in the Wuku Profile since local influences other than tectonics are not observed in sediment records. When sea level reached similar elevation to that of Taipei Basin plain (resembling the present configuration) since the recent major marine incursion in the basin at 10-9 ka (Teng et al., 2000b), sediments piled up across the entire profile, including the footwall, hanging wall and extensional fault block areas. Given the high rate of erosion and hence rapid sediment accumulation of the Taiwan Island in the present day (Dadson et al., 2003), the room of sedimentation created by rising eustasy is considered to be filled up contemporaneously, therefore producing flat topography similar to the modern one.

Under this assumption, the topography at beginning of the deposition for the C1 unit of the Sungshan Formation would be approximately flat. Because the C1 unit of SCF-1 lies in the footwall area, hence it would not involve significant vertical motion of the faulting. Referring to the growth normal faulting scheme, the bases of C1 units in the hanging wall side would be expected to be consequently downward displaced by dip-slips of the Shanchiao Fault which provided additional sedimentation rooms resulting in lateral thickening of the units. The elevation differences between the base of C1 unit at SCF-2 and SCF-1 (7.8 m), and SCF-2 and WK-1 (11.3 m) thus are interpreted to represent cumulative vertical displacements on the branch and main faults, respectively, from 8.4 ka till present (Fig. 3-6a). Furthermore, we can observe that the height of sea level e (around -16 m) at the onset of the C1 (~ 8.4 ka) is close to the depth of the base of the C1 unit (-14.5 m) in the footwall area (SCF-1).

Back to 8.4 ka, because that the top of the basin deposits (C2 unit) in the footwall appears to be near the sea level (level e), therefore the height of the top of the estuarine deposits of the C2 unit across the profile would be considered to be very much flat. Under this assumption, the fault zone stratigraphic configuration by then can be approximated by removing the C1 unit above and re-leveling the C2 unit tops in WK-1 (hanging-wall region) and SCF-2 (extension fault block) to the one at SCF-1 (footwall region) as restoration by 'back-stripping' (Fig. 3-6b). We calculate the remaining vertical differences of the depths of C2 unit between three holes as mentioned above. We then obtain 3.3 m and 7.4 m, which hence denote to be cumulative vertical offsets on the branch and main faults respectively during the 9 ka to 8.4 ka period (Fig. 3-6b). These relative large amounts of vertical offset at a short time span of 600 years appear to be consistent with two possible earthquake events

occurred during this period inferred by previous study (Huang et al., 2007). We will discuss it in more details in the later section.

The above approach became much difficult to apply to deeper sediments of the Sungshan Formation because the 10 ka datum is obscure at SCF-2 and WK-1, and synchronicity of sedimentation along the Wuku profile was absent during 23 ka to 10 ka. However, the Jingmei Formation alluvial fan deposits of 25 – 23 ka resulted in a relatively flat topography at the end of the river-capture event. Provided the comparable thicknesses of the Jingmei conglomerates (C4 unit) at SCF-2 and WK-1, the ancient topography of the Wuku profile is considered to be roughly even at around 23 ka, therefore permitting the ‘back-stripping’ of C3 unit and evaluation of fault vertical displacements during the deposition of the C3 unit. Under this assumption, we then obtain that the Shanchiao branch fault slipped 13.6 m vertically and the main fault 32.2 m during ~23 ka to 9 ka according to constraints from top horizons of the C3 unit and the Jingmei Formation (Fig. 3-6c).

Details of sediment accumulation and fault throws between ~23 ka to 9 ka cannot be accurately resolved, while the stacking pattern of the deposits does show westward onlapping of layers which is closely tied to tectonic modification on local geomorphology and base level changes controlled by eustacy. Regional sedimentation rate (modulated by tectonic movements) was zero at the LGM as the sea level (level a) was low at about -140 m compared to the present day level. Since LGM the sedimentation rate is expected to be rapidly increasing in pace with the rising sea level, and again dropped to trivial numbers when eustacy stabilized to elevations similar to that of today at ~6 ka (Fig. 3-5).

In summary, the total vertical offset across the Shanchiao fault zones since 23 ka can be yielded by summing the above results during different periods, as shown in Fig. 3-6. We thus obtain a total vertical offset of 75.6 m, with 24.7 m and 50.9 m for the branch fault and the main fault, respectively, since the LGM of 23 ka. It can translate to an average vertical fault slip rate of 3.3 mm/yr across the Shanchiao fault zone in Wuku profile, with 1.1 mm/yr for the branch fault and 2.2 mm/yr for the main fault, since 23 ka.

Evolution model for the Shanchiao Fault zone
along Wuku profile since 23000 yrBP
(Assuming negligible sediment compaction)

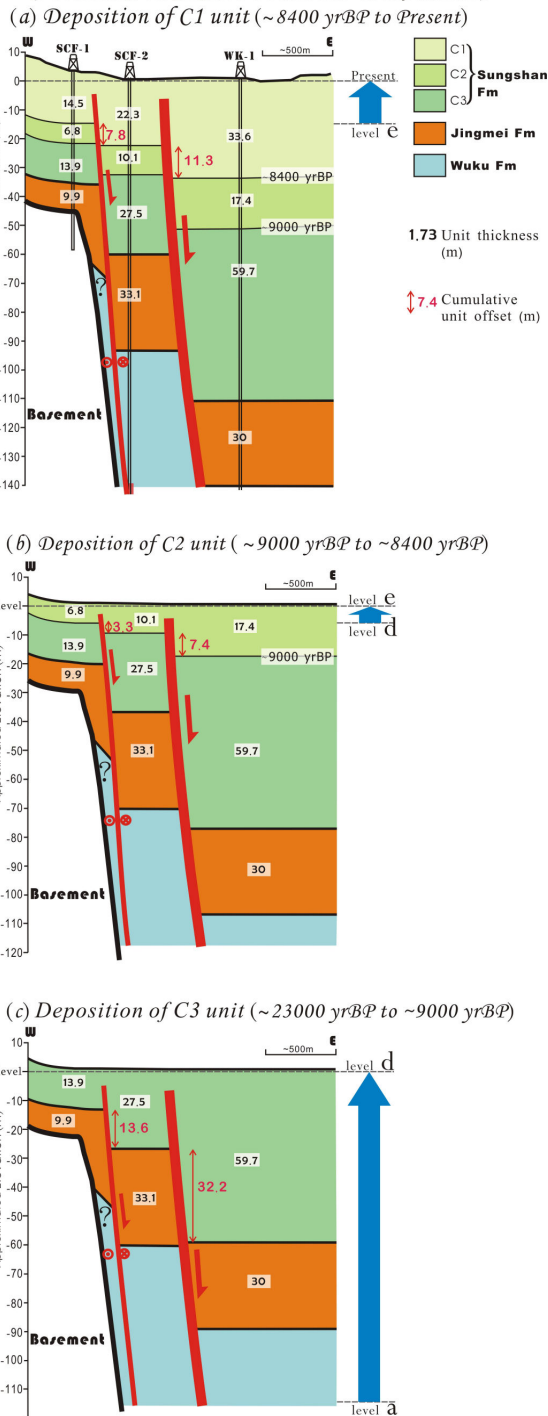


Fig. 3-6. Back-stripping method and reconstruction of cumulative deformation on the Shanchiao Fault since the LGM of about 23 ka. Three periods of 8.4 ka – present (a), 9 – 8.4 ka (b), and 23 - 9 ka (c), which correspond to depositional ages of Units C1, C2, and C3, respectively, are adopted for explaining the evolution of the growth faulting of the Shanchiao Fault. Numbers in black color: thickness of stratigraphic units. Numbers in red color: vertical differences of thickness for each stratigraphic unit between drilling holes. Levels a to e are paleo-sea levels trough time, which are denoted in Fig. 3-5.

3.5.3 Evolution of sedimentation vs. growth faulting

Combining information on stratigraphic architecture and knowledge on sea level changes since the LGM, the fault zone evolution is depicted in five scenes shown in Fig. 3-7.

(1) Shortly before 25 ka (Fig. 3-7i)

Global and East Asian eustatic sea level plunged to more than 100 m below the present level since 30 ka, as the LGM began (Yokoyama et al., 2007). The sea level around Taiwan stabilized at approximately -140 m (level *a*) from about 28 ka compared to the present day. The 25-ka paleo-topography as to of the Wuku formation can be estimated by adding the present day -140.8 m deep with 75.6 m of total vertical subsidence due to faulting with our back-stripping method, as described above. We obtain a depth roughly at -65 m for the top of Wuku formation along the Wuku profile (Fig. 3-7i). It means that the Wuku formation was about 75 m high above the sea level at that time. As a result, sediments of the Wuku formation were subject to strong erosion by drainage system in the Taipei basin.

The relatively high local topography 75 m above sea level indicates that no major channels, neither the Tanshui River nor the creeks originated from the Linkou Tableland in the west, existed in the investigated profile, which would form gorge-like incised valleys. The shallow basement at SCF-1 was exposed without cover of late-Quaternary deposits and thus was subject to be weathered (Fig. 3-7i). Surface scarps resulted from slips on the Shanchiao Fault were likely to be rapidly erased or retreated westward on topography by intense erosion, obscuring attempts to estimate fault activity during this period.

(2) 25 ka to 23 ka (Fig. 3-7ii)

The Jingmei sediments were interpreted to be quickly deposited when the Tahan River was captured into the Taipei Basin during 25-23 ka (Teng et al., 2004a). These alluvial fan conglomerates accumulated within a time span of 2000 year and attained ~30 m thick in the Wuku region. Top of the Jingmei conglomerates should be rather flat by the time deposition ceased in the Wuku Profile because sediment transport was normal to the profile towards the north and no major channels were present. The gravel bed of the Jingmei Formation is 10 m thick onlapping onto the weathered Mio-Pliocene basement at SCF-1, implying an ancient topographic scarp located between SCF-1 and SCF-2. However, we interpret that the Shanchiao Fault was inactive during this 2000-yr-long period because the Jingmei Formation is of uniform thicknesses (i.e. 30 – 33 m) across the main fault between SCF-2 and WK-1.

On the other hand, during 25 ka to 23 ka, the sea level did not change significantly,

thus remained about -140 m compared to the present level. So that the top of the Jingmei formation lies about -35 m compared to the present, that is, about 105 m high above the sea level.

(3) 23 ka to ~12 ka (Fig. 3-7iii)

We anticipate that the Taipei basin started to subside along the Shanchiao Fault after completion of the Jingmei conglomerate with probably both the hanging-wall block and the extensional fault block displaced downward. However, braid plain to floodplain sediments of 23-12 ka (lower part of C3 Unit of the Sungshan Formation) exist only at WK-1. It implies that during this 10000-year-long period the hanging wall had subsided enough to accumulate braid plain and flood plain fluvial growth sediments of while the Jingmei gravel would be exposed in the footwall and the extensional fault block region. In the meantime, sea level rose rapidly from -140 m (level *a*) to -55 m (level *b*) from ~18 ka to 12 ka (Fig. 3-5) during this period. So that the elevation of the basin floor decreased drastically from 105 m to 10-20 m high above the sea level from 23 ka to 12 ka.

(4) ~12 ka to 10 ka (Fig. 3-7iv)

The situation of next 2000 years in 12-10 ka was similar to the previous period as the sea level rose rapidly, except that the growth strata of fluvial deposits (middle part of Unit C3 of the Sungshan Formation) started to lap on to the area of the extensional fault block between the main and branch faults. This suggests that the subsidence in the extensional fault block region allowed fluvial sediments to accumulate. Sea level rose from -55 m (level *b*) to about -37 m (level *c*) during this period, while it still kept slightly lower than the basin ground.

(5) 10 ka to 8.4 ka (Fig. 3-7v)

The start of this period marked the onset of major marine incursions in the basin (Teng et al., 2000b) as sea level gradually rose from -37 m (level *c*) to -16 m (level *e*) from 10 to 8.4 ka. Sediments began to pile up across the entire section, and the accommodation space was filled contemporaneously with the rising sea level. Since then the regional topography should be very similar to the flat one today, with less than 5 meters of difference in elevation between the borehole sites. The top horizons of C3 and C2 units, the estuarine deposits during that time, are therefore assumed to be similar in elevation along the Wuku profile in the three boreholes at around 9 ka and 8.4 ka, respectively. Accordingly, while the sea level continued to rise from level *d* to level *e* from 9 to 8.4 ka (Fig. 3-7v), we estimate that an extraordinarily rapid sedimentation of Unit C2 with 6.8, 10.1, and 17.4 m thickness at SCF-1, SCF-2, and WK-1, respectively. In the mean time, the Shanchiao Fault slipped vertically 3.3 m on the branch fault and 7.4 m on the main fault during the 600-year interval when C2

rapidly deposited in a relative deep, lower estuarine environment.

(6) 8.4 ka to present (Fig. 3-7vi)

From 8.4 ka till present, as the sea level continued to rise from level e (-16 m) to present level and coupled with tectonic fault movement, the estuarine deposits of the C1 unit piled up and completed the uppermost sediments of the Taipei basin in the Wuku profile. The extensional fault block has been observed to subside (relative to the footwall) 7.8 meters and additional 11.3 meters for the hanging wall of the main fault.



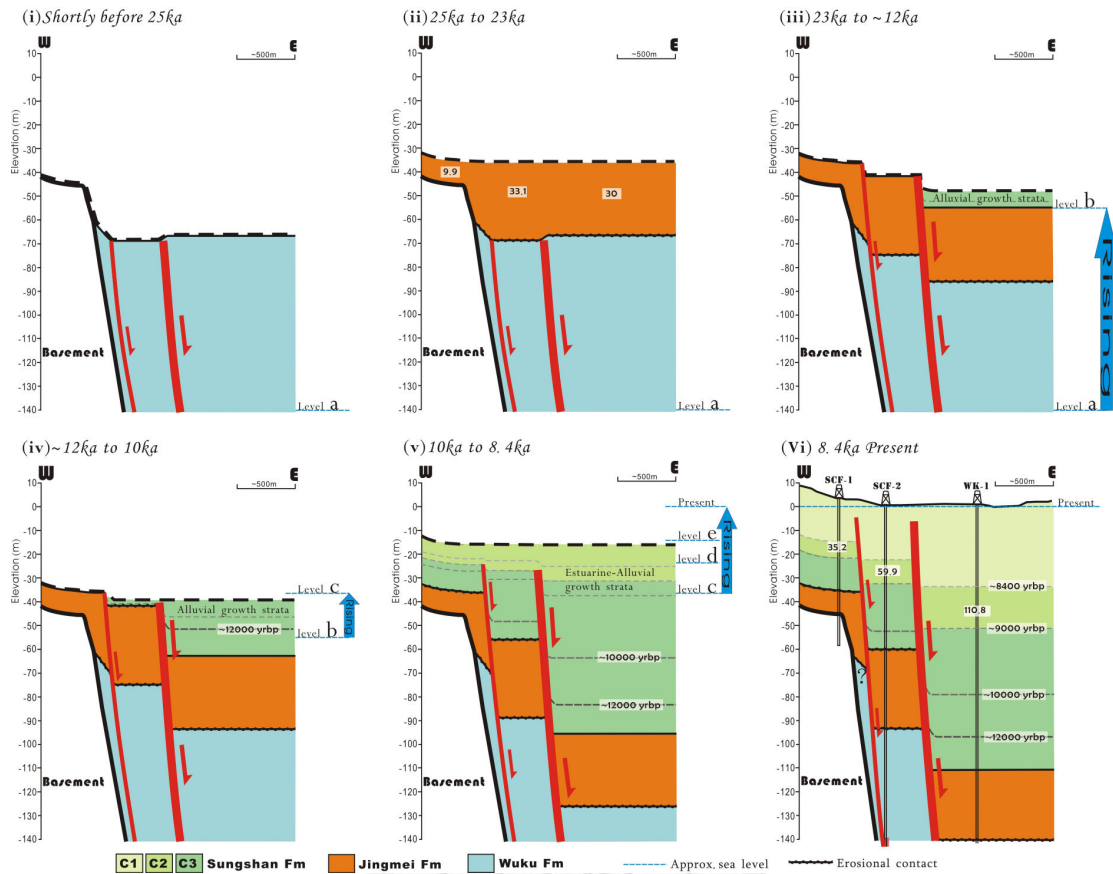


Fig. 3-7. Interpreted sedimentation and growth faulting and post-LGM development history of the Shanchiao Fault zone in the Wuku profile. Several geological events with confident age controlled were adopted to divided the period into six stages: (i) shortly before the deposition of the Jingmei formation (25ka), (ii) deposition of the Jingmei conglomerates (25 – 23 ka), (iii) shortly before the sea level rising to reach the basin ground level (23 – 12 ka), (iv) the sea level beginning to surpass the basin ground level (12 – 10 ka), (v) basin-wide sedimentation containing a 600-year time span with possible earthquake events coupled with rapid sedimentation (9 – 8.4 ka), and (vi) the latest stage of the sedimentation and growth faulting with gradual sea level rise and stabilized (8.4 – 0 ka). Levels a to e are denoted in Fig. 3-5.

3.6 Discussion

3.6.1 Tectonic loading rates and earthquake events

Given that the rate of sediment supply and the rate of increasing accommodation space from rising sea level and tectonic subsidence are at balance, the sedimentation rate provides a direct way to estimate the effects of these components through time. When this is the case, sedimentation rate of growth strata across the fault offers explicit evaluation of both regional deposition rate and additional contribution from tectonic subsidence, with that obtained on the footwall containing only the former one.

Sedimentation rate investigation as described above is conducted on the C1 and C2 units of the Sungshan formation in the Wuku Profile, that is from 9 ka to present. The reason why constraining to the Holocene time is mainly because of the synchronicity of deposition and quality of age controls. We obtain the Holocene sedimentation rates (dividing the unit thickness by the time span of deposition) for three blocks: (a) derived from units on the footwall at SCF-1 block stand for the regional deposition rate, while (b) derived on the extensional fault block at SCF-2 and (c) the hanging wall block at WK-1 include excess rates representing tectonic subsidence. The estimations are presented in Table 3-4 and Fig. 3-8A. The yielded sedimentation rates are 1.7, 2.7, and 4.0 mm/yr for footwall, extensional fault block, and hanging wall, respectively, during 8.4 ka – present (C1 unit). However, we obtain a much higher sedimentation rate of 11.3, 16.8, and 29.2 mm/yr for footwall, extensional fault block, and hanging wall, respectively, during 9 – 8.4 ka (C2 unit). Note that difference in compaction rate of these Holocene units between the boreholes (i.e. different parts across the fault) would be well lower than 1 mm/yr (Meckel et al., 2006) and is thus ignored in the evaluation. By incorporating sea level rise, we obtain rate excess which we interpreted as tectonic subsidence rate (Table 3-4, Fig. 3-8A): 0.9 and 2.3 mm/yr for branch fault and main fault, respectively during 8.4 ka – present (C1 unit) and 5.5 and 17.8 mm/yr for branch fault and main fault, respectively during 9 – 8.4 ka (C2 unit).

Based on the above results, the period of 9 – 8.4 ka when C2 was laid is characterized by both rapid base level rise and high tectonic subsidence rate. Two paleo-earthquake events documented on the branch fault zone by Huang et al. (2007) coinciding the start and end of C2 deposition may lead to the much enhanced sedimentation rate and tectonic rate calculated. The total vertical tectonic subsidence of 3.3 m and 7.4 m for branch and main fault during this period of 9 – 8.4 ka would mainly be subject to these two possible earthquake events. The rates derived from the C1 unit, embodying averages for a longer time period of 8.4 – 0 ka, are considered to

better represent the Holocene and late Quaternary long-term tectonic subsidence rate of the Shanchiao Fault which is 2.3 mm/yr on the hanging wall and 0.9 mm/yr on the extensional fault block, with a regional sedimentation rate of 1.73 mm/yr, and yield a rather high growth index (defined as fault throw rate divided by footwall sedimentation rate; Childs et al., 2003) of 1.3.

Tectonic subsidence rates of the Shanchiao Fault since 23 ka can also be inferred from vertical offsets of the horizons (Fig. 3-8B). Differences to the top depths of the Jingmei Formation (Unit C4) encompass the total vertical offsets of the Shanchiao Fault system since 23 ka, indicating the average vertical slip rates of 3.3 mm/yr with 1.1 mm/yr on the branch fault and 2.2 mm/yr on the main fault since the LGM. We also obtain about 1.0 mm/yr and 2.3 mm/yr of averaged vertical slip rates on the branch and main faults, respectively, during 23 – 9 ka. The faulting rates obtained from various time periods and criteria are quite consistent with the exception of those from C2 unit. We can also conclude that the hanging wall down-throw rates were higher than the regional sedimentation rates since at least 9 ka.

Comparing to the long-term tectonic subsidence rate of the Shanchiao Fault, which was estimated to be 1.75 mm/yr since 0.4 Ma (Chen et al., 2007), the results of short-term rate of 3.3 mm/yr since 23 ka appears to be significantly higher (Fig. 3-8B). Although it is possible that the Shanchiao Fault has being more rigorous during the last tens of thousands of years, however, without study to complete the gap between 0.4 Ma and 23 ka, it is too early to draw a conclusion right now.

Table 3-4: Sedimentation rate and inferred tectonic subsidence rate of the Shanchiao Fault zone in the Wuku Profile since ~9 ka (assuming negligible differences in compaction rates).*

	Footwall (SCF-1)	Extensional fault block (SCF-1)	Hanging wall (WK-1)
C1 (~8.4 ka – present)	14.5 / 1.7 / -	22.3 / 2.7 / 0.9	33.6 / 4 / 2.3
C2 (~9 ka – ~8.4 ka)	6.8 / 11.3 / -	10.1 / 16.8 / 5.5	17.5 / 29.2 / 17.8

*: The values displayed are arranged as: thickness (m) / sedimentation rate (mm/yr) / rate excess (tectonic subsidence rate)

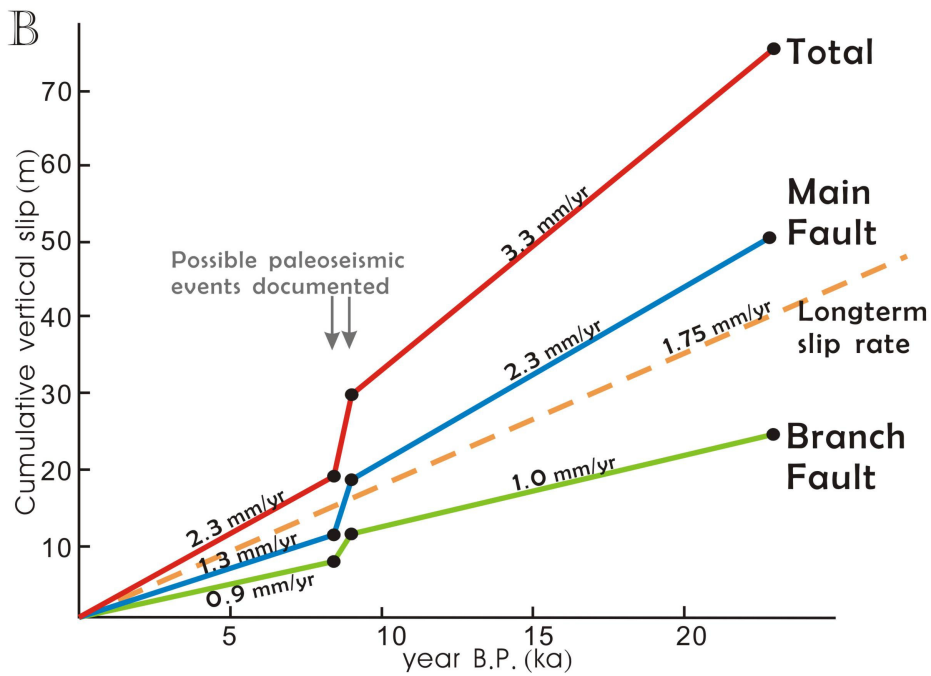
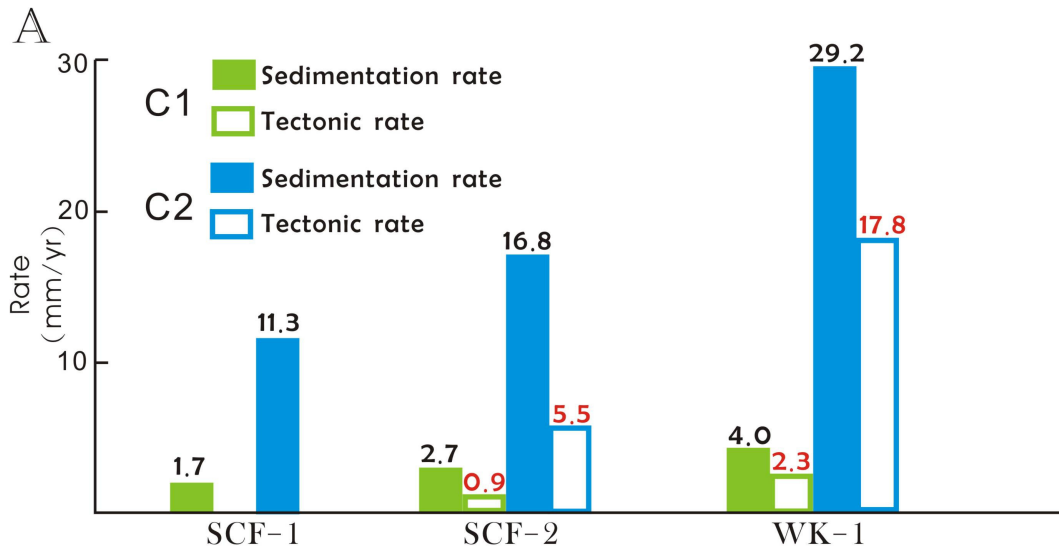


Fig. 3-8. (A) Sedimentation rate and tectonic subsidence rate of the C1 and C2 units at the Wuku boreholes. (B) Accumulative vertical slips for the Shanchiao fault since the LGM documented in the Wuku Profile.

3.6.2 Correlation between surface topography and subsurface geology

Previous study of topographic mapping aiming at characterizing Shanchiao Fault zone geomorphology has identified a series of fault-related scarps arranged in an en-echelon array (Chen et al., 2006), which are present along the western edge of the Taipei Basin (Fig. 3-2A). The locations of fault-related scarps are generally in good agreement with existing borehole analyses which placed the surface trace of the Shanchiao Fault between borehole pairs including SCF-1 and 2, SCF-5 and 6, SCF-3 and 4 (Fig. 3-2A; Huang et al., 2007, Lin, 2001). In the Wuku Profile, however, these traces and geomorphic features actually correspond to the branch fault zone; the main fault zone of the Shanchiao Fault may reach land surface east of SCF-2 where ground elevation is close to zero. We speculate that any topographic depressions caused by activities on the main fault zone would be readily erased since such troughs below the sea level tend to be rapidly filled by sediments given frequent typhoons and floods of Taiwan. This demonstrates that young faults without clear geomorphic evidences do not preclude the possibility of their recent activities, and hence the potential seismic threats.

Figure 3-9 shows a 3-D block diagram summarizing structural and geomorphic characteristics of the Shanchiao Fault zone. Structures of faulted and tilted strata within the basement rocks mainly reflect deformation features occurred in the mountain-building stage in the Taipei region consisting of thrust sheets, as the Hsinchuang Fault and the one seen in WK-1. The Hsinchuang Fault, by then the mountain frontal thrust some 2 Ma, only broke in the lower part of the Linkou Formation, and the basement rocks are buried within the fan-delta Linkou conglomerates (Teng et al., 2001). The uplift of the Linkou Tableland on the footwall block may be closely associated with the development of the normal faulting of the Shanchiao fault. The eastern border of the tableland, consisting of steep cliffs bearing some triangular facets and generally two threads of terraces (Chen et al., 2006), is composed of colluvial deposits with local outcrops of basement rocks (Teng et al., 2001). Geomorphic scarps bordering these terraces of uncertain origin might be related to past earthquake events as retreated fault scarps enhanced by fluvial processes. The only in situ fault-related scarps are associated with the branch fault, and exhibit right-stepping segmentation which denotes sinistral transcurrent tectonic environment, in line with the fault striation recovered in the drilling hole (SCF-2; Lee et al., 1999) and with the regional GPS measurements (Rau et al., 2008).

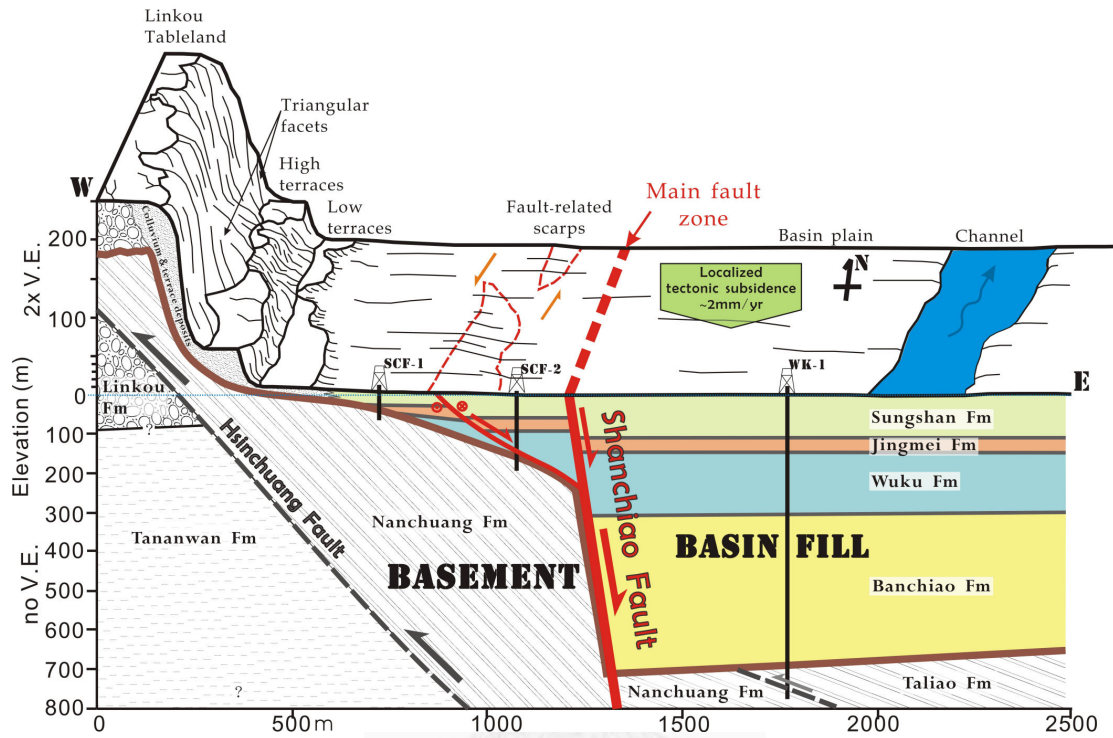


Fig. 3-9. Schematic 3-D diagram of the fault zone in the Wuku area, central portion of the Shanchiao Fault, displaying regional subsurface geology and its relation to surface topographic features.

3.7 Concluding remarks

The Shanchiao Fault zone is interpreted to be composed of a main fault zone and a westerly shallower branch fault zone, with an extensional fault block in between. Left-lateral transcurrent motion in addition to normal faulting is present at least on the branch fault. The Shanchiao Fault has been highly active by almost incessant faulting since the Last Glacial Maximum of 23 ka. By comparing stratigraphy and its age, we are able to correlate stratigraphic units in a great detail across the three drilling holes along the Wuku profile. Under the assumption that the rapid rise of the sea level since the LGM would provide immense sediments to keep the topography flat in Taipei basin, we reconstructed history of growth strata, which shows sedimentation significantly reflecting a combination effect of sea level rise and tectonic subsidence across the Shanchiao Fault since 23 ka. Furthermore, we calculated averaged vertical throw rates of about 2.2 mm/yr and 1.1 mm/yr on the main and branch faults, respectively. The branch fault, corresponding to the major fault designated in previous documentations, made up about a third of total vertical displacement on the entire Shanchiao Fault zone since around 23 ka. Holocene tectonic subsidence rate of the fault appears to be similar and is constrained to be 2.3 mm/yr in the near-fault part of the hanging wall block, and 0.9 mm/yr in the extensional fault block area during 8.4 – 0 ka. However, an episode with possible two earthquake events revealed substantial tectonic subsidence of 7.4 and 3.3 m in the main fault and the branch fault, respectively, during a 600-yr time span of 9 – 8.4 ka. At the present day, only the branch fault has geomorphic expressions; any topographic depressions caused by faulting on the main fault seem to be quickly filled. This has important implication for neotectonic investigations that faults of suspected status may still be active even though no clear direct geomorphic evidences can be found.

Chapter 4: Fault zone characteristics and basin-wide distribution of post-Last Glacial Maximum tectonic subsidence of the active Shanchiao Fault in the Metropolitan Taipei Basin, northern Taiwan

4.1 Introduction

Continental extensional provinces are common sites of concentrated population and urban development given the presence of arable and habitable plains or basins, as well as seismic threat from active normal faults (e.g. Machette et al., 1991; Boncio et al., 2004). However the efforts to accurately assess the posing earthquake hazard are usually hampered by the scarcity of outcrops to derive geological information useful in precisely characterizing the active fault, including the fault trace, the fault zone width, (Quaternary) offset and slip rate. Other means to explore the paleoseismic history and future earthquake scenario are historical and instrumental records, archaeoseismology, and tectonic geomorphology, while their relevance varies from region to region (Caputo and Helly, 2008). For places without confirmed historical earthquake events, one of the key tasks is to map the fault trace and the spatial extent of tectonic deformation. With leveling and triangulation measurements and the recent advent of advanced geodetic tools like InSAR, scientists are able to monitor ground deformation associated to fault activity; while given the short observation period to the usually much longer earthquake cycle, these data only hold for interseismic behavior of the targeted faults (Scholz, 2002). Furthermore, these surface deformation observations are often contaminated by contributions from effects such as groundwater fluctuations and human activities, obscuring precise determination of fault movements (e.g. Amelung et al., 1999; Bawden et al., 2001). More reliable constraints come from syn-tectonic sediments, namely the growth strata common in these extensional provinces; when coupled with other analyses the long-term activity and kinematics of the fault are better illuminated.

The Taipei metropolis, home to several million people and the capital of Taiwan, is situated in the Taipei Basin under the influence of the extensional tectonics of northern Taiwan and Ryukyu backarc system (Teng, 1996). The Taipei Basin is a half-graben formed by repeated slips of the active Shanchiao normal fault and filled with late-Quaternary unconsolidated sediments (Teng et al., 2001). Despite the huge significance on hazard mitigation and regional geodynamics, the geological

characteristics of the Shanchiao Fault remain not well understood. There is no known fault outcrop preventing definite mapping of the fault trace (Lin, 2005), and heavy urban development makes geomorphic analysis difficult (Chen et al., 2006). The Taipei area is low in shallow crust seismicity (Wang et al., 2006; Wang, 2008) except in the Tatun Volcanoes north of the Taipei Basin where volcano-related seismic signals are identified (e.g. Lin et al., 2005), thwarting attempts to image active faults by the clustering of microseismicity. Contemporary surface deformation measurements by GPS (Yu et al., 1999a; Lin et al., 2010), leveling (Chen et al., 2007) and InSAR (Chang et al., 2010) confirmed the existence of extension and subsidence caused by the Shanchiao Fault, but were unable to extract the exact values as aquifer deformation was also present. While analyses of growth sediments from boreholes in the central portion of the fault demonstrated a promising growth faulting scheme to unravel fault activity since the Last Glacial Maximum (LGM) around 23 ka (Chen et al., 2010) when the recent basin deposits began to accumulate (Teng et al., 2000b), along with possible paleoearthquake events within the Holocene proposed by Huang et al. (2007).

In this work, fault zone topography and growth faulting analysis join force to delineate the detailed Shanchiao Fault zone, and a key horizon within the growth sediments is traced laterally across the entire Taipei Basin to illuminate the magnitude and spatial distribution of long-term post-LGM tectonic subsidence. The growth sedimentation and fault zone architecture documented in the central portion of the fault in the Wuku Profile (Chen et al., 2010) is confirmed to be a common phenomenon for the Shanchiao Fault as similar growth faulting and half-tulip structure is recognized in the Luzhou Profile in the central-north portion of the fault; considering the fault configuration the trace mapped from fault-related scarps represents only part of the fault zone. The top of the Jingmei Formation, an event strata in the lower part of the growth sediments and widespread in the Taipei Basin, records the fault throw since the LGM both in the fault zone and throughout the basin; the resultant tectonic subsidence pattern shows that the hanging wall of the Shanchiao Fault is deformed in a roll-over fashion while the fault slip is largest in Wuku-Luzhou area and decrease systematically towards the south and east.

4.2 Regional setting

4.2.1 Geology of the Taipei Basin

Taiwan results from active convergence between the Chinese Continental Margin on the Eurasian Plate and the Luzon Arc on the Philippine Sea Plate since around 5 Ma (Suppe, 1981; Teng, 1990; Wu et al., 1997) with a rapid convergent rate of about 82 mm/yr in the NW direction (Seno, 1977; Yu et al., 1997; Fig. 4-1A). This oblique

convergence leads to the southward-propagation of the Taiwan orogeny (Suppe, 1981). While central and southern Taiwan are presently in full and mature collision (Angelier et al., 1986; Yu et al., 1997; Shyu et al., 2005), the northern part of the mountain belt, including the Taipei region, is now in a state of post-collision with an extensional or transtensional tectonic setting rather than a compressional one (Teng, 1996; Hu et al., 2002), as evidenced by the presence of Quaternary extensional structures (Lee and Wang, 1988; Lee, 1989; Lu et al., 1995), extensional earthquake focal mechanisms (Yeh et al., 1991; Kao et al., 1998), and GPS displacement fields (Yu et al., 1997; Rau et al., 2008; Lin et al., 2010). The Taipei half-graben of Quaternary deposits is therefore formed in a close association with down-dip slips on the Shanchiao Fault, which is considered as the major neotectonic structures responsible for the negative tectonic inversion from compression to extension across the Taipei region (Teng et al., 2001; Fig. 4-1).

The flat low-lying Taipei Basin, a triangular-shaped half-graben filled with late-Quaternary fluvial deposits since c. 0.4 Ma (Wei et al., 1998; Teng et al., 2001), developed on top of the folded Oligo-Mio-Pliocene shallow marine sedimentary rocks, as a fold-and-thrust belt during the earlier stage of mountain building. The late Quaternary terrestrial deposits in the Taipei basin form an asymmetric sedimentary wedge: reaching a maximum depth of about 700 m near the western margin and rather drastically becoming thinner toward the east and south (Fig. 4-1C). These unconsolidated deposits are divided into four major lithostratigraphic units (Teng et al., 1999). From bottom to top, they are: (1) the Banchiao Formation: consisting of intercalated fluvial sands, muds and conglomerates, with occasional pyroclastics and topped by thick laminated mud, with maximum thickness of 380 m with ages ranging from 250 to 400 ka; (2) the Wuku Formation: consisting of fluvial sands and conglomerates, with minor mud and lateritic conglomerates, reaching a maximum thickness of c. 160 m with ages ranging from 80 to 250 ka; (3) the Jingmei Formation: composed of lateritic fluvial (alluvial-fan) conglomerates with an utmost thickness of 50 m. These particular conglomerates layers are interpreted as the products when the Tahan River was captured into the Taipei basin at 25 to 23 ka (Teng et al., 2004a); (4) the Sungshan Formation, composed of estuarine interbedded sand-mud deposits with a thickness of 50-100 m, was deposited from 23 ka till present (Teng et al., 2000b; Chen et al., 2010). The basin deposits exhibit prominent lateral facies changes with frequent pinch-outs. However, the widespread lateritic gravels of the Jingmei Formation and the laminated muds in the upper Banchiao Formation (Teng et al., 2004b) usually serve as basin-wide marker beds (Teng et al., 1999).

Geological evolution of the Taipei Basin was proposed by Teng et al. (2001), based

on interpretation of regional geology. While the Plio-Pleistocene orogeny of mountain building reached its climax in northern Taiwan in Quaternary, the Paleo-Tanshui River, the major river in the Taipei Basin, provided sediments to produce the Linkou fan-delta around the ancient mountain front (Chen and Teng, 1990). Accompanying the waning of compression in the northernmost Taiwan during the middle to late Quaternary (Lee and Wang, 1988) is the vigorous eruptions of the Tatun volcanoes to the north of the Taipei Basin (Wang and Chen, 1990; Song et al., 2000), closely related to the onset of regional extension. Subsidence along western margin of the Taipei basin, as evidenced by several hundred meters thick fluvial deposits, is interpreted to result from the repeated normal faulting of the Shanchiao Fault as inverted from the Hsinchuang fault, an ancient frontal thrust in northern Taiwan (Chiu, 1968; Hsieh et al., 1992). The extensional tectonics turned the Taipei area from rugged mountains gradually into a sediment-receiving basin, and accumulation of fluvial and lacustrine sediments started at about 0.4 Ma (Wei et al., 1998; Teng et al., 2001). Since then the Taipei Basin has kept expanding due to erosion and continual asymmetric subsidence along the Shanchiao Fault in the western edge of the basin. Under the combining influences of sea level fluctuations, volcanic activities, drainage system changes, and tectonic processes, the basin was infilled with various types of sediments, including alluvial, lacustrine, marine and pyroclastic deposits, up to 700 m thick as mentioned above.

4.2.2 The active Shanchiao Fault

The Shanchiao Fault was mapped (Chang et al., 1998; Lin et al., 2000; Lin, 2001; Huang et al., 2007; Chen et al., 2004, 2006) along the topographic boundary between the Linkou Tableland and the Taipei Basin, sub-parallel to the Hsinchuang Fault (Lin, 2001; Teng et al., 2001), with features indicating that the steeper Shanchiao normal fault may merge into the Hsinchuang thrust fault at depth (e.g. Hsieh et al., 1992). Following the late-Quaternary tectonic inversion, tectonic subsidence from down-dip slips on the Shanchiao Fault led to formation and development of the Taipei Basin. Left-lateral transcurrent motion together with clockwise block rotation is also present along the Shanchiao Fault, based on studies on regional structural geology, paleomagnetism, and GPS measurements (Lu et al., 1995; Lee et al., 1999; Rau et al., 2008).

Many efforts have been made to characterize this active fault. Shallow reflection seismic profiling across the Shanchiao Fault imaged vertical offsets of Holocene sediments at shallow depth, although the location of the main fault remains questionable (Wang and Sun, 1999; Shih et al., 2004). GPS surveys of the Taipei area showed WNW-ESE extension with a slow rate of 0.08 μ strain/yr across the fault (Yu

et al., 1999a). Asymmetric tectonic subsidence related to the Shanchiao Fault across the basin was illuminated through recent study on 30-year-long levelling data (Chen et al., 2007) as well as recent InSAR data (Chang et al., 2010). Huang et al. (2007) correlated stratigraphy of three sets of boreholes, and proposed three paleoseismic events during the Holocene (i.e. at 8500, 9200, and 11100 years b.p., respectively). Radon and helium anomalies in soil-gas along the fault zone were documented (Walia et al., 2005) indicating the presence of possible active faults and deep fracture-advection system. Growth faulting analysis at the central portion of the fault in Wuku area demonstrated that the fault has been constantly active in the last 23000 years and the shallow fault zone seems to possess half-tulip structure (Chen et al., 2010). Preliminary geomorphology analysis (Chen et al., 2006) also revealed a series of scarps closely related to the development of the Shanchiao Fault. The Shanchiao Fault is therefore considered currently active (Chang et al., 1998; Lin et al., 2000) while our knowledge toward it is still limited.

In the following the detailed topographic analysis in the fault zone is first presented, and then what have been found in the Wuku Profile at the central of the fault are demonstrated to be extended along strike and across the basin to illuminate fault zone structure and tectonic subsidence. The results shed light on basic information including the location of the fault zone and fault displacement pattern, as well as insights on rheological controls on shallow fault zone structure and the surface imprint of active faulting.

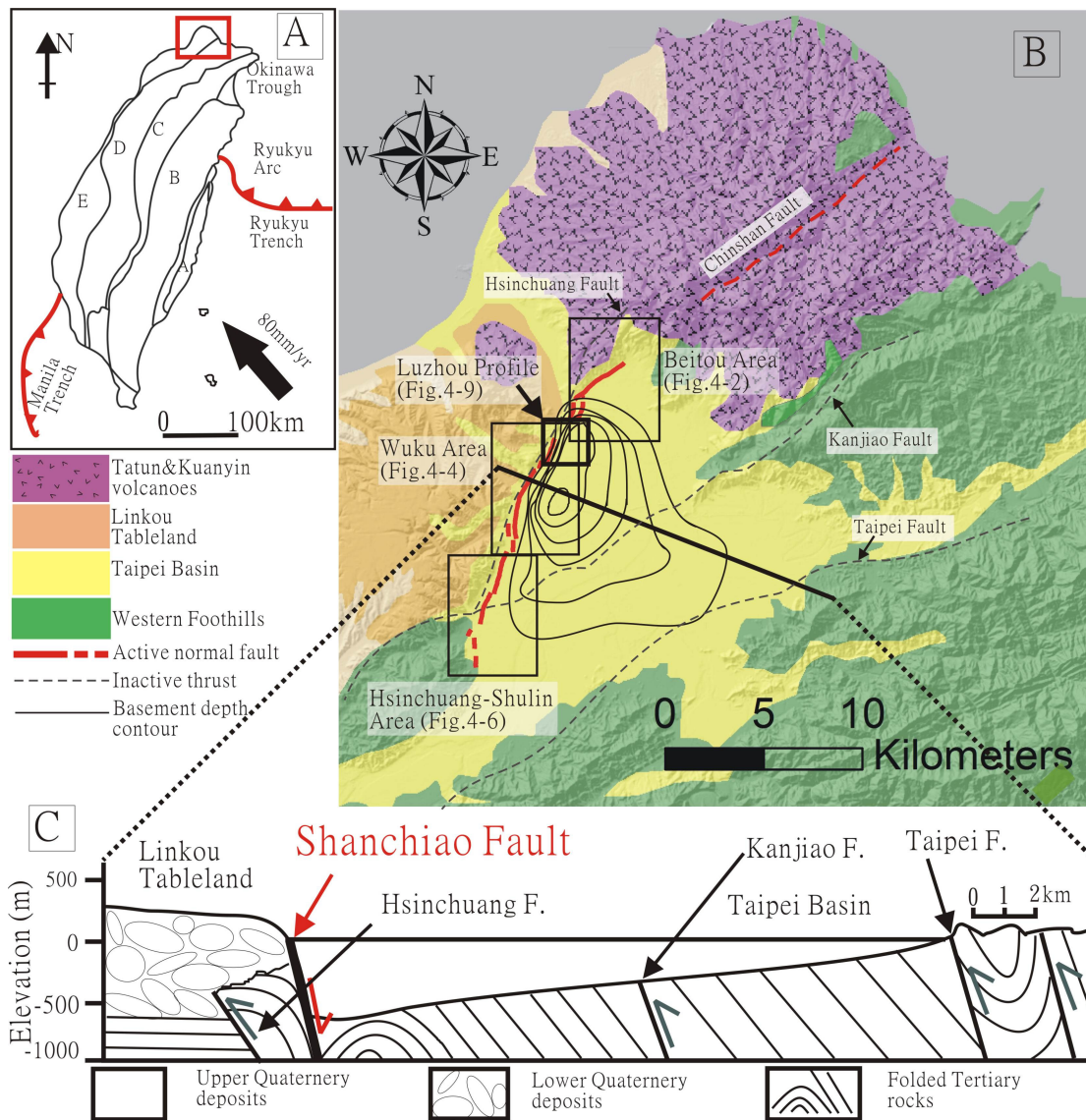


Fig. 4-1. (A) General tectonic framework of Taiwan. A: Coastal Range; B: Backbone Range; C: Hsueshan Range; D: Western Foothills; E: western Coastal Plain. (B) Simplified geology of the Taipei area. Four geological domains are defined in the Taipei area as indicated by different colors shown in the legend. The thick red lines are the Shanchiao Fault traces (Chen et al., 2006). Thin black lines within the Taipei Basin are the basement depth contour of 100 m interval (adapted from Teng et al., 2001). The areas shown in Figs. 4-2, 4, 6, and 9 are marked. (C) Geological cross section of the Taipei Basin (modified from Teng et al., 1999).

4.3 Fault zone geomorphology

In the search for evidence of geomorphic features of the Shanchiao Fault, the widely-available 40-m Digital Terrain Model (DTM) is analyzed. Although the spatial resolution of 40 meters is seemingly poor, the resolution on elevation of the 40-m DTM is within one meter, which is rather good and is the main reason for the analyses. Several cross sections of high-precision topographic measurements were carried out where artificial impacts on topography are visibly less intense. Results of analyses from boreholes of the Central Geological Survey (Lin et al., 1999; Lin, 2001; Huang, 2003; Huang et al., 2007; Song et al., 2007; Chen et al., 2010) are also taken into account, which suggested that the possible fault trace and related geomorphic features should be parallel and east of the eastern topographic boundary of the Linkou Tableland within the Taipei Basin. However, these features like fault scarps are prone to fluvial and artificial modification, making their identification challenging. In order to better describe its geomorphic characteristics, the Shanchiao Fault zone is divided into 3 areas from north to south: the northern Beitou area which is north of the Tanshui River (Fig. 4-2), the middle Wuku area (Fig. 4-4), and the southern Hsinchuang-Shulin area (Fig. 4-6).

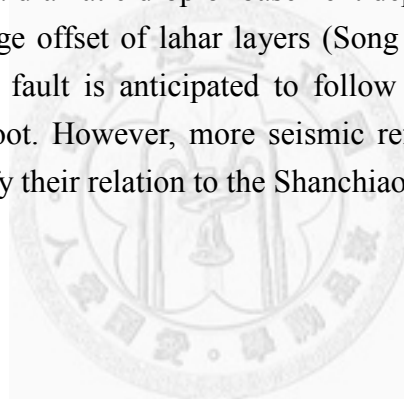
Topographic profiles extracted from 40 m DTM in regions where borehole data were available are first examined. By comparing them local topographic pattern in the fault zone is constructed; then the features are traced laterally. Field measurements were carried out in places where original landform was thought better preserved. After eliminating artificial effects on topography, the area maps of the surface fault scarp traces of the Shanchiao Fault are constructed based on remnant natural geomorphic features.

4.3.1 North of the Tanshui River (Beitou area)

To the northwestern part of the Beitou area, the northernmost of the Shanchiao fault within the basin is probably covered by a large alluvial fan where fluvial effects made geomorphic interpretation difficult. Southwest away of this fan one river terrace is clearly visible along the edge of the NE-SW trending hills (terrace level V, Fig. 4-2) with a few small higher flat surfaces possibly representing remnant older terraces (i.e., terrace level II and III). A break of slope can be observed southeast of the terrace risers (see Profile 1 in Fig. 4-3), which is interpreted as the remaining of geomorphic scarp of the Shanchiao fault. A pair of CGS boreholes showed a drastic difference of basement depth across this slope break (SCF-12 with basement depth 4 m and SCF-10 with basement depth 78 m), supporting that these subtle scarps are in close relation to normal faulting on a branch of the Shanchiao Fault. These scarps about 1 m in height represent gentle slopes fringing the hillsides and terrace cliffs to the west. It can be

speculated that they might be formed through incremental faulting of the Shanchiao Fault. These scarps generally follow the MRT subway route in the northern part of this area, and become vague (also possibly branched) near the MRT Guandu station (Fig. 4-2). Combining analysis of borehole SCF-11 further southeast with SCF-10 and 12, Song et al. (2007) suggested the main offset of the fault should be located between SCF-10 and SCF-11 based on the correlation and depth displacement of lahar deposits, while no clear geomorphic features corresponding to this offset can be found.

Further southwest in the southern part of Beitou-Guandu area human constructions and land use have significantly altered the original topography. Two steps of topographic scarps have been recognized (see Profile 2 in Fig. 4-3) and mapped (Fig. 4-2). The western scarp is roughly 3 m in height, and the eastern one is a gentle slope of 2 m in height. The western one is of similar topographic location and configuration of identified fault scarp in Profile 1. On the other hand, the borehole data (SCF-7~9) indicate that the main Shanchiao fault lies possibly between boreholes SCF-8 and SCF-9, where a dramatic drop of basement depth observed from 140 m to 365 m together with a large offset of lahar layers (Song et al., 2007; Fig. 4-3). The surface trace of the main fault is anticipated to follow a subtle geomorphic scarp sub-parallel to the hills foot. However, more seismic reflections and borehole data would be helpful to identify their relation to the Shanchiao Fault.



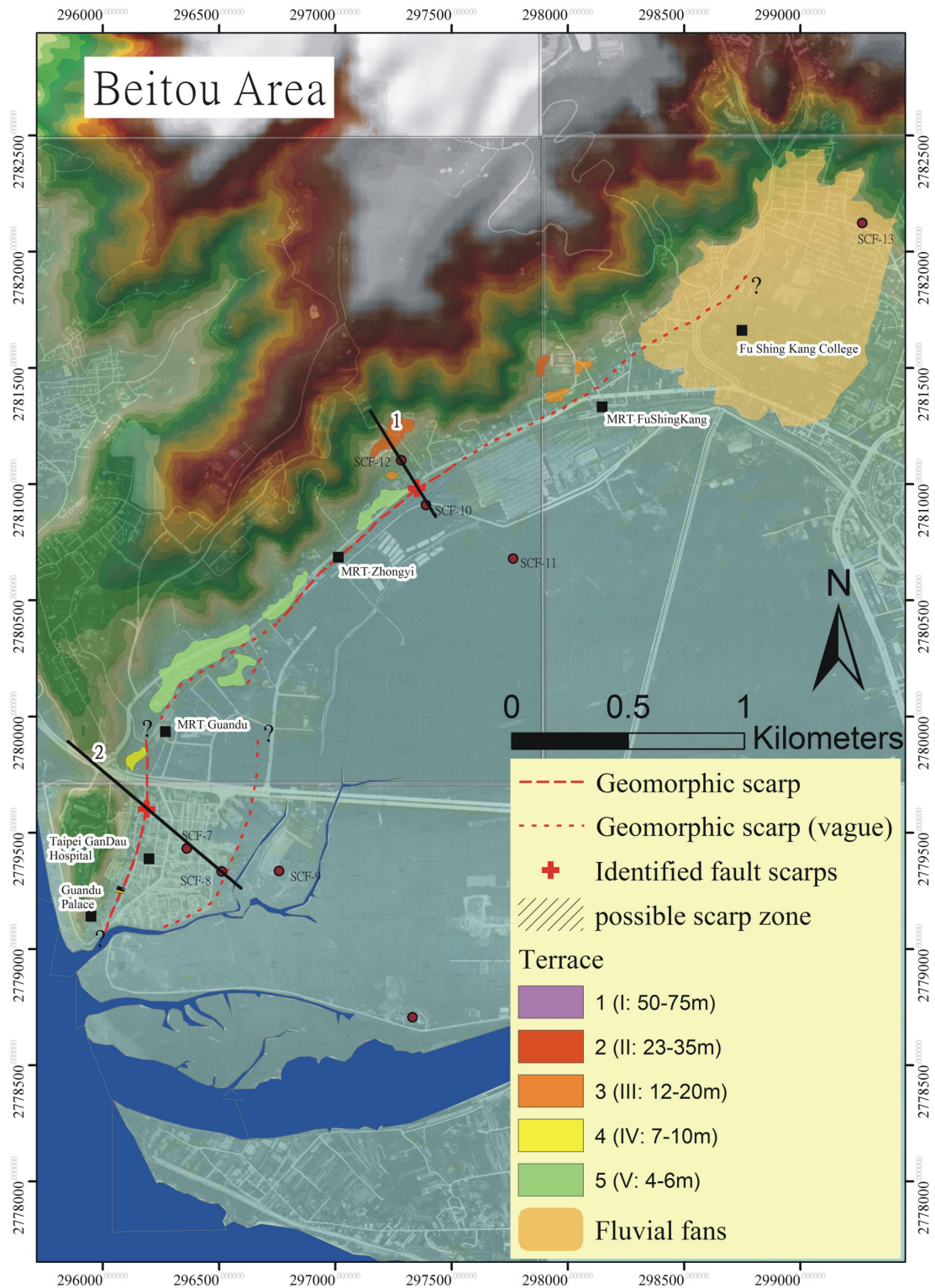


Fig. 4-2. Map of the surface trace of the Shanchiao Fault in the Beitou area. The coordinate shown is of TWD 67 Transverse Mercator system.

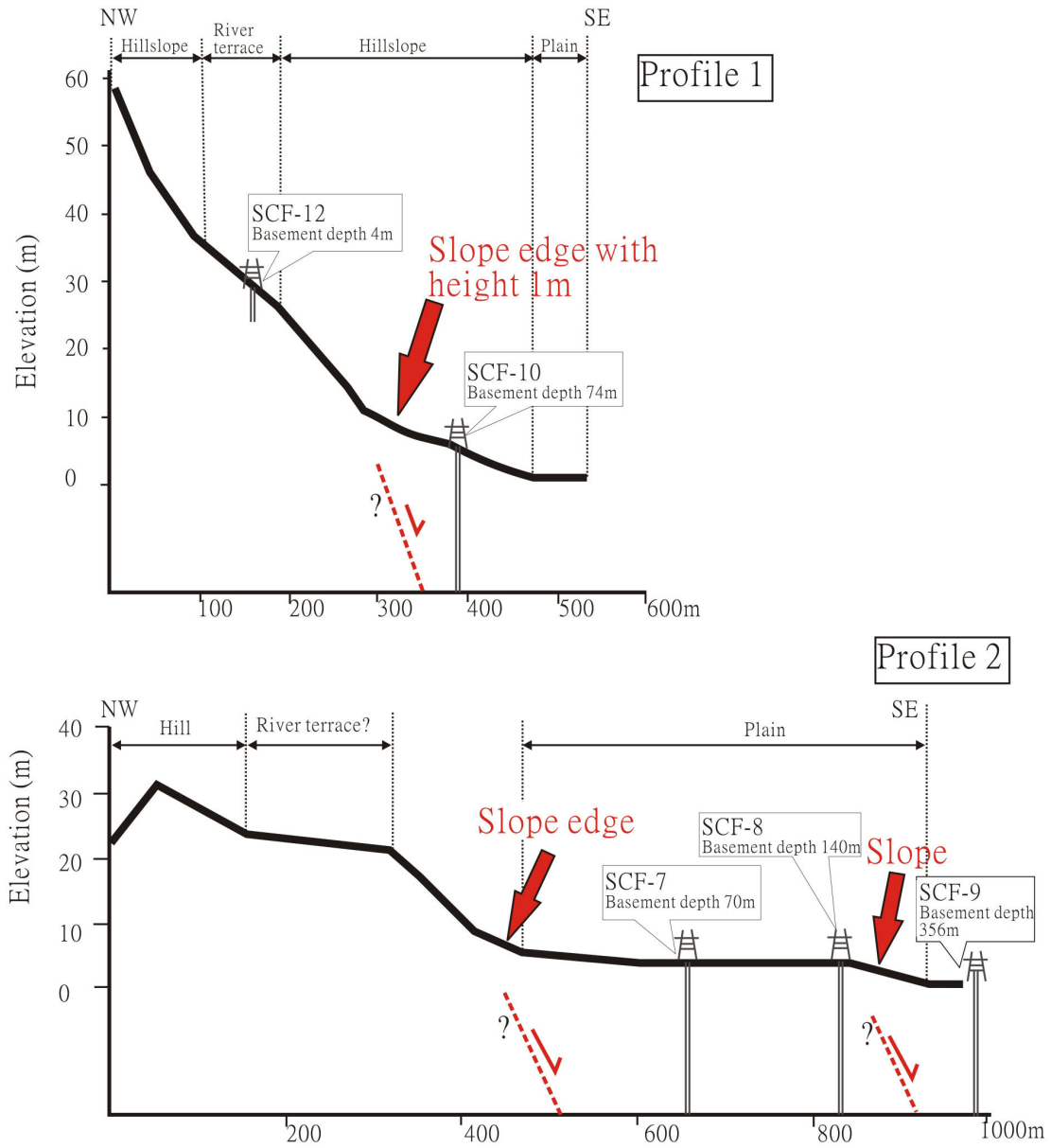


Fig. 4-3. Topographic profiles across the Shanchiao fault in the Beitou Area.

4.3.2 Wuku area

In the Wuku area, more than two different levels of terraces and three alluvial fans (from north to south, Guanyinkeng, Wukukeng, and Taishan) are recognized (Fig. 4-4). Series of gentle slopes are commonly present east of the terraces and alluvial fans are noticed and interpreted to be the remaining of geomorphic scarps of the Shanchiao Fault as described in the following.

In the northernmost Wuku area, the geomorphic features are much obliterated by the Guanyinkeng alluvial fan. The boreholes SCF-5 (basement depth 122m) and SCF-6 (basement depth 222m) are located across a gentle slope with a height of 0.5 m east of the Guanyinkeng fan (see Profile 3 in Fig. 4-5). This slope is interpreted as a geomorphic scarp of the Shanchiao fault, which has been modified by human construction. This scarp extends north along the edge of Guanyinkeng fan, and does not appear to extend far toward the south because scarp-like forms are no longer recognized, where the fault surface trace is interpreted to have jumped a little to the west (Fig. 4-5, the western scarp on Profile 3) which might also extend further north. Patches of level V terraces (the lowest terrace) can be mapped between the Guanyinkeng Fan and the Wukukeng Fan. The linear terrace risers are interpreted to be possible fault-related features as illustrated on the map (Fig. 4-4).

Farther south around the Wukukeng alluvial fan, the fault scarp is interpreted to closely follow the margin of the fan. In this region, the surface trace of the Shanchiao fault seems to extend to an embankment in the north and to follow a N-S trending road in the south. A series of profiles (Profiles 4, 5, and 6 in Fig. 4-5) demonstrate various observed geomorphic features, including river channel, ancient river bed, scarp, etc. After discriminating fluvial and artificial effects to topography in Profile 4 (Fig. 4-5), a scarp with height 2 m is recognized bounding the edge of the Wukukeng Fan which is interpreted to be a possible fault scarp. In Profile 5 (Fig. 4-5), boreholes SCF-3 (which didn't reach the basement at the depth of 75 m) and SCF-4 (basement depth 40m) might be located across the Shanchiao Fault, although the conclusion can not be drawn because of the insufficient depth reached of the SCF-3. A vague scarp is present near SCF-3, however, has been modified due to human land use. By contrast, to the south near the Taishan Fan, a scarp of about 2 m in height, across which drilled cores (SCF-1 and SCF-2, see Profile 6 in Fig. 4-5) revealed vertical offsets of upper tens of meters layers in stratigraphy (Huang et al., 2007), is considered the fault scarp here.

Between the Wukukeng Fan and the Taishan Fan, several levels of terraces can be mapped, while whether all of them were fluvial in origin is uncertain, especially for the higher ones. Two prominent terrace risers are present between level III and level

IV terraces, and the eastern edge of the level IV terraces (Fig. 4-4). The interpreted fault trace delineated from scarps recognized from Profiles 4, 5, 6 lies east of all the above terrace risers. Around the Taishan alluvial fan, sedimentary features dominate topography which made identification of the fault scarps difficult. Together with dense human constructions, the geomorphic features in the southern part of the Wuku area are significantly altered. Nevertheless, series of gentle slopes as drawn by the dashed south-trending lines can still be observed (Fig. 4-4), but the surface trace of the fault remains uncertain.



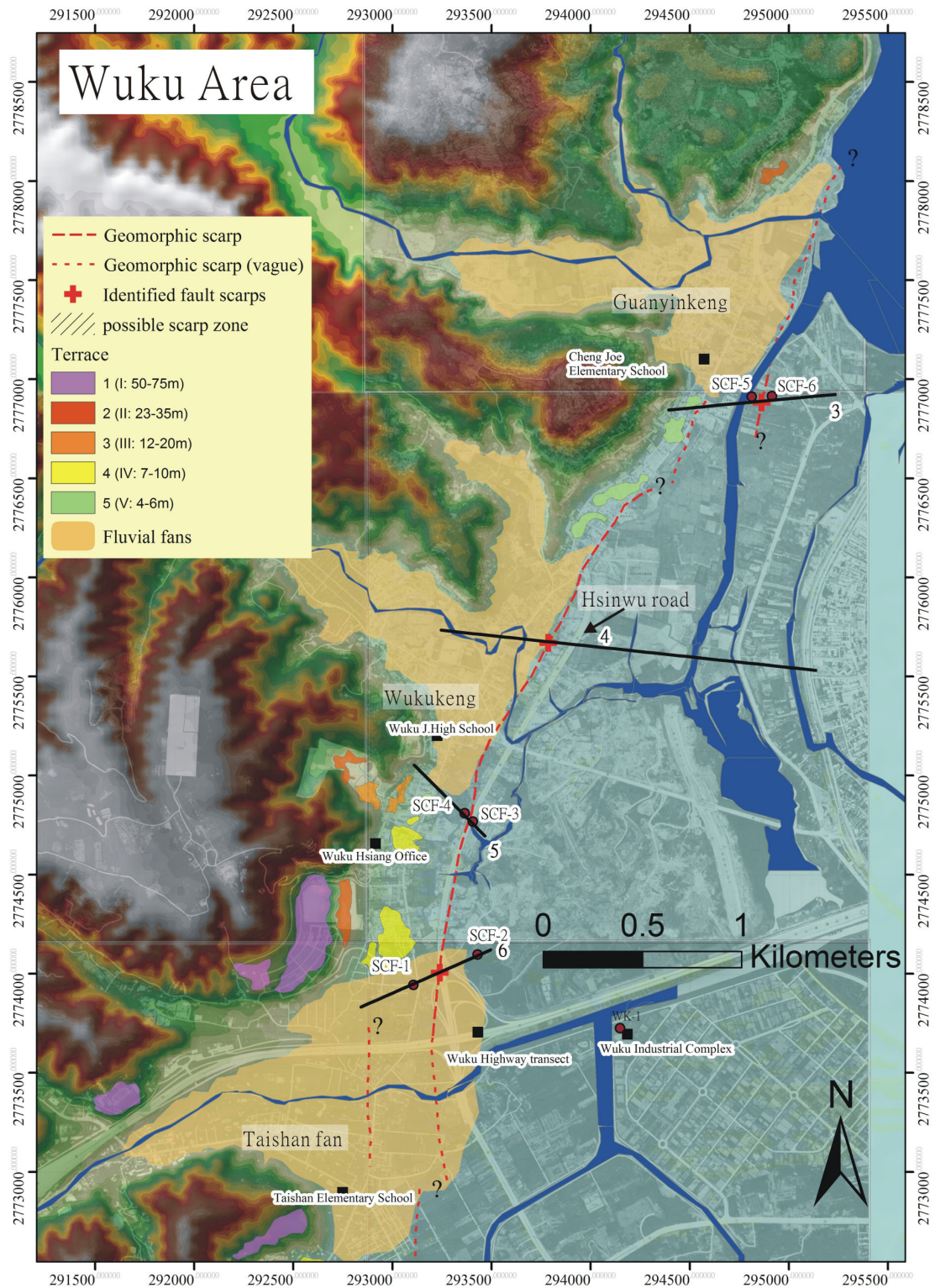


Fig. 4-4. Map of the surface trace of the Shanchiao Fault in the Wuku area. The coordinate shown is of TWD 67 Transverse Mercator system.

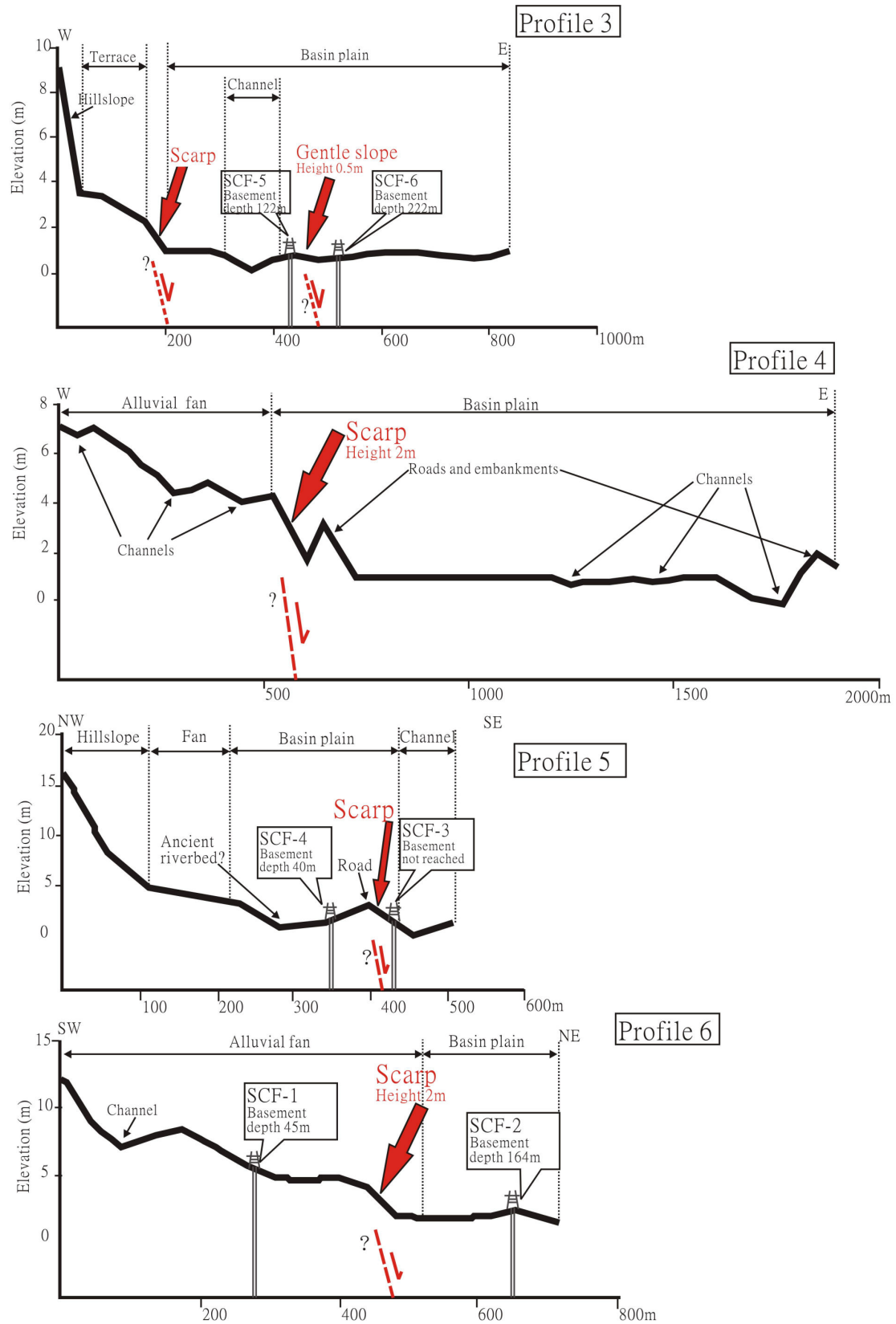


Fig. 4-5. Four topographic profiles in the Wuku Area.

4.3.3 Hsinchuang-Shulin area

In this section, the 40-m DTM indicates relatively clear geomorphic scarps with height around 1 m in the middle-northern part (Fig. 4-6 and Profile 7 in Fig. 4-7). In this area, high-resolution topographic surveys are carried out along four E-W trending roads (Fig. 4-6 and 4-8): from north to south, Hsinsheng road, Tali street, Hankou street, and Hsoushan road. The trends of the roads are approximately perpendicular to the strike of the Shanchiao Fault, in order to better characterize geomorphic features associated with fault scarp. Detailed topography on the four roads is mapped using a Trimble Geomatics total station. The topographic profiles obtained through these measurements have a precision of 1-2 centimeters for both horizontal and vertical components. Distinct geomorphic scarps can be observed to lie along east of the N-S trending Mingchih road (Figs. 4-6 and 4-8). On the Hsinsheng road section (profile A) a geomorphic scarp of approximately 30 cm in height is interpreted to be related to the Shanchiao Fault (Fig. 4-8). In profile B of the Tali street, a subtle topographic scarp 70 cm high is present in the eastern half of the profile. Near the western end of the profile, the rugged slope may correspond to the northern termination of the next segment to the south. Profile C (measured along the western part of Profile 7), about 300 m south of Profile B, shows a similar but westward-displaced geomorphic scarp with height of around 65 cm, although it may have been slightly enhanced by road construction. Further south in profile D a clear scarp 80 cm in height is present on the Hsoushan road; however, the original landform of this scarp seems also to be enhanced during road construction. The interpreted fault trace from the geomorphic scarps observed on Profiles A and B extends northward into a geomorphically diffuse zone and becomes obscure around Yi-Shiue Junior High School. In this section, the fault trace appears to be segmented in an en-echelon manner near Mingchi Technological University between Profiles B and C (Fig. 4-6). Although there are large population and dense buildings in the survey area, it is found that original geomorphic features and patterns are still present despite artificial alteration, probably due to lack of mass building projects in the region which usually involve higher degree of landform modification over larger portions of land. The similar topography shown on Profile 7 (extracted from 40-m DTM) and Profile C (obtained from field measurement) further strengthens the reliability of the analysis.

Southwards into the southern part of the Hsinchuang-Shulin area, the topographic scarps become increasingly difficult to be recognized. In this area where two large fans dominate topography, a scarp identified from Profile D travels south into a zone of subtle slopes observed on the topographic profile of 40-m DEM (Fig. 4-7, Profile 8), which is considered to be the most-likely geomorphic fingerprint of the Shanchiao Fault. Further south series of roughly N-S trending scarps/slopes are mapped on two

subtle slopes within the fan with much speculation.

In the southernmost part of the Shulin area, the topography is controlled by fluvial processes of the Tahan River. Along with dense constructions of buildings and roads, identification of fault scarps becomes extremely difficult. A group of four boreholes (SCF-14~17) by Central Geological Survey are located near the Shulin industrial park (Fig. 4-6 and Profile 9 in Fig. 4-7). Based on stratigraphic analysis of the boreholes, a normal fault, possibly a branch of the Shanchiao fault, was interpreted to lie between SCF-15 (footwall) and SCF-16 (hanging wall) (Huang et al., 2007). A scarp zone was therefore mapped on Fig. 4-6 and Profile 9 which has poor lateral persistency. It can be speculated that lack of clear topographic marks related to the Shanchiao Fault might be a result of depositional effect from the Tahan River; another possibility is that the offset of the Shanchiao fault decreased significantly in the southernmost tip of the Shanchiao Fault. The second speculation is consistent to results from borehole analysis (Huang et al., 2007) and will be addressed in section 4.4.3.



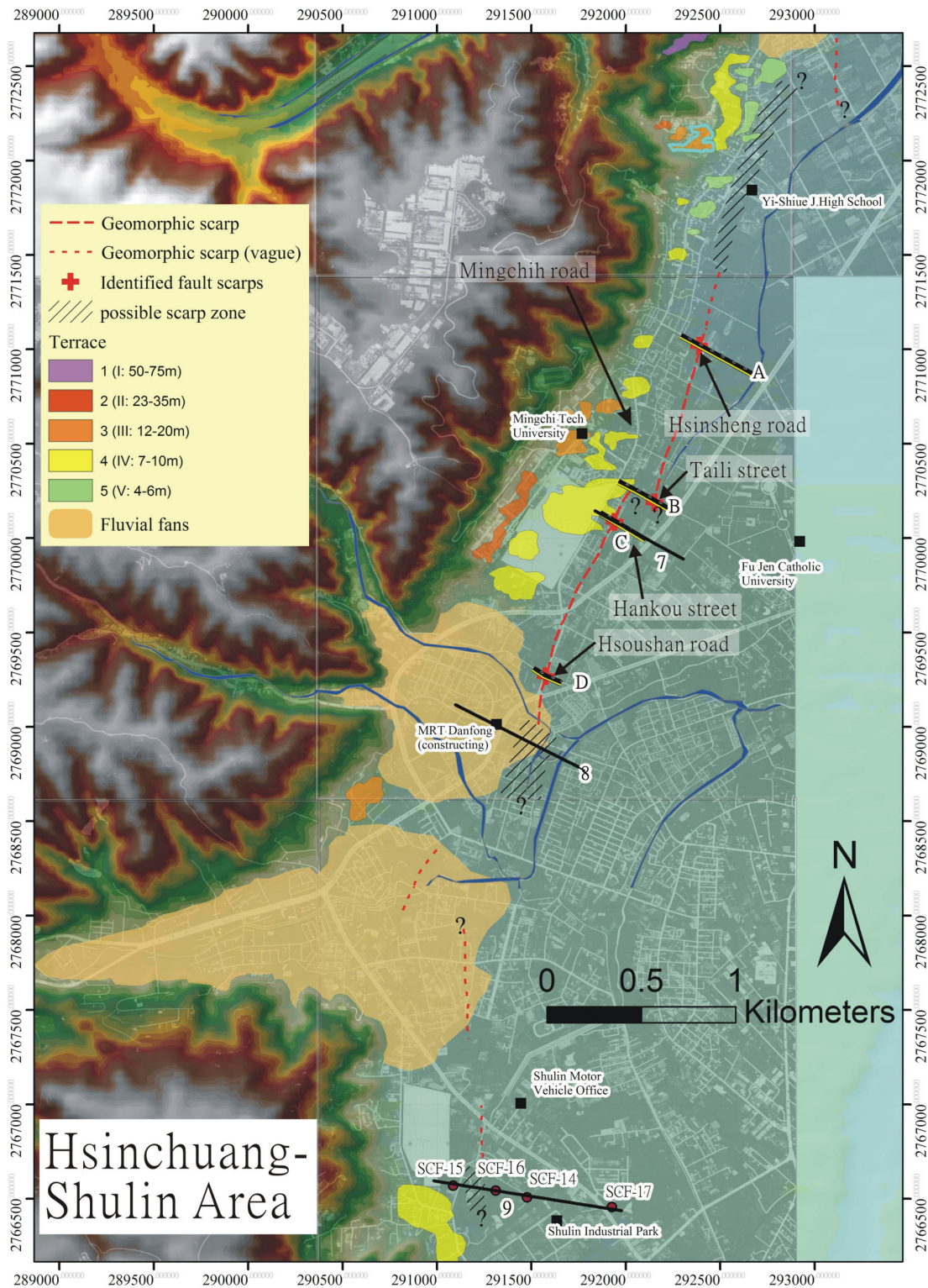


Fig. 4-6: Map of the surface trace of the Shanchiao Fault in the Hsinchuang-Shulin area. We carried out four field measurements in the northern portion of this area as Profiles A - D. The coordinate shown is of TWD 67 Transverse Mercator system.

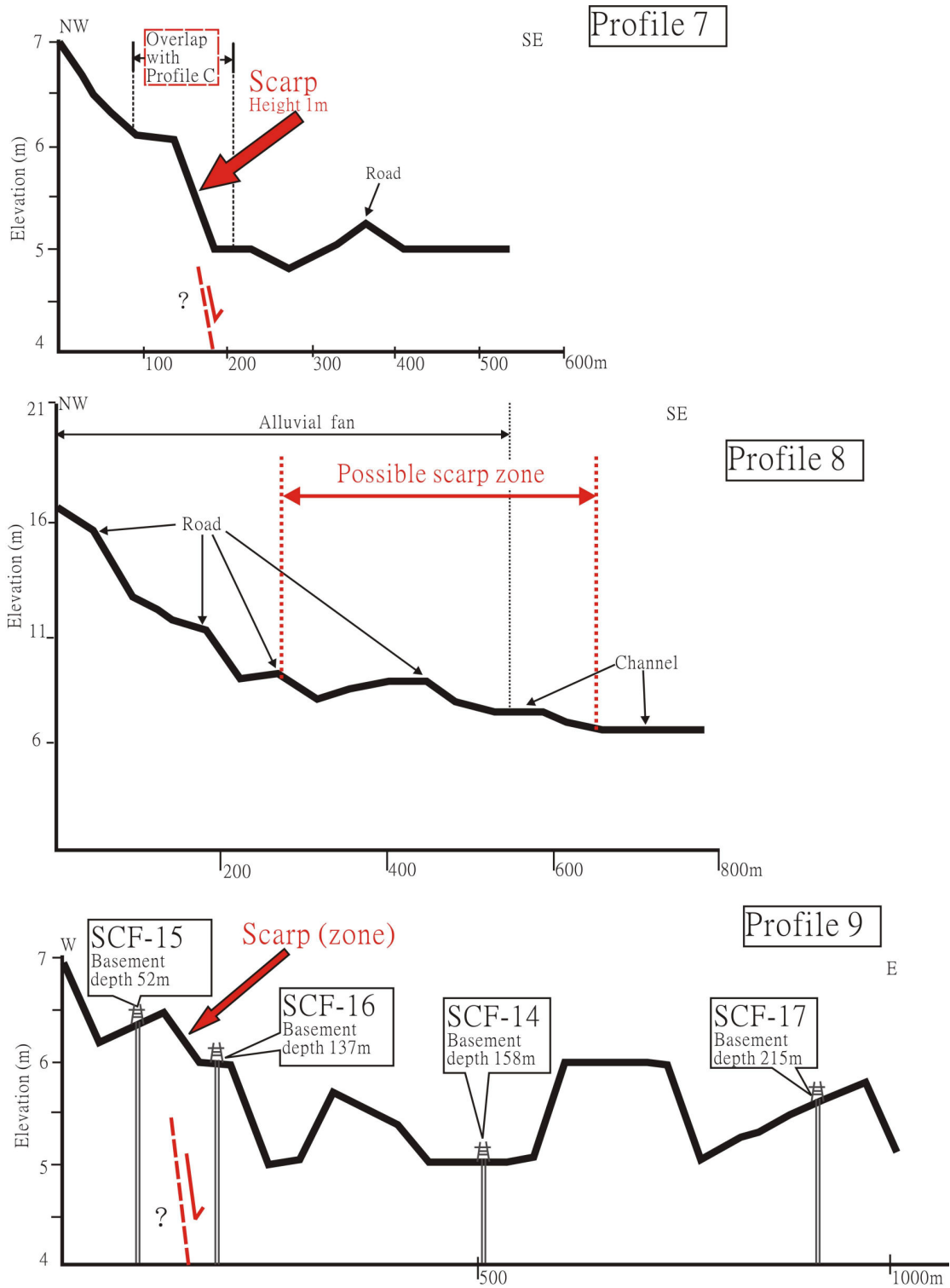


Fig. 4-7. Topographic profiles in the Hsinchuang-Shulin area. The anticipated fault scarp in Profile 7 was measured in great detail as Profile C in Fig. 4-8.

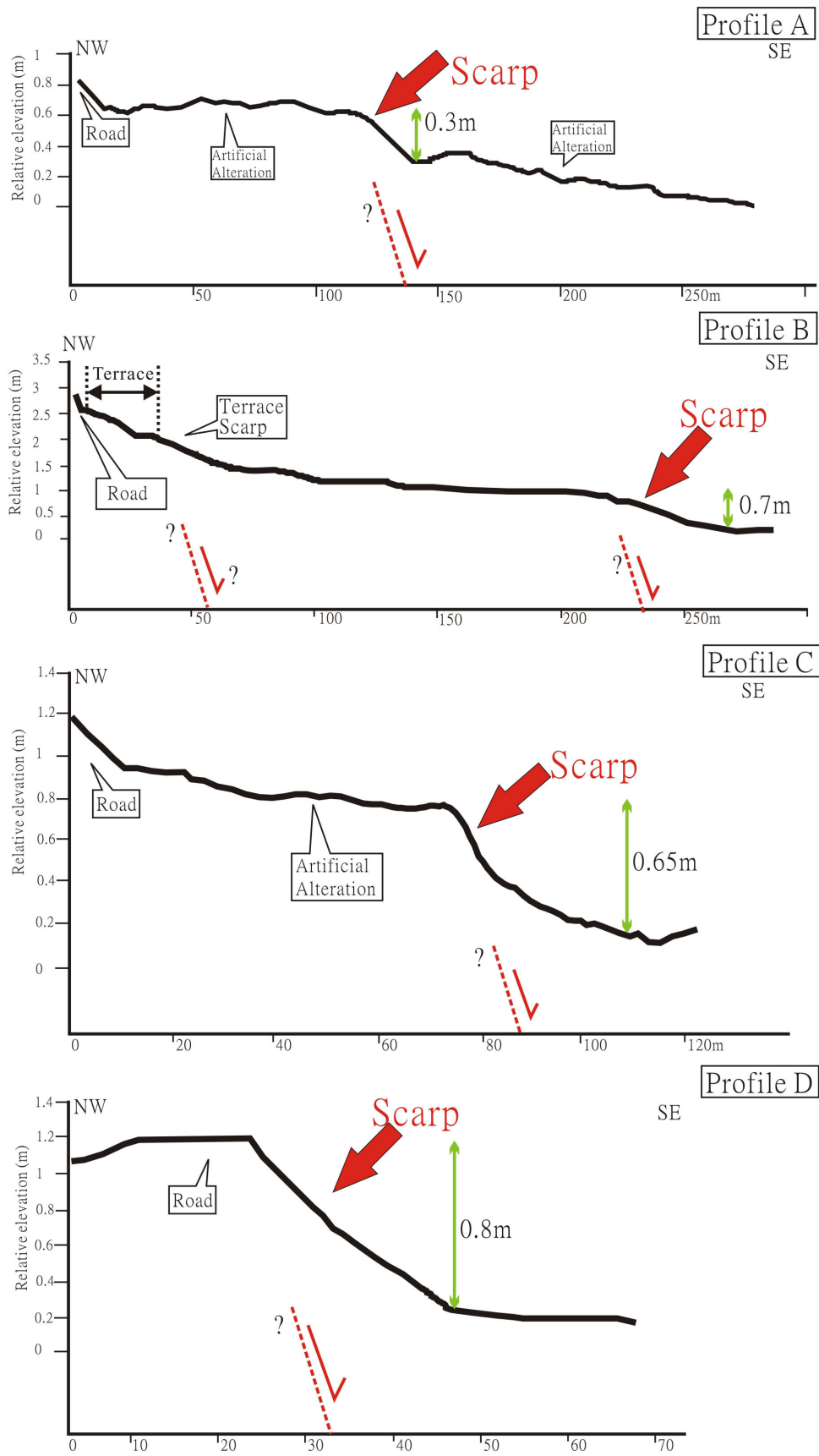


Fig. 4-8. High-resolution topographic profiles in north Hsinchuang-Shulin area. These four profiles of topography were obtained by field measurements using Trimble Geomatics total station. Various features we identified are marked.

4.4 Fault zone structure

In highly urbanized regions like the Taipei metropolis, contemporary records are usually contaminated by artificial activities, preventing accurate determination of fault location and activity history such as slip rates and past events. For instance, both leveling data and InSAR data of the past few decades contain signals from not only the tectonic subsidence from the Shanchiao Fault and the natural compaction of the loose Holocene basin deposits, but also groundwater pumping-related aquitard compression and post-pumping aquifer elastic rebound (Chapter 2; Chen et al., 2007; Chang et al., 2010); topography along the western margin of the Taipei Basin is significantly altered by construction and transportation development making fault scarp identification difficult (section 4.3; Chen et al., 2006). Direct constraints should rest within the syn-faulting sediments recovered by boreholes. In the central portion of the Shanchiao Fault three closely-located and well-documented boreholes in the Wuku Profile revealed growth faulting dominated by slips of the Shanchiao Fault and tied to the eustatic sea level change (Chapter 3; Chen et al., 2010). Below the sedimentation history and the inferred fault structure in the Wuku Profile is briefed, and analysis of boreholes in the north-central portion of the fault in the Luzhou Profile is presented indicating such growth faulting is characteristic to the Shanchiao Fault.

4.4.1 Growth faulting at the Wuku Profile in the central portion of the fault

The SCF-1, 2, and WK-1 boreholes are located east of the Taishan Fan within the Taipei Basin (Fig. 3-2). All of the three boreholes penetrated the basin sediments and reached the basement rocks. The basement is shallow in the western SCF-1 well (45 m) and shows a dramatic dive between SCF-2 and WK-1 (from 164 m to 679 m; Figs. 3-2B and 3-3). The lowermost of the basin deposits, the Banchiao Formation, exists only in the easternmost WK-1 well and the overlying Wuku Formation found in SCF-2 and WK-1 thickens and deepens to the east (Fig. 3-3). A considerable hiatus preceded the sedimentation of the Jingmei Formation (or called the Jingmei Conglomerate) as alluvial fan deposit resulted from the diversion of the Tahan River into the Taipei Basin around 25 ka (Teng et al., 2000b, 2004), which is of roughly the same thickness (~30 m) in SCF-2 and WK-1 and capped weathered basement rock in SCF-1 with thickness of 10 m. Mimicking the basement geometry, the Jingmei Formation is deeper toward the east and the youngest basin deposit the Sungshan Formation above forms a eastward-thickening wedge. The Sungshan Formation in the Wuku area can be divided into three members: the lower C3 unit consists of fluvial sands and mud, deposited right after the completion of the Jingmei Formation (~23 ka) at WK-1, but in SCF-2 and 1 the deposition lagged much behind starting at 12 and 10 ka, respectively, indicating substantial and westward-increasing hiatus between the Sungshan and Jingmei sedimentation (Huang et al., 2007; Chen et al., 2010). Since 10

ka, the entire Taipei Basin was flooded with contemporaneous deposition, leading to a major marine incursion at 9 ka forming the C2 estuarine-lacustrine sediments till 8.4 ka, followed by the C1 deposition of alternating estuarine and fluvial sediments. Marine mollusks are frequently encountered in the C1 and C2 units but not in the C3 unit across the wells confirming the synchronous change of sedimentary environment and facies, while the top horizons of the C3 and C2 units at 9 and 8.4 ka, which are probably pretty horizontal at the time of formation, are downward-displaced to the east. In summary, within the one-kilometer-long Wuku Profile, all basin sediment units are thickened and down-offset to the east as the hanging wall of the Shanchiao Fault.

To understand how these sediments were stacked in the fault zone it's necessary to consider the eustacy as the basin floor is close to sea level and the proximity of the sea to the basin. During the LGM the basin ground, composed of the Wuku Formation, stood out roughly 70 m higher than the then sea level, and was therefore subject to erosion preventing sustainable preservation of fault-related topographic features. Around 25 ka in the height of the LGM, the Tahan River, which flew westward into the Taiwan Strait through Taoyuan before, was captured into the basin and rapidly dumped a large alluvial fan originated from the southwest and covers most of the basin, forming the Jingmei Formation in a very short period within 25 to 23 ka (Teng et al., 2004) with its top horizon being flat and regular as the expected alluvial fan surface. The present configuration of the eastward deepening of the Jingmei Formation top horizon in the Wuku Profile, which was at right angle to the river channel during sedimentation, is the result of normal faulting after the alluvial fan deposition was finished. Following the Jingmei fan formation, although the sea level began to rise at ~20 ka (Yokoyama et al., 2007), the basin ground was still much elevated relative to the then sea level until ~12 ka and fluvial sediments were only allowed to accumulate on the near-fault hanging wall region like the site of WK-1, as the Shanchiao Fault continued to be active since at least ~23 ka. It was around 12 ka the sea level was approaching basin ground and the fluvial sediments were able to onlap to the less-subsided area as the site of SCF-2. At 10 ka the basin ground surface and sea level were even permitting basin-wide sedimentation and led to simultaneous sedimentation in all of the three borehole sites across the fault zone. The excellent age-depth correlation between unit horizons and corresponding sea level height in the Sungshan Formation at SCF-1 confirms that the SCF-1 sits on the footwall and the basin deposits were dominated by the rise of sea level since the Last Glacial Maximum (Chen et al., 2010). The deepening of horizons and thickening of units in the east at SCF-2 and WK-1 came from additional room for sedimentation provided by tectonic subsidence of slips on the Shanchiao Fault (Huang et al., 2007), thereby

allowing estimations on vertical fault slips during the deposition of the units by simple ‘back-stripping’ demonstrated in Fig. 3-6.

It’s revealed that the Shanchiao Fault zone in the Wuku area is composed of a main fault between the SCF-2 and WK-1, and a branch fault between SCF-1 and 2 which was considered to be the master fault (Lin, 2005) with Holocene paleo-earthquakes (Huang et al., 2007) but actually accounts for only about 1/3 of total vertical deformation. The main fault which slipped 51 m since the LGM seems to follow the steep basement drop between SCF-2 and WK-1 then extend upward, and the branch fault which slipped only about 28 m in the same period is developed on the sediment-basement rock interface as the sheared section containing slickensides of normal plus sinistral sense recovered in the lowermost basin deposits in SCF-2 (Lee et al., 1999), together the fault zone exhibits a half negative flower structure, or half tulip structure, inherited from the transtensional nature of the Shanchiao Fault (Fig. 3-2B; Lee et al., 1999; Rau et al., 2008). The post-LGM averaged tectonic subsidence rate as calculated from offsets of the top of the Jingmei Formation is about 3 mm/yr on the hanging wall and is about 1 mm/yr on the extensional fault block bordered by the main and branch faults, and the Holocene rate calculated from C1 deposition is quite similar (Fig.3-8). Concerning the link between topography and the fault zone structure, the fault scarp delineated in this area (section 4.3.2; Chen et al., 2006) corresponds to branch fault; region east of the scarp is flat except some channel and artificial features, and the elevation is very close to sea level (about 2 m.a.s.l.) that any fault scarps are easy to be erased by sedimentation (Fig. 3-9; Chen et al., 2010).

4.4.2 Structure and growth faulting at the Luzhou Profile in the north-central portion of the fault

In the Luzhou area immediately south of the Tanshui River, several well-documented boreholes are available east of the Guanyinkeng Fan in the basin plain (Fig. 4-4, 4-9A). The SCF-5, 6, and LC-1 are boreholes drilled by the Central Geological Survey (CGS) aimed at studying the basin deposits and the Shanchiao Fault (Lin et al., 1999; Huang et al., 2007), and the BH-1 to 9 are boreholes drilled for construction purposes (available from the CGS engineering geology data bank). The Shanchiao Fault was considered to be located between the SCF-5 and 6 boreholes (Lin, 2005) and two paleoseismic events at 11 ka and 9 ka were proposed (Huang et al., 2007). All of the boreholes are close to each other, within a one-km-long profile normal to the trend of the Shanchiao Fault (Fig. 4-9).

Situated in a geological environment similar to that at the Wuku area, analysis of basin sediments recovered in the SCF-5, 6 and LC-1 boreholes reveals analogue growth strata architecture. The basement is 125 m deep at SCF-5, 221 m at SCF-6 and

deeper than 300 m in LC-1, meanwhile members of basin deposits including the Banchiao, Wuku and Sungshan formations are significantly thickened and down-shifted in the east (Fig. 4-10). As shown in the Wuku Profile, the Jingmei Formation and the Sungshan Formation were accumulated during the latest sea level rise and therefore better preserve the interactions between faulting and sedimentation (Chen et al., 2010). The Jingmei Formation is thicker towards the east (21.5 m, 26.5 m, 31 m at SCF-5, 6 and LC-1, respectively), probably reflecting the difference in height of the eroded basin ground composed of the Wuku Formation before the formation of the Jingmei alluvial fan; while the top horizon of the Jingmei Formation should be rather flat and regular as the surface of a broad alluvial fan should be, but now it's much deeper in the east (112 m in LC-1 compared to 72.5 m in SCF-6 and 62.1 m in SCF-5). The Sungshan Formation on top again forms an eastward-thickening wedge and exhibits a significant westward-increasing hiatus with the underlying Jingmei Formation (radiocarbon age data summarized in Table 4-1). The three units in the shallowest Sungshan Formation defined in the Wuku area can also be applied in the SCF-5, 6 and LC-1 boreholes due to the similar sedimentary characteristics and identical horizons, while a 4-unit scheme previously defined in SCF-5 and 6 (Huang et al., 2007) for the Sungshan Formation is difficult to be applied to the LC-1 borehole. The lower C3 unit is found between 62 and 50.4 m deep and started deposition at ~ 11 ka in SCF-5, 72.5 to 39.2 m deep starting at ~ 14 ka in SCF-6, and 111.7 to 50 m deep starting at ~ 23 ka as continuous with Jingmei deposition in LC-1 (Teng et al., 2000b). The C2 unit is present at 30.4 to 23.7 m in SCF-5, 39.2 to 29.4 m in SCF-6, and 50 to 33.5 m in LC-1; both the C2 and C1 units thicken and deepen towards the east. Mollusks are abundant in the C1 and C2 units signifying the marine presence in the Taipei Basin since 9 ka. The depths of the key horizons including the tops of the Jingmei Formation, C3 and C2 units in LC-1 are quite similar to those found in WK-1, as well as transgression records inferred from foraminifer assemblages (Huang, 2006).

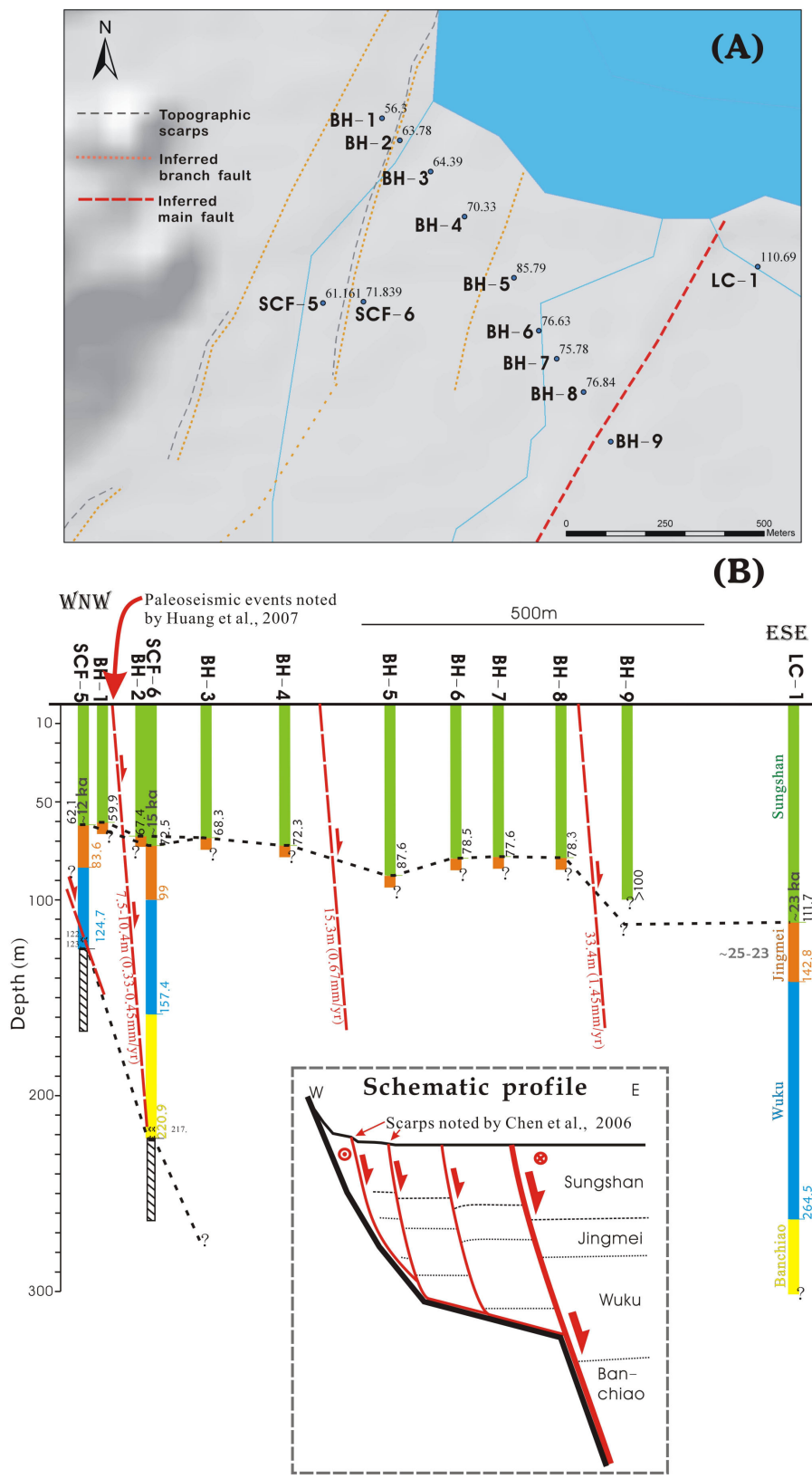


Fig. 4-9. (A) Map of the Luzhou area indicated in Fig. 4-1B, showing locations of the boreholes used in this study, the interpreted Shanchiao Fault trace (dashed lines), and geomorphic features. (B) Interpreted Luzhou geological profile consisted of three westerly branch faults and a main fault to the east, resembles a half-tulip structure.

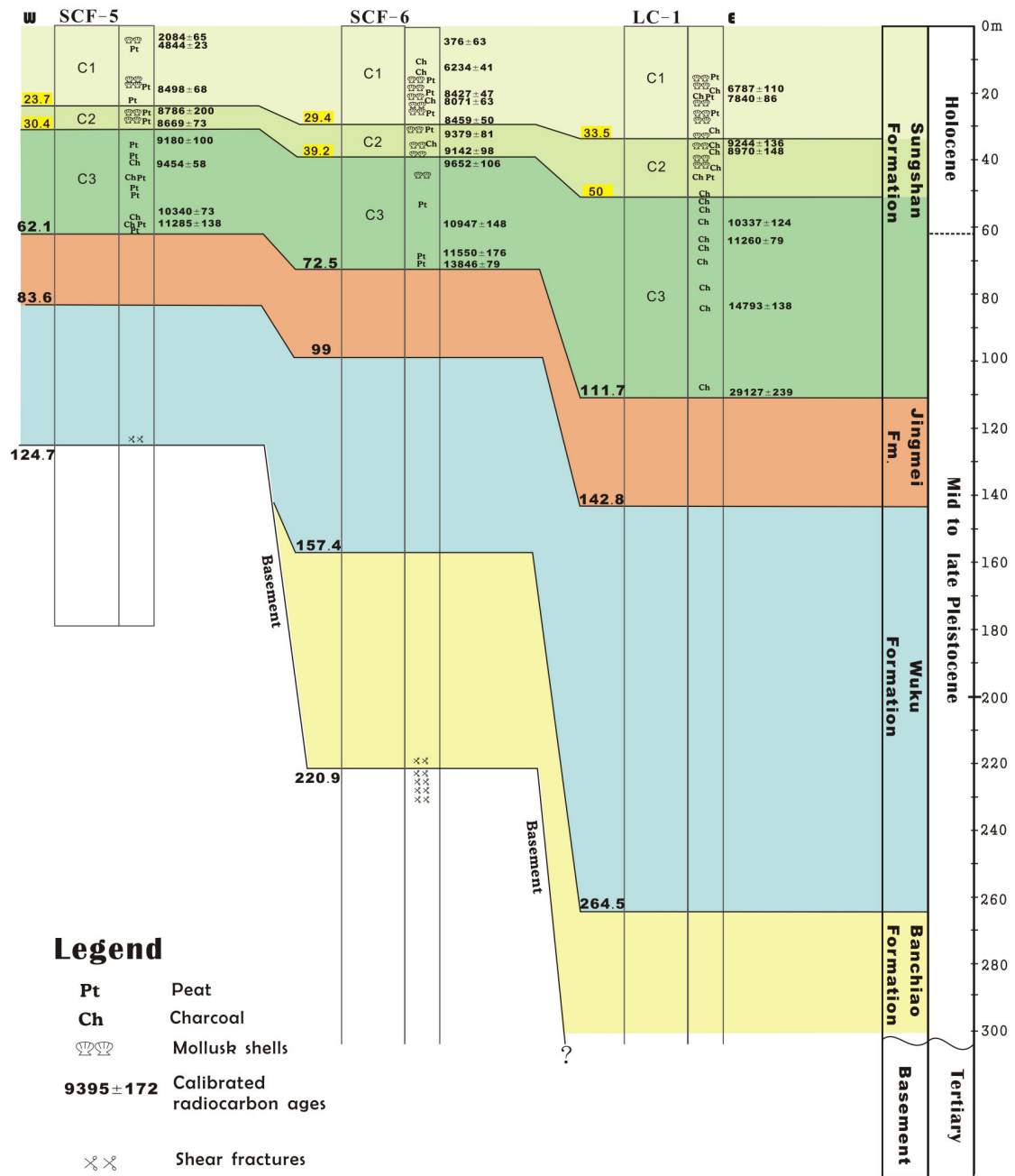


Fig. 4-10. Stratigraphic correlation between boreholes (SCF-5, SCF-6, and LC-1) of the Luzhou Profile. Location of the boreholes is indicated in Fig. 4-9A.

Table 4-1: Radiocarbon age data incorporated in the Luzhou Profile.

Borehole	Data source ^a	¹⁴ C age (yr B.P.±2σ)	Calendar year range ^b (cal. yr B.P.)	Depth (m)	Unit
SCF-5	(1)	2110±40	2019-2149	3.6	C1
	(1)	4280±40	4821-4867	3.9	C1
	(1)	7720±70	8430-8566	18.1	C1
	(1)	7940±130	8586-8986	23.8	C2
	(1)	7890±40	8596-8742	28.4	C2
	(1)	8220±60	9080-9280	34.4	C3
	(1)	8430±70	9396-9280	41.2	C3
	(1)	9200±40	10267-10413	56.8	C3
	(1)	9870±110	11147-11423	58.8	C3
SCF-6	(1)	230±40	313-439	4.35	C1
	(1)	5420±40	6193-6275	12.5	C1
	(1)	7640±60	8380-8474	20.1	C1
	(1)	7263±51	8008-8134	22.7	C1
	(1)	7682±52	8409-8509	29.2	C1
	(1)	8350±60	9298-9460	32	C2
	(1)	8195±63	9044-9240	38.7	C2
	(1)	8700±70	9546-9758	40.4	C3
	(1)	9590±60	10799-11095	58.9	C3
	(1)	10040±70	11374-11726	67.9	C3
	(1)	12044±79	13767-13925	71.1	C3
LC-1	(2)	5960±90	6677-6897	18.3	C1
	(2)	7010±80	7754-7926	21.1	C1
	(2)	8260±90	9108-9380	33.8	C2
	(2)	8060±100	8822-9118	35.7	C2
	(2)	9180±100	10213-10461	58.1	C3
	(2)	9860±80	11181-11339	63.8	C3
	(2)	12700±90	14655-14931	85.1	C3
	(2)	24350±180	28888-29366	109.1	C3

In addition to SCF-5, 6, and LC-1, nine boreholes (BH-1 to 9) for construction use aligned NW-SE were drilled in this area. These boreholes recorded the depth variation of the Jingmei Formation top horizon, as the Jingmei Formation is the last conglomerate to be deposited in most of the Taipei Basin especially the western part. The Jingmei Formation top horizon in the Luzhou Profile displays down-east staircase geometry with three steps (Fig. 4-11A): 7.5 m between BH-1 and 2 where a 10 m offset is also present between SCF-5 and 6, ~ 15 m between BH-4 and 5, and more than 22 m between BH-8 and 9 or up to 33 m between BH-8 and LC-1. Such spaced plunges of Jingmei Formation top depth were not likely to be present when it was deposited considering the form of the original alluvial fan.

Based on stratigraphic correlation of the Sungshan Formation it is revealed that fault offset occurs both between SCF-5 and 6 and Between SCF-6 and LC-1, with the latter containing greater slips. The offset is 4 m between LC-1 and SCF-6 and 5.7 m between SCF-6 and 5 from 8.4 ka till present, and 6.8 m between LC-1 and SCF-6 and 3.1 m between SCF-6 and 5 from 9 ka till 8.4 ka. Taking account the depth changes of Jingmei Formation top horizon in the entire Luzhou Profile, the Shanchiao Fault is made up of a main fault in the east (between BH-8 and 9) and at least two branch faults in the west (one between BH-4 and 5, another between BH-1/SCF-5 and BH-2/SCF-6), whose averaged slip rate since ~ 23 ka is around 1.5, 0.7, and 0.4 mm/yr (Fig. 4-9B). The LC-1 is situated on the hanging wall as the WK-1 in the Wuku area. The branch fault located between SCF-5 and 6 may again rooted in the basin sediment-basement interface as the sheared section at the base of basin deposits recovered in SCF-6. The existence of another sheared section at the base of basin sediment in SCF-5, as well as the deeper depths of key horizons in SCF-5 compared to those in SCF-1 of the upstream Wuku area (Chen et al., 2010), suggests that at least one more branch fault exists west of the SCF-5. As a whole, the Shanchiao Fault in the Luzhou Profile has a form of half tulip structure, containing a main fault extended from the steep basement rise east of borehole SCF-6 and three westerly branch faults developed within the loose basin sediments (Fig. 4-9B). Correlation of lahar layers in the Wuku Formation also agrees with the proposed fault configuration (Song et al., 2007). The entire Shanchiao Fault zone is therefore of several hundred meters wide, and only the two westernmost branches have corresponding fault scarps. Although none of the boreholes of the Luzhou Profile seems to be on the actual footwall of the Shanchiao Fault, exact fault vertical throw and subsidence rate can be inferred by taking the data of SCF-1 on the footwall in the Wuku Profile. The calculated tectonic subsidence rate since ~ 23 ka of the Luzhou Profile is shown in Fig. 4-11D; the hanging wall has been subsiding about 3 mm/yr since the LGM, a rate identical to that obtained in the Wuku Profile in the central portion of the fault (Chen et al., 2010). The

detailed evolution of post-LGM tectonic subsidence in the fault zone is rather complicated as exhibited in Fig. 4-12. The westernmost branch fault west of SCF-5, probably equivalent to the one between SCF-1 and 2 in the Wuku Profile, has had a nearly constant subsidence rate of 1 mm/yr except for non-activity during the C2 deposition (9-8.4 ka). Slip was variably divided among the branch fault between SCF-5 and 6 (Huang et al., 2007) and the main fault between SCF-6 and LC-1; while the two faults combined yielded the slip rates almost identical to that on the main fault (between SCF-2 and WK-1) in the Wuku Profile. Such pattern of varying slip rate partitioning among main and branch faults suggests that fault displacement was not constantly distributed within the fault zone; one particular branch fault may be highly active in some periods or earthquake events while be dormant in other times.

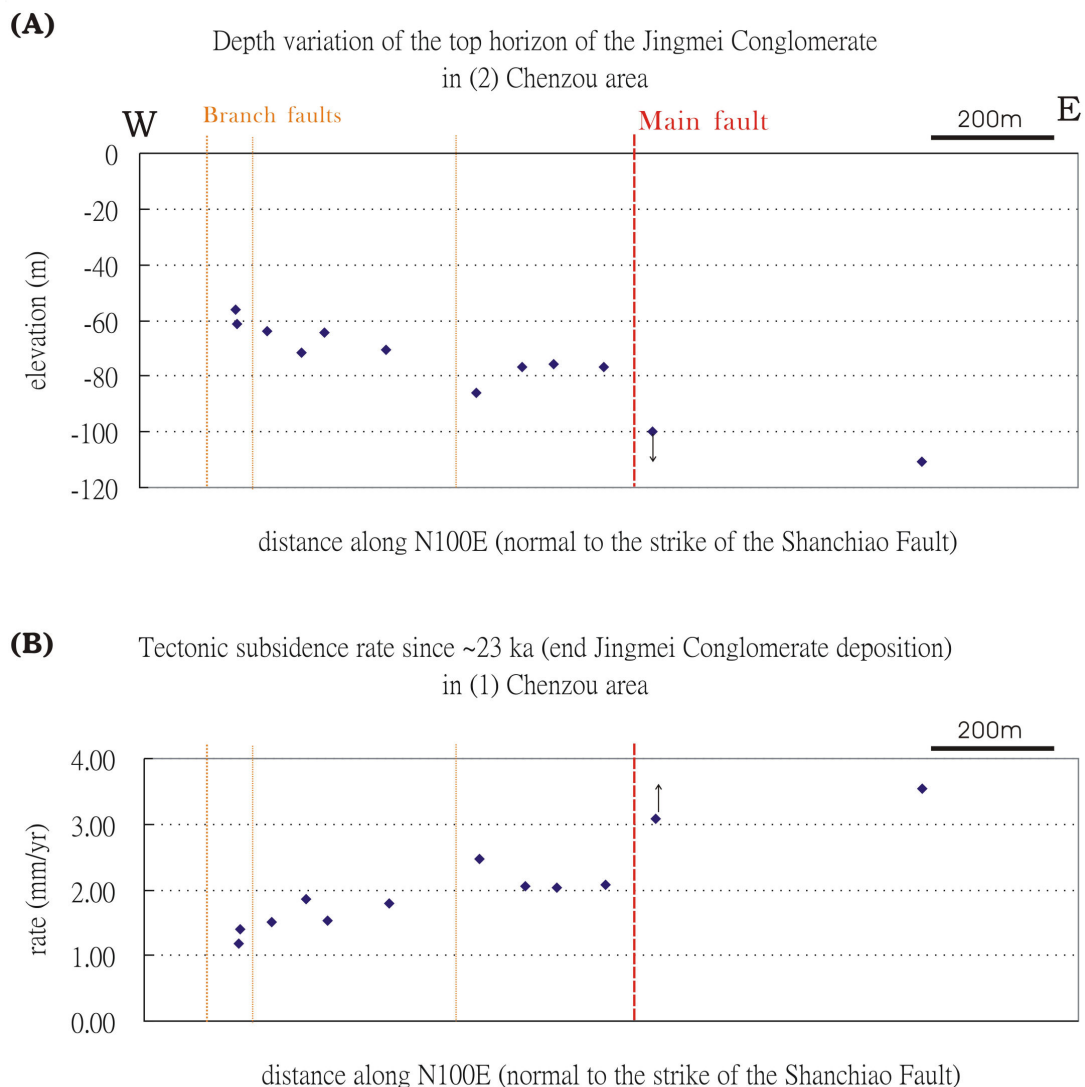


Fig. 4-11. Depth variations of the Jingmei Formation top horizon and the deduced tectonic subsidence rates since ~ 23 ka in the Luzhou Profile

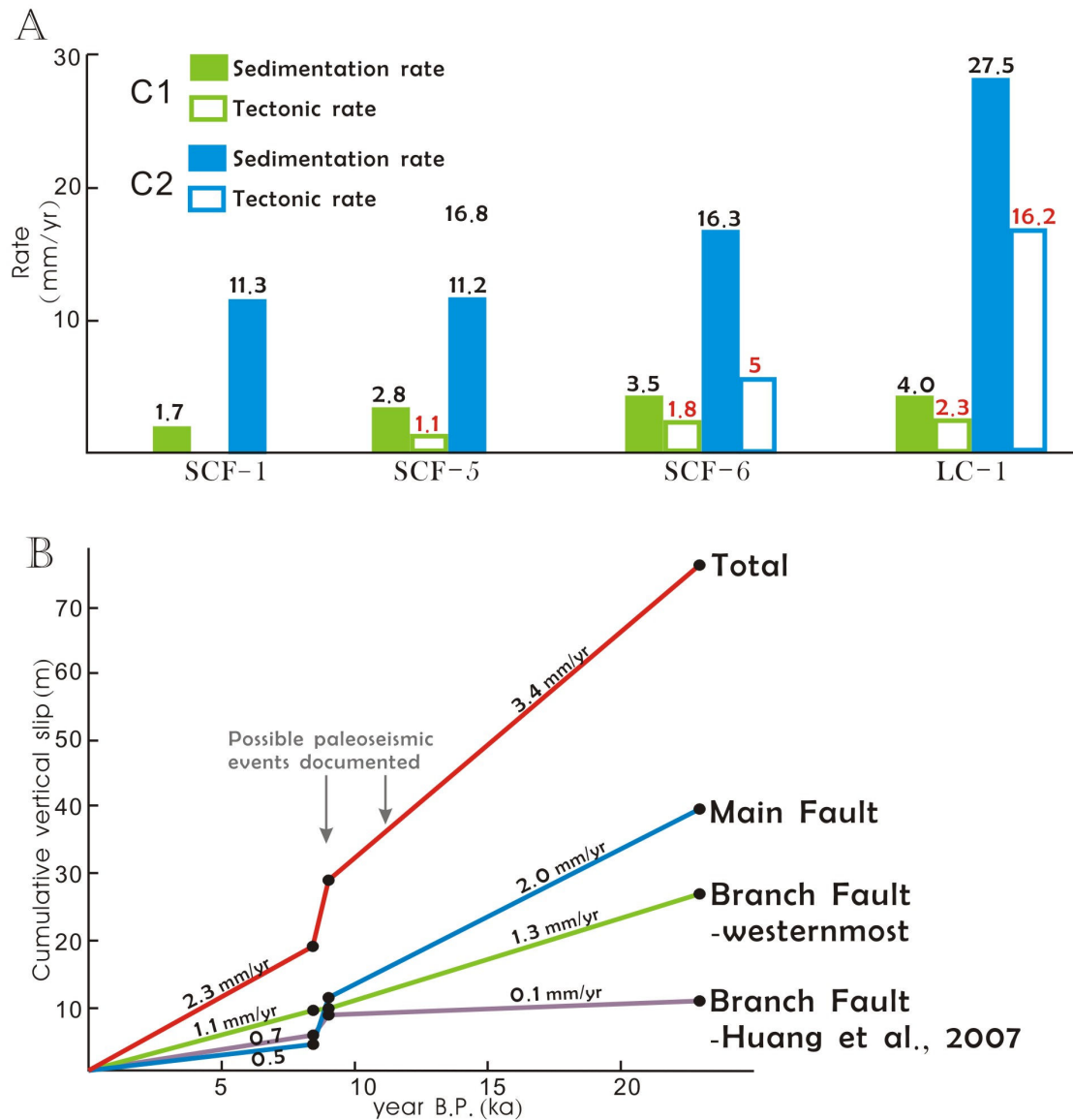


Fig. 4-12. (A) Sedimentation rate and tectonic subsidence rate of the C1 and C2 units at the Luzhou boreholes. (B) Accumulative vertical slips for the Shanchiao fault since the LGM documented in the Luzhou Profile.

4.4.3 Geological interpretation of the Shulin Profile in the southern end of the fault

Four boreholes SCF-14 to 17 located in the Shulin area in the southwest corner of the Taipei Basin (Fig. 4-6) were studied by Huang et al. (2007) aimed at deciphering the exact site of the Shanchiao Fault at its southernmost portion. In great contrast to what is observed in the Wuku and Luzhou areas, the Sungshan Formation is essentially of the same thickness across the Shulin Profile and the Jingmei Formation directly covers the Tertiary basement without the presence of neither the Wuku nor the Banchiao formations (Huang et al., 2007). The lack of Jingmei Formation top offsets and Sungshan Formation thickness variations demonstrates the absence of faulting in the Shulin Profile since ~ 23 ka. The dramatic eastward increase of Jingmei Formation thickness and basement depth can be the product of intense erosion followed by channel deposition during the Tahan River capture event (Teng et al., 2004) other than faulting predating 23 ka, which should either permitted the preservation of older basin sediments (the Wuku or the Banchiao formations) or indicate more than 100 m of fault slips within the 25 to 23 ka period. The Wuku and Banchiao sediments might be present in SCF-14, 16, and 17 before 25 ka but was eroded away during the river capture. The onset of Sungshan Formation deposition was almost at the same time around 10 ka across the wells, suggesting sedimentation here was mostly controlled by the rising eustacy without differential fault-offset on topography. All information available points to the fact that the Shanchiao Fault is not present within the basin plain in the Shulin area. In comparison to records in SCF-1 of the Wuku Profile downstream to the Shulin Profile, the Jingmei Formation top horizon (also the 10 ka sedimentation onset horizon) is slightly lower in the Shulin Profile than in the confirmed footwall in SCF-1. It's tempting to speculate that the entire Shulin Profile is on the hanging wall, and the southernmost Shanchiao Fault is actually westward outside of the Taipei Basin probably following the trace of the Hsinchuang Thrust on the western border of the Shantzujiào terrain.

4.5 Distribution of tectonic subsidence since the Last Glacial Maximum across the Taipei Basin

4.5.1 Jingmei Formation top horizon as a key marker

From growth faulting analysis performed in the Wuku (Chen et al., 2010; section 4.4.1) and the Luzhou profiles (section 4.4.2) in the central portion of the Shanchiao Fault, it's noted that the top of the Jingmei Formation as the original Jingmei alluvial fan surface serves to be a good marker documenting tectonic subsidence succeeding its completion at about 23 ka. The Jingmei Formation top horizon is therefore considered a precious key horizon with the following advantages: 1. the Jingmei Formation was formed in a snapshot in geological sense and is widespread across the basin except in the northwestern corner; 2. the Jingmei Formation top horizon is expected to possess a regular, flat to conical geometry as the top surface of a broad alluvial fan should be; 3. it's a distinct and easy-to-recognize lithological boundary in boreholes as the Jingmei Formation is the last conglomerate to be deposited in the basin except in the northern corner (pyroclastic deposits sourced from the Tatun volcanoes) and the southeastern part (later fan deposits from the Xindian River). What's more, many boreholes drilled for engineering or construction purposes in the Taipei Basin encountered the conglomerate before finishing, making the depth information of this particular horizon widely available. Taking the possible earthquake recurrence interval as 1000 years from paleoseismic investigations by Huang et al. (2007), the Jingmei Formation top horizon has documented fault displacement over ten earthquake cycles and is thus representative of late-Quaternary fault behavior. This work integrates the available borehole records throughout the Taipei Basin to investigate spatial variation of the Jingmei Formation top horizon and the inferred vertical deformation caused by the Shanchiao Fault.

4.5.2 Data and result

The geological drilling data incorporated in this study is acquired from the online open-source borehole data bank maintained by the Central Geological Survey, available on <http://210.69.81.70/geo/frame/gsb88.cfm>. In total 520 borehole records in the Taipei Basin reached the target horizon with clear geological information are assembled in the compilation. While some of them belong to the deep drillings carried out by the Central Geological Survey for research purpose, most of the data are coming from engineering consultation companies for construction purposes. The compilation is presented in Fig. 4-13. The values shown are meters below the (present-day) sea level corrected for the ground elevation of the drilling sites. The Jingmei Formation top horizon exhibits a sharp dive from about 30 m to over 100 m deep in about 1 km at the western border of the basin as documented in Wuku and Luzhou areas (section 4.4.1, 2; Chen et al., 2010). East of the trough the horizon

rapidly rises to 60 m deep in 4 km in the central part of the basin, followed by a much slower ascend back to around 40 m deep at the eastern margin of the basin. The horizon is deeper or non-existent near and north of the lower reach of the Tanshui River channel. The horizon depth is also greater in the central part than in the southern part of the basin, while a slight cone-shape bulge exists in the southeast.

Despite the easy-recognition of the Jingmei Formation top horizon, some minor conglomerate layers deposited later on is known to exist along the borders of the basin, many are colluvial in origin and are thus very limited in spatial and temporal scale, while some may be originated from tributaries of the Tanshui River. When the identification is in doubt, records of nearby boreholes are cross-checked to discriminate local conglomerates from the Jingmei Formation. Nonetheless some data compiled in the eastern part of the basin is marked ‘less certain’ as a caution that the true Jingmei Formation top horizon in the area is ambiguous (Fig. 4-13).

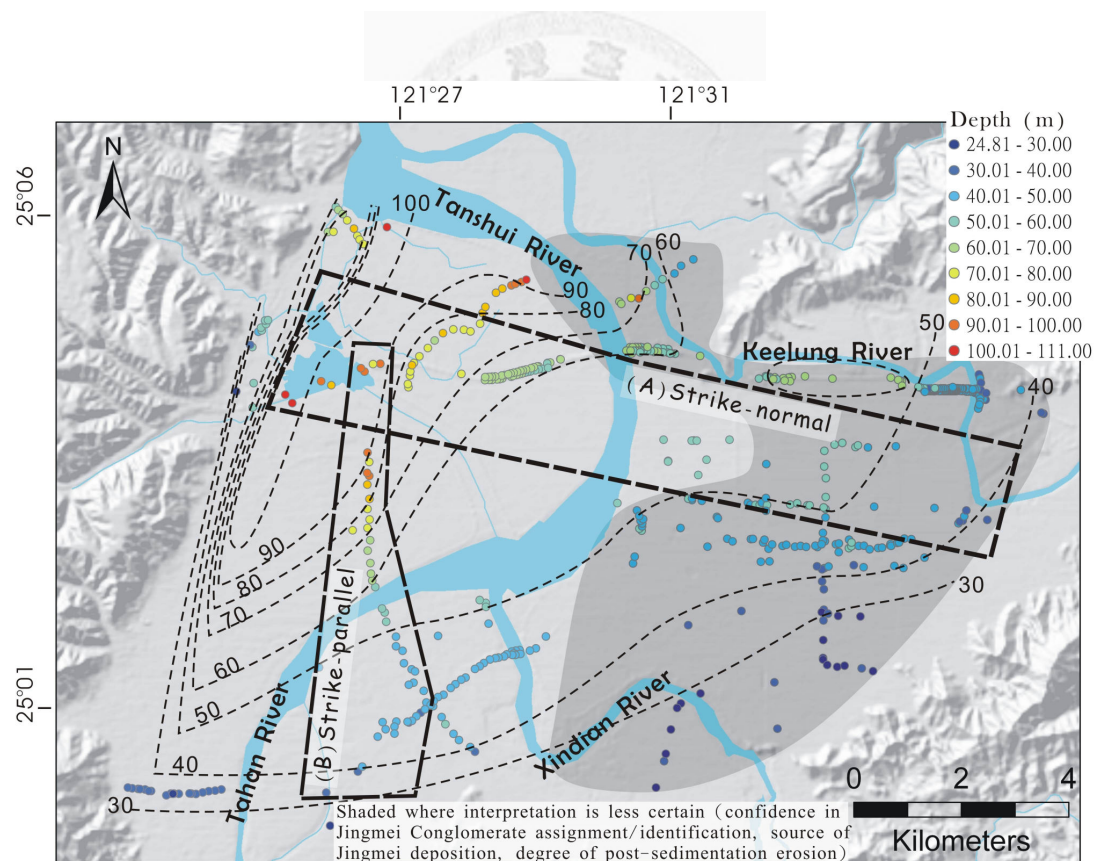


Fig. 4-13. Basin-wide compilation of depth distribution of the Jingmei Formation top horizon. A prominent trough near the western boundary of the basin is observed and is a product of fault offset.

4.5.3 Factors affecting the depth distribution of the Jingmei Formation top horizon

Contrary to the spatial extent and thickness distribution of the Jingmei Formation (Teng et al., 2004), the present configuration of the Jingmei Formation top horizon does not resemble its alluvial fan origin. The first order control is held by slips of the Shanchiao Fault which produced the offset in the western basin margin and the gradual return in depth across the basin. The resultant tectonic subsidence is therefore largest and almost equal in Luzhou and Wuku areas, and then decreases along strike towards south. The deeper horizon depth found near and north of the lower reach of the Tanshui River is probably resulted from river erosion, leading to speculation that the Tanshui River has not changed its course significantly since the LGM as the associated depression is quite localized along its present channel; another possible reason is that the area is located on the outer boundary of the original alluvial fan, which might help explaining a similar northward plunging of Jingmei Formation top horizon depths south of the Keelung River course in the eastern part of the basin. Another depression in the northeast boundary of the basin near the channel of the Keelung River is also likely the result of fluvial erosion of lesser extent. The conical hump in the southeast is the sub-alluvial fan drained by the Xindian River, which was formed together with the main fan produced by the Tahan River and continued to be active beyond 23 ka till more recently (Teng et al., 2004).

The Jingmei Formation top horizon depth variation in the western to central Taipei Basin is mainly the product of tectonic deformation by activities of the Shanchiao Fault. Taking the horizon depth 29.1 m in SCF-1 in Wuku Profile as the undeformed reference on the footwall, tectonic subsidence since LGM after the deposition of the Jingmei paleo-alluvial fan around 23 ka can be inferred and calculated. The central part of the Shanchiao Fault zone is composed of at least two long, narrow extensional fault blocks with offsets about 25 and 50 m before reaching the exact hanging wall with offset more than 70 m in the Wuku-Luzhou region. Moving further away from the fault in the fault-normal Wuku-Sanchung-Taipei Profile (Fig. 4-14) the offset quickly decreases to about 30 m in the center of the basin in the Sanchong area, and is then gradually reduced to 10 m in the Xinyi-Nankang region at the eastern extreme of the basin, while most of the central Taipei City has a tectonic subsidence between 20 to 30 m. The along-strike variation of offset from the central portion to the southern portion of the fault (Fig. 4-15) is also significant and rather systematic, which drops from about 60 m to 30 – 40 m north of the Tahan River in Hsinchuang and 20 – 0 m south of the Tahan River in Banchiao. Such southward fault-parallel changes in the horizon depth may be reflecting the fault deformation but contribution from the original fan geometry, which should be higher upstream in the south with unresolved gradient, is of unknown proportion and difficult to be excluded.

Wuku-Sanchung-Taipei profile / strike-normal

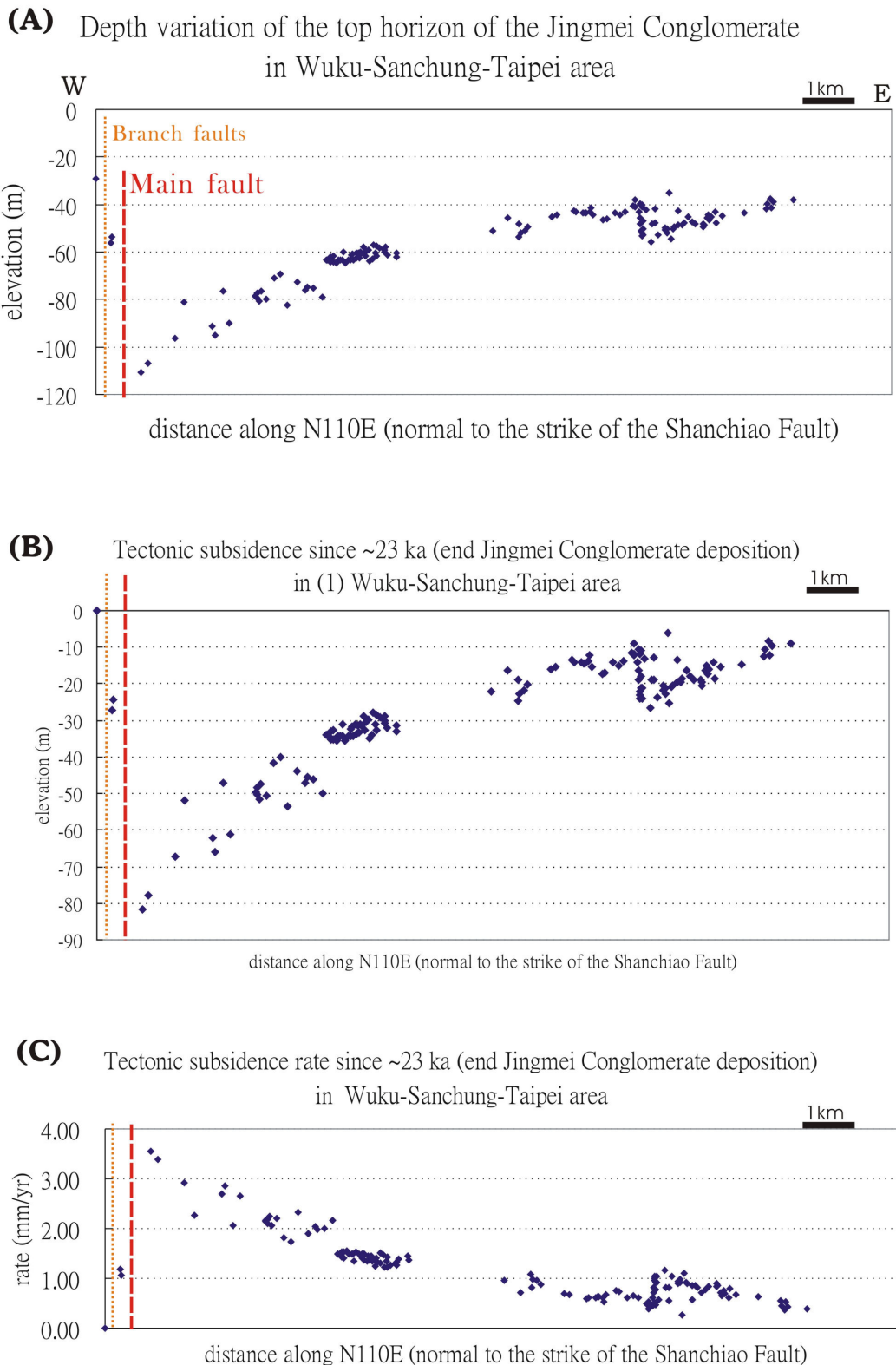


Fig. 4-14. Variations of the Jingmei Formation top horizon depth (A), and the deduced tectonic subsidence amount (B) and rate (C) since ~ 23 ka in the Wuku-Sanchung-Taipei profile normal to the fault trace across the fault.

Wuku-Hsinchuang-Banchiao profile / strike-parallel

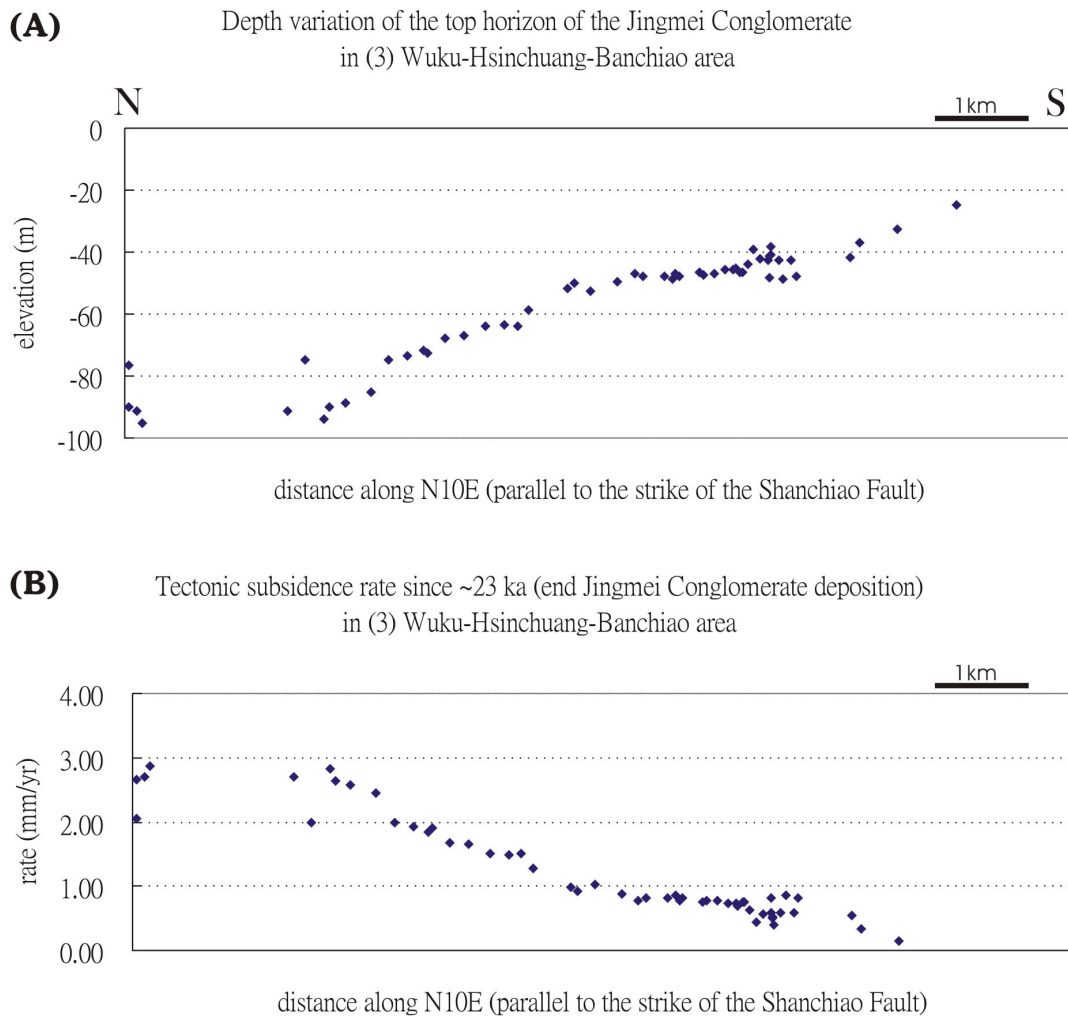


Fig. 4-15. Variations of the Jingmei Formation top horizon depth (A), and the deduced tectonic subsidence rate (B) since ~ 23 ka in the Wuku-Hsinchuang-Banchiao profile sub-parallel to the fault trace across the fault.

4.6 Discussions

4.6.1 Delineating the Shanchiao Fault zone

The Shanchiao Fault was previously mapped as a single string of trace slightly east of the topographic divide between the Linkou Tableland and the Taipei Basin based on geomorphic analysis (e.g. Shyu et al., 2005; Chen et al., 2006) and/or limited borehole synthesis (e.g. Lin et al., 2000; Lin, 2005; Huang et al., 2007). Regional borehole analysis and synthesis in the central Wuku and north-central Luzhou areas along the fault reveal that fault displacement is distributed in a fault zone with two or more faults, other than localized on a one particular fault plane. In both cases, the fault zone is of several hundred meters wide with the major offset on its eastern boundary and the (presently-) morphogenic branch fault marking its western border (Fig. 4-16).

To the north on the right bank of the lower reach of the Tanshui River, the major Shanchiao Fault offset is also believed to be situated southeast of the topographic boundary the southwestern extension of the Tatun Volcanoes and the recognized western fault-related scarps (Chen et al., 2006) within the Guandu Plain in northern Taipei Basin, as among borehole pairs SCF-8, 9 and SCF-10, 11 (Song et al., 2007). The northern portion of the Shanchiao Fault is therefore also better perceived as a fault zone up to hundreds of meters across in map view as imaged in shallow seismic reflection profiling (Shih et al., 2004), while the main fault between SCF-8 and 9 may have produced a scarp as a gentle topographic slope (Chen et al., 2006). Further north it's still far from clear how the Shanchiao Fault might be extending into the Tatun Volcanoes and it's relation with the active Chinshan Normal Fault (Chan et al., 2008).

The position of the Shanchiao Fault in its southern portion in the southwestern corner of the Taipei Basin remains uncertain as the lack of borehole data providing depth information of the Jingmei Formation top horizon in the region (Fig. 4-13). The topographic scarps mapped south of the Taishan Fan (Fig. 4-6) which is similar to the one belongs to the branch fault in the Wuku Profile may still marks the western boundary of the fault zone, and the main fault as the eastern fault zone border continues south-southwest altogether. On the southeastern edge of the Linkou Tableland near the conjunction of the Hsinchuang and Shulin districts, the Hsinchuang Thrust which is reactivated by the Shanchiao Fault along the western border of the Taipei Basin turns southwest and runs on the western margin of the Shantzujiao terrain. This portion of the 'diverted' Hsinchuang Thrust is often named as the Kueishan Thrust. Borehole synthesis in the Shulin Profile suggests the Shanchiao Fault is still active since the LGM but the fault is outside west of the basin. As the Shanchiao Fault is genetically related to the Hsinchuang Thrust, it's natural to

hypothesize the Shanchiao Fault follows the former thrust plane to divert westward and reactivates the Kueishan Thrust (Fig. 4-16). Further geological investigation is crucial to confirm or disprove this speculation on the whereabouts of the southernmost Shanchiao Fault.

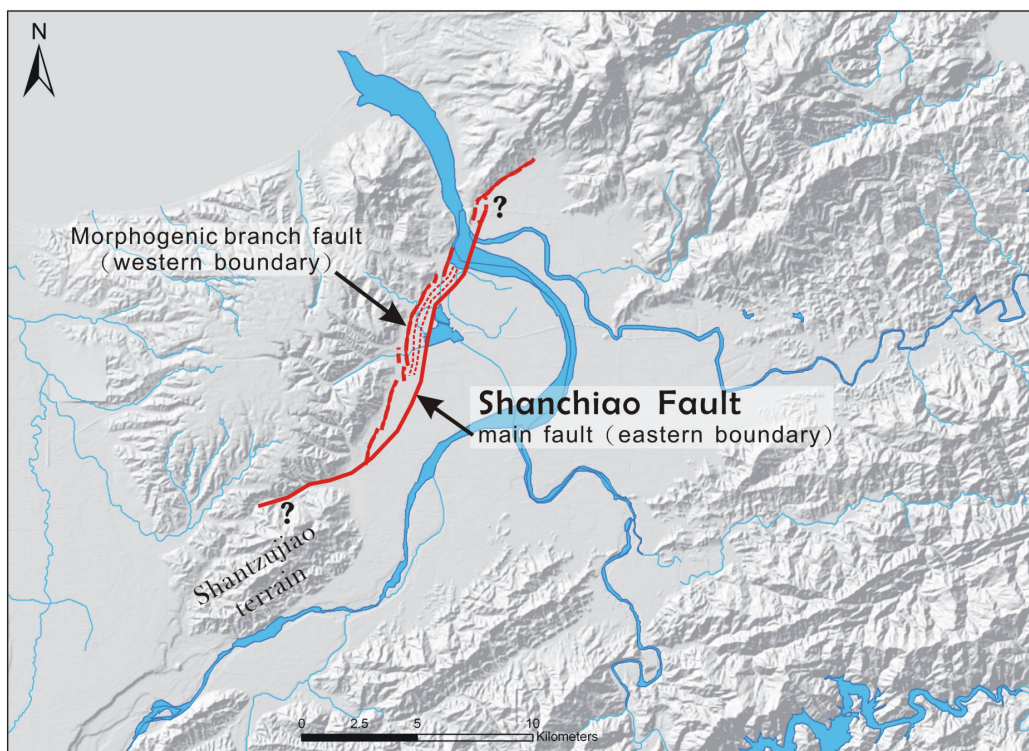


Fig. 4-16. Updated mapping of the Shanchiao Fault zone.

4.6.2 Characteristics of the fault zone structure

The Shanchiao Fault zone examined in the Wuku and Luzhou areas in its central part possesses a half-tulip structure containing concave-upward minor branch faults west of the main fault, and comparable configuration might be expected for the northern part of the fault. Growth faulting and the presence of branch faults developed within loose basin sediments thus appear to be key phenomena operating along the entire length of the Shanchiao Fault. The topography produced by faulting controlled loci of sedimentation when eustasy began rising but was far lower than the basin ground; when the ground floor was close to sea level deposition spanned the entire fault zone with thicker strata and deeper horizons on the hanging wall and extensional fault blocks than on the footwall. Among the growth sediments the Jingmei Formation is a good marker for fault offsets since the LGM due to its particular spatial and temporal distribution as event alluvial fan deposits, as well as its distinct lithology. From the mapping of the Jingmei Formation top horizon depth in Fig. 4-13, there are up to three longitudinal extensional fault blocks with post-LGM tectonic subsidence of about 25, 40, and 50 m that can be recognized from the Luzhou Profile and traced laterally along strike to the Wuku area (e.g. the extensional fault block the SCF-2 situates in Wuku Profile may extend to the block of SCF-5 in Luzhou Profile, while the one SCF-6 sits on in Luzhou Profile extends to the Wuku Profile between SCF-2 and WK-1), and may persist further south to where the fault trace left the basin (Fig. 4-16).

The fact that the development of the branch faults and the widening of the fault zone are limited to the unconsolidated basin sediments at shallow depth is most likely a result of the great rheological and strength contrast between the basement rocks and the loose deposits, as well as the changing geometry of basement in the fault zone. From borehole analysis, the Shanchiao Fault is supposed to be a single shear zone following the steep western wall of the basin basement when it enters the western trough of the basin from depth, and the shear zone splays to form branch faults when the single shear zone travels upward to where the basement slope is much lessened at 300 to 200 m deep. The main fault seems to be the direct extension of the steep basement wall to the surface and is totally within the sediments, while the remaining displacement continues to be concentrated along the sediment-basement rheological boundary as evidenced by the sheared sections at the bottom of basin deposits recovered in the SCF-2, 5 and 6 boreholes before diverging upward to form branch faults probably at loci of basement slope changes (Figs. 3-9, 4-9B; Chen et al., 2010). Such fault zone configuration in the central part of the Shanchiao Fault is depicted in Fig. 4-17, emphasizing the relation between basement geometry, shallow fault zone structure, and corresponding topographic features. Therefore the Shanchiao Fault

dictates the basin-scale basement geometry while the fault zone structure looks in turn controlled by the detailed basement topography underneath.

A further complication revealed in fault zone analysis from the Luzhou area is the variable percentage of total fault vertical slips taken up by each branch or main faults for different periods or earthquake events, as demonstrated by the complex vertical fault slip rate compile in Fig. 4-12. Therefore one needs to examine the entire fault zone for a complete paleo-earthquake and fault evolution investigation.

The half-tulip form of the Shanchiao Fault zone is also the product of its transcurrent component of motion, as this kind of structure is commonly perceived to indicate transtensional tectonics. Although the sinistral movement is substantiated by geological records as the fault striation recovered in the borehole (Lee et al., 1999), geomorphic documentation as the right-stepping fault scarp alignment (Chen et al., 2006; section 4.3), and by geodetic data as regional GPS survey (Rau et al., 2008), its percentage in total displacement of the fault is yet constrained based on current knowledge.



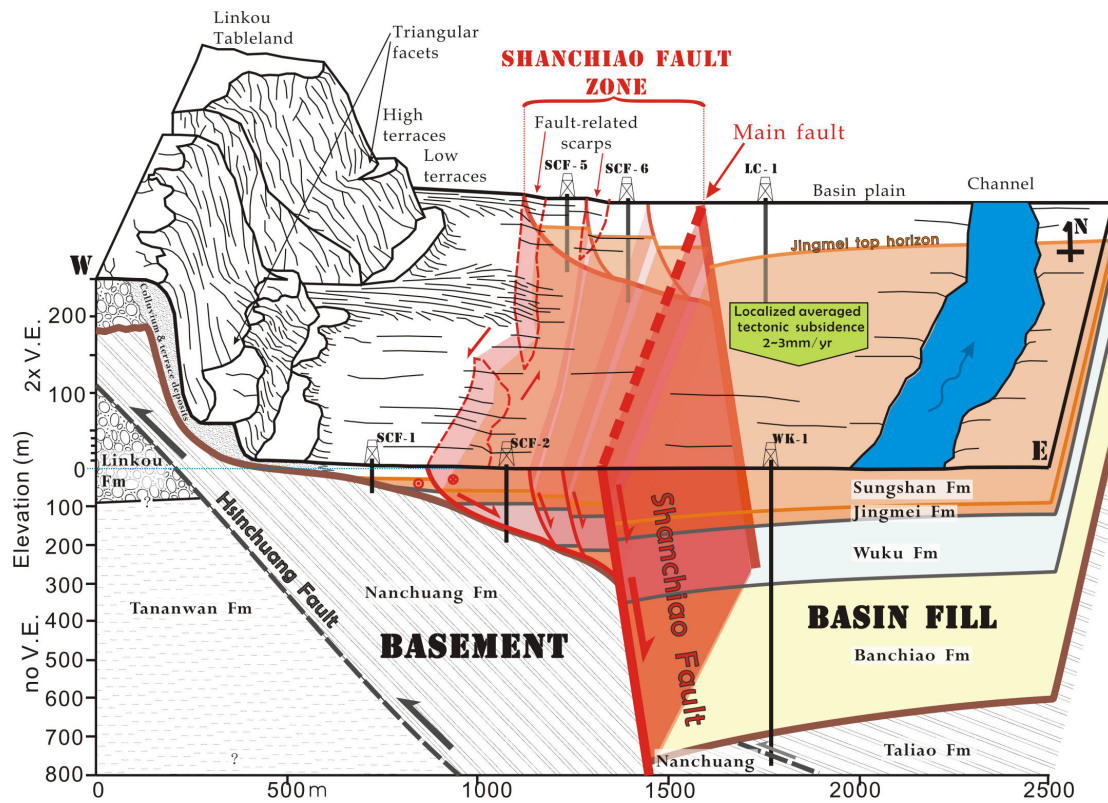


Fig. 4-17. Schematic 3-D diagram of the fault zone in the Wuku area, central portion of the Shanchiao Fault, displaying regional subsurface geology and its relation to surface topographic features.

4.6.3 Extent of the magnitude and rate of fault-related vertical deformation since the Last Glacial Maximum

The basin-wide mapping of Jingmei Formation top horizon depth offers insights to the long-term tectonic deformation encompassing numerous earthquake cycles the Shanchiao Fault imposed in the region. As already described in section 4.5, for the central Taipei Basin the hanging wall closest to the main fault experienced more than 70 m of vertical offset since the LGM (Fig. 4-14) which rapidly decreases to about 30 m in 4 km away from the fault followed by a slower decline to about 10 m in the eastern basin margin 12 km away, resulting in a roll-over geometry (Fig. 4-18); while this deformation is achieved in 23 kyr the averaged tectonic subsidence rate is calculated to be more than 3, 1.3 and about 0.4 mm/yr, respectively. Based on the data and the rationale, fault-caused tectonic subsidence may persist further away from the fault into the foothills east of the basin. For the along-strike changes of the tectonic offset a few kilometers away from the fault (Figs. 4-13, 15), the amount and rate declined somewhat steadily from the center of the fault in Luzhou-Wuku area at more than 60 m (over 2.5 mm/yr) to 30-40 m (1.5 mm/yr) in Hsinchuang and about 10 m (0.4 mm/yr) in Banchiao. Combining the Banchiao and Shulin data the Shanchiao Fault is considered still active nonetheless weak in the southern end of the basin since the LGM, as the depths of the Jingmei Formation top horizon in these areas are deeper than that of SCF-1 in Wuku area (Fig. 4-18) despite being upstream in the original alluvial fan. Present-day ground elevation monitoring by leveling (Chen et al., 2007) exhibited the presence of modern tectonic subsidence in the central portion of the fault from southern Guandu through Luzhou to Wuku areas although the rate and lateral extent were not clear, a pattern probably stands for interseismic behavior and is similar to the long-term one imaged by the Jingmei Formation top horizon.

The fault-parallel changes of vertical fault deformation may be related to the diminishing displacement towards the fault tip, while the fault-normal variation of vertical offset is most likely been governed by the crustal fault plane geometry which is the topic of investigation for the next chapter.

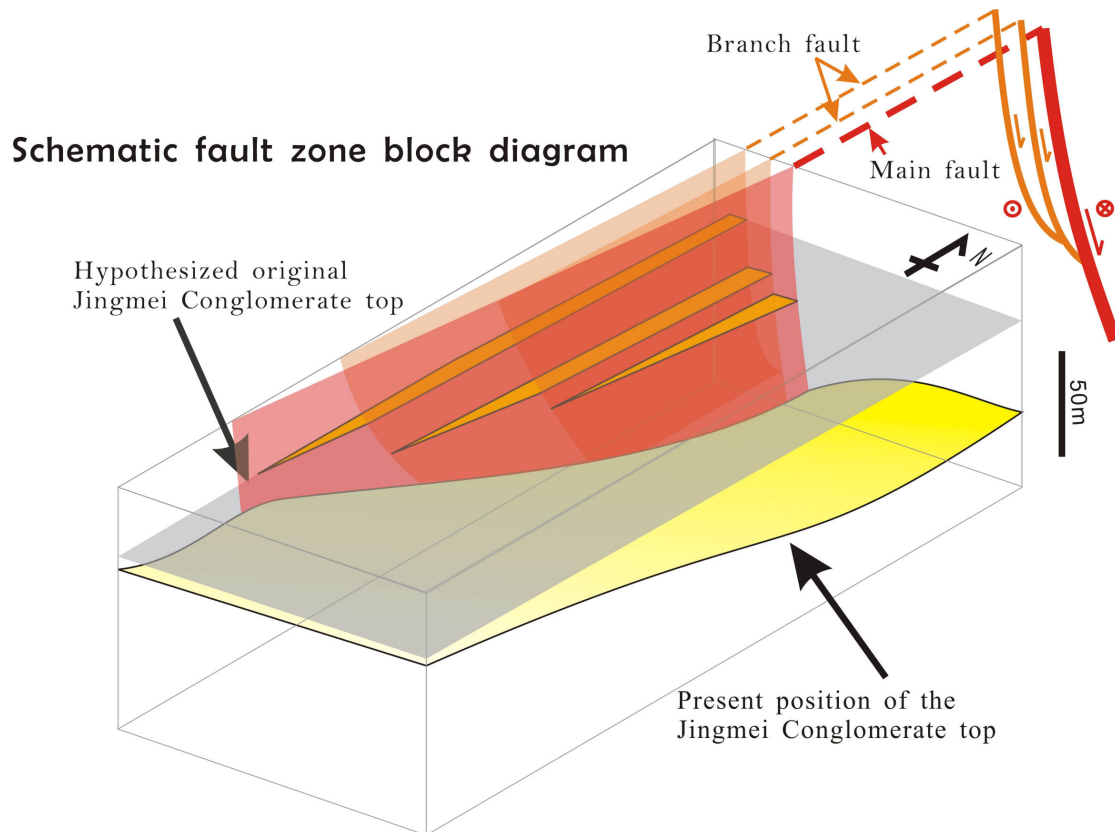


Fig. 4-18. Cartoon exhibiting the deformation of the Jingmei Formation top horizon by the Shanchiao Fault, emphasizing the pronounced roll-over monocline in the hanging wall immediate east of the fault, and the rather systematic decrease of offset towards the southern end of the fault.

4.7 Summary

The Shanchiao Fault, instead of a single trace, is better mapped as a fault zone up to several hundred meters wide on land surface. The main-branch fault configuration and growth faulting influenced by the rising sea level identified in the Wuku and Luzhou areas in the central portion of the fault are characteristics of the Shanchiao Fault. The fault zone structure has a half-tulip form signaling its transtensional nature. For the fault zone south of the Tanshui River only the western branch faults have corresponding scarps while the main fault is devoid of surface expression. The Jingmei Formation top horizon in the growth sediments of the latest sequence in the Taipei Basin serves to be a key tectonic subsidence marker in most of the basin area and its depth distribution is mapped; it's revealed that the fault displacement decreases rather systematically along-strike to the south, and the hanging wall of the fault is deformed in a roll-over style with the peak value of post-LGM tectonic subsidence reaches more than 70 m as over 3 mm/yr in average.



Chapter 5: Active post-collisional normal fault reactivating syn-convergence thrust detachment and involvement of deep-seated pre-orogen rift faults: a case study of the Shanchiao Fault in the Taipei Metropolis, northern Taiwan

5.1 Introduction

Pre-existing fabrics as weak planes or zones are the favored sites for the development of subsequent structures resulting in reactivation. While in thrust belts many reverse faults are known to reactivate former normal faults in positive tectonic inversion (e.g. Schmidt et al., 1996), culmination of post-collisional normal fault is also significantly influenced by the past thrusts (e.g. Constenius, 1996; D'Agostino et al., 1998) though complicated by its mechanical feasibility as this gives rise to the activation of low angle normal faults (e.g. Sibson, 1985; Faccenna et al., 1995; Collettini and Sibson, 2001; Collettini, 2011). The previous thrusts which can possess a dip gentler than 30° are inevitably prone to rupture upon loading but their orientations are quite unfavorable given the vertical σ_1 in the extending upper crust (Sibson, 1985, 2000). From analogue modeling's point of view, former thrusts may be truncated (cut through), or partially to entirely reactivated by the newly formed normal fault depending on the dip of the thrust fault plane with cut-off points around 32 and 41 degrees respectively (Faccenna et al., 1995). Despite this, development of new low angle normal faults rooted into near-horizontal master detachments formed during convergence is widely recognized and documented in the mid-Cenozoic collapse of the Cordilleran Orogen, which is no longer active today and led to the doming of a metamorphic core complex (e.g. Constenius, 1996). For the late-Cenozoic destruction of the Apennines mountain chain, various relationships between the previous thrusts and successive normal faults have been proposed; low angle normal faults whether partially reactivate former thrust planes or are formed independently are mapped and described (D'Agostino et al., 1998; Tavarnelli et al., 2003; Collettini et al., 2006). With other similar documentations worldwide it is undisputed that former thrust planes of all ranges of dip can be reactivated as later normal faults, while details on the mechanical preconditions permitting such inversion, their seismogenic potential, and structural evolution remain much speculated (Collettini, 2011).

What's less discussed is the possible role of pre-orogen normal faults on the

post-orogen evolution of structures. Continental margins involved in collision belts often contain normal faults and rift structures overlain by margin sediments followed by foreland sequences. These pre-existing fabrics may have been reactivated as or influenced the allocation and geometry of syn-orogen thrusts before or during the incorporation and underthrusting of the continental margin basement. Though deeper in the orogenic pile when mountain building processes have reached climax, the pre-existing normal faults may still have attitudes favorable for reactivation when they are under vertical σ_1 extensional environments. The Taiwanese mountain belt presents a live example of such system that a mature orogenic wedge fed by the rifted Chinese Continental Margin is experiencing post-orogenic mountain collapse in its northern part (Teng, 1996). Sequence of thrust faults developed mainly within the margin and foreland sediments become inactive towards the north of the island as the compressive tectonic regime yielded to the extensional one (Lee and Teng, 1988), and the underthrusted Chinese Continental Margin contains series of normal faults mapped both in front of the foreland and beneath the fold-thrust belt (Lin et al., 2003; Teng and Lin, 2004). The Shanchiao Fault, an active fault located in the northern tip of Taiwan Island, is a good candidate to explore how the possible relations the late normal faults can engage in with former thrusts and even previous normal faults. Given the clustering of moderate to large earthquakes at flat-ramp junctions and branch points found in the extensional fault systems of the Apennines (e.g. Boncio and Lavecchia, 2000a), the geometrical characteristics of the Shanchiao Fault may have important implications for its seismic hazard assessment as the Taipei Metropolis is situated on the hanging wall of the fault.

In this work late-Quaternary vertical displacement distribution across the Shanchiao Fault documented by a key horizon within the growth sediments is modeled to infer the upper crustal fault geometry. In light of regional tectonics the fault plane shape is found to be closely associated with pre-existing structures, allowing us to address the patterns of fault reactivations and earthquake risks of the Shanchiao Fault.

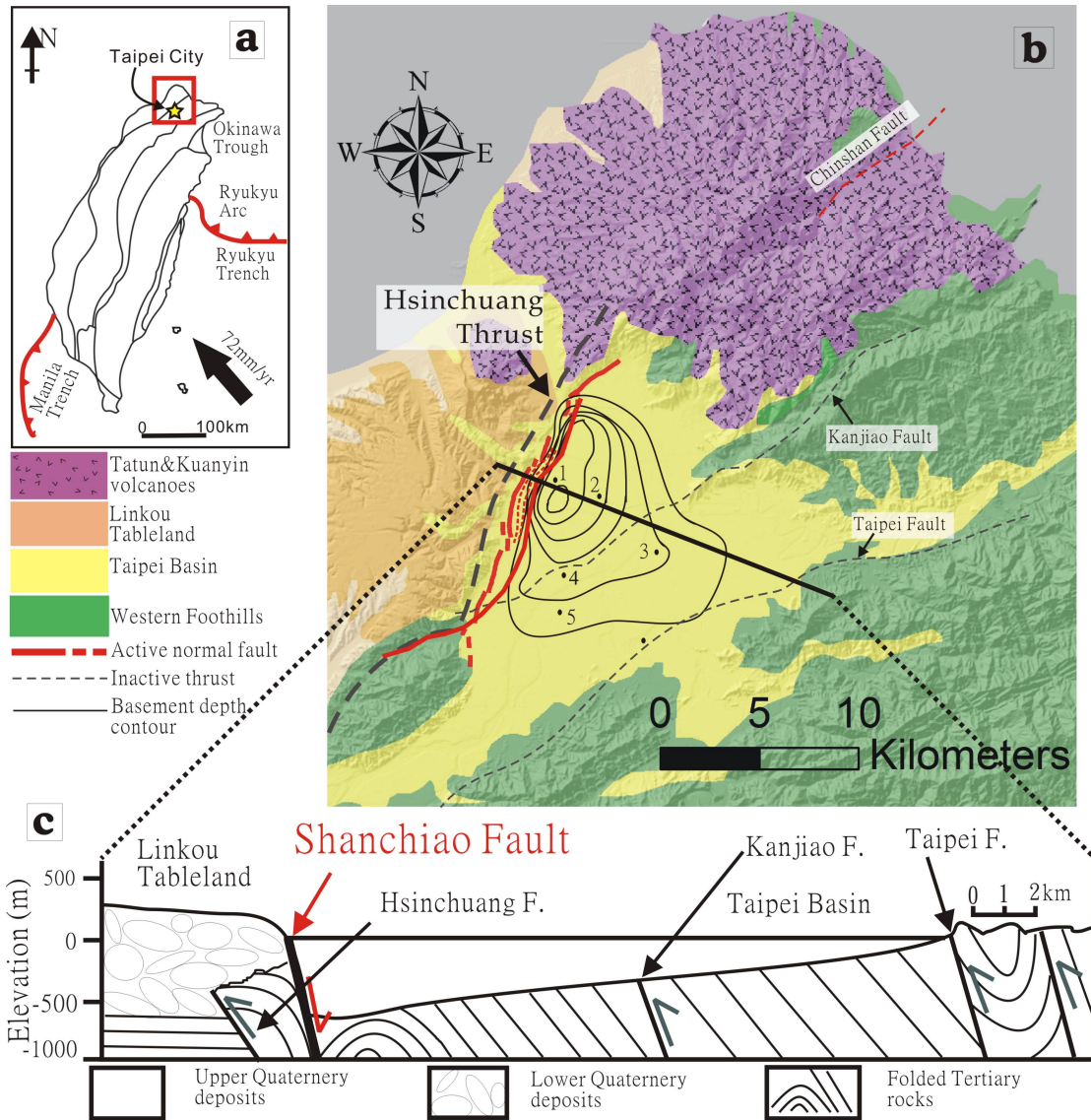


Fig. 5-1. (a) General tectonic framework of Taiwan. A: Coastal Range; B: Backbone Range; C: Hsueshan Range; D: Western Foothills; E: western Coastal Plain. (b) Simplified geology of the Taipei area. Four geological domains are defined in the Taipei area as indicated by different colors shown in the legend. The thick red lines are the Shanchiao Fault traces. Thin black lines within the Taipei Basin are the basement depth contour of 100 m interval (adapted from Teng et al., 2001). The black dots mark local district names in the Taipei Basin: 1. Wuku, 2. Sanchung, 3. central Taipei, 4. Hsinchuang, 5. Banchiao. (c) Simplified geological cross section of the Taipei Basin (modified from Teng et al., 1999). The Hsinchuang, Kanjiao, and Taipei Faults are inactive thrust faults (denoted with grey arrows) which slipped during the collision phase in the Taipei area.

5.2 Regional setting

5.2.1 The Taiwan Orogen and post-collisional tectonics in northern Taiwan

Taiwan is the product of active convergence between the Chinese Continental Margin and the Luzon Arc since around 5 Ma (Ho, 1986; Suppe, 1981; Teng, 1990; Lu and Hsu, 1992; Wu et al., 1997) with a rapid convergent rate of about 82 mm/yr currently in the NW direction (Seno, 1977; Yu et al., 1997; Fig. 5-1A). Prior to the Neogene orogeny, the Chinese Continental Margin south and east of the Chinese coast was highly rifted and drifted since Eocene until Miocene due to the opening of the South China Sea (Briais et al., 1993; Lee and Lawver, 1994; Lo et al., 2000) leaving numerous rift-related normal faults and (half-) grabens whose magnitude of extension and subsidence increased eastward (Lin et al., 2003; Teng and Lin, 2004). On land the deformed and metamorphosed Chinese Continental Margin basement crops out along the eastern part of the Central Range against the accreted Luzon Arc of the Coastal Range. To the west sediments on the rifted continental margin were deformed forming the slate belt and the foothills fold-thrust belt with sequence of west-vergent thrust faults which may root into some detachments (e.g. Suppe, 1980; Yue et al., 2005; Chen et al., 2011). These thrusts may have been affected or partially re-slipped the rift normal faults (e.g. Mouthereau and Lacombe, 2006).

The oblique nature of the convergence leads to the southward-propagation of the Taiwan orogeny (Suppe, 1981), while in the northern part of the island the developed orogen architecture is dissected by extensional structures due to the westward advance of the Ryukyu subduction system and the post-collisional orogen collapse (Suppe, 1984; Teng, 1996; Wang et al., 1999). Central and southern Taiwan are presently in full and mature collision (Angelier et al., 1986; Yu et al., 1997; Shyu et al., 2005), in contrast the northern part of the mountain belt, including the Taipei Metropolis region, is now in an extensional or transtensional tectonic setting (Teng, 1996; Hu et al., 2002) as evidenced by the presence of Quaternary extensional structures (Lee and Wang, 1988; Lee, 1989; Lu et al., 1995), extensional earthquake focal mechanisms (Yeh et al., 1991; Kao et al., 1998), and GPS displacement fields (Yu et al., 1997; Rau et al., 2008; Lin et al., 2010). The Taipei Basin where the Taipei Metropolis resides is a half-graben formed by repeated slips of the Shanchiao Fault, an active normal fault considered as the major neotectonic structures responsible for the negative tectonic inversion from compression to extension across the Taipei region, and is filled with late-Quaternary unconsolidated sediments since 0.4 Ma (Teng et al., 2001; Wei et al., 1998). The basin basement is composed of folded Oligo-Mio-Pliocene shallow marine sedimentary rocks as a fold-and-thrust belt during the earlier stage of mountain building, and also outcrops to the east and south of the basin. The late Quaternary terrestrial deposits in the Taipei basin as growth sediments of the Shanchiao Fault

form an asymmetric sedimentary wedge: reaching a maximum depth of about 700 m near the western margin and rather drastically becoming thinner toward the east and south (Fig. 5-1C). Regional geological synthesis (Teng et al. 2001) illustrates the effects reflecting the tectonic regime change. While the Plio-Pleistocene orogeny of mountain building reached its climax in northern Taiwan in Quaternary, the Paleo-Tanshui River, the major river in the Taipei Basin, provided sediments to produce the Linkou fan-delta around the ancient mountain front (Chen and Teng, 1990). Accompanying the waning of compression in the northernmost Taiwan during the middle to late Quaternary (Lee and Wang, 1988) is the vigorous eruptions of the Tatun volcanoes to the north of the Taipei Basin (Wang and Chen, 1990; Song et al., 2000), closely related to the onset of regional extension. The extensional tectonics turned the Taipei area from rugged mountains gradually into a sediment-receiving basin, and accumulation of fluvial and lacustrine sediments started at about 0.4 Ma (Wei et al., 1998; Teng et al., 2001). Since then the Taipei Basin has kept expanding due to erosion and continual asymmetric subsidence in the western edge of the basin along the Shanchiao Fault, which is evidenced by several hundred meters thick fluvial growth deposits with its repeated normal faulting, and the fault is interpreted to be inverted from the Hsinchuang fault, the frontal thrust in northern Taiwan during the compressional phase (Chiu, 1968; Hsieh et al., 1992). Under the combining influences of sea level fluctuations, volcanic activities, drainage system changes, and tectonic processes, the basin was infilled with various types of sediments, including alluvial, lacustrine, marine and pyroclastic deposits, up to 700 m thick as mentioned above (Fig. 5-2).

Taipei Basin deposits

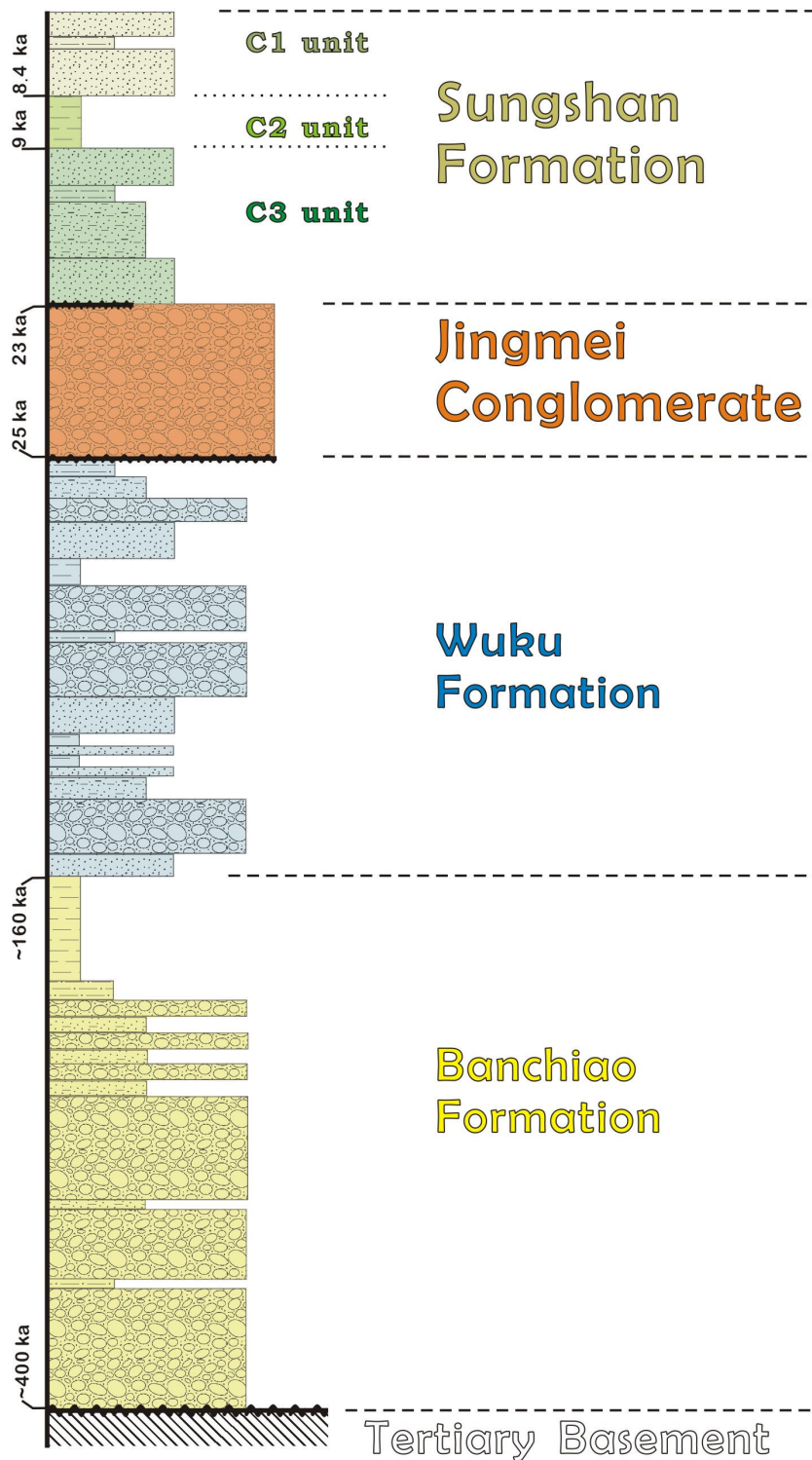


Fig. 5-2. Lithostratigraphic column of the Taipei Basin deposits (After Teng et al., 1999).

5.2.2 The active Shanchiao Fault

The Shanchiao Fault was mapped (Chang et al., 1998; Lin et al., 2000; Lin, 2001; Huang et al., 2007; Chen et al., 2004, 2006; Chapter 4) close to the topographic boundary between the Linkou Tableland and the Taipei Basin, sub-parallel to the Hsinchuang Fault (Lin, 2001; Teng et al., 2001), with features indicating that the steeper Shanchiao normal fault may merge into the Hsinchuang thrust fault at depth (e.g. Hsieh et al., 1992). Following the late-Quaternary tectonic inversion, tectonic subsidence from down-dip slips on the Shanchiao Fault led to formation and development of the Taipei Basin. Left-lateral transcurrent motion together with clockwise block rotation is also present along the Shanchiao Fault, based on studies on regional structural geology, paleomagnetism, and GPS measurements (Lu et al., 1995; Lee et al., 1999; Rau et al., 2008).

Many efforts have been made to characterize this active fault. Shallow reflection seismic profiling across the Shanchiao Fault imaged vertical offsets of Holocene sediments at shallow depth, although the location of the main fault remains questionable (Wang and Sun, 1999; Shih et al., 2004). Preliminary geomorphology analysis (Chen et al., 2006; section 4.3) also reveals a series of scarps closely related to the development of the Shanchiao Fault. GPS surveys of the Taipei area showed WNW-ESE extension with a slow rate of $0.08 \mu\text{strain/yr}$ across the fault (Yu et al., 1999a). Asymmetric tectonic subsidence related to the Shanchiao Fault across the basin was illuminated through 30-year-long levelling data (Chen et al., 2007) as well as recent InSAR data (Chang et al., 2010). Huang et al. (2007) correlated stratigraphy of three sets of boreholes, and proposed three paleoseismic events during the Holocene (i.e. at 8500, 9200, and 11100 years b.p., respectively). Radon and helium anomalies in soil-gas along the fault zone were documented (Walia et al., 2005) indicating the presence of possible active faults and deep fracture-advection system. Growth faulting analysis at the central portion of the fault in Wuku and Luzhou areas demonstrated that the fault has been constantly active in the last 23000 years and the shallow fault zone possesses half-tulip structure (Chen et al., 2010; Chapter 4). The Shanchiao Fault is therefore considered currently active (Chang et al., 1998; Lin et al., 2000), and it's seismogenic based on the Holocene paleoseismic events proposed by Huang et al. (2007) and a possible historic earthquake in 1694 which induced severe subsidence and inundation in the Taipei Basin forming the Kanshi Taipei Lake (Hsu, 1983).

Despite the knowledge gathered mostly about the current deformation and shallow underground properties of the fault, the geometry of the Shanchiao Fault within the brittle crust has not been constrained. The unavailability of deep seismic profiling

data and the scarcity of upper crust microseismicity across northern Taiwan (Wang et al., 2006; Wang, 2008) except in the Tatun Volcanoes north of the Taipei Basin where volcano-related seismic signals are identified (e.g. Lin et al., 2005), hamper efforts to delineate the fault plane shape at depth. From analysis of growth faulting in the fault zone a key horizon widespread in the Taipei Basin was identified which encompasses vertical tectonic offset accumulated over at least ten earthquake cycles in 23 kyr; the distribution of tectonic offset revealed by this key marker should reflect the fault geometry beneath that drives hanging wall deformation. In the following the key horizon, the Jingmei Formation top horizon, and the long-term tectonic subsidence it reveals are described. The displacement distribution across the fault is then modeled with simple elastic half-space boundary element method to figure out the best fit fault geometry by try-and-error process. The resultant upper crust fault geometry is discussed for its relations with pre-existing tectonic fabrics including syn-convergence thrusts and pre-orogen normal faults, and for the seismic hazard the geometry may imply.

5.3 Reconstruction of late-Quaternary post-Last Glacial Maximum vertical tectonic deformation

5.3.1 The Jingmei Formation top horizon as a key marker

The proximity of location and elevation to the sea means sedimentation in the Taipei Basin is controlled by eustatic changes alongside tectonic subsidence (Teng et al., 2000b). As revealed in back-stripping of growth sediments in the fault zone (Chen et al., 2010), the latest sequence of basin sediments was deposited during the recent sea level rise. The bottommost of the last growth sediment sequence is the Jingmei Formation (Fig. 5-2), which resulted from the capturing of the Tahan River channel into the basin in the Last Glacial Maximum at 25 to 23 ka (Teng et al., 2004a). The Jingmei Formation was an alluvial fan rapidly deposited by the diverted Tahan River, filling up the incised valleys caused by the much-lowered eustasy and covered the entire basin except the northwestern corner (Teng et al., 2004a). The top of the Jingmei Formation as the original alluvial fan surface is expected to be a smooth, flat or slightly conical plane. The present configuration of the eastward deepening of the Jingmei Formation top horizon in the Wuku and Luzhou profiles (Chen et al., 2010; Chapter 4), which was at right angle to the river channel during sedimentation, is the result of normal faulting after the alluvial fan deposition was finished. The Sungshan Formation, the most recent basin deposits consisted of fluvial to estuarine sands and mud (Fig. 5-2), also exhibits onlap features in the fault zone demonstrating faulting-controlled sedimentation during sea level rise.

The top of the Jingmei Formation as the original Jingmei alluvial fan surface

therefore serves to be a good marker documenting tectonic subsidence succeeding its completion at about 23 ka. The Jingmei Formation top horizon is considered a precious key horizon with the following advantages: 1. the Jingmei Formation was formed in a snapshot in geological sense and is widespread across the basin except the northwestern corner; 2. the Jingmei Formation top horizon is expected to possess a regular, flat to conical geometry as the top surface of a broad alluvial fan should be; 3. it's a distinct and easy-to-recognize lithological boundary in boreholes as the Jingmei Formation is the last conglomerate to be deposited in the basin (Fig. 5-2) except the northern corner (pyroclastic deposits sourced from the Tatun volcanoes) and the southeastern part (later fan deposits from the Xindian River). Besides, many boreholes drilled for engineering or construction purposes in the Taipei Basin encountered the conglomerate before finishing, making the depth information of this particular horizon widely available. Taking the possible earthquake recurrence interval as 1000 years from paleoseismic investigations by Huang et al. (2007), the Jingmei Formation top horizon has documented fault displacement over ten earthquake cycles and is thus representative of late-Quaternary fault behavior.

5.3.2 Mapping of tectonic subsidence across the Taipei Basin

In total 520 borehole records in the Taipei Basin reached the target Jingmei Formation top horizon with clear geological information are assembled in the data compilation (Fig. 5-3; Chapter 4). Before proceeding to evaluate the tectonic displacement, some other factors affecting the horizon depth distribution should be discussed. The deeper horizon depth found near and north of the lower reach of the Tanshui River is probably resulted from river erosion or from been on the edge of the alluvial fan; it might be contemplated that the Tanshui River has not changed its course significantly since the LGM as the associated depression is quite localized along its present channel. Another depression in the northeast boundary of the basin near the channel of the Keelung River is also likely the result of fluvial erosion of lesser extent. The conical hump in the southeast is the sub-alluvial fan drained by the Xindian River, which was formed together with the main fan produced by the Tahan River and continued to be active beyond 23 ka till more recently (Teng et al., 2004a). The factors identified above are relatively local effects and the first order control is still exerted by the slips of the Shanchiao Fault.

To extract the tectonic subsidence values the horizon depth at SCF-1 in Wuku area is taken as reference since the borehole is confirmed to be situated on the footwall (Chen et al., 2010). The resultant distribution map of tectonic subsidence since ~ 23 ka is presented in Fig. 5-4. For the central Taipei Basin the hanging wall closest to the main fault experienced more than 70 m of vertical offset since the LGM which rapidly

decreases to about 30 m in 4 km away from the fault followed by a slower decline to about 10 m in the eastern basin margin 12 km away, resulting in a roll-over geometry. Along-strike changes of the tectonic offset is also significant, showing somewhat steady decline from the center of the fault in Luzhou-Wuku area at more than 60 m to 30-40 m in Hsinchuang and about 10 m in Banchiao. Based on the data and the rationale, fault-caused tectonic subsidence may persist further away from the fault into the foothills east and south of the basin. The fault-parallel changes of vertical fault deformation may be related to the diminishing displacement towards the fault tip, but contribution from the original fan geometry, which should be higher upstream in the south with unresolved gradient, is of unknown proportion and difficult to be excluded. The fault-normal variation of vertical offset shown in the Wuku-Sanchung-Taipei profile (Fig. 5-5) at the central part of both the Shanchiao Fault and the Taipei Basin is most likely been governed by the crustal fault plane geometry, as the local factors mentioned ahead are not apparently affecting the profile, and the orientation of the profile is roughly normal to the paleocurrent direction when the fan was deposited meaning the absence of major topographic gradient inherited from original fan morphology. The fault-normal Wuku-Sanchung-Taipei profile (Table 5-1) is therefore chosen for investigating the upper crustal geometry of the Shanchiao Fault.

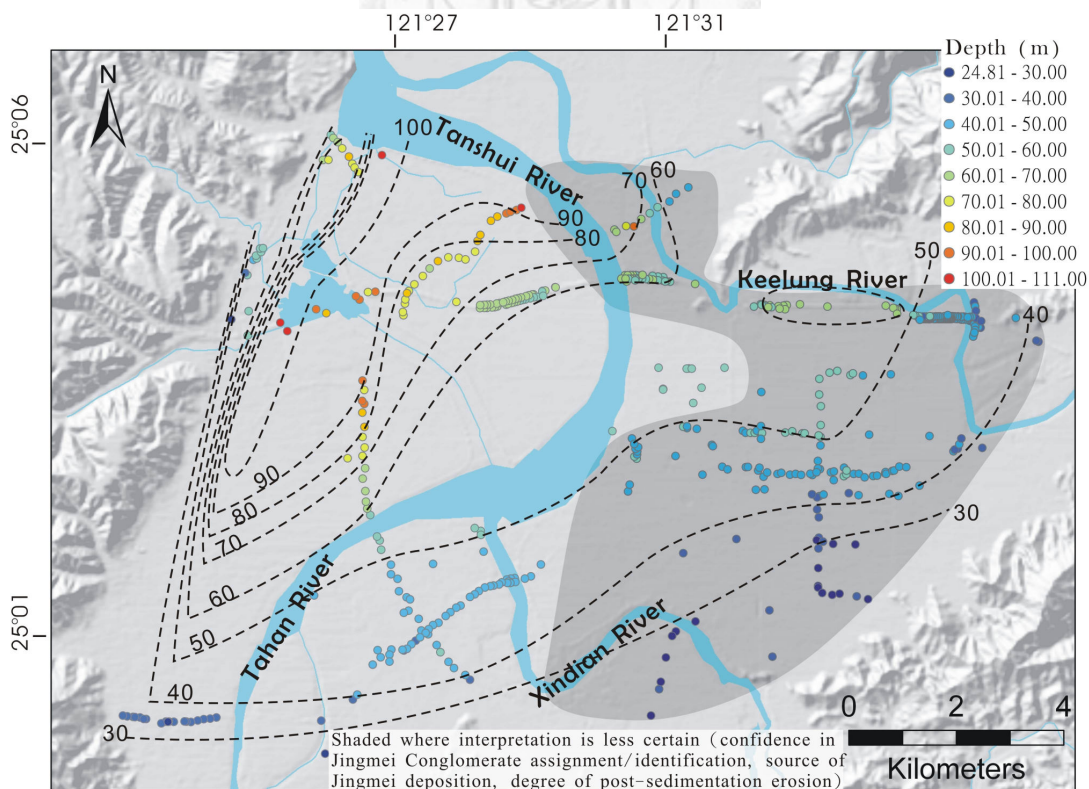


Fig. 5-3. Basin-wide compilation of depth distribution of the Jingmei Formation top horizon.

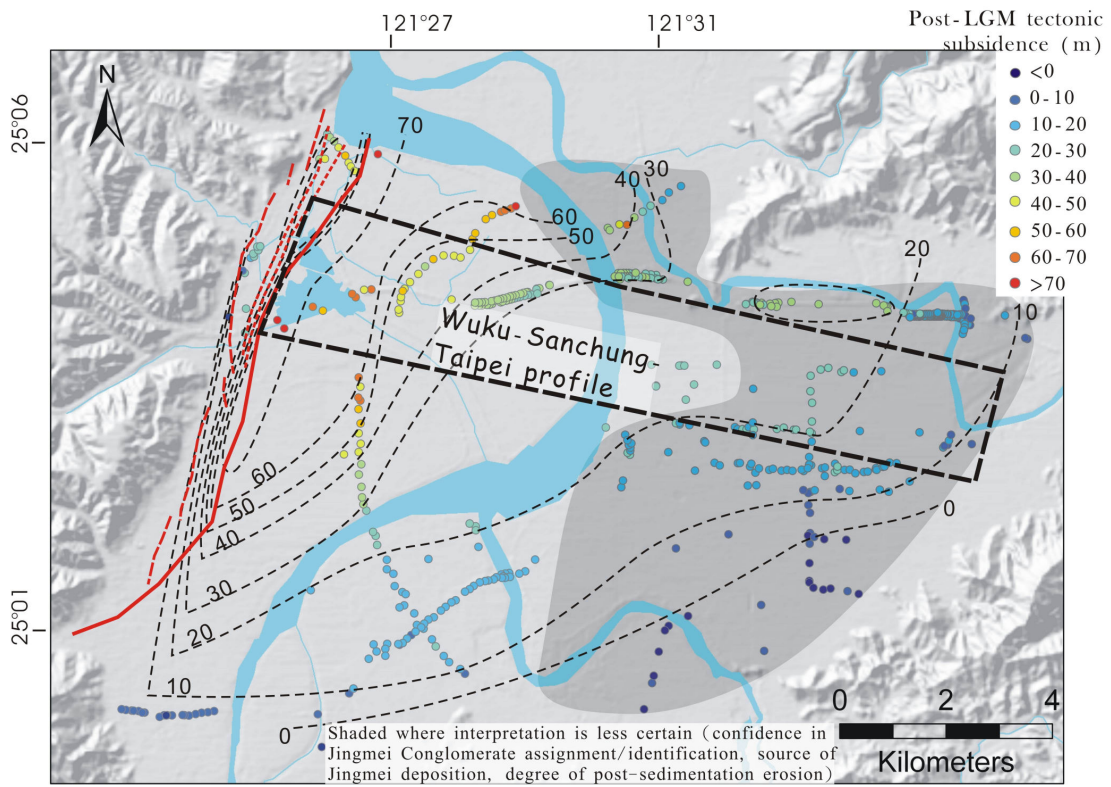


Fig. 5-4. Basin-wide variation of post-LGM tectonic subsidence revealed by the depth distribution of the Jingmei Formation top horizon.

Wuku-Sanchung-Taipei profile / strike-normal

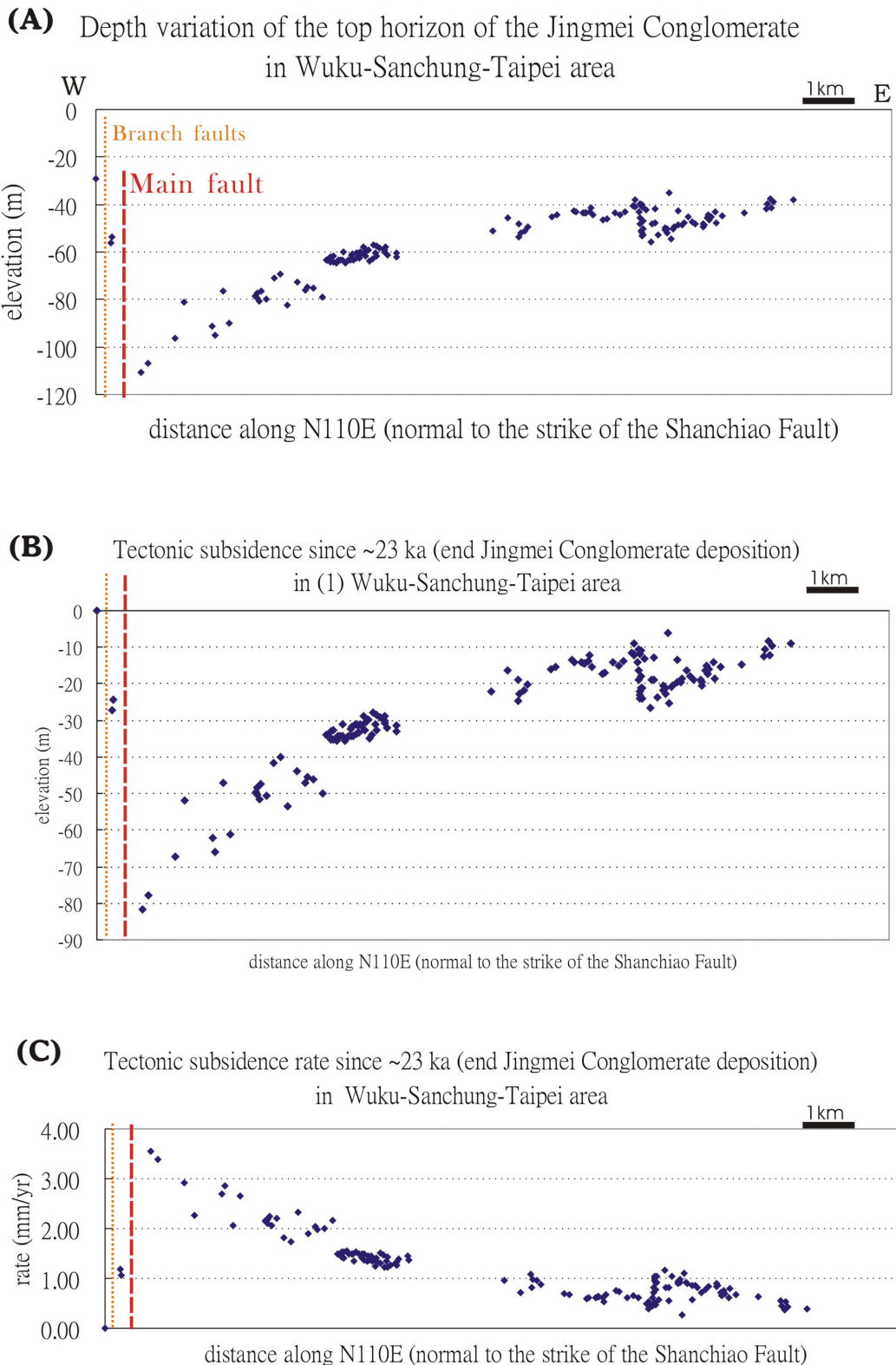


Fig. 5-5. Variations of the Jingmei Formation top horizon depth (A), and the deduced tectonic subsidence amount (B) and rate (C) since ~ 23 ka in the Wuku-Sanchong-Taipei profile normal to the fault trace across the fault.

Table 5-1. Borehole records of Jingmei Formation top horizon in the Wuku-Sanchong-Taipei profile.

Borehole	Easting	Northing	Horizon depth (m)	Distance N110E (m)	Elevation (m)	Horizon depth corrected (m)	Tectonic subsidence (m)	Subsidence rate (mm/yr)
SCF-1	293105	2773943	35.2	0	6.066	29.134	0.0	0.00
SCF-2	293430	2774097	59.9	305	6.358	53.542	24.4	1.06
WK-1	294148	2773725	110.8	980	3.971	106.829	77.7	3.38
BH-30	293411	2773646	60.4	287	4.2	56.2	27.1	1.18
BH-29	294018	2773883	111.1	858	0.25	110.85	81.7	3.55
A-47	294876	2774059	82.2	1664	1.042	81.158	52.0	2.26
A-48	294686	2774133	99	1485	2.737	96.263	67.1	2.92
A-46	295428	2774375	92.1	2182	0.798	91.302	62.2	2.70
BH-28	295494	2774314	96.5	2245	1.43	95.07	65.9	2.87
BH-27	295789	2774459	91.4	2522	1.2	90.2	61.1	2.66
A-45	295652	2774454	78.1	2393	1.744	76.356	47.2	2.05
ORDB25	296312	2774020	80.6	3013	1.97	78.63	49.5	2.15
ORDB26	296303	2774081	80.55	3004	1.83	78.72	49.6	2.16
ORDB27	296342	2774237	79.2	3041	1.72	77.48	48.3	2.10
ORDB28	296347	2774315	80.8	3046	1.33	79.47	50.3	2.19
BH-26	296381	2774432	82.1	3078	1.37	80.73	51.6	2.24
ORDB29	296414	2774474	77.8	3109	1.21	76.59	47.5	2.06
ORDB30	296516	2774598	81	3205	1.21	79.79	50.7	2.20
ORDB31	296675	2774753	72.3	3354	1.48	70.82	41.7	1.81
ORDB32	296799	2774892	70.78	3471	1.58	69.2	40.1	1.74
ORDB33	296955	2775029	84.2	3617	1.63	82.57	53.4	2.32
ORDB34	297148	2775097	74.4	3799	1.53	72.87	43.7	1.90
ORDB35	297344	2775092	76.4	3983	1.73	74.67	45.5	1.98
ORDB36	297468	2775059	76.9	4099	1.6	75.3	46.2	2.01
ORDB37	297645	2775204	80.6	4266	1.51	79.09	50.0	2.17
BH-25	297297	2774269	77.6	3939	1.36	76.24	47.1	2.05
PU13N	298062	2774185	63	4658	2.948	60.052	30.9	1.34
PU14N	298013	2774172	65.35	4612	2.015	63.335	34.2	1.49
PU15N	297962	2774168	65.3	4564	1.814	63.486	34.4	1.49
PU17N	297867	2774158	63.6	4474	1.94	61.66	32.5	1.41
PU18N	297817	2774157	64.23	4427	2.25	61.98	32.8	1.43
PU19N	297738	2774154	66.2	4353	2.999	63.201	34.1	1.48
PU01N	298737	2774353	62.5	5292	5	57.5	28.4	1.23
PU02N	298673	2774338	63.1	5232	5.95	57.15	28.0	1.22

PU03N	298580	2774315	62.9	5144	3.955	58.945	29.8	1.30
PU04N	298527	2774305	63.3	5095	3.614	59.686	30.6	1.33
PU05N	298478	2774290	61.35	5049	3.461	57.889	28.8	1.25
PU06N	298421	2774275	63.3	4995	3.21	60.09	31.0	1.35
PU07N	298373	2774262	64.4	4950	3.86	60.54	31.4	1.37
PU08N	298325	2774249	64.25	4905	3.95	60.3	31.2	1.36
PU09N	298257	2774232	64.6	4841	3.9	60.7	31.6	1.37
BH-23	298227	2774219	65.1	4813	3.65	61.45	32.3	1.41
A-44	298800	2774362	61.2	5351	2.89	58.31	29.2	1.27
PD10P	298110	2774251	67	4703	2.429	64.571	35.4	1.54
PD11P	298051	2774238	65.8	4647	2.382	63.418	34.3	1.49
PD13P	297928	2774222	66.7	4532	1.935	64.765	35.6	1.55
PD14P	297868	2774216	66.6	4475	2.309	64.291	35.2	1.53
PD15P	297818	2774213	66	4428	1.621	64.379	35.2	1.53
PD16P	297740	2774210	64.85	4355	1.672	63.178	34.0	1.48
PD01P	298649	2774392	65.3	5209	2.35	62.95	33.8	1.47
PD02P	298596	2774376	66.25	5159	2.35	63.9	34.8	1.51
PD03P	298504	2774352	66.5	5073	4.845	61.655	32.5	1.41
PD04P	298442	2774336	64.7	5015	4.158	60.542	31.4	1.37
PD05P	298398	2774325	66.4	4973	3.974	62.426	33.3	1.45
PD06P	298338	2774307	66	4917	3.35	62.65	33.5	1.46
PD07P	298272	2774291	66.3	4855	2.762	63.538	34.4	1.50
PD08P	298216	2774276	66.5	4802	2.94	63.56	34.4	1.50
PD09P	298168	2774264	66.2	4757	2.81	63.39	34.3	1.49
BH-22	298734	2774409	63.5	5289	1.62	61.88	32.7	1.42
BH-24	297780	2774212	65.8	4393	2.33	63.47	34.3	1.49
A-42	299140	2774544	64.1	5671	1.832	62.268	33.1	1.44
A-43	298902	2774475	61.64	5447	1.831	59.809	30.7	1.33
PD12N	299146	2774541	62.45	5676	1.943	60.507	31.4	1.36
PD15N	298954	2774482	63	5496	1.819	61.181	32.0	1.39
PD16N	298897	2774464	61.35	5442	2.076	59.274	30.1	1.31
PD19N	298706	2774407	64.7	5263	4.461	60.239	31.1	1.35
PU19M	298914	2774382	63.25	5458	5.178	58.072	28.9	1.26
NHB01	301062	2773044	54.9	7477	3.8	51.1	22.0	0.96
HCB31	301627	2773029	54	8008	2.117	51.883	22.7	0.99
RAB10	301710	2772389	53.2	8086	2.15	51.05	21.9	0.95
RAB14	301586	2773028	56.4	7969	2.61	53.79	24.7	1.07
SS-1	305389	2772923	50.33	11542	6.108	44.222	15.1	0.66

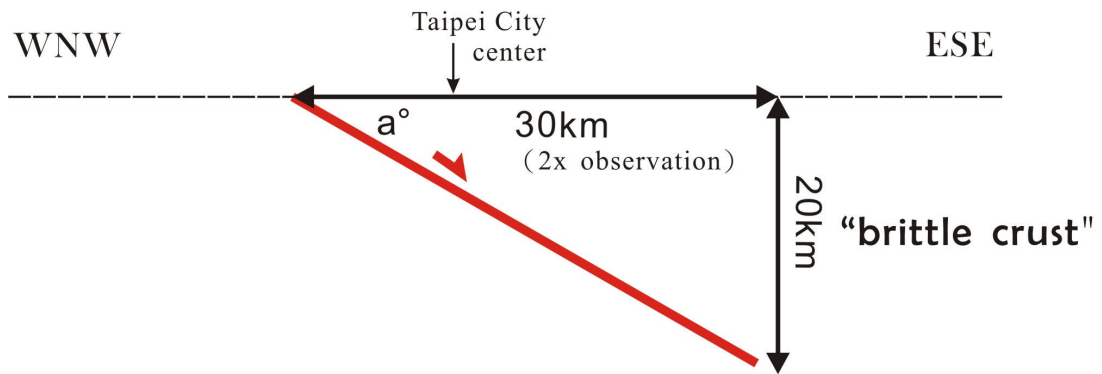
ME-B10	304087	2772328	57.3	10319	4.28	53.02	23.9	1.04
ME-B11	304054	2772545	57.8	10288	4.57	53.23	24.1	1.05
ME-B13	304057	2772839	56.1	10291	4.05	52.05	22.9	1.00
ME-B14	304246	2772953	59.3	10469	3.57	55.73	26.6	1.16
ME-B15	304393	2772984	56.6	10606	3.63	52.97	23.8	1.04
ME-B16	304638	2772908	58	10837	3.48	54.52	25.4	1.10
ME-B17	304683	2772938	53.6	10880	3.51	50.09	21.0	0.91
ME-B18	304869	2772900	53.6	11054	4.92	48.68	19.5	0.85
ME-B07	304079	2771757	54.4	10312	4.19	50.21	21.1	0.92
ME-B08	304043	2771784	55.4	10278	4.24	51.16	22.0	0.96
ME-B09	304083	2771978	54.7	10316	4.35	50.35	21.2	0.92
SS-B-39	306107	2771775	48.3	12218	4.58	43.72	14.6	0.63
SS-B-32	304986	2771799	50.7	11164	5.31	45.39	16.3	0.71
A-1	306634	2771538	43.8	12712	6.37	37.43	8.3	0.36
A-6	307093	2771554	46	13144	8.01	37.99	8.9	0.39
AH-43	306554	2771489	48	12637	6.23	41.77	12.6	0.55
AH-44	306579	2771521	46	12661	6.32	39.68	10.5	0.46
AH-45	306665	2771619	47.7	12741	6.38	41.32	12.2	0.53
AH-46	306703	2771727	44.4	12777	5.54	38.86	9.7	0.42
CH31	302633	2771872	49.6	8953	1.04	48.56	19.4	0.84
CH32	302686	2771834	49.9	9003	1.04	48.86	19.7	0.86
CH33	302778	2771833	51.9	9089	1.04	50.86	21.7	0.94
CH34	302855	2771833	53.1	9162	1.04	52.06	22.9	1.00
CH35	302892	2771871	50.6	9196	1.04	49.56	20.4	0.89
CH36	302992	2771830	54	9290	1.04	52.96	23.8	1.04
A-04	302976	2772592	53.15	9275	3.54	49.61	20.5	0.89
A-12	301682	2773026	53	8059	2.15	50.85	21.7	0.94
A-02	302968	2771959	49.1	9268	3.83	45.27	16.1	0.70
AD-5	303424	2771838	52.9	9696	1.04	51.86	22.7	0.99
BH-06	303551	2771862	56.1	9816	4.79	51.31	22.2	0.96
BH-08	303742	2771822	55.2	9995	4.69	50.51	21.4	0.93
BH-09	303785	2771822	55.2	10036	4.74	50.46	21.3	0.93
BH-3	301149	2772653	55.9	7558	2.87	53.03	23.9	1.04
BH-5	301151	2772644	55.7	7561	2.98	52.72	23.6	1.03
BH-6	301148	2772636	55.7	7557	2.99	52.71	23.6	1.03
BH-2	301863	2772671	56	8229	3.05	52.95	23.8	1.04

5.4 Half-space elastic dislocation modeling

5.4.1 Model setup

The long-term vertical tectonic deformation imposed by the Shanchiao Fault on the Jingmei Formation top horizon is modeled by a boundary element method (BEM), the Poly3D software developed by the Stanford University (Thomas, 1993). The modeling helps to resolve how slip on a fault patch (or element) can produce displacement within the half-space. If the fault geometry and fault slip distribution are known or determined, forward modeling can yield the corresponding (near-) surface displacement. In the case of the Shanchiao Fault, for which no exact information on its crustal geometry is available, numerous possible fault geometries whose dip varies with depth are tested against the offset pattern exhibited by the key horizon assuming uniform slip along the entire fault plane. The medium in which the fault slipped is assumed to be homogeneous, isotropic and elastic half-space as considered applicable in a variety of geological settings globally (Okada, 1985) with the amount of deformation/strain with respect to the modeled space. The parameters of crust elasticity applied in the forward modeling are adopted from those commonly used in previous works: the Young's modulus 75000 bars and Poisson's ratio 0.25. The fault is restricted to extend to either 20 km deep or 30 km away from the fault trace, the former one is constrained from the probable thickness of brittle crust in the Taipei region, and the later one is determined to be double of the length of the observation profile in order to prevent boundary effects (Fig. 5-6). The model results within 15 km away from the fault are taken for comparison, and the readings are taken every 500 m. As the geological constraint from the key horizon contains only the vertical component of fault displacement, only the vertical component of the model displacement is taken into analysis. For realistic comparison between geological record and model outcomes, both are converted to ratios of offset at each point to that of the maximum offset; in the geological record the maximum vertical offset about 80 m is set by the horizon depth record in borehole BH-29 near borehole WK-1 (the confirmed near-fault hanging wall location; Chen et al., 2010), and the two boreholes are probably located around 500 m away from the main fault trace; in the model results the value 500 m away from the fault is taken as the maximum for each experiment (Fig. 5-7).

(A) "Single-plane"



(B) "Listric"

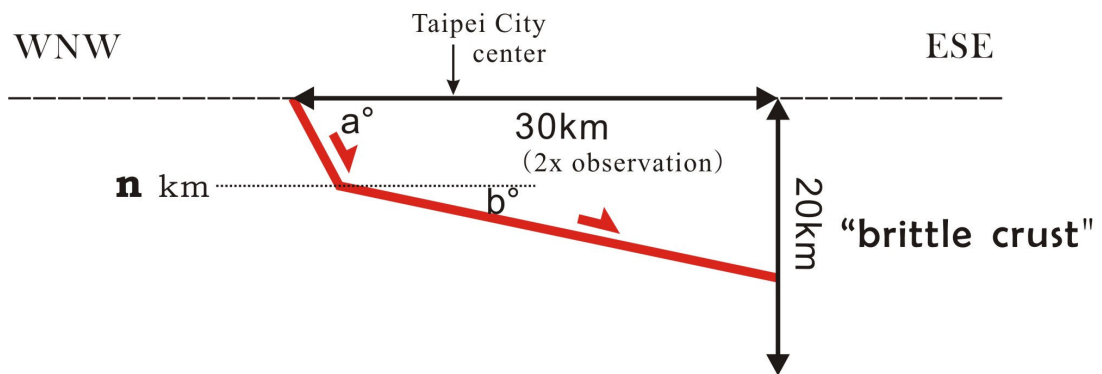


Fig. 5-6. Settings of the uniform dip and listric models in elastic half-space dislocation modeling.

5.4.2 Fault plane models with uniform dip

The first set of experiments assume the Shanchiao Fault has a constant dip within the brittle crust as consisted of only one fault patch. The dip angle, denoted as ‘a’ in Fig. 5-6A, is tested with a as 45°, 60° and 75°. The model results cannot reproduce the rapid decline of tectonic subsidence within 4 km of the fault trace (Fig. 5-7). While all models overestimate the vertical offset, the higher dip angle model of 75° has result closer to the observation and does not possess an unrealistic concave-upward trend near the fault as seen in lower angle models. What can be inferred is the Shanchiao Fault may be high angle in some portions of its fault plane but the uniform dip geometry does not fit to the observed deformation pattern.



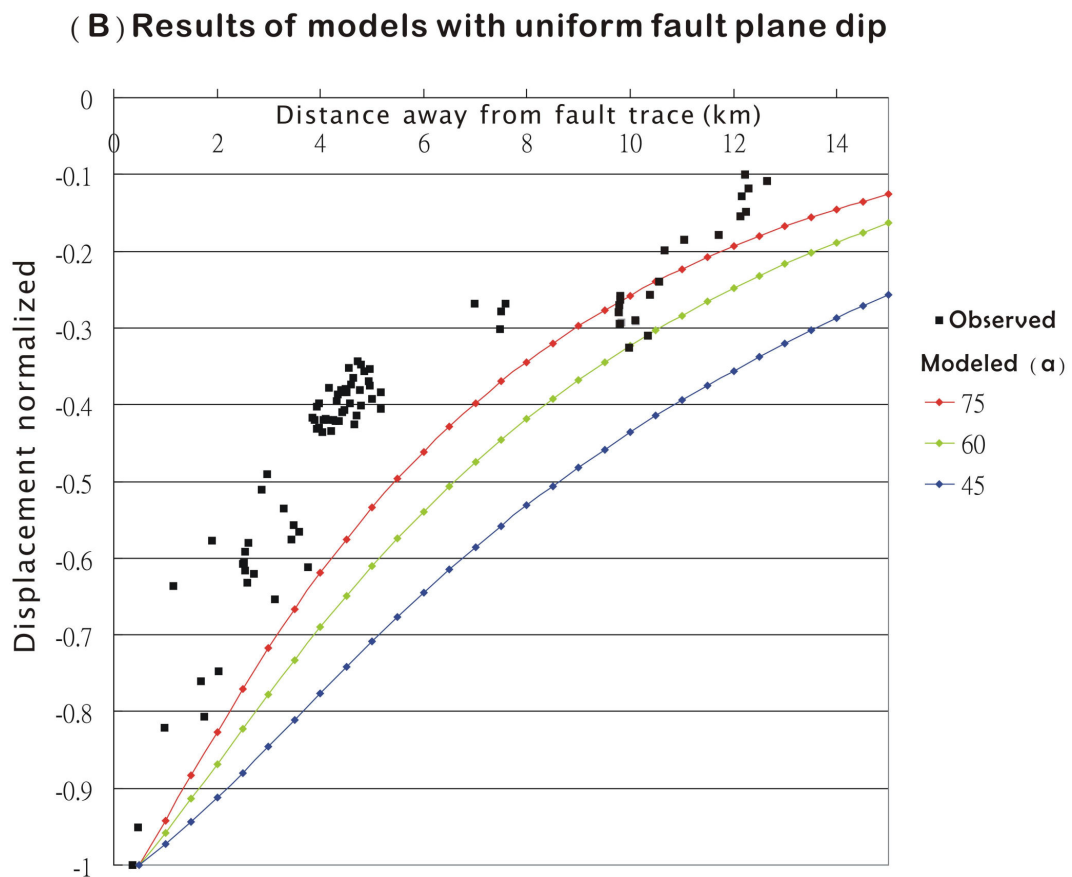
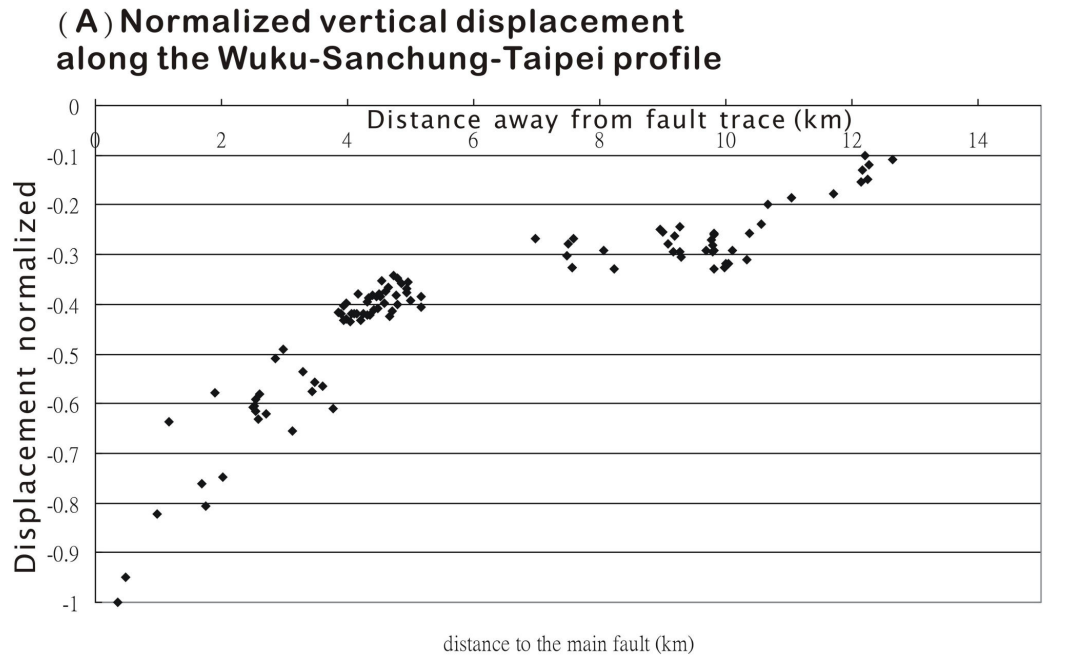


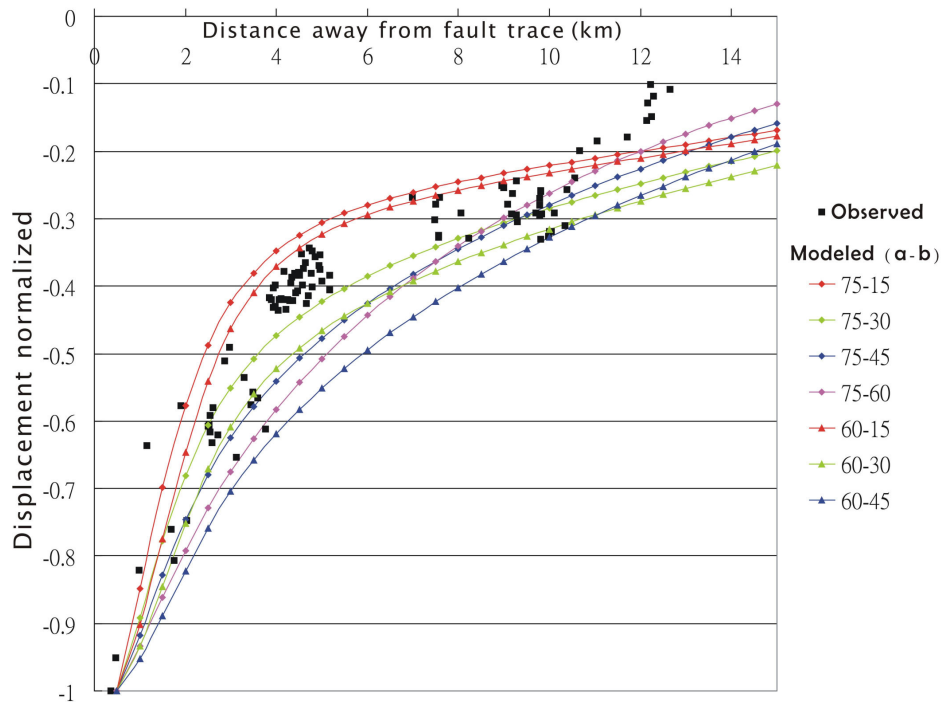
Fig. 5-7. (A) The geological constraint of long-term vertical tectonic deformation by the Shanchiao Fault recorded by the Jingmei Formation top horizon, with the offset values normalized. (B) Modeling outcomes of the uniform dip models. None of the models reproduce the roll-over monocline observed, while the higher angle model ($\alpha=75$) is relatively closer to the geologic constraints.

5.4.3 Fault plane models with listric geometry

The fact that the hanging wall of the Shanchiao Fault is deformed in a roll-over fashion (Figs. 5-4, 5; Chapter 4) indicates the fault plane is likely to possess listric geometry (Wernick and Burchfiel, 1982). Here a simplified listric geometry is achieved by joining a shallow steep-dipping fault patch with a deeper gentle-dipping fault patch (Fig 5-6B), which contains three independent variables: the dip of the upper and lower fault patches ('a' and 'b' degrees) and the depth of the junction point ('n' km). From the outcomes of the uniform dip experiments, the shallow patch is likely to be of high angle (not less than 60°). The listric experiments is grouped in four according to the fault plane nodal point depth (n) shown in Fig. 5-8. For each nodal depth, experiments with the values of 75 and 60, b values of 15, 30, 45 and 60 (for a=75) are carried out; if the experiments have results closely resemble the geological observation detailed dip variations are examined (e.g. a values of 85, 80, 70; b values of 5, 10, 20, 25). Several good fits are obtained from experiments with nodal depth over 3 km deep and a strong dip contrast between the upper and lower fault patches. If the junction is at 3 km deep, the upper patch should be no gentler than 75° and the lower patch is 15°; for a 4 km node depth the upper patch is again of very steep dips over 75° and the lower patch is 10°; when the junction depth is at 5 km deep, the upper patch needs to be sub-vertical (over 80°) while the lower patch is sub-horizontal at 5°. It's notable that slight variations (5°) in the dip angle of the lower patch can bring about large deviations of the output displacement pattern. There exists a trend that with increasing flat-ramp nodal depth (n) the shallower part of the fault has to be more upright while the deeper part of the fault is required to be further horizontal. Despite the excellent fitting between the above listric model outcomes and the geological data within 5 km away from the fault, the model results either overestimate the offset farther than 10 km (for nodal depth at 3 km) or underestimate the displacement between 6 and 11 km (for nodal depths at 4 and 5 km).

Results of Listric Models

(A) Nodal depth $n=2$ km



(B) Nodal depth $n=3$ km

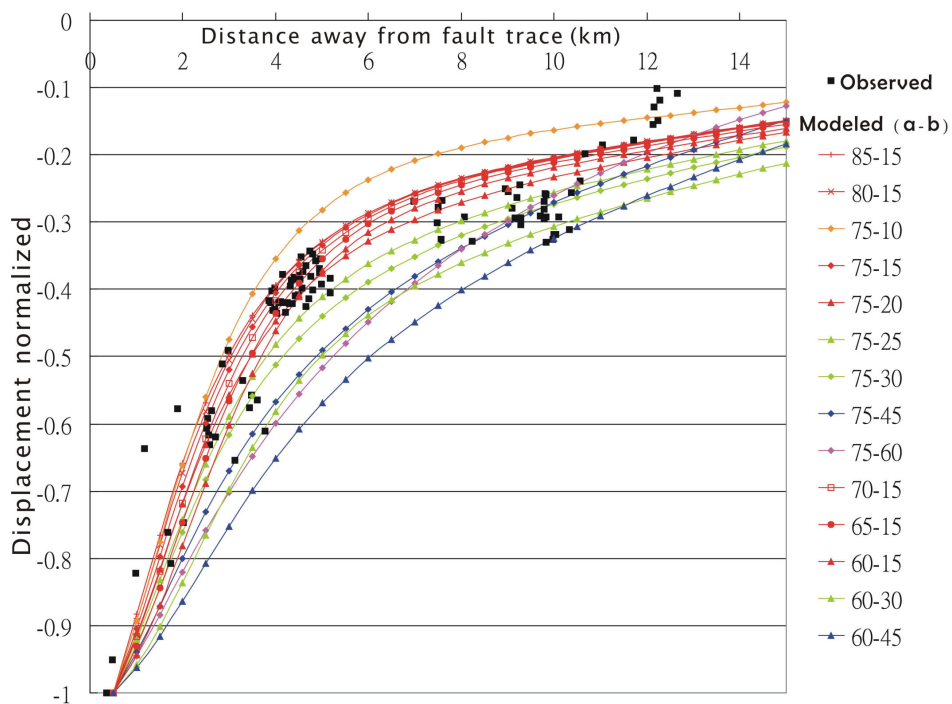


Fig. 5-8. Modeling outcomes of the listric models. From the good-fit experiments, when the flat-ramp nodal depth (n) is increased (from 3 to 5 km) the shallower part of the fault has to be more upright (no less than 75°) while the deeper part of the fault is required to be further horizontal (ranging from 15° to 5°).

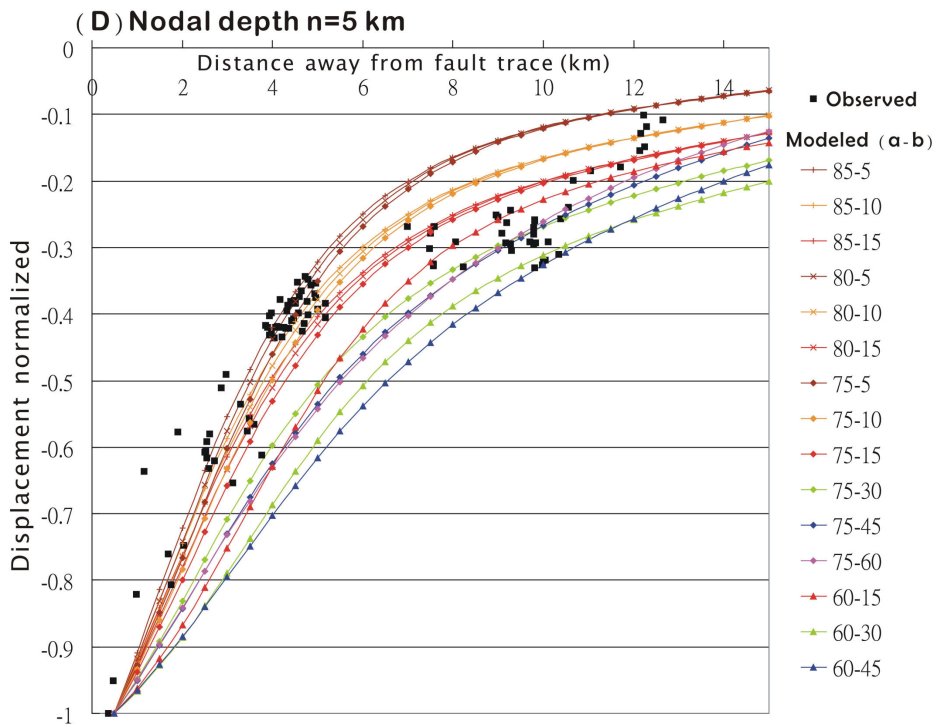
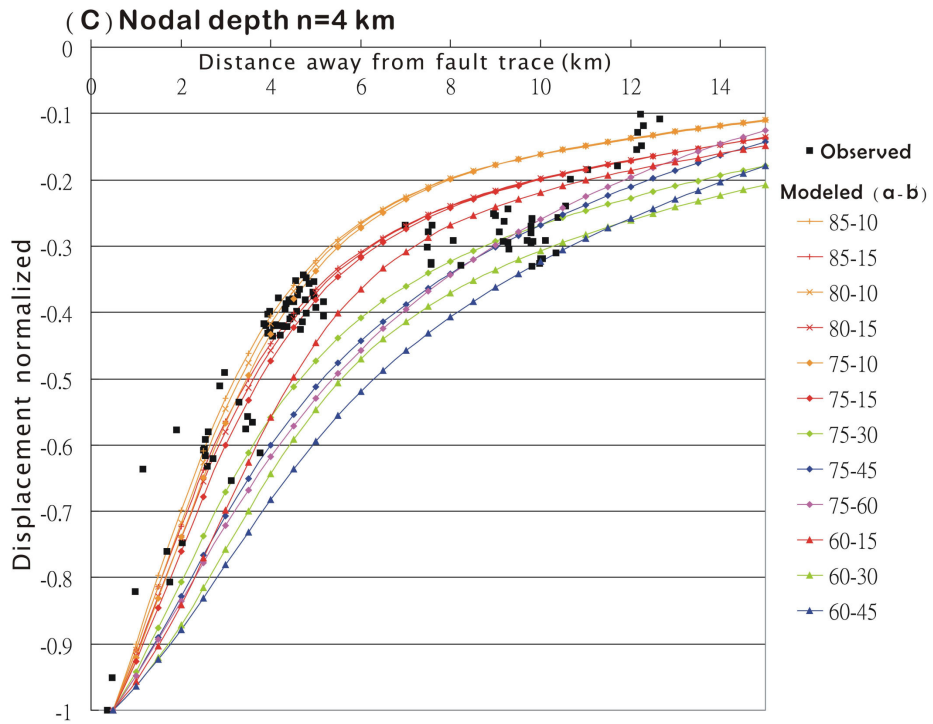


Fig. 5-8. (continued)

5.5 Discussions

5.5.1 Shallow crust fault geometry and its relation with syn-convergence thrust detachment

The modeling results, albeit performed under very simplified and idealistic conditions and geometrical settings, provide us first-order control on the shallow crust geometry of the Shanchiao Fault. A drastic bend of the fault plane from near-vertical to sub-horizontal at 3 to 5 km depths is the characteristics of Shanchiao Fault in shallow crust. The upper part of the fault plane above the bend dips from 75° to vertical ('ramp'), and the fault plane below the bend dips from 15° to 5° ('flat'). The fault plane of all the models producing good fit does not go deeper than 12 km within the modeled space. The sub-vertical dip at shallow depth and the extreme curve toward sub-horizontal is necessary to produce the pronounced roll-over folding of the hanging wall and the fast decline of tectonic subsidence away from the fault (Fig. 5-5). In other words, the near-fault hanging wall deformation pattern (in the Shanchiao Fault case, about within 5 km away from fault trace) reflect the shallow crust fault plane geometry. The misfit of model output with observed displacement pattern further away from fault about 6 to 13 km, though uncertainties in the geological record may exist, demonstrates the ambiguity of the fault plane dipping at deeper depth.

The abrupt fault plane bend illustrate above is a clear evidence that the Shanchiao Fault is a negative tectonic inversion product from a pre-existing thrust fault plane. The best candidate of the reactivated structure is the Hsinchuang Thrust, the former deformation front in northern Taiwan when the region was in its compressive phase (Chiu, 1968; Suppe, 1980). The Hsinchuang Thrust outcrops along or slightly west of the topographic divide between the Linkou Tableland and the Taipei Basin (Fig. 5-1), more than 1 km west of the main fault. The Hsinchuang Thrust has a snakehead-like structure at near surface and rapidly turned to be a flat and gentle-dipping plane a few kilometers deep (Chiu, 1968; Suppe, 1980). The Hsinchuang Thrust is therefore very low-dipping (~15° or less) from around 3 km deep onwards and may root into the master detachment of the Western Foothills at the frontal part of the Taiwan orogenic wedge (Suppe, 1980). The sub-horizontal lower fault patch in the good fit models may be the inverted Hsinchuang Thrust plane. At shallow depth normal faulting is not sustained on the pre-existing gentle plane and branches upward to form a new sub-vertical fault plane, a process probably related to the decreased confining pressure under vertical σ_1 stress regime. The newly-formed sub-vertical upper fault patch extends to the land surface producing the steep basement gradient along the main fault in the Shanchiao Fault zone (Chen et al., 2010; Chapter 4).

In spite of excellent correlation of the regional pre-existing thrust plane, normal faulting is thought to be difficult, if not impossible, to be initiated or continue to be active with very gentle dipping configuration in the brittle upper crust (Anderson, 1951; Profett, 1977; Sibson, 1985, 2000). The dips of the lower fault patch of the considered models and the Hsinchuang Thrust itself are all below the lower bound value for partial reactivation of former thrust plane demonstrated by Faccenna et al. (1995). Faulting on such extreme curved surface may also be kinematically unviable without the presence of branch or splay faults co-active in conjunction with the master Shanchiao Fault, which are not found on geological, geodetic or geomorphic evidences (Rau et al., 2008; Lin et al., 2010; Chan et al., 2005). Below a brief review of the low-angle normal fault enigma is summarized, and then further changes in fault plane geometry at depth is proposed advising the plausible involvement of other pre-existing structures for the Shanchiao Fault.

5.5.2 Deeper fault geometry and the low-angle-normal-fault enigma

5.5.2.1 Global debate on seismogenesis on low angle normal faults

Although been mapped in the brittle crust of many extending tectonic provinces and accommodate significant crustal extension, activity especially seismic slips on low-angle normal faults has long been questioned (Collettini, 2011, and references therein). In a simple brittle extensional regime with vertical maximum principle stress (Anderson, 1951) containing isotropic and fluid saturated (hydrostatic) rock mass, according to frictional sliding failure criterion pre-existing planar discontinuity dipping lower than 30° is unable to be reactivated unless the pore fluid pressure exceeds the minimum principle stress; similar situation applies for normal fault initiation that based on Coulomb shear fracturing failure criterion fault planes dip less than 30° cannot be formed (Sibson, 1985, 2000; Collettini and Sibson, 2001). Another way to keep slips on the low-dipping planes is to radically reduce its frictional coefficient by the massive presence of phyllosilicates. However significant fluid overpressure in extensional regimes is thought to difficult to be maintained as tensile environment promotes permeability and is vulnerable to hydrofracturing, meaning the high-pressure fluid is easily drained (Sibson, 2000). Presence of massive phyllosilicate on the fault zone results from intense fluid-assisted diffusion mass transfer or the incorporation of particular lithology (e.g. serpentinite), while the velocity-strengthening behavior of the phyllosilicates permits only aseismic slips on the fault as creeping (e.g. Moore and Rymer, 2007; Collettini et al., 2009). For the Hsinchuang Thrust and the main decollement in northern Taiwan both the strong mineralization of phyllosilicates and significant fluid overpressure are not observed. What adds to the dilemma is the absence of moderate to large ($M > 5.5$) normal faulting earthquakes occurring on rupture planes dipping less than 30° globally

(Jackson and White, 1989; Colletini and Sibson, 2001), rendering further doubts on the seismogenic potential of low-angle normal fault systems.

5.5.2.2 Half-space elastic dislocation modelling of fault plane models with double-ramp geometry

Based upon the above arguments, a set of experiment is designed to explore if the now deep-seated normal faults can be involved in the Shanchiao Fault. The shallow part of the fault plane is listric as previously constrained, and a deeper steeper fault patch is introduced resulting in a ramp-flat-ramp geometry with two bends (Fig. 5-9). Geometry of the shallow listric part is taken from one of the good fits (Fig. 5-8) with parameters a , b and n (Fig. 5-6B) as 75° , 15° and 3 , respectively. The deeper fault patch as the second ramp is set to be dipping at 60° , the optimal angle for normal fault initiation and slip. The experiments are aimed at resolving the depth of the flat-ramp junction where the fault is bend downward (' m ' in Fig. 5-9). The modeling outcome is presented in Fig. 5-10. When the junction depth is shallower than 8 km the double-ramp geometry produces an anticline in the hanging wall (axis at 7 km away from the fault when $m=5$, and at 13 km when $m=7$) instead of the roll-over monocline revealed by the horizon depth distribution, and the model results in the anticline area significantly underestimate the tectonic offset. When the bend depth from the middle sub-horizontal patch to the deep ramp patch is 8 to 9 km deep excellent fits with the Jingmei Formation top horizon record are obtained. Compared with the listric good fits, the double-ramp good fits are able to envelope or contain the geologic data of the entire profile with lessened underestimations for data 7 to 11 km away from the fault, and exhibit smoother trends between 5 and 13 km away from the fault. Therefore the double-ramp geometry with the deeper bend at 8 to 9 km depth is a good candidate for the upper crustal configuration of the Shanchiao Fault.

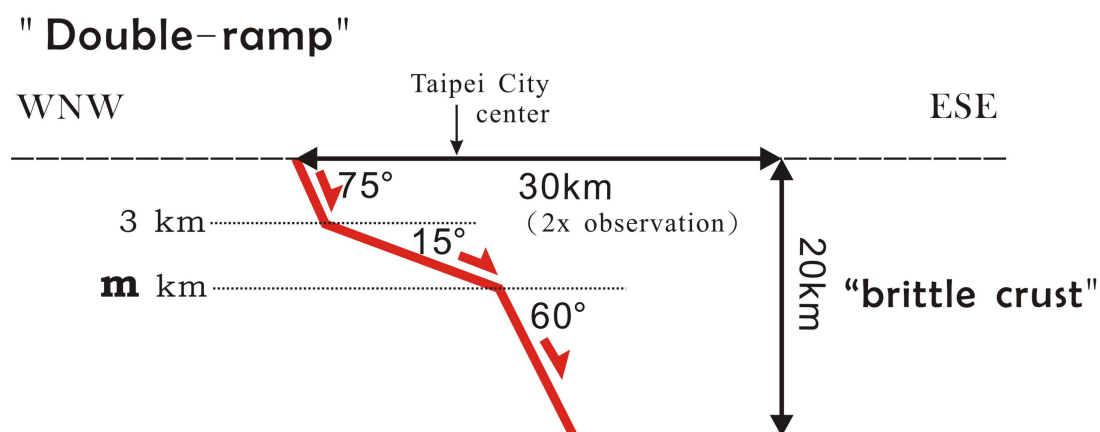


Fig. 5-9. Settings of the double-ramp models in elastic half-space dislocation modeling.

Results of Double - Ramp Models

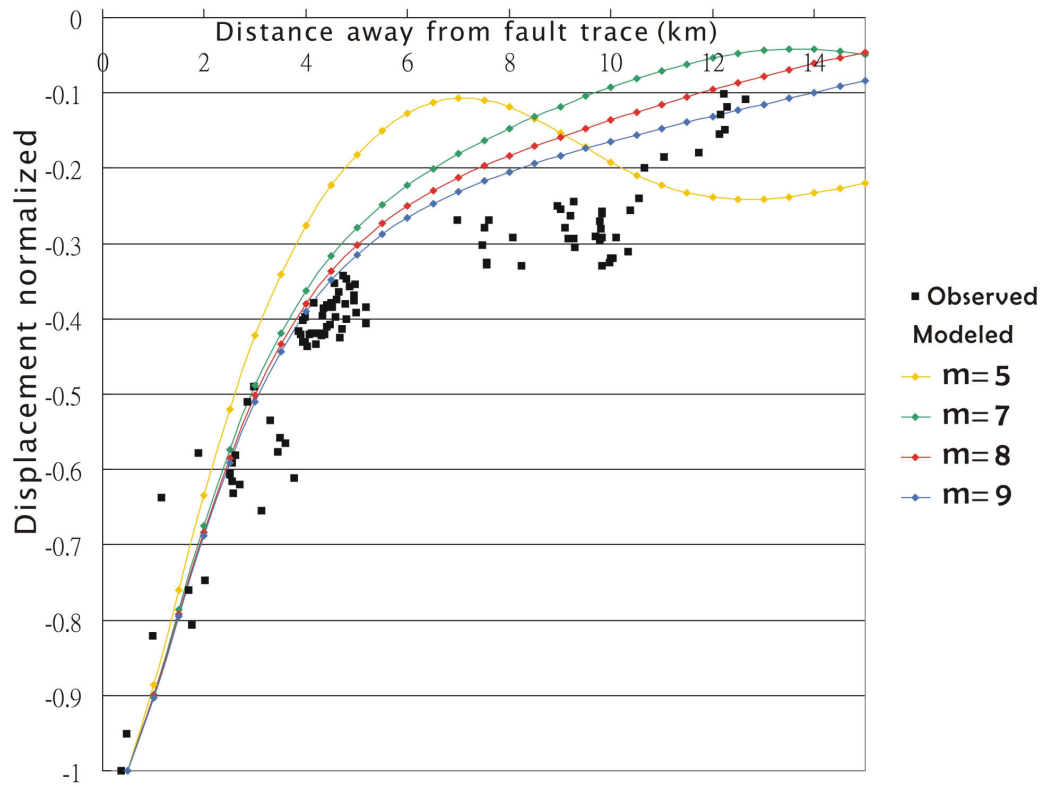


Fig. 5-10. Modeling outcomes of the double-ramp models. When $m=8$ to 9 km deep, excellent fits with the Jingmei Formation top horizon record are obtained with lessened underestimations for data 7 to 11 km away from the fault and smoother trends between 5 and 13 km away from the fault, compared with the listric good fits.

5.5.2.3 The role of pre-orogen rift normal faults on post-collisional extension tectonics

The deeper steep fault patch in the double-ramp geometry illustrated above is a possible manifestation of the pre-orogen normal fault buried under the orogenic wedge. Although this deep patch might be a newly-formed structure during the formation of the Shanchiao Fault in the post-orogenic processes, the fact that the Shanchiao Fault evidently re-slipped the pre-existing thrust décollement and the widespread presence of rift normal faults on the Chinese Continental Margin (Teng and Lin, 2004) strongly advocates its reactivation origin. The rift normal faults were mainly active from Eocene to late Oligocene or early Miocene and extend from the continental margin sediments into the basement till probably mid-crustal depth (Teng et al., 1992; Lin et al., 2003). When incorporated into the collision zone, the pre-orogen normal faults are mostly concealed beneath the wedge as the main detachment in the Western Foothill fold-thrust belt is located in Miocene and late Oligocene strata (Suppe, 1980), though their reverse faulting reactivation are also postulated (e.g. Mouthereau and Lacombe, 2006). For northern Taiwan the detachment level for the Hsinchuang Thrust and regional décollement is considered to be in the Wuchishan Formation deposited in late Oligocene. Thus the rift-related normal faults contained within the continental margin basement and lower sediments were underthrust below the frontal part of the wedge during the convergence and are difficult to be delineated from surface geological data. The modeling results thereby suggest that in northern Taiwan around the Taipei region pre-orogen rift normal fault is present under the fold-thrust pile and is currently re-slipped by the post-orogenic / post-collisional extensional faulting. To summarize, the modeling results indicate the Shanchiao Fault has reactivated both the Hsinchuang Thrust at intermediate depth and a rift normal fault further deep (Fig. 5-11).

A further supporting evidence for the deep-steepening of the Shanchiao Fault plane comes from detailed relocation and focal mechanism determination of a recent M_w 3.8 earthquake happened on 23 October 2004. The epicenter is located slightly east of the eastern border of the Taipei Basin within the foothills, at depth estimated between 7 and 10 km (Lin, 2005; Chen et al., 2010b; Lee et al., 2010). With improved inversion methods, the earthquake rupture source parameters from the determined focal mechanism point to a normal fault striking northeast and dipping about 60° to southeast (Chen et al., 2010b; Lee et al., 2010). The fault plane dip estimates are in agreement with the proposed double-ramp geometry, and the rupture was likely to have occurred on the upper boundary of the lower ramp fault patch (Fig. 5-11).

The continuing deviations between geological data and modeling outcomes from 7

to 12 km on the Wuku-Sanchung-Taipei profile, though narrowed down in the double-ramp models, implies more complexities exist about the deeper fault plane geometry or other geological agents affecting the Jingmei Formation top horizon depth variation in the region, and is subject to further investigation.

5.5.3 Seismic hazard implication

Detailed fault plane geometry is crucial in evaluating its seismic hazard, as the width and hence area of the ruptured fault plane is proportional to the seismic moment, and the districts where sections the fault plane lie within the seismogenic zone depths project to land surface are probable epicenter sites. Moderate to large earthquakes in extensional provinces are found able to be generated at very shallow depths less than 5 km deep in areas like the northern Apennines (e.g. Boncio et al., 2004; Chiaraluse et al., 2005). For the double-ramp geometry proposed above, the possible seismogenic zone of the Shanchiao Fault may cover the eastern half of the Taipei Basin and the neighboring foothill areas, as the 5-km-depth contour on the fault plane lies about 8 to 9 km away from the fault trace. Given the optimal attitude and its location within the seismogenic zone depths, the reactivated rift normal fault might be the driving source of fault movement especially during seismic rupturing.

Another lesson from northern Apennines seismotectonics is the tendency of major earthquakes to cluster and nucleate at loci of fault plane bends with prominent changes in fault plane dip angle or development of splaying branch faults, as revealed in the Narcia, Gubbio and Colfiorito earthquake events (Boncio and Lavecchia, 2000a, b). Although the Shanchiao Fault lacks the presence of microseismicity along the fault plane as observed on the Altotiberina extensional detachment in the northern Apennines (Chiaraluse et al., 2007), the shallow and deep ramp-flat junction of the proposed fault plane geometry might be nucleation sites for important seismic events. This inference is also substantiated by the 23 October 2004 Taipei Earthquake (Lee et al., 2010; Chen et al., 2010b) and two more following seismic events (M_L 3.2 and 3.7 on 23 March 2005 and 5 December 2005, respectively; Chen et al., 2010b) which all occurred in the same area and depth correlated to the shallow border of the lower ramp fault patch near the junction with the inverted thrust detachment. In map view the shallow (about 3 km deep listric bending) and deep (about 8 km deep connection to rift normal fault) are positioned around 1 and 20 km away from the fault line. Such speculation puts almost the entire Taipei Metropolis within the potential epicentral region, and needs to be verified when further constraints including crustal rheology and fault zone properties are available, as well as the transcurrent motion present on the fault which is largely neglected in the present study due to the difficulty to quantify its contribution to fault offset and fault plane geometry.

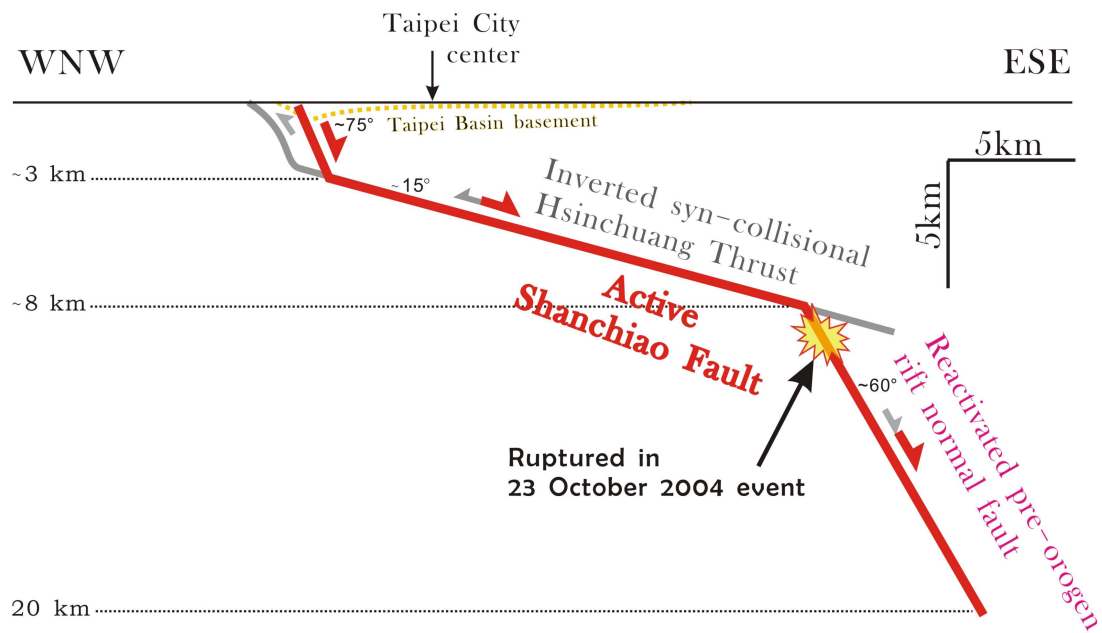
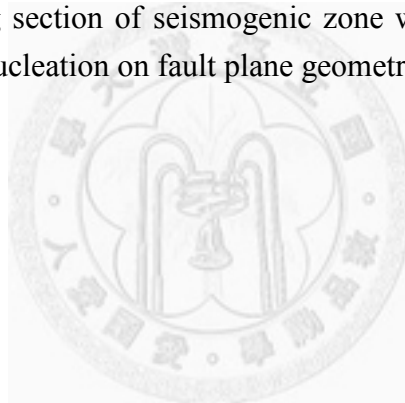


Fig. 5-11. Interpretation of modeling results on the upper crust geometry of the Shanchiao Fault, highlighting the clear inversion of syn-convergence Hsinchuang Thrust detachment and the likely reactivation of the pre-orogen rift normal fault.

5.6 Concluding remarks

With the aid of basin-wide geological record of long-term tectonic subsidence since the Last Glacial Maximum, the upper crustal geometry of the Shanchiao Fault is first illuminated by simple half-space elastic dislocation modeling. The shallow portion of the fault plane is listric with a sudden change between 3 and 5 km deep from sub-vertical to near-horizontal dips as reflected by the prominent roll-over monoclinical folding in the immediate hanging wall. The deeper portion of the fault is considered to possess another bending from sub-horizontal to steep dipping when taking into account of the tectonic subsidence in the eastern half of the basin, the existence of pre-orogen normal fault underneath the fold-thrust pile, the few but well-resolved focal mechanisms, and the debated seismogenic ability of extensional detachment. The Shanchiao Fault is therefore found to have acquired a complex double-ramp configuration by reactivating both a syn-convergence thrust detachment (the Hsinchuang Thrust) and a pre-orogen rift normal fault. Such geometry place much of the Taipei Metropolis region within the epicentral area of the Shanchiao Fault judged by the overlapping section of seismogenic zone with the fault plane and the likelihood of earthquake nucleation on fault plane geometrical singularities.



Chapter 6: Conclusions and future scope

6.1 Mapping the Shanchiao Fault with illumination of fault zone structure

The Shanchiao Fault is composed of a main fault and several westerly branch faults within shallow basin deposits as illuminated from borehole syntheses in the Wuku and Luzhou areas in the central portion of the fault. A fault zone up to several hundred meters wide on land surface is therefore defined with the main fault bounding in the east and the morphogenic westernmost branch fault as the western boundary (Fig. 4-16).

6.2 Continued and ongoing activity of the Shanchiao Fault since 23 ka to present constrained by growth faulting study and leveling data analysis

Stacking of post-Last Glacial Maximum basin deposits in the fault zone has been constantly enhanced by subsidence resulted from normal faulting in addition to the rising eustasy, indicating continued activity on the fault with calculated tectonic subsidence rate on the hanging wall immediately east of the main fault around 3 mm/yr in the Holocene and since 23 ka. Analysis of modern leveling data across the basin also confirms the existence of contemporary tectonic subsidence in the near-fault hanging-wall region after tentative removing of shallow soil compaction and discussion on aquifer-related deformation. Basin-wide mapping of a key marker in the growth sediments for cumulative tectonic subsidence since 23 ka, the Jingmei Formation top horizon, exhibits that the hanging wall of the Shanchiao Fault is deformed into a roll-over monocline with maximum offset in the central part of the fault in Wuku and Luzhou areas, and fault displacement decreases rather systematically toward the southern tip of the fault.

6.3 Joint reactivation of syn-convergence thrust and pre-orogen rift fault by the Shanchiao Fault during orogen wedge collapse

The Shanchiao Fault is interpreted to be composed of a shallow sub-vertical patch joining a near-horizontal patch at 3 to 5 km depth, and a further deep steep patch starting at 8 to 9 km depth based on simple elastic dislocation modeling of post-LGM tectonic subsidence. Such shallow listric geometry with a deep ramp is a manifestation of reactivating both syn-convergence thrust detachment and pre-orogen rift normal fault in the post-collisional extensional tectonics. As substantiated by the 23 October 2004 and following similar events, pre-orogen rift fault is first elucidated contributing to post-orogenic tectonic processes in northern Taiwan. Such complex fault plane geometry may have implications on seismic hazard evaluation concerning the possible sites for earthquake nucleation.

6.4 Future Scope: Unresolved dilemmas and some directions for further investigations

One of the critical questions neglected in the thesis work is the contribution percentage of transcurrent motion on fault slips. Lee et al. (1999) suggested the Taipei Basin was formed as a releasing bend with the Shanchiao Fault as a sinistral fault, despite the oblique fault striation they reported in SCF-2. GPS-derived deformation field in the vicinity of the Shanchiao Fault is also characterized by both extensional and sinistral shear strain (Rau et al., 2008; Lin et al., 2010). How much the proportion of transcurrent component of strain observed during the interseismic period (GPS data) or from the branch fault (recovered in SCF-2) can be projected to the complete seismic cycle or the entire fault zone is difficult to resolve. Although fault scarp arrangement and few earthquake focal mechanisms (Lee et al., 2010; Chen et al., 2010c) also denote the presence of sinistral movement, more geologic constraints (what kind of data can be useful?) are needed for solid estimations.

Another difficulty met is the study and quantification of fault structure and fault slip rates north of the Tanshui River in the northernmost part of the Taipei Basin. The absence of the Jingmei Formation in the Guandu and Beitou (probably Shilin, too) precludes the methodology applied in the work. More radiocarbon dating results from shallow sediments in the SCF-7, 8 and 9, and neighboring boreholes may help. A more radical and time-consuming way is to correlate volcanic ash layers with known age (e.g. Chen et al., 2010c). Besides, borehole analysis for areas south of Wuku area along the fault is also needed to better constrain the Shanchiao Fault zone towards south.

The paleoseismic events noticed by Huang et al. (2007) span only from 11 ka to 8 ka, which led to doubts on the recent activity of the Shanchiao Fault and the trouble in estimating the earthquake recurrence interval. Consider the sea-level-coupled growth faulting operating in the fault zone, the borehole pairs Huang et al. studied lie in the western part of the fault zone experiencing less tectonic subsidence (none if on footwall as SCF-1) while the sea level stabilized to current level at around 6 ka without further rising (e.g. Chen and Liu, 1996); this means that sediments later than 6 ka was hard to accumulate on the footwall as room for deposition did not increase. Syn-faulting sediments may remain between SCF-2 and WK-1 in the Wuku Profile due to stronger tectonic subsidence; drilling and correlation in the section proposed above might facilitate recognizing more recent paleo-earthquake events.

In this work the southern tip of the Shanchiao Fault is anticipated to divert west outside the basin following the trace of the Hsinchuang Thrust; such statement is still far from mature and requires more evidences for confirmation. Another more

significant question is how the Shanchiao Fault in the Taipei Basin extends northward into the Tatun Volcanoes and the possible co-activation with the Chinshan Normal Fault farther north (Shyu et al., 2005; Huang et al., 2007). Again, multi-discipline efforts are needed to complete the mapping of the entire Shanchiao Fault.

The upper crustal structure of the Shanchiao Fault proposed in Chapter 5 is rather a bold adventure, especially on involving a second deeper ramp as reactivation of pre-orogen normal fault associated with the opening of the South China Sea. Although substantiated with modeling results, mechanical arguments, and few well-constrained seismic events, solid confirmation on the existence and geometry of the deeper ramp is not yet achieved. Besides means including cross section construction, detailed analysis of regional seismicity and modeling under more realistic settings (viscous-elastic instead of only elastic), studying the more evolved and exhumed post-collisional collapsed mountain belt northeast and east of the Taipei Basin may yield insights to the active structures and possible reactivations at the collision-subduction junction in northern Taiwan.



References

- Abidin, H.Z., Djaja, R., Darmawan, D., Hadi, S., Akbar, A., Rajiyowiryono, H., Sudiby, Y., Meilano, I., Kasuma, M.A., Kahar, J., Subarya, C., 2001. Land subsidence of Jakarta (Indonesia) and its geodetic monitoring system. *Natural Hazards* 23, 365-387.
- Allen, D. R., Mayuga, M. N., 1969. The mechanics of compaction and rebound, Wilmington Oil Field, Long Beach, California, U.S.A. *Proceedings of the Tokyo Symposium on Land Subsidence* 2, 410-423, International Association of Scientific Hydrology and UNESCO, September 1969, Tokyo.
- Amelung, F., Galloway, D.L., Bell, J.W., Zebker, H.A., Laczniak, R.J., 1999. Sensing the ups and downs of Las Vegas: InSAR reveals structural control of land subsidence and aquifer-system deformation. *Geology* 27-6, 483-486.
- Anderson, E.M., 1951. *The dynamics of faulting*, 2nd edition. Oliver and Boyd, Edinburgh, p. 206.
- Angelier, J., Barrier, E., Chu, H.-T., 1986. Plate collision and paleostress trajectories in a fold-thrust belt: the Foothills of Taiwan. *Tectonophysics* 125, 161-178.
- Bawden, G.W., Thatcher, W., Stein, R.S., Hudnut, K.W., Peltzer, G., 2001. Tectonic contraction across Los Angeles after removal of groundwater pumping effects. *Nature* 412, 812-815.
- Boncio, P., Lavecchia, G., 2000a. A structural model for active extension in central Italy. *Journal of Geodynamics* 29, 233-244.
- Boncio, P., Lavecchia, G., 2000b. A geological model for the Colfiorito earthquakes (September – October 1997, central Italy). *Journal of Seismology* 4, 345 –356.
- Boncio, P., Lavecchia, G., Pace, B., 2004. Defining a model of 3D seismogenic sources for Seismic Hazard Assessment applications: The case of central Apennines (Italy). *Journal of Seismology* 8-3, 407-425.
- Briais, A., Patriat, P., Tapponnier, P., 1993. Updated interpretation of magnetic anomalies and seafloor spreading stages in South China Sea: implications for the tertiary tectonics of Southeast Asia. *Journal of Geophysical Research* 98, 6299–6328.
- Brown, L.F.Jr., Loucks, R.G., Treviño, R.G., Hammes, U., 2004. Understanding growth-faulted, intraslope subbasins by applying sequence-stratigraphic principles: Examples from south Texas Oligocene Frio Formation. *AAPG Bulletin* 88-11, 1501-1522.
- Bull, J.M., Barnes, P.M., Lamarche, G., Sanderson, D.J., Cowie, P.A., Taylor, S.K., Dix, J.K., 2006. High-resolution record of displacement accumulation on an active normal fault: Implications for models of slip accumulation during repeated earthquakes. *Journal of Structural Geology* 28, 1146-1166.

- Caputo, R., Helly, B., 2008. The use of distinct disciplines to investigate past earthquakes. *Tectonophysics* 453, 7-19.
- Caputo, R., Helly, B., Pavlides, S., Papadopoulos, G., 2004. Palaeoseismological investigations of the Tyrnavos Fault (Thessaly, Central Greece). *Tectonophysics* 394, 1-20.
- Cappa, F., Guglielmi, Y., Fenart, P., Merrien-Soukatchoff, V., Thoraval, A., 2005. Hydromechanical interactions in a fractured carbonate reservoir inferred from hydraulic and mechanical measurements. *International Journal of Rock Mechanics and Mining Sciences* 42, 287-306.
- Chai, J.-C., Shen, S.-L., Zhu, H.-H., Zhang, X.-L., 2004. Land subsidence due to groundwater drawdown in Shanghai. *Géotechnique* 54-2, 143-147.
- Chang, C.-P., Yen, J.-Y., Hooper, A., Chou, F.-M., Chen, Y.-A., Hou, C.-S., Hung, W.-C., Lin, M.-S., 2010. Monitoring of surface deformation in northern Taiwan using DInSAR and PSInSAR techniques. *Terrestrial, Atmospheric and Oceanic Sciences* 21-3, 447-461.
- Chang, H.-C., Lin, C.-W., Chen, M.-M., Lu, S.-T., 1998. An introduction to the active faults of Taiwan, explanatory text of the active fault map of Taiwan (in Chinese with English abstract). Special Publication of Central Geological Survey 10, 103 pp.
- Chan, Y.-C., Lee, J.-C., Chen, R.-F., Chang, K.-J., Liu, J.-K., Hsu, W.-C., Hu, J.-C., Chen, W.-S., Yang, C.-C., Chen, Y.-G., Cheng, D.-Y., Tsao, S., Hsieh, Y.-C., 2005. Airborne laser swath mapping of the Metropolitan Taipei Area: preliminary results and geological interpretations. Workshop on Volcanic Activities and Sanchiao Fault in the Taipei Metropolitan Area. p. 87-102. (in Chinese)
- Chan, Y.-C., Chang, K.-J., Chen, R.-F., Lee, J.-C., Hsieh, Y.-C., 2008. Characteristics of active normal faulting in the northern Taiwan mountain belt: Evidence from LiDAR-derived DTM and geologic observations. AGU Fall Meeting 2008, abstract # T53D-1983.
- Chan, Y.-C., Song, S.-R., Tsao, S., 2010. Preface to the special issue on potential geohazards of the Taipei Metropolitan Area. *Terrestrial, Atmospheric and Oceanic Sciences* 21, I-III.
- Chen, C.-H., Lee, C.-Y., Lin, S.-B., 1995. The eruption age of volcanic ashes in the Wuku Well, Taipei Basin: constraints on mineral chemistry and $^{40}\text{Ar}/^{39}\text{Ar}$ dating. *Journal of Geological Society of China* 38, 371-382.
- Chen, C.-H., Burr, G.S., Lin, S.-B., 2010c. Time of a near Holocene volcanic eruption in the Tatun Volcano Group, northern Taiwan: evidence from AMS radiocarbon dating of charcoal ash from sediments of the Sungshan Formation in Taipei Basin. *Terrestrial, Atmospheric and Oceanic Sciences* 21-3, 611-614.

- Chen, C.-T., Lin, K.-H., Jen, Y.-W., Lee, J.-C., Chan, Y.-C., 2004. Geomorphic studies of the Shanchiao Fault in the Taipei Basin, the Xth Symposium on Quaternary of Taiwan, Taipei, Taiwan, 151-154.
- Chen, C.-T., Lee, J.-C., Hu, J.-C., Chan, Y.-C., Lu, C.-Y., 2006. The active Shanchiao Fault in the Metropolitan Taipei Area, Northern Taiwan: geomorphic and geodetic analyses. *Eos Trans. AGU* 87-52, Fall Meeting Supplement, Abstract T33D-0543.
- Chen, C.-T., Hu, J.-C., Lu, C.-Y., Lee, J.-C., Chan, Y.-C., 2007. Thirty-year land elevation change from subsidence to uplift following the termination of groundwater pumping and its geological implications in the Metropolitan Taipei Basin, Northern Taiwan. *Engineering Geology* 95, 30-47.
- Chen, C.-T., Lee, J.-C., Chan, Y.-C., Lu, C.-Y., 2010a. Growth normal faulting at the western edge of the Metropolitan Taipei Basin since the Last Glacial Maximum, northern Taiwan. *Terrestrial, Atmospheric and Oceanic Sciences* 21-3, 409-428.
- Chen, C.-T., Chan, Y.-C., Lu, C.-Y., Simoes, M., Beyssac, O., 2011. Nappe structure revealed by thermal constraints in the Taiwan metamorphic belt. *Terra Nova* 23, 85-91.
- Chen, K.-C., Huang, B.-S., Huang, W.-G., Wang, J.-H., Kim, K.-H., Lee, S.-J., Lai, Y.-C., Tsao, S., and Chen, C.-H., 2010b. A blind normal fault beneath the Taipei basin in northern Taiwan. *Terrestrial, Atmospheric and Oceanic Sciences* 21-3, 495-502.
- Chen, Y.-G., Liu, T.-K., 1996. Sea level changes in the last several thousand years, Penghu Islands, Taiwan Strait. *Quaternary Research* 45, 254-262.
- Chen, W.-F., Teng, L.S., 1990. Depositional environment of Quaternary deposits of the Linkou Tableland, northwestern Taiwan. *Proceedings of the Geological Society of China* 33, 39-63.
- Chia, Y.-P., Chang, M.-H., Liu, W.-I., Lai, T.-C., 1999. Hydrogeologic characterization of Taipei Basin (in Chinese with English abstract). *Central Geological Survey Special Publication* 11, 393-406.
- Chiaraluce, L., Barchi, M., Collettini, C., Mirabella, F., Pucci, S., 2005. Connecting seismically active normal faults with Quaternary geological structures in a complex extensional environment: The Colfiorito 1997 case history (northern Apennines, Italy). *Tectonics* 24, TC1002.
- Chiaraluce, L., Chiarabba, C., Collettini, C., Piccinini, D., Cocco, M., 2007. Architecture and mechanics of an active low-angle normal fault: Alto Tiberina Fault, northern Apennines, Italy. *Journal of Geophysical Research* 112, B10310.
- Childs, C., Nicol, A., Walsh, J.J., Watterson, J., 2003. The growth and propagation of synsedimentary faults. *Journal of Structural Geology* 25, 633-648.
- Chiu, H.T., 1968. The Hsinchuang Fault in the Taoyuan area, northern Taiwan.

- Proceedings of Geological Society of China 11, 60-73.
- Cho, W.-C., 2006. Groundwater level change and elevation fluctuation of the Taipei Basin. Master thesis, National Taiwan University, Taipei, 73 pp.
- Clark, J.A., Farrelle, W.E., Peltier, W.R., 1978. Global changes in post glacial sea level: A numerical calculation. *Quaternary Research* 9, 265-287.
- Collettini, C., 2011. The mechanical paradox of low-angle normal faults: current understandings and open questions. *Tectonophysics* 510, 253-268.
- Collettini, C., Sibson, R.H., 2001. Normal faults normal friction? *Geology* 29, 927 – 930.
- Collettini, C., De Paola, N., Holdsworth, R.E., Barchi, M.R., 2006. The development and behaviour of low-angle normal faults during Cenozoic asymmetric extension in the Northern Apennines, Italy. *Journal of Structural Geology* 28, 333-352.
- Collettini, C., Niemeijer, A., Viti, C., Marone, C.J., 2009. Fault zone fabric and fault weakness. *Nature* 462, 907 – 910
- Constenius, K.N., 1996. Late Paleogene extensional collapse of the Cordilleran foreland fold and thrust belt. *Geological Society of America Bulletin* 108, 20-39.
- Dadson, S.J., Hovius, N., Chen, H., Dade, W.B., Hsieh, M.-L., Willett, S.D., Hu, J.-C., Horng, M.-J., Chen, M.-C., Stark, S.P., Lague, D., Lin, J.-C., 2003. Links between erosion, runoff variability and seismicity in the Taiwan orogen. *Nature* 426, 648-651.
- D'Agostino, N., Chamot-Rooke, N., Funicello, R., Jolivet, L., Speranza, F., 1998. The role of pre-existing thrust faults and topography of the styles of extension in the Gran Sasso range (central Italy). *Tectonophysics* 292, 229-254.
- Dokka, R.K., 2006. Modern-day tectonic subsidence in coastal Louisiana. *Geology* 34, 281-284.
- Faccenna, C., Nalpas, T., Brun, J.-P., Davy, P., 1995. The influence of pre-existing thrust faults on normal fault geometry in nature and in experiments. *Journal of Structural Geology* 17-8, 1139-1149.
- Fairbanks, R.G., Mortlock, R.A., Chiu, T.-C., Cao, L., Kaplan, A., Guilderson, T.P., Fairbanks, T.W., Bloom, A.L., 2005. Marine radiocarbon calibration curve spanning 0 to 50000 years B.P. based on paired $^{230}\text{Th}/^{234}\text{U}/^{238}\text{U}$ and ^{14}C dates on pristine corals. *Quaternary Science Reviews* 24, 1781-1796.
- Gambolati, G., Teatini, P., 1998. Natural land subsidence due to compaction of the upper Adriatic Sea Basin. *IGEA* 11, 29-40.
- Gambolati, G., Teatini, P., Tomasi, L., Gonella, M., 1999. Coastline regression of the Romagna region, Italy, due to natural and anthropogenic land subsidence and sea level rise. *Water Resources Research* 35-1, 163-184.
- Gatto, P., Carbognin, L., 1981. The Lagoon of Venice: natural environmental trend

- and man-induced modification. *Hydrological Sciences-Bulletin* 26-4, 379-391.
- Gawthorpe, R., Hardy, S., 2002. Extensional fault-propagation folding and base-level change as controls on growth-strata geometries. *Sedimentary Geology* 146, 47-56.
- Ho, C.-S., 1975. An introduction to the geology of Taiwan. Ministry of Economic Affairs, Republic of China, 143 pp.
- Holzer, T.L., 1984. Ground failure induced by groundwater withdrawal from unconsolidated sediments. *Reviews in Engineering Geology* 6, 67-105.
- Hori, K., Tanabe, S., Saito, Y., Haruyama, S., Nguyen, V., Kitamura, A., 2004. Delta initiation and Holocene sea-level change: Example from the Hong Song (Red River) delta, Vietnam. *Sedimentary Geology* 164, 237-149.
- Hsieh, C.-H., Chang, Y.-F., Sun, R.-H., 1992. Seismic investigate Hsin-Chuan fault on the west of Taipei Basin (in Chinese with English abstract). *Ti-Chih* 12-1, 13-26.
- Hsu, M. T., 1983. Estimation of earthquake magnitude and seismic intensities of destructive earthquakes in the Ming and Ching eras. *Meteorological Bulletin Central Weather Bureau* 29, 1-18. (in Chinese)
- Huang, C.-Y., 2006. On foraminifers of Taipei Basin. *Western Pacific Earth Sciences* 6, 29-58.
- Hu, J.-C., Yu, S.-B., Chu, H.-T., Angelier, J., 2002. Transition tectonics of northern Taiwan induced by convergence and trench retreat. *Geological Society of America Special Paper* 358, 149-162.
- Hu, J.-C., Chu, H.-T., Hou, C.-S., Lai, T.-H., Chen, R.-F., Nien, P.-F., 2006. The contribution to tectonic subsidence by groundwater abstraction in the Pingtung area, southwestern Taiwan as determined by GPS measurements. *Quaternary International* 147, 62-69.
- Huang, S.-Y., 2003. Prehistoric earthquakes along the Shanchiao Fault, Taipei Basin, Northern Taiwan. Master thesis, Central Washington University, 83p.
- Huang, S.-Y., Rubin, C.M., Chen, Y.-G., Liu, H.-C., 2007. Prehistoric earthquakes along the Shanchiao Fault, Taipei Basin, northern Taiwan. *Journal of Asian Earth Sciences* 31, 265-276.
- Hubert-Ferrari, A., Suppe, J., Gonzalez-Mieres, R., Wang, X., 2007. Mechanisms of active folding of the landscape (southern Tian Shan, China). *Journal of Geophysical Research* 112, B03S09.
- Hwang, J.-M., Wu, C.-M., 1969. Land subsidence problems in Taipei Basin. *Proceedings of the Tokyo Symposium on Land Subsidence* 1, 21-34, International Association of Scientific Hydrology and UNESCO, September 1969, Tokyo.
- Jackson, J.A., White, N.J., 1989. Normal faulting in the upper continental crust: observations from regions of active extension. *Journal of Structural Geology* 11, 15 - 36.

- Jelgersma, S., 1996. Land subsidence in coastal lowlands. In: Milliman J.D., Haq, B.U. (Eds.), *Sea-Level Rise and Coastal Subsidence*, pp. 47-62.
- Kao, H., Shen, S.J., Ma, K.-F., 1998. Transition from oblique subduction to collision: Earthquakes in the southernmost Ryukyu arc-Taiwan region. *Journal of Geophysical Research* 103, 7211-7229.
- Karig D.E., Hou G., 1992. High-stress consolidation experiments and their geologic implications. *Journal of Geophysical Research* 97, 289–300.
- Lam, D.D., Boyd, W.E., 2001. Some facts of sea-level fluctuation during the late Pleistocene-Holocene in Ha Long Bay and Ninh Binh area. *Journal of Sciences of the Earth* 23, 86-91.
- Lee, C.-T., Wang, Y., 1988. Quaternary stress changes in northern Taiwan and their tectonic implication. *Proceedings of the Geological Society of China* 31-1, 154-168.
- Lee, J.-C., 1989. Neotectonics of northern Taiwan based on the faults and paleostress analyses. Master thesis, National Taiwan University, Taipei, Taiwan., 128pp (in Chinese).
- Lee, J.-F., Lin, C.-Z., Lai, D.-C., Su, .T.-W., Chiu, Z.-L., Zeng, C.-J., 1999. The study on the formation of Taipei Basin. *Special Publication of Central Geological Survey* 11, 207-226 (in Chinese with English abstract).
- Lee, S.-J., Huang, B.-S., Liang, W.-T., Chen, K.-C., 2010. Grid-based moment tensor inversion techniques by using 3-D green's function database: a demonstration of the 23 October 2004 Taipei earthquake. *Terrestrial, Atmospheric and Oceanic Sciences* 21-3, 503-514.
- Lee, T.-Y., Lawver, L.A., 1994. Cenozoic plate reconstruction of the South China Sea region. *Tectonophysics* 235, 149-180.
- Lin, C.-C., 1957. *Geomorphology of Taiwan*. Taiwan Province Literature Communication, Taipei, 424 pp (in Chinese).
- Lin, C.-H., 2005. Seismicity increase after the construction of the world's tallest building: an active blind fault beneath the Taipei 101. *Geophysical Research Letters* 32, L22313, doi : 10.1029/2005GL024223.
- Lin, C. -H., Konstantinou, K. I., Liang, W.-T., Pu, H.-C., Lin, Y.-M., You, S.-H., Huang, Y.-P., 2005. Preliminary analysis of tectonic earthquakes and volcanoseismic signals recorded at the Tatun volcanic group, northern Taiwan. *Geophysical Research Letters* 32-10, L10313
- Lin, C.-W., Chang, H.-C., Lu, S.-T., Shih, T.-S., Huang, W.-J., 2000. An introduction to the active faults of Taiwan, 2nd ed., explanatory text of the active fault map of Taiwan (in Chinese with English abstract). *Special Publication of Central Geological Survey* 13, 122 pp.

- Lin, C.-Z., 2001. Geologic environment of the Taipei metropolis. Symposium on Geological Hazards in the Taipei Metropolis, 1-19 (in Chinese).
- Lin, C.-Z., 2005. Shanchiao Fault and the geological structures along the western margin of the Taipei Basin. Symposium on Volcanic Activities and the Shanchiao Fault in the Taipei Metropolis, 191-198 (in Chinese).
- Lin, C.-Z., Lai, T.-C., Fei, L.-Y., Liu, H.-C., Chi, C.-C., Su, T.-W., 1999. Results of deep borehole investigations in the Taipei Basin between 1992 to 1996. Special Publication of Central Geological Survey 11, 7-39 (in Chinese).
- Lin, K.-C., Hu, J.-C., Ching, K.-E., Angelier, J., Rau, R.-J., Yu, S.-B., Tsai, C.-H., Shin, T.-C., Huang, M.-H., 2010. GPS crustal deformation, strain rate, and seismic activity after the 1999 Chi-Chi earthquake in Taiwan. *Journal of Geophysical Research* 115, B07404.
- Lin, M.-L., Huang, T.-H., Hung, J.-J., Chi, C.-C., 1999. A study on in situ measurement of ground subsidence of Taipei Basin (in Chinese with English abstract). Central Geological Survey Special Publication 11, 317-344.
- Lo, C.-H., Chung, S.-L., Lee, T.-Y., Wang, K.-L., Wu, C.-T., 2000. Cenozoic magmatism and rifted basin evolution around the Taiwan Strait, SE China continental margin. *Eos Transactions AGU*, 81, 1111.
- Lu, C.-Y., Hsu, K.J., 1992. Tectonic evolution of the Taiwan mountain belt. *Petroleum Geology of Taiwan* 27, 21– 46.
- Lu, C.-Y., Angelier, J., Chu, H.-T., Lee, J.-C., 1995. Contractional, transcurrent, rotational and extensional tectonics: examples from Northern Taiwan. *Tectonophysics* 246, 129-146.
- Machette, M. N., Personius, S. F., Nelson, A. R., Schwartz, D. P., Lund, W. R., 1991. The Wasatch fault zone, Utah: Segmentation and history of Holocene earthquakes. In: Hancock, P. L., Yeats, R. S., Sanderson, D. J. (Eds.), *Characteristics of Active Faults*, *Journal of Structural Geology* 13, 137-150.
- McCalpin, J.P., Nishenko, S.P., 1996. Holocene paleoseismicity, temporal clustering, and probability of future large ($M > 7$) earthquakes on the Wasatch fault zone, Utah. *Journal of Geophysical Research* 101, 6233-6253.
- Meckel, T.A., ten Brink, U.S., Williams, S.J., 2006. Current subsidence rates due to compaction of Holocene sediments in southern Louisiana. *Geophysical Research Letters* 33, L11403, doi:10.1029/2006GL026300.
- Moore, D.E., Rymer, M., 2007. Talc-bearing serpentinites and the creeping section of the San Andreas fault. *Nature* 448, 795 – 797.
- Mouthereau, F., Lacombe, O., 2006. Inversion of Paleogene Chinese continental margin and thick-skinned deformation in the western foreland of Taiwan. *Journal of Structural Geology* 28, 1977-1993.

- Okada, Y., 1985. Surface deformation due to shear and tensile faults in a halfspace. *Bulletin of Seismological Society of America* 75-4, 1135 – 1154.
- Oliver, M.A., Webster, R., 1990. Kriging: a method of interpolation for geographical information system. *International Journal of Geographical Information Systems* 4-3, 313-332
- Ota, Y., Chappell, J., 1999. Holocene sea-level rise and coral reef growth on a tectonically rising coast, Huon Peninsula, Papua New Guinea. *Quaternary International* 55, 51-59.
- Peng, C.-H., Teng, L.S., Yuan, P.B., 1999. Facies characteristics of Taipei Basin deposits. *Special Publication of Central Geological Survey* 11, 67-99.
- Phien-wej, N., Giao, P.H., Nutalaya, P., 2006. Land subsidence in Bangkok, Thailand. *Engineering Geology* 82, 187-201.
- Proffett, J.M., 1977. Cenozoic geology of the Yerington district, Nevada, and implications for the nature of Basin and Range faulting. *Geological Society of America Bulletin* 88, 247 – 266.
- Rau, R.-J., Ching, K.-E., Hu, J.-C., Lee, J.-C., 2008. Crustal deformation and block kinematics in transition from collision to subduction: Global positioning system measurements in northern Taiwan, 1995-2005. *Journal of Geophysical Research* 113, B09404, doi: 10.1029/2007JB005414.
- Schmid, S. M., Pfiffner, O. A., Froitzheim, N., Schönborn, G., Kissling, E., 1996. Geophysical-geological transect and tectonic evolution of the Swiss-Italian Alps. *Tectonics* 15, 1036–1064.
- Scholz, C. H., 2002. *The mechanics of earthquakes and faulting*, 2nd ed., Cambridge University Press, New York.
- Seno, T., 1977. The instantaneous rotation vector of the Philippine Sea Plate relative to the Eurasian Plate. *Tectonophysics* 42, 209-226.
- Sharp, I.R., Gawthorpe, R.L., Underhill, J.R., Gupta, S., 2000. Fault-propagation folding in extensional settings: Examples of structural style and synrift sedimentary response from the Suez rift, Sinai, Egypt. *Geological Society of America Bulletin* 112-12, 1877-1899.
- Shih, R.-C., Chan, Y.-H., Liu, H.-C., 2004. Shallow seismic reflection surveys of the Shanchiao Fault in the Guandu Plain. *Special Publication of Central Geological Survey* 15, 1-11 (in Chinese with English abstract).
- Shyu, J.B.H., Sieh, K., Chen, Y.-G., Liu, C.-S., 2005. Neotectonic architecture of Taiwan and its implications for future large earthquakes. *Journal of Geophysical Research* 110, B08402, doi:10.1029/2004JB003251.
- Sibson, R.H., 1985. A note on fault reactivation. *Journal of Structural Geology* 7, 751 – 754.

- Sibson, R.H., 2000. Fluid involvement in normal faulting. *Journal of Geodynamics* 29, 469 – 499.
- Song, S.-R., Tsao, S.-J., Lo, H.-L., 2000. Characteristics of the Tatun volcanic eruptions, north Taiwan: implications for a cauldron formation and volcanic evolution. *Journal of Geological Society China* 43, 361-378.
- Song, S.-R., Chen, T.-M., Tsao, S., Chen, H.-F., Liu, H.-C., 2007. Lahars in and around the Taipei Basin: implications for the activity of the Shanchiao Fault. *Journal of Asian Earth Sciences* 31, 277-286.
- Suppe, J., 1980, A retrodeformable cross section of northern Taiwan. *Proceedings of Geological Society of China* 23, 46-55.
- Suppe, J., 1981. Mechanics of mountain building and metamorphism in Taiwan. *Memoir of the Geological Society of China* 4, 67–89.
- Suppe, J., 1984. Kinematics of arc-continent collision, flipping of subduction and back-arc spreading near Taiwan. *Memoir of the Geological Society of China* 6, 21–33.
- Tavarnelli, E., Renda, P., Pasqui, V., Tramutoli, M., 2003. The effects of post-orogenic extension on different scales: an example from the Apennine-Maghrebide fold-and-thrust belt, SW Sicily. *Terra Nova* 15, 1-7.
- Taylor, S.K., Nicol, A., Walsh, J.J., 2008. Displacement loss on growth faults due to sediment compaction. *Journal of Structural Geology* 30, 394-405.
- Teatini, P., Ferronato, M., Gambolati, G., Bertoni, W., Gonella, M., 2005. A century of land subsidence in Ravenna, Italy. *Environmental Geology* 47, 831-846.
- Terzaghi, K.T., 1925. *Erdbaumechanik auf Bodenphysikalischer Grundlage*: Wien, Deuticke, 399 pp.
- Teng, L.S., 1990. Late Cenozoic arc-continent collision in Taiwan. *Tectonophysics* 183, 57– 76.
- Teng, L.S., 1996. Extensional collapse of the northern Taiwan mountain belt. *Geology* 24, 949–952.
- Teng, L.S., Yuan, P.B., Chen, P.-Y., 1993. Study on stratigraphy and sedimentary environment. Report on Taipei Basin subsurface geology and engineering environment research project 1992, Central Geological Survey, MOEA, R.O.C.
- Teng, L.S., Yuan, P.B., Chen, P.-Y., Peng, C.-H., Lai, T.-C., Fei, L.-Y., Liu, H.-C., 1999. Lithostratigraphy of Taipei Basin deposits. Central Geological Survey Special Publication 11, 41-66 (in Chinese with English abstract).
- Teng, L.S., Lee, C.-T., Tsai, Y.-B., Hsiao, L.-Y., 2000a. Slab breakoff as a mechanism for flipping of subduction polarity in Taiwan. *Geology* 28, 155-158.
- Teng, L.S., Yuan, P.B., Yu, N.-T., Peng, C.-H., 2000b. Sequence stratigraphy of the Taipei Basin deposits: A preliminary study. *Journal of the Geological Society of*

- China 43-3, 497-520.
- Teng, L.S., Lee, C.-T., Peng, C.-H., Chen, W.-F., Chu, C.-J., 2001. Origin and geological evolution of the Taipei Basin, Northern Taiwan. *Western Pacific Earth Sciences* 1-2, 115-142.
- Teng, L.S., Liu, T.-K., Chen, Y.-G., Liew, P.-M., Lee, C.-T., Liu, H.-C., Peng, C.-H., 2004a. Influence of Tahan River capture over the Taipei Basin. *Geographical Research* 41, 61-78 (in Chinese with English abstract).
- Teng, L.S., Lee, C.-T., Liew, P.-M., Song, S.-R., Tsao, S.-J., Liu, H.-C., Peng, C.-H., 2004b. On the Taipei dammed lake. *Geographical Research* 36, 77-100 (in Chinese with English abstract).
- Thomas, A.L., 1993. Ploy3D: a three-dimensional, polygonal element, displacement discontinuity boundary element computer program with application to fractures, faults and cavities in the Earth's crust. M.S. Thesis, Stanford University, Stanford, CA, pp 97.
- van Wagoner, J.C., Posamentier, H.W., Mitchem, R.M., Vail, P.R., Sarg, J.F., Loutit, T.S., Hardenbol, J., 1988. An overview of the fundamentals of sequence stratigraphy and key definitions, in Wilgus, C.K. et al. (eds.), *Sea-Level Changes: An Integrated Approach*. Society of Economic Paleontologists and Mineralogists Special Publication 42, 39-45.
- Vergés, J., Marzo, M., Muñoz, J.A., 2002. Growth strata in foreland settings. *Sedimentary Geology* 146, 1-9.
- Walia, V., Su, T.-C., Fu, C.-C., Yang, T.F., 2005. Spatial variations of radon and helium concentrations in soil gas across the Shan-Chiao fault, Northern Taiwan. *Radiation Measurements* 40, 513-516.
- Waltham, T., 2002. Sinking cities. *Geology Today* 18-3, 95-100.
- Wang, C.-Y., Sun, C.-T., 1999. Interpretation of seismic stratigraphy in the Taipei Basin (in Chinese with English abstract). *Central Geological Survey Special Publication* 11, 273-292.
- Wang, J.-H., 2008. Urban seismology in the Taipei metropolitan area: Review and perspective. *Terrestrial, Atmospheric and Oceanic Sciences* 19-3, 213-233.
- Wang, J.-H., Huang, M.-W., Huang, W.-G., 2006. Aspects of $M \geq 4$ earthquakes in the Taipei metropolitan area. *Western Pacific Earth Sciences* 6, 169-190.
- Wang, K.-L., Chung, S.-L., Shinjo, R., Chen, C.-H., Yang, T. F., Chen, C.-H., 1999. Post collisional magmatism around northern Taiwan and its relation with opening of the Okinawa Trough. *Tectonophysics* 308, 363-376.
- Wang-Lee, C.-M., Cheng, Y.-M., Wang, Y., 1978. Geology of the Taipei Basin (in Chinese). *Taiwan Mining Industry* 30-4, 350-380.
- Wang, W.-S., Chen, C.-H., 1990. The volcanology and fission track age dating of

- pyroclastic deposits in Tatun volcano group, northern Taiwan. *Acta Geologica Taiwan* 28, 1-40.
- Wei, K., Chen, Y.-G., Liu, T.-K., 1998. Sedimentary history of the Taipei Basin with constraints from thermoluminescence dates. *Journal of Geological Society of China* 41, 109-125.
- Wernicke, B., Burchfiel, B.C., 1982. Modes of extensional tectonics. *Journal of Structural Geology* 4, 105-115.
- Woodcock, N.H., Schubert, C., 1994. Continental strike-slip tectonics, in Hancock, P.L. (ed.), *Continental Deformation*. Pergamon Press, New York, 251-263.
- Woodroffe, S.A., Horton, B.P., 2005. Holocene sea-level change in the Indo-Pacific. *Journal of Asian Earth Sciences* 25, 29-43.
- Wu, C.-M., 1987. Reviews on the land subsidence of the Taipei Basin (in Chinese). *Sino-Geotechnics* 20, 34-49.
- Wu, F.-T., 1965. Subsurface geology of the Hsinchuang structure in the Taipei Basin. *Petroleum Geology of Taiwan* 4, 271-282.
- Wu, F.T., Rau, R.-J., Salzberg, D.Z., 1997. Taiwan orogeny: Thin-skinned or lithospheric collision? *Tectonophysics* 274, 191-220.
- Yeh, Y.-H., Barrier, E., Lin, C.-H., Angelier, J., 1991. Stress tensor analysis in the Taiwan area from focal mechanisms of earthquakes. *Tectonophysics* 200, 267-280.
- Yokoyama, Y., Kido, Y., Tada, R., Minami, I., Finkel, R.C., Matsuzaki, H., 2007. Japan Sea oxygen isotope stratigraphy and global sea-level changes for the last 50000 years recorded in sediment cores from the Oki Ridge. *Palaeogeography, Palaeoclimatology, Palaeoecology* 247, 5-17.
- Yu, S.-B., Chen, H.-Y., Kuo, L.-C., 1997. Velocity field of GPS stations in the Taiwan area. *Tectonophysics* 274, 41– 59.
- Yu, S.-B., Chen, H.-Y., Kou, L.-C., Hou, C.-S., Lee, C.-F., 1999a. A study on the fault activities of the Taipei Basin (in Chinese with English abstract). *Central Geological Survey Special Publication* 11, 227-251.
- Yu, S.-B., Kuo, L.-C., Punongbayan, R.S., Ramos, E.G., 1999b. GPS observation of crustal deformation in the Taiwan-Luzon region. *Geophysical Research Letters* 26-7, 923-926.
- Yue, L.-F., Suppe, J., Hong, J.-H., 2005. Structural geology of a classic thrust belt earthquake: the 1999 Chi-Chi earthquake Taiwan (Mw=7.6). *Journal of Structural Geology* 27, 2058–2083.
- Zang, S.X., Chen, Q.Y., Ning, J.Y., Zheng, K.S., Liu, Y.G., 2002. Motion of the Philippine Sea plate consistent with the NUVEL-1A model. *Geophysical Journal International* 150, 809-819.

Appendices

A1. Note on Chapter 2

The content of Chapter 2 is a published manuscript with detailed citation below:

Chen, C.-T., Hu, J.-C., Lu, C.-Y., Lee, J.-C., Chan, Y.-C., 2007. 30 years land elevation change from subsidence to uplift following the termination of groundwater pumping and its geological implications in the Metropolitan Taipei Basin, Northern Taiwan. *Engineering Geology* 95, 30-47, doi: [10.1016/j.enggeo.2007.09.001](https://doi.org/10.1016/j.enggeo.2007.09.001).





Thirty-year land elevation change from subsidence to uplift following the termination of groundwater pumping and its geological implications in the Metropolitan Taipei Basin, Northern Taiwan

Chih-Tung Chen^{a,*}, Jyr-Ching Hu^a, Chia-Yu Lu^a, Jian-Cheng Lee^b, Yu-Chang Chan^b

^a Department of Geosciences, National Taiwan University, Taipei 106, Taiwan, ROC

^b Institute of Earth Sciences, Academia Sinica, Taipei 115, Taiwan, ROC

Received 12 February 2007; received in revised form 16 August 2007; accepted 4 September 2007

Available online 21 September 2007

Abstract

Several levelling routes in the metropolitan Taipei Basin have been repeatedly conducted during the past decades, mainly in order to monitor the anthropogenic ground subsidence due to massive pumping of groundwater. We analysed the levelling data released from government and investigated the rate of ground level change from 1975 to 2003, which postdate the massive groundwater exploitation in Taipei area. Based on the contour maps created from the levelling data of 406 benchmarks, the overall subsidence rate in the Taipei Basin gradually decreased since 1975, and around 1989 the basin switched to slight uplift throughout a large part of the basin. Three mechanisms are proposed to be responsible for the observed land elevation changes, including shallow soil compaction, deformation within aquifer, and tectonic subsidence. The trend of the ground level change in 1975–2003 essentially demonstrated the effects of natural recharge to previously depleted aquifers, and is explained by the hydro-mechanical coupling of aquifer materials, i.e., elastic rebound, to the rising piezometric level. The rate of shallow soil compaction is estimated about 1–8 mm/yr throughout the basin according primarily to the shallow clay thickness. Asymmetric tectonic subsidence related to the Shanchiao Fault was estimated to be 1.75 mm/yr and 0.9 mm/yr in the western part and the central part of the basin, respectively. By subtracting the components of the soil compaction and tectonic subsidence from the surface land elevation change, the rebound of aquifer strata was estimated to be about 6.7 cm and 16 cm in western margin and Central Taipei, respectively. The amount of rebound is approximately 10% in magnitude comparing to the amount of previous anthropogenic subsidence due to massive groundwater pumping, totally about 2 m.

© 2007 Elsevier B.V. All rights reserved.

Keywords: Groundwater pumping; The Taipei Basin; Ground subsidence; Aquifer deformation; The Shanchiao Fault

1. Introduction

Excessive groundwater utilization in agricultural and urban area is known to cause rapid human-induced land

subsidence and pose severe problems including damage to building and infrastructures, exhaustion of groundwater resources, increase of risks of inundation, and inland sea water intrusion, as documented in many places around the world (e.g. Bangkok, Thailand, Phien-vej et al., 2006; Jakarta, Indonesia, Abidin et al., 2001; Ravenna, Italy, Teatini et al., 2005; Pingtung Plain,

* Corresponding author. Tel.: +886 2 33662927; fax: +886 2 23636095.
E-mail address: kthomasch@gmail.com (C.-T. Chen).

Taiwan, Hu et al., 2006). Pumping-induced subsidence is resulted primarily from irreversible compaction of aquitard material composed of fine-grained silt and clay layers during prolonged drainage process, and from minor amount of presumably elastic compaction from compression of coarse-grained conglomerate and sand deposits in aquifers (Holzer, 1984; Waltham, 2002). Ground surface change due to pumping generally reflects the response to dropping piezometric level (Fig. 1). Ban or controls on pumping are the actions usually taken by many authorities to mitigate the hazards, and regional groundwater table rises accordingly due to natural groundwater recharge. Ground elevation change during groundwater recovery after long-term extensive pumping should exhibit some amount of uplift. This effect is considered to be originated from relaxation of elastically compressed aquifer materials when pore pressure regained, as illustrated by injection experiment carried out at the

severely subsided Wilmington oilfield in the Long Beach harbour area of California (Allen and Mayuga, 1969), a phenomenon commonly referred as elastic rebound (Waltham, 2002). Characterization of such post-pumping behaviour, however, has not yet been studied in detail.

Typical ground response during fast artificial recharge for short-period pumping tests (e.g. Cappa et al., 2005) is well known as curve A in Fig. 1, indicating immediate and direct coupling of changes between ground elevation and hydraulic head. On the other hand, ground surface variations following cessation of prolonged groundwater pumping are mainly characterized by a transition of minor movements from subsidence to uplift (curve B in Fig. 1), as reported in Venice, Italy (e.g., Gatto and Carbognin, 1981). It demonstrates a more complicated scheme when groundwater production is of greater spatial and temporal scales. Characteristics and mechanisms of regional land elevation

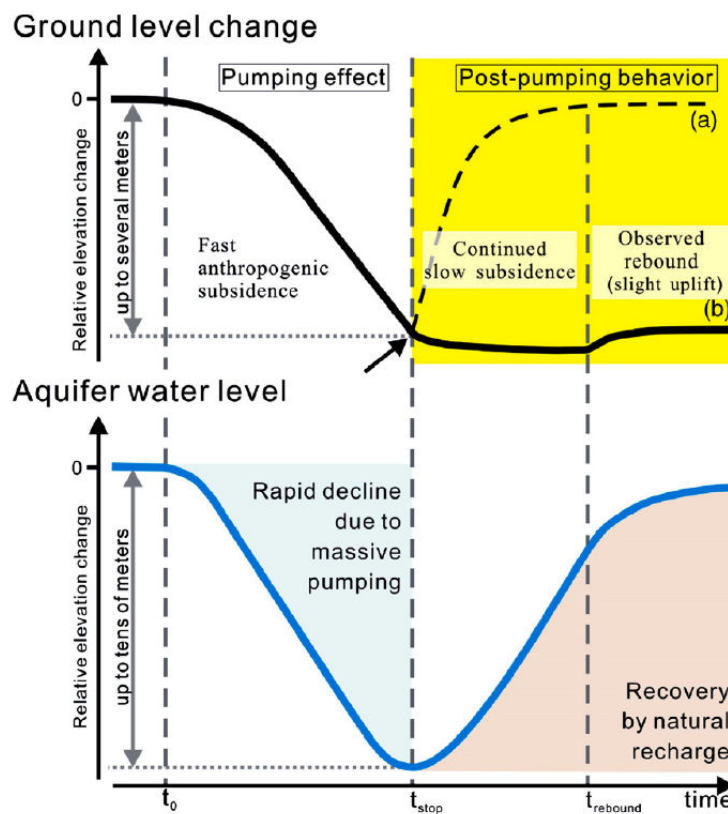


Fig. 1. General conceptual model of ground elevation change due to artificial piezometric head drawdown and recovery. Note that two different post-pumping behaviours of ground level change: (a) short-term pumping test and (b) long-term artificial pumping. See text for details.

change, particularly the elastic rebound after experiencing basin-wide groundwater over-extraction, remain unclear. The history of pumping and recovery of the groundwater in the Taipei Basin in northern Taiwan, therefore, provides a good opportunity for better understanding of this post-pumping mechanism.

The Taipei City is the political and economical centre of Taiwan (Fig. 2a) with dense population of about 3 million habitation and another several million inhabitants in the surrounding suburban areas. Like many big cities in the world, early development of the Taipei city was partly facilitated by its rich groundwater resources. However, unrestricted of groundwater over-pumping

resulted in both dry-ups of wells and severe land subsidence, especially during 1955–1970 (Hwang and Wu, 1969; Wu, 1987). In order to prevent more ground subsidence and further associated damage, the government put a stop on the use of groundwater in the Taipei Basin during the early 1970s. Rapid land subsidence has therefore significantly decreased (Wu, 1987), and the groundwater table was gradually recovered and became approximately stable since late 90s (Chia et al., 1999; Fig. 3c). In this paper, we intend to examine recent vertical change of ground surface in response to the post-pumping groundwater recharge in more details. Thanks to several annually measured levelling routes

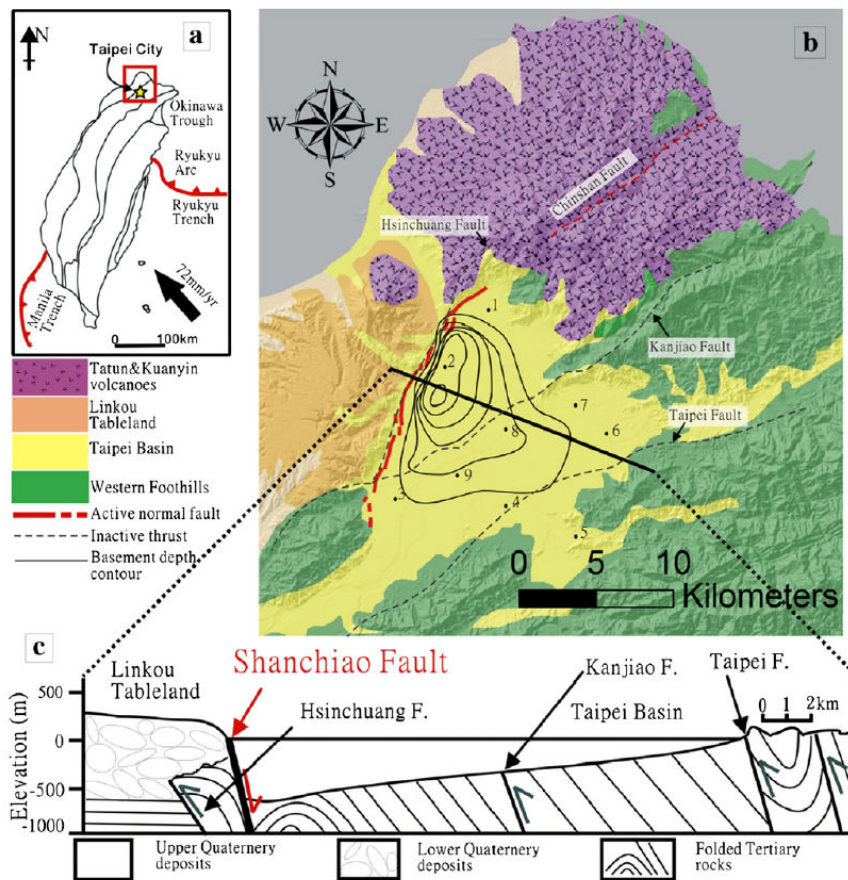


Fig. 2. (a) Tectonic framework of Taiwan. The converging rate and direction of Philippine Sea Plate relative to Eurasia plate is adapted from Yu et al. (1999b) and Zang et al. (2002). (b) Four geological domains of Taipei area (see text for details). The thin grey lines within the Taipei Basin are the basement depth contour of 100 m interval (after Teng et al., 2001). The red line along the western margin of the Taipei Basin is the Shanchiao Fault (after Chen et al., 2006). The black dots mark local district names in the Taipei Basin: 1. Guandu, 2. Wuku, 3. Shulin, 4. Zhonghe, 5. Jingmei, 6. Sungshan, 7. Dazhi, 8. central Taipei, 9. Banchiao. (c) Simplified geological cross section of the Taipei Basin (modified from Teng et al., 1999). The Hsinchuang, Kanjiao, and Taipei Faults are inactive thrust faults (denoted with grey arrows) which slipped during the collision phase in the Taipei area.

across the Taipei Basin, we are able to reconstruct the history of the land vertical change following the recharge of the aquifers.

Furthermore, while severe anthropogenic land subsidence has been stopped in the Taipei metropolitan area, concerns on potential earthquakes and related geohazards due to possible reactivation of the active

Shanchiao fault continue to be discussed (e.g., Teng et al., 2001; Shyu et al., 2005; Huang et al., 2007). Taiwan is situated in a plate boundary between the actively converging Eurasian and Philippine Sea plates beginning about 5 Ma (Suppe, 1981; Teng, 1990). At present, the collision process is manifested in southern and central Taiwan as demonstrated by the intense

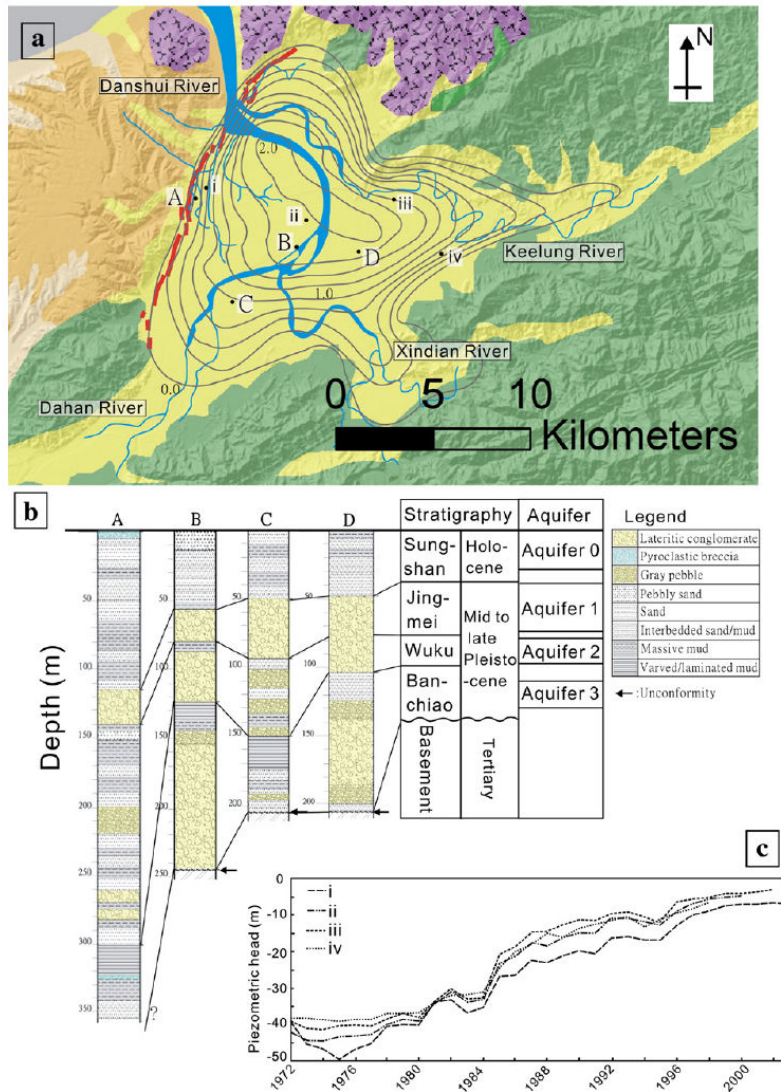


Fig. 3. (a) Cumulated subsidence in the Taipei Basin from 1955 to 1991 (after Lin et al., 1999). Contour interval is 0.25 m. Borehole sites: A: Wuku (WK-1), B: Sanchung (SC-1), C: Banchiao (PC-2), D: Shingongyuan (Shingongyuan No.1). Groundwater monitoring wells: i: Wuku, ii: Sanchung, iii: Shingtien Palace, iv: Sungshan. (b) Stratigraphic architecture of late-Quaternary deposits within the basin, along with the four aquifers (modified from Teng et al., 1999). (c) Piezometric head records of Aquifer 1 at four monitoring wells since 1972 to 2003 (Chia et al., 1999; Cho, 2006).

crustal shortening, according to data from the GPS and seismic networks of Taiwan. In contrast, north-eastern Taiwan underwent post-collisional processes and has been considered to be incorporated in the opening of the southern Ryukyu back-arc system (Teng et al., 2000), as evidenced by the presence of Quaternary extensional structures (Lee and Wang, 1988; Lu et al., 1995) and extensional earthquake focal mechanisms (Yeh et al., 1991; Kao et al., 1998). The Shanchiao Fault, which bounds the western edge of the Taipei Basin, has attracted attention in terms of earthquake hazards during the last decades. Tectonic subsidence related to this possible active fault is illuminated through recent levelling data, and should have an influence on the land elevation change in the Taipei Basin especially in the western part.

Levelling data in the Taipei area from 1975 to 2003 postdating the massive groundwater exploitation is utilized in the present study to examine the general conceptual model relating ground level response to recharge of aquifers. The various depth-related processes responsible for the observed occurrences of subsidence and uplift are discussed, including shallow soil compaction, crustal-scale tectonic movement, and irreversible compaction and elastic rebound within aquifer. A schematic model explaining recent 30 years land elevation change in the Taipei Basin is proposed.

2. Regional setting

2.1. Geological background

The Taipei region can be divided into four geological domains (Fig. 2b): (1) the Foothills, hilly terrains north, east, and south of the Taipei Basin, consisting of fold-and-thrust belt of Miocene continental margin sedimentary packages; (2) the Tatun and Kuanyinshan volcanoes, north and northwest of the Taipei Basin, piled up of late-Quaternary andesitic volcanic formations; (3) the Linkou Tableland, west of the Taipei Basin, covered by Quaternary thick lateritic conglomerates as an ancient fan-delta which rests above Miocene/Pliocene sedimentary rocks (Chen and Teng, 1990); (4) the Taipei Basin, a triangular-shaped half-graben filled with late-Quaternary fluvial deposits since about 0.4 Ma (Wei et al., 1998; Teng et al., 2001), which lie unconformably over the deformed Miocene sedimentary packages.

The late-Quaternary deposits of the Taipei Basin form an asymmetric wedge shape in thickness: reaching a maximum depth of about 700 m in the western margin and gradually becoming thinner toward the east and south (Fig. 2c). These unconsolidated deposits in the

Taipei Basin are divided into four lithostratigraphic units (Teng et al., 1999), from bottom to top (Fig. 3b): (1) the lowest Banchiao formation, consisting of fluvial sand, mud and conglomerates, with minor pyroclastic debris and thick varved mud in the upper section; (2) the Wuku formation, consisting of fluvial sand and conglomerates with minor mud and lateritic conglomerates; (3) the Jingmei formation, comprising of lateritic alluvial-fan conglomerates; (4) the Sungshan formation, composed of estuary interbedded sand–mud deposits. The basin deposits are marked by prominent facies changes and most of the sedimentary layers laterally pinch out rapidly. However, the widespread lateritic gravel of the Jingmei formation and the varved layers in upper Banchiao formation serve as basin-wide marker beds (Teng et al., 1999).

Brief geological evolution of the Taipei Basin is summarized in the following, based on previous studies. In Pliocene, the Taiwan Orogeny has initiated as the Luzon Arc of the Philippine Sea plate approaching to continental margin of Eurasia (e.g. Suppe, 1981). The Miocene shallow marine sedimentary rocks of the Taipei area were deformed into imbricated fold-and-thrust sheets with several major faults including the Hsinchuang, Kanjiao, and Taipei Faults (Fig. 1b, c) as mountainous ranges (Ho, 1975; Wang-Lee et al., 1978). While the orogeny reached climax in northern Taiwan about 2 Ma, the Paleo-Tanshui River, the major river in the Taipei Basin, produced the Linkou fan-delta around the ancient mountain front thrust (Chen and Teng, 1990), the Hsinchuang Fault which runs approximately parallel to the western margin of the Taipei Basin (Teng et al., 2001). The compressive stress regime of the northernmost Taiwan appeared to cease during the middle to late Quaternary (Lee and Wang, 1988). The eruption of the Tatun volcanism to the north of the Taipei Basin might reflect the onset of regional extension which was interpreted to be related to the Okinawa trough back-arc opening and/or lateral extraction in the corner of plate convergence (Lee and Wang, 1988; Lu et al., 1995; Hu et al., 2002). Subsidence along western margin of the Taipei Basin is interpreted to result from the repeated normal faulting on the Shanchiao Fault as tectonic inversion on the Hsinchuang thrust fault (Chiu, 1968; Hsieh et al., 1992). It turned the Taipei area from rugged mountains into a sediment-receiving basin. The accumulation of fluvial and lacustrine sediments was estimated to be started at about 0.4 Ma (Wei et al., 1998; Teng et al., 2001). Since then the Taipei Basin has kept expanding due to continual asymmetric subsidence along the Shanchiao fault in the western edge of the basin (Wang-Lee et al., 1978). Under the combining influences

of sea level fluctuations, volcanic activities, drainage system changes, and tectonic processes, the basin was filled with various types of sediments, including alluvial, lacustrine, marine and pyroclastic deposits, as mentioned above.

As a consequence, the Shanchiao Fault, which separates the Linkou Tableland from the Taipei Basin, is considered the major active structure responsible for accommodating the extension across the Taipei region and thus for the formation of the half-graben Taipei Basin (Teng et al., 2001). Shallow seismic reflections across the Shanchiao Fault imaged an offset of Holocene sediments at shallow tens of meters depth (Wang and Sun, 1999). GPS surveys of the Taipei area showed extension with a rate of $0.08 \pm 0.02 \mu\text{strain/yr}$ in the direction of SEE–NWW across the fault (Yu et al., 1999a). Huang et al. (2007) correlated stratigraphy of three sets of boreholes across the Shanchiao Fault, and identified three paleoseismic events within the Holocene time (8400–8600, 9000–9300, and 11,100 years b.p.). Geomorphology analysis also exhibits series of scarps closely related to the development of the Shanchiao Fault (Chen et al., 2006). Thus the Shanchiao Fault is considered active (as stated in reports of Central Geological Survey, Chang et al., 1998; Lin et al., 2000).

2.2. Hydrogeologic framework and utilization of groundwater

Four major aquifers, which generally correspond to the stratigraphic formations, have been defined in the late-Quaternary sediments of the Taipei Basin (Fig. 3b; Wu, 1987). The topmost free aquifer (Aquifer 0), which extends from ground surface to depth around 50 m (except in the western edge of the basin being deeper to about 120 m in maximum), is composed of interbedded clay, sand and pebbles. Aquifer 0 is thus considered to correspond to the Sungshan formation. The confined Aquifer 1 sits at depth between 50 to around 100 m (again except in the western edge of basin, about 115–140 m) in the conglomerate layer covered by laterite. This conglomerate layer is interpreted to correspond to the Jingmei formation, with hydraulic diffusivity around 0.12 to 0.18 m^2/s and storage coefficient ranging from 0.001 to 0.004 (Chia et al., 1999). The lower aquifers (Aquifers 2 and 3) are present approximately 100 to 130 m and 140 to 160 m underground (depths for the central portion of the basin), as two layers of conglomerates within the Wuku and Banchiao formations, respectively (Fig. 3b). Among them Aquifer 1 appeared to be the major groundwater source of the pumping wells in the Taipei Basin. The groundwater of the lower

three aquifers comes mainly from two of the major rivers in the Taipei Basin, the Xindian River and the Dahan River (Fig. 3a). On the other hand, rainfall is the major water source for Aquifer 0 (Chia et al., 1999).

First massive utilization of groundwater source in the Taipei Basin (primarily Aquifer 1) was initiated by an English engineer W. K. Bardon in 1895. Under his advisory the government set up 150 wells (Wu, 1987). Since then the number of wells was rapidly increasing and the groundwater resource drained twice in 1906 and 1960 to early 1970s. The second event was accompanied by severe land subsidence. Piezometric head of Aquifer 1 decreased more than 40 m and reached the lowest point around 1975 (Wu, 1987; Chia et al., 1999; Fig. 3c). The basin-wide subsidence resulted from over-pumping was particularly concentrated in the central portion of the Taipei Basin where maximum land subsidence exceeded 2 m (Fig. 3a), corresponding to the site of major pumping at that time. Severe restriction taken by the government on groundwater pumping in the early 1970s had successfully stopped the fast decline of groundwater table which immediately began to rise as the piezometric head having gradually recovered 30–40 m in 30 years (Chia et al., 1999; Cho, 2006; Fig. 3c). Water resource of the Taipei metropolitan since the 1970s has been supplied by surface water mainly from two reservoirs in upstream Dahan and Xindian Rivers.

3. Analyses and results

3.1. Description of data analyses

For the purpose of monitoring the land subsidence due to groundwater pumping, several levelling routes were established by government authorities since 1948 in the Taipei Basin. More than 406 benchmarks were constructed in different periods of the levelling (Fig. 4). Most of the benchmarks were installed on concrete foundation or rock basement. In this study, we analysed the levelling data from 1975 to 2003, in order to decipher effects of post-pumping. Only benchmarks with repeated measurements were taken into account. The observed elevations from these surveys were orthometrically corrected. The more recent data (since 1989) were additionally corrected for temperature variations for rod and instrumental biases. The levelling was deployed conventionally by closing a series of double-run sections. These data sets called TWVD2001 (Taiwan Vertical Datum, the reference of absolute elevation of benchmarks, calculated from the tide data of Keelung tide station) are stored in archive centre of the Ministry of the Interior and Land Subsidence

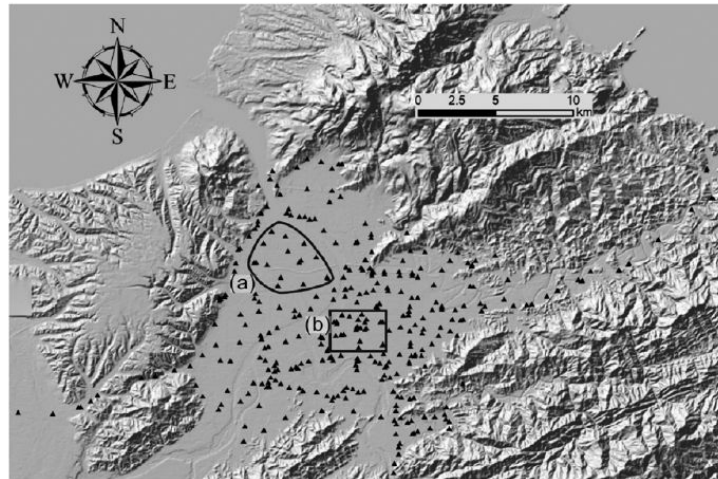


Fig. 4. Distribution of the 406 benchmarks of levelling routes analysed in this study. Benchmarks in groups (a) and (b) are used to represent the average movements in western Taipei Basin and Central Taipei, respectively.

Prevention and Reclamation Corp of National Cheng-kung University. The survey adopted the standard procedures of the first order high precision levelling, which is of a standard error of about $2\sqrt{D}$ mm, where D is the distance of measurement (unit of km). As a result, the uncertainties of the elevations for each benchmark during surveys are usually within 1–3 mm.

For the sake of discontinuity of measurements, we divided the data into 7 periods from 1975 to 2003 (1975–1980, 1980–1985, 1985–1989, 1989–1994, 1994–1996, 1996–2000, and 2000–2003). For each period, the elevation changes of the benchmarks are transferred to elevation change rates, in order for comparison. Based on the rates of elevation change for each benchmark, we then construct contour map of land change for each period (1975–1989 for Fig. 5 and 1989–2003 for Fig. 6), adopting the commonly used extrapolation technique of kriging (Oliver and Webster, 1990). For each period, the contours were derived from data of more than 76 benchmarks. Note that ground level fluctuation shown outside the basin plain is mostly a result of extrapolation which may contain large errors and should not be taken into account.

3.2. Results of post-pumping land elevation change

Several interesting and important characteristics of the land surface level change (subsidence and uplift) in the Taipei Basin during the post-pumping time can be inferred from the contour maps. First, the whole basin still subsided after the stop of groundwater pumping, but with

a decreasing trend from 40–70 mm/yr to 0–30 mm/yr, during 1975 to 1989, denoted here as Phase 1 (Fig. 5). Second, a large part of the land became to uplift since 1989, denoted as Phase 2 (Fig. 6). However, the surface elevation change was far from homogeneous. For instance, enhanced and persistent subsidence occurred in north-western margin of the basin near Guandu (for the place names mentioned, please refer to Fig. 2b) throughout the entire time span (1975–2003), and concentrated subsidence in western margin of the basin (Wuku, Shulin) and north-eastern basin (Dazhi-Sungshan) was also very persistent before 1996. Other locus of subsidence (e.g., Banchiao, Zhonghe, Jingmei) as well as irregular and short-lived subsidence or uplift were also observed.

A period-by-period account of land elevation change in the Taipei Basin is presented as followed. Basin-wide decreasing subsidence characterized all three periods in Phase 1. During 1975–1980 (Fig. 5a; 94 benchmark), subsidence was dominant and was mostly concentrated in the northwestern (Guandu, exceeded 60 mm/yr; and Wuku, maximum 75 mm/yr) and northeastern portions (Dazhi, nearly 70 mm/yr). In 1980–1985 (Fig. 5b; 76 benchmark), significant subsidence continuously occurred along the western margin of the basin (Guandu, reached 12 mm/yr; Wuku, over 10 mm/yr) and in the northeastern corner (Dazhi, more than 20 mm/yr), however, with smaller rates compared to the previous period. For 1985–1989 (Fig. 5c; 157 benchmark), a large part of areas in the basin were continuous to subside (in particular, the western margin), but some small areas began to show

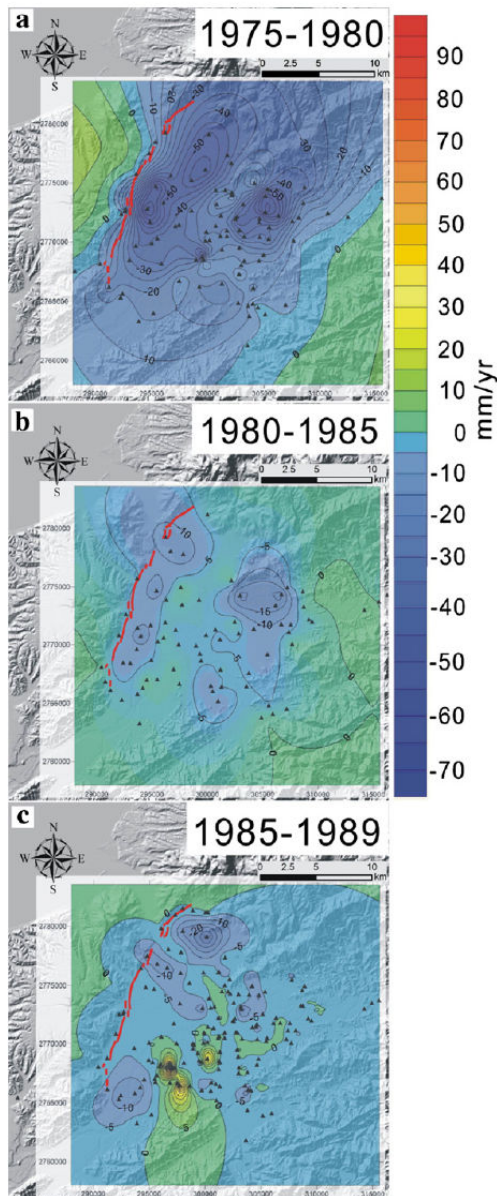


Fig. 5. Contour maps of observed land surface elevation change in Phase 1 (1975–1989) of post-pumping period. (a) 1975–1980. (b) 1980–1985. (c) 1985–1989. Negative rate values indicate subsidence, and vice versa. Contour interval is 5 mm/yr. Coordinates shown are of TWD 67 Transverse Mercator system. The whole basin revealed a general subsidence from 1975–1985, with some localized effects. See detailed discussion in text.

slight uplifting, especially in the central and southern parts, although some of the benchmark records showing extremely sharp uplift might be anomalies. In general, the subsidence rate continued to decrease, comparing to the two previous periods; nonetheless, localized subsidence was still persistent along the western margin of the basin (Guandu, attained 30 mm/yr; northern Wuku, >10 mm/yr; Shulin, 10 mm/yr) and other patches in the basin (south Dazhi, maximum 15 mm/yr; and Jingmei, around 5 mm/yr).

Starting from about 1989 (Phase 2), uplift began to appear significantly in the Taipei Basin and declined in magnitude in the later half of this Phase. During 1989 to 1994 (Fig. 6a; 111 benchmark), we observed that the surface subsidence almost ceased and a large portion of the Taipei Basin began to slight uplift, especially in the centre of the basin (central Taipei, 10 to 15 mm/yr; Banchiao, 10 to 15 mm/yr). Nevertheless, slight subsidence still persisted in western margin of the basin (e.g., 0 to 5 mm/yr in Guandu and Wuku). In 1994–1996 (Fig. 6b; 146 benchmark), slight subsidence continuously occurred and was localized in western side of the basin (Guandu, as high as 14 mm/yr; Wuku, maximum 10 mm/yr; and Shulin to Banchiao, up to 6 mm/yr), and in southern Taipei (Zhonghe, reached 10 mm/yr). On the other hand, uplift seemed to dominate the eastern half of the basin, but with a lesser magnitude. In 1996–2000 (Fig. 6c; 103 benchmark), the whole Taipei Basin was generally experiencing mild uplift, except for north-western margin of the basin (Guandu–Wuku, subsidence with a possible bull-eye reaching maximum over 20 mm/yr), and other local areas (Dazhi, Zhonghe, and Jingmei). During the most recent period, 2000–2003 (Fig. 6d; 94 benchmark), slight uplift prevailed in the Taipei Basin (0–5 mm/yr) with subsidence in north-western basin (Guandu, Wuku, 0 to 5 mm/yr), and other local areas along the southern and eastern edge of the basin (Sungshan, Zhonghe and Jingmei).

In summary, the subsidence rate for the Taipei Basin as a whole generally decreased from 1975 to 1989 (Phase 1), and then the elevation change of the basin gradually switched to slight uplift since about 1989 during Phase 2 (Fig. 7). The waning subsidence during the 1975–1989 of Phase 1 is interpreted to be mainly ascribed to the compaction of the water-depleted aquifers, resulting from the residual effect of the rapidly declined piezometric head due to over-pumping of groundwater. While massive pumping was ceased, recharge of groundwater from two major rivers (Xindian and Dahan Rivers) to the aquifers has raised the water table for more than 30 m from the 1970s to 2003

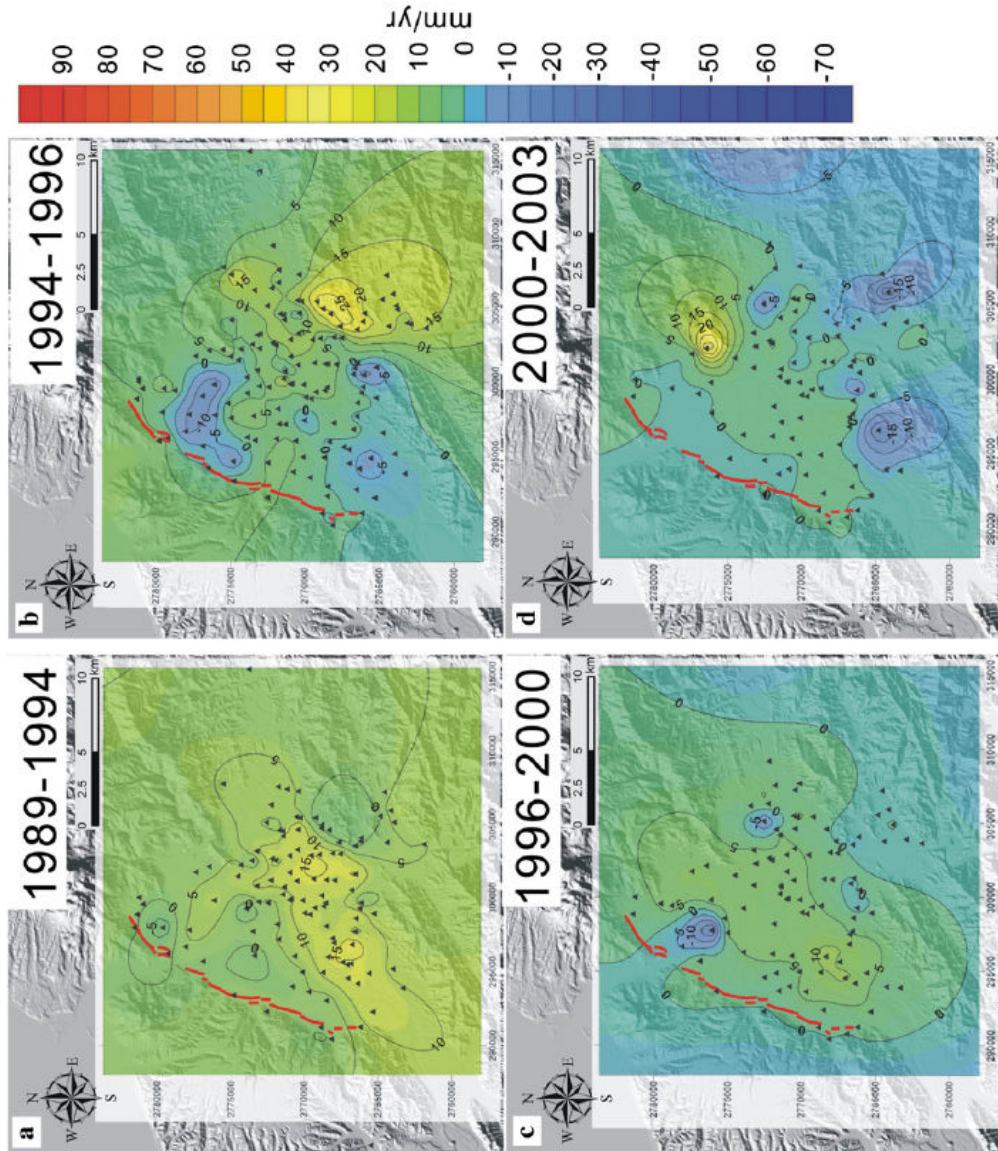


Fig. 6. Contour maps of observed land surface elevation change in Phase 2 (1989–2003) of post-pumping period. (a) 1989–1994, (b) 1994–1996, (c) 1996–2000, (d) 2000–2003. Annotations see Fig. 5. The basin showed a general uplift from 1989 to 2003; however, local subsidence occurred at several places. See details in text.

(Fig. 3c). We anticipate that the recovery of the groundwater level would produce an elastic rebound for the aquifers, thus caused basin uplift since 1989 in Phase 2. However, the concentrated and rather persistent subsidence and the reduced uplift occurred along the western margin and northern part of the Taipei Basin, compared to the central part of the basin, suggesting under impacts of other factors.

4. Mechanisms of land elevation changes during post-pumping

The land elevation change of the Taipei Basin could be a product of complexly interfering natural and artificial processes. The heterogeneous pattern of land vertical changes in the Taipei Basin certainly reflects the spatial and temporal context of different agents. In the spatial domain, these agents, according to where the processes take place, can be described and classified by their operation depth. Here we propose main mechanisms to explain the land elevation changes in the Taipei Basin, attributing effects of land elevation change of the Taipei

Basin to three major components: (1) surface soil compaction (the shallow component), (2) deformation of aquifers, including compaction and elastic rebound due to groundwater effect (the intermediate component), and (3) tectonic load (the deep and crustal-scale component).

4.1. Near surface soil compaction (the shallow component)

Local enhanced subsidence can be observed in several areas within the Taipei Basin in many periods we analysed. Subsidence caused by construction (loads of new buildings) cannot be omitted, but such phenomenon might be extremely localized and short-lived. Otherwise, subsidence in several places, such as Dazhi, Sungshan, Jingmei, Banchiao and Shulin, occurred throughout many periods although not always present (Figs. 5 and 6). Since their close proximity to the three major river channels in the Taipei Basin (i.e., Keelung, Dahan and Xindian Rivers), we intend to interpret that a large part of subsidence in these areas to be contributed by compaction of recent flood or overbank deposits (especially mud). Effect of in situ sediment compaction,

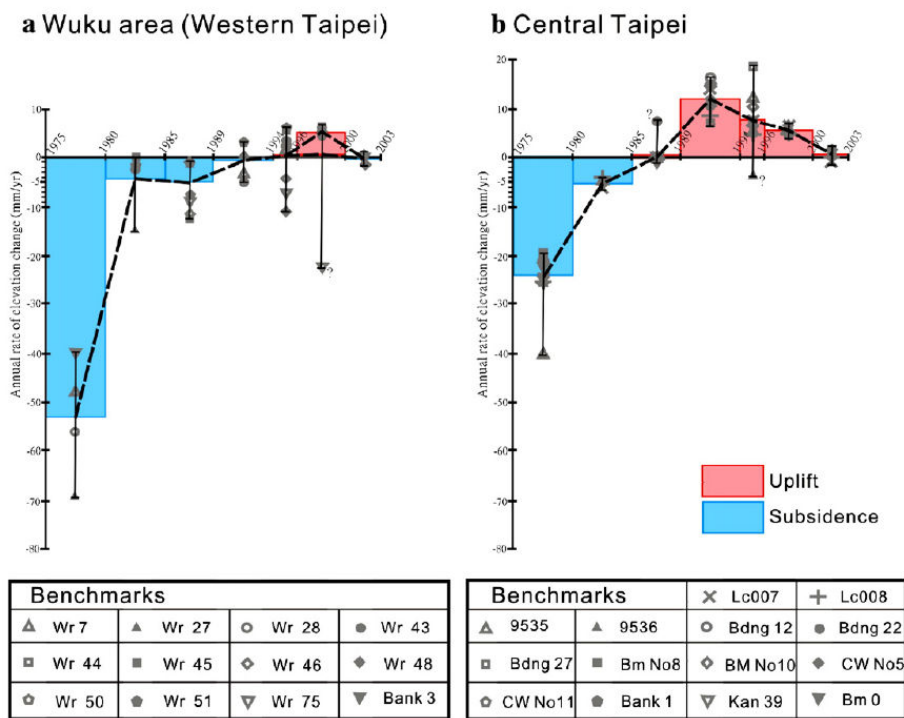


Fig. 7. Evolution of ground elevation change rate in post-pumping period from 1975 to 2003. (a) Western Taipei as the Wuku area. (b) Central Taipei. Distribution of the benchmarks used for calculation is shown on Fig. 4.

Table 1

The in situ compaction in clayey layers of top 50 m basin sediments recorded by Lin et al. (1999)

Well	Presence of clayey layers (meters in depth)	Cumulated compaction (mm)	Calculated annual compaction rate (mm/yr per meter of clayey layers)
Wuku (Industrial Park)	~27–35 ~42–48	4 (14–10) 4 (6–2)	0.1429 0.1905
Banchiao (Veterans Affairs Office)	~10–20	10 (18–8)	0.2857

The averaged annual rate of compaction in 1-meter-thick clayey layers is deduced.

often referred as natural subsidence (Waltham, 2002), therefore must be evaluated in order to further distinguish the role and intensity of natural and artificial factors played on the observed ground level change.

According to a recent in situ study in the Taipei Basin conducted by Lin et al. (1999), compaction of the loose sediments occurred mainly in the clayey layers of the uppermost 50 m Holocene deposits (generally corresponding to the Sungshan Formation) in three monitored wells in the western part of the basin at Wuku and Banchiao, in a time span of three and a half years from March, 1994 to September, 1997. For older sediments underneath, the compaction and consolidation were observed to be rather slow and was ignorable regardless

of the types of the deposits. Based on their results, we estimated the averaged annual rate of compaction for 1-meter-thick clayey layers to be ranging from 0.14 to 0.28 mm/yr (Table 1) by dividing the cumulative compaction of the clay sections in the monitored wells by the monitoring interval of three and half years. Meanwhile we reconstructed an isopach map for clay thickness within the topmost deposits of the Sungshan Formation in the basin (Fig. 8a) based on 350 borehole records from Central Geological Survey (open source, available on <http://210.69.81.69/geo/frame/gsb88.cfm>). The proxy of present variation of shallow soil compaction rate in the Taipei Basin can be obtained by multiplying the deduced average annual compaction rate for 1-meter-thick clay (i.e., 0.2 ± 0.07 mm/yr) with the shallow clay thickness isopach. We estimate contemporary shallow soil compaction to contribute 1–8 mm/yr of subsidence in the basin with most land ranging 2 to 5 mm/yr (Fig. 8b).

Natural subsidence rates of surface soil documented elsewhere in similar flood plain and deltaic environments fall in the same order of magnitude (Jelgersma, 1996), such as Ravenna (4–6 mm/yr, Teatini et al., 2005), Romagna (0–5 mm/yr, Gambolati et al., 1999), Venice (0.5–1.3 mm/yr, Gatto and Carbognin, 1981), and Po River Delta (3–5 mm/yr, Gambolati and Teatini, 1998) in Italy and coastal Louisiana, USA (shallow component 1.5–2.5 mm/yr, Dokka, 2006). In addition, the modelling results of Meckel et al. (2006) based on Holocene

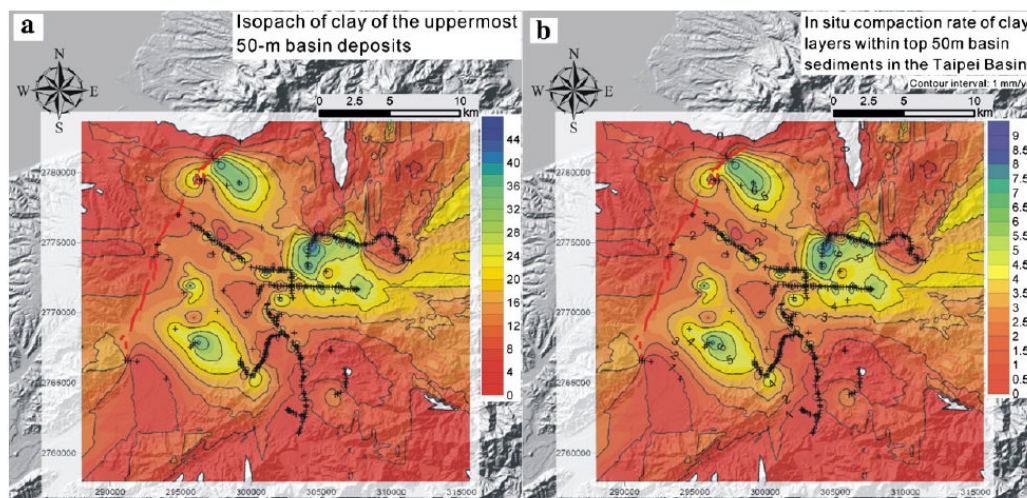


Fig. 8. (a) Isopach of the Holocene clayish sediments (topmost 50-m deposits) in Taipei Basin, constructed from 350 borehole records from Central Geological Survey (borehole sites marked in cross). (b) Estimated compaction rate of clayey layers within the Holocene deposits (soil compaction). See text for reference.

stratigraphy of lower Mississippi River Delta in southern Louisiana, which closely resembles the compacting shallow sediments of the Sungshan formation in the Taipei Basin, is applied to evaluate our proxy. Taking the surface soil in the Taipei Basin (50-meter-thick and deposited within the Holocene) into their cumulative distribution functions of compaction rate model, the 90th percentile compaction rate (Fig. 2 of Meckel et al., 2006) ranges from 1.5 to 4 mm/yr. This suggests that our estimate is reasonable and not likely to underestimate present soil compaction.

Comparison between the contour maps of the observed elevation change (Figs. 5 and 6) and the estimated shallow soil compaction (Fig. 8b) shows that concentrated subsidence are indeed in a close relation with thicker soil/clay layers, especially along the main river courses (Fig. 3a). For example, ultra thick clay with resultant peak soil compaction is likely the main source of continuous subsidence in the marshy Guandu area along the Danshui River in the north-western corner of the basin. However, the Wuku area in western Taipei, on the contrary, is not subject to high soil compaction. As a consequence, persistent subsidence in the western margin of the Taipei Basin (Guandu, Wuku, and sometimes extending to Shulin) cannot be attributed totally to natural compaction especially during Phase 2, and requires other explanations to decipher its origin.

4.2. Tectonic load (the deep and crust-scale component)

Tectonic subsidence from activities of the Shanchiao Fault is thought to affect ground surface elevation change since present extensional deformation across the fault was documented (Yu et al., 1999a). It's expected to be most pronounced in the near-fault hanging-wall region, that is, the western margin of the basin, where the basin basement is dramatically deepened and reaches maximum depth. The long-term averaged tectonic subsidence rate in western Taipei Basin thus can be estimated by stratigraphic offset across the fault. The onset of basin sediment deposition was estimated to be around 0.4 Ma when basin basement was lowered to near sea level (Chen et al., 1995; Wei et al., 1998; Teng et al., 2001) and since then approximately 700 m of basin sediments were accumulated. Dividing the total thickness of late-Quaternary basin deposits (700 m) by the time span of sedimentation (0.4 Myr) we obtain the late-Quaternary averaged tectonic subsidence rate to be 1.75 mm/yr since 0.4 Ma. Note that it may contain contributions from co-seismic slips (Huang et al., 2007), thus representing the upper limit of value for inter-seismic tectonic subsidence rate. In the central part of

the basin tectonic subsidence may attain half of the rate in western Taipei, approximately 0.88 mm/yr. We consider the tectonic subsidence rates to be constant over the investigated time intervals since no major earthquakes were recorded in shallow crust of the Taipei area during 1975 to 2003. More accurate assessment of the ongoing tectonic subsidence could be derived from levelling of benchmarks attached to deep boreholes (e.g. Dokka, 2006) and is in urgent need for earthquake hazard research and mitigation in the Taipei metropolis.

4.3. Deformation of aquifers (the intermediate component)

In the hydro-mechanical coupling scheme as illustrated by Waltham (2002), abstracting groundwater would reduce pore-water pressure in aquifers, usually as sand or conglomerate beds, which behave in a seemingly elastic manner (Karig and Hou, 1992). However, this would be followed by reduced pore-water pressure in usually intercalated clay and aquitard materials in order to regain hydraulic equilibrium. Clay compaction is largely an irreversible one-way process, and is the major source for severe pumping-induced land subsidence (Terzaghi, 1925; Holzer, 1984; Phien-wej et al., 2006). When groundwater is recharged into the starved aquifers to recover the pore pressure, expansion of aquifer sand and gravel layers occurs and contributes to uplift of ground surface as elastic rebound (Waltham, 2002). In detail of this hydro-mechanical coupling, during piezometric head rise, the recharged sections of the aquifer will release the formerly imposed compressive strain to show dilatation, producing elastic rebound. On the other hand, the starved sections of aquifer and aquitard will continue to show compression as the result of time-dependent consolidation behaviour caused by past piezometric drawdown, until groundwater table has risen to remove deficits of pore pressure in these sections. Ground level change reflected on groundwater recovery is the competition between subsidence from starved aquifer (plus aquitard) section and uplift from the recharged aquifer section. The evolution generally follows the pattern of curve B in Fig. 1. Similar mechanism was also invoked to explain land level fluctuation in Las Vegas controlled by seasonal water table variations (Amelung et al., 1999).

According to well monitor records in the Taipei Basin (Fig. 3c), groundwater table started to rise as soon as pumping ceased in 1975. Compaction of Aquifer 1 during massive groundwater extraction would arrest gradually, following the recharge of groundwater in the aquifer. Near the end of Phase I as piezometric head was largely recovered, deformation of aquifer would become

neutral as that rebound had developed to surpass remaining compaction. The uplift due to elastic rebound of Aquifer 1 was not visible on land surface until 1989 at the beginning of Phase 2 (Fig. 6). We interpret that at this time the amount and rate of elastic rebound outpaced residual aquifer clay compaction and other subsidence effects including the compaction of surface soil and tectonic subsidence of normal faulting. Elastic rebound of recharged aquifer would then gradually decrease in amount and rate since the groundwater level stabilized from mid 1990s. Ground level change pattern of the Taipei Basin after cessation of massive pumping with natural groundwater recharge thus fits well with the scheme of curve B in Fig. 1. The evolution of the post-pumping elevation change is characterized by a relatively longer period of waning subsidence (Phase

1: 1975–1989) followed by a shorter period of slight uplift (Phase 2: 1989–2003), due to a combination of decreasing compaction and increasing refill in Aquifer 1. The time lag between the start of piezometric level rise (t_{stop} in Fig. 1) and the first occurrence of the observed uplift of land surface ($t_{rebound}$ in Fig. 1) in Taipei Basin is about 15 years, which is believed to be closely related to the recharge rate of Aquifer 1. The contrast on amount between the non-revertible, plastic clay compaction and the elastic rebound of aquifer strata may be a viable explanation to the fact that the recent uplift (since 1989) in the Taipei Basin has a much lesser magnitude than that of the severe subsidence during massive pumping as before the 1970s. Most surface uplift due to rebound was observed in the central to eastern portion of the basin, roughly corresponding to

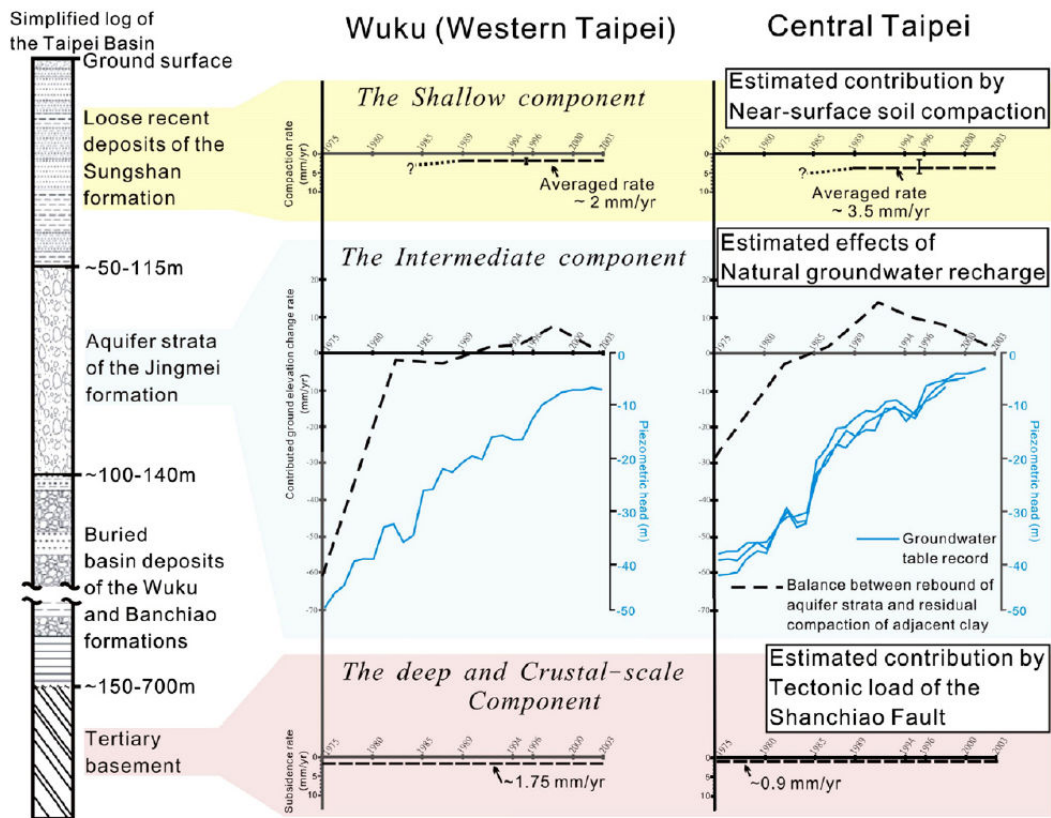


Fig. 9. Mechanisms of three depth-related component responsible for land elevation change in Western Taipei (Wuku) and Central Taipei. The shallow component represents the surficial soil compaction with the average rates estimated after Lin et al. (1999). The intermediate component represents the aquifer deformation consists of compaction and elastic rebound within Aquifer 1. The deep and crustal-scale component represents asymmetric tectonic subsidence due to the activity of the Shanchiao fault in the western margin of the basin. Calculation of each component is explained in the text.

area of most intense anthropogenic subsidence during pumping (compare Fig. 6 and Fig. 3a).

Similar phenomenon following cessation of massive groundwater exploitation was documented in Venice, Italy by Gatto and Carbognin (1981) where a land rebound of 2 cm, 15% of subsidence due to groundwater withdraw, occurred about 5 years later than the onset of regional piezometric head recovery from natural recharge. Artificial recharge of a severely depleted hydrocarbon reservoir in Long Beach, California, induced an observed rebound of 33.5 cm where precedent subsidence due to petroleum production reached 9 m in maxima (Allen and Mayuga, 1969). Both cases demonstrated that aquifer rebound is generally about one order less in magnitude than the preceding subsidence. This is in good accordance with the situation in the Taipei Basin, whose subsidence is of 2 m and rebound is of 10–20 cm in general. Recent studies of geodetic records in regions including Ravenna, Italy (Teatini et al., 2005) and Shanghai, China (Chai et al., 2004) displayed a sharp change on subsidence rates showing a switch from severe to slight subsidence while groundwater utilization was controlled or stopped; however, no uplift due to aquifer rebound was observed in these above regions yet. Differences in groundwater exploitation history, piezometric level evolution, and local hydrogeological properties (e.g. aquifer compressibility, porosity, permeability) are major factors for the discrepancies documented in the localities cited above.

As mentioned above in Section 2.2, most groundwater extraction in the Taipei Basin was from Aquifer 1, which is generally located about 50 to 100 m underground within the Jingmei Formation. We intend to call the direct resultant effects from post-pumping compaction and rebound of aquifer strata due to natural recharge of groundwater as the “intermediate” component, compared with the compaction of the surface soil above the Aquifer 1 and the possible crust-scale subsidence due to the normal faulting of the Shanchiao Fault. This component is expected to have basin-wide impact since the Aquifer 1 is distributed throughout the entire basin.

4.4. Synthesis and discussion

The mechanisms of land elevation change in the Taipei Basin during the past 30-year post-pumping period are summarized in Fig. 9, showing the effect from three major depth-related components in the central and western parts of the basin. Soil compaction (the shallow component) is estimated with averaged rates of 3.5 mm/yr and 2 mm/yr for Central Taipei and the western margin, respectively (see Fig. 8, Section 4.1.). The tectonic load from the Shanchiao Fault (the deep and crustal-scale component) contributes subsidence of approximately 1.75 mm/yr for the western margin of the basin and 0.9 mm/yr for Central Taipei (discussed in Section 4.2.). As for aquifer deformation (the intermediate component), due to combination of

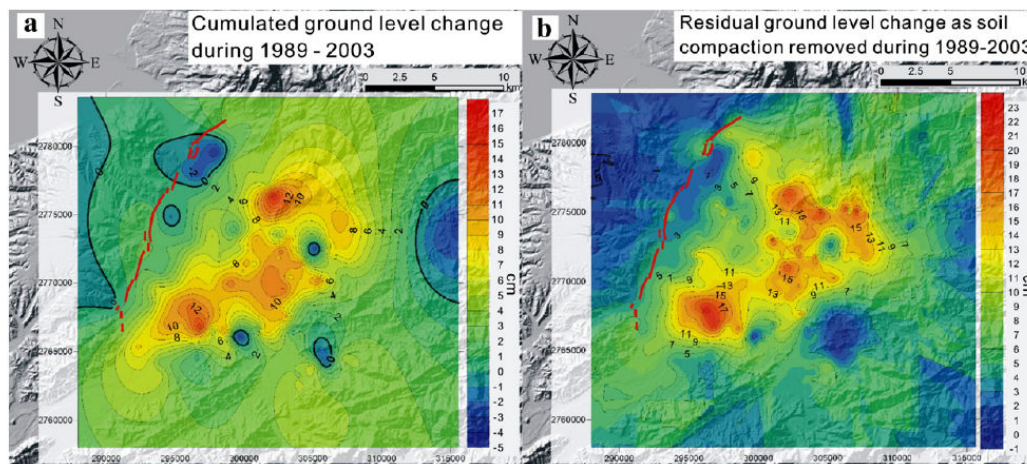


Fig. 10. Ground level changes during Phase 2 of post-pumping period. (a) Cumulated ground elevation change from 1989 to 2003. (b) Residual ground elevation change from 1989 to 2003 as soil compaction (shallow component) removed.

compaction and rebound of natural recharge, its deformation rate is estimated by subtracting the soil compaction rate and the tectonic subsidence rate from the land elevation change rate. We thus obtain the evolution of the aquifer deformation rate in western and central Taipei Basin, as the dashed curve in Fig. 9.

As revealed by Fig. 9, among the three major mechanisms, the aquifer deformation appears to be the main driving source of ground elevation changes, that is, subsidence in Phase 1 and uplift in Phase 2. Further-

more, the observed prominent land uplift in Phase 2, which is interpreted to be mainly related to the aquifer rebound, was significantly less in western margin than in Central Taipei.

In order to illuminate the actual extent of effects from aquifer deformation (compaction versus rebound) and tectonic load, we sum up the ground level change in the Taipei area during Phase 2 (1989–2003, Fig. 10a) then remove estimate of shallow soil compaction to create the map of residual cumulative ground level change

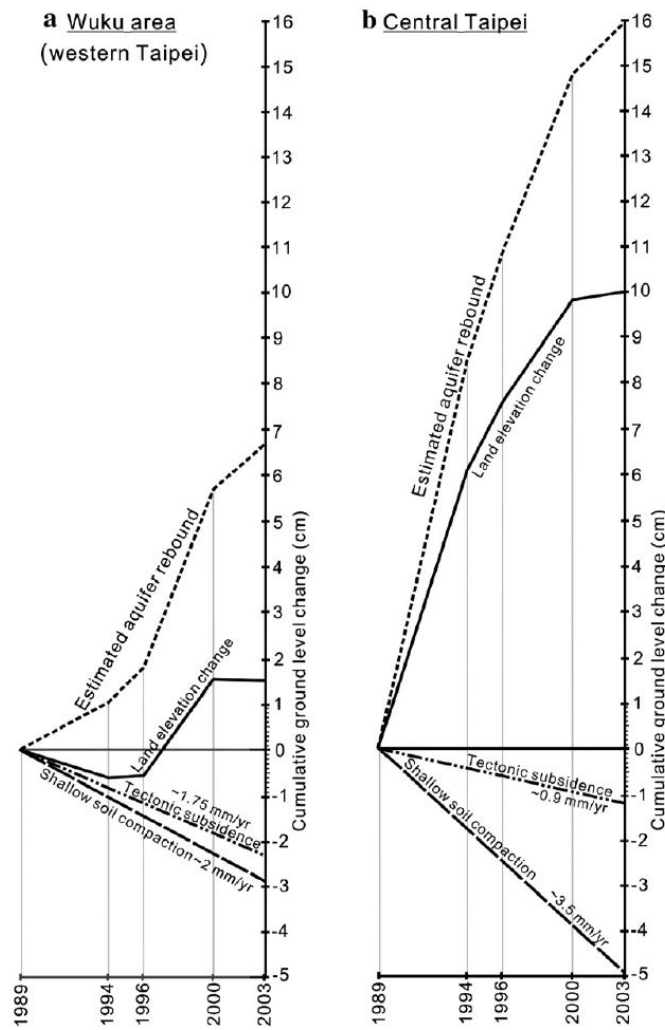


Fig. 11. A schematic model for evaluating aquifer elastic rebound during the Phase 2 of the post-pumping period 1989–2003, in (a) Wuku (Western Taipei) and (b) Central Taipei.

(Fig. 10b). The major remaining factors affecting land elevation fluctuation during Phase 2 are (1) elastic rebound of recharged Aquifer 1 contributing uplift and (2) tectonic subsidence. Note that the residual compaction of Aquifer 1 had declined to a neglected minimal rate as groundwater table almost fully recovered and stabilized. Most of the Taipei Basin, except the western margin, showed rather homogeneous uplift of 13–18 cm (spatial variation) during 1989–2003 (or 9–13 mm/yr in average), and is interpreted as a manifestation of elastic rebound of Aquifer 1 due to natural recharge. The western part of the basin, in contrast, exhibited less amount of uplift (1–9 cm, or 0–6 mm/yr in average throughout the area) which decreased toward the west and northwest (also exhibited in Fig. 7). The “differential uplift” was partially resulted from variations of elastic rebound of Aquifer 1 possibly related to changes in sedimentary facies (hence the thickness and composition of the aquifer strata) and hydrological parameters. However, the pattern of uplift diminishing toward the Shanchiao Fault also demonstrated a likely effect of tectonic load especially for the near-fault hanging-wall regions including Guandu, Wuku, and Shulin.

A schematic model of mechanisms for the cumulative land elevation changes of Central and Western Taipei areas during Phase 2 of post-pumping from 1989 to 2003 is presented in Fig. 11. For Central Taipei, adapting 3.5 mm/yr of shallow soil compaction and 0.9 mm/yr of long-term tectonic subsidence, we obtain a total aquifer rebound of 16 cm in 1989–2003 (Fig. 11b). For the Wuku area of western Taipei in the same manner by adopting averaged shallow soil compaction of 2 mm/yr and the long-term tectonic subsidence rate of 1.75 mm/yr, we come to an estimation of rebound in the region as 6.7 cm in 1989–2003 (Fig. 11a). The values of total rebound are of reasonable magnitude as the preliminary test given below. Based on injection experiments carried out in Wilmington oilfield, California, Allen and Mayuga (1969) proposed a simplified empirical equation: the amount of rebound (u) is a function of thickness of the recharged aquifer strata (t_{aquifer}):

$$u = a \cdot b t_{\text{aquifer}}$$

Where a is the ratio of surface uplift to actual amount of aquifer elastic rebound and was given as 0.5, b is the expansion factor per aquifer unit and was estimated to be 0.005 per unit. Taking averaged thickness of Aquifer 1 (the Jingmei formation) of 50 m in Central Taipei into calculation, the aquifer rebound is estimated to be 12.5 cm. For Western Taipei by adapting known

minimum thickness of Aquifer 1 in the region as 25 m, amount of the aquifer rebound is estimated to be 6.25 cm. Although minor amount of aquifer rebound may still be in operation after 2003, fair agreement is found between the above estimation and our results (16 cm versus 12.5 cm in Central Taipei, and 6.7 cm versus 6.25 in Western Taipei).

Improvements from these preliminary results and statements will come from more comprehensive study on geotechnical and hydrological properties of the basin deposits to contribute a realistic modelling, and further level monitoring of both ground surface and down-hole benchmarks.

5. Summary

Land elevation change during post-pumping in 1975–2003 in the Taipei Basin illuminated by levelling data was documented in details. The post-pumping behaviour is characterized by an interval of waning subsidence followed by one of slight uplift, as Phase 1 and Phase 2, respectively. This behaviour was dominated by aquifer internal deformation in response to piezometric level changes. The aquifer is observed to exhibit substantial elastic rebound in the later stage of groundwater recharge, whose magnitude is about 10% of that of the former pumping-induced subsidence. This further confirms that land subsidence caused by aquifer/reservoir overdraft is largely an irreversible process and should be avoided especially in critical areas of flat low-lying topography and flood risk.

Two other major mechanisms also imposed significant effects on basin ground level change. Shallow soil compaction contributed enhanced subsidence especially near river courses and marshy areas. Regional tectonic asymmetric subsidence related to the Shanchiao normal Fault, whose effect is observable from the elevation change data, is interpreted to be the main agent responsible for continued subsidence in the western margin of the basin on the hanging wall near the fault line.

Acknowledgements

We thank LSPRC (Land Subsidence Prevention and Reclamation Corp) of National Chengkung University for kindly providing levelling data and Central Geological Survey, MOEA for borehole data. We also thank H.-T. Chu, Y.-G. Chen, L. S. Teng, K.-C. Chang, and C. Huang for helpful comments and suggestions. This work is supported by National Science Council of R.O.C. (grant NCS-95-2922-I-002-239).

References

- Abidin, H.Z., Djaja, R., Darmawan, D., Hadi, S., Akbar, A., Rajiowiryono, H., Sudibyoy, Y., Meilano, I., Kasuma, M.A., Kahar, J., Subarya, C., 2001. Land subsidence of Jakarta (Indonesia) and its geodetic monitoring system. *Natural Hazards* 23, 365–387.
- Allen, D.R., Mayuga, M.N., 1969. The mechanics of compaction and rebound, Wilmington Oil Field, Long Beach, California, U.S.A. Proceedings of the Tokyo Symposium on Land Subsidence 2, 410–423, International Association of Scientific Hydrology and UNESCO, September 1969, Tokyo.
- Amelung, F., Galloway, D.L., Bell, J.W., Zebker, H.A., Lacznak, R.J., 1999. Sensing the ups and downs of Las Vegas: InSAR reveals structural control of land subsidence and aquifer-system deformation. *Geology* 27–6, 483–486.
- Cappa, F., Guglielmi, Y., Fenart, P., Merrien-Soukatchoff, V., Thoraval, A., 2005. Hydromechanical interactions in a fractured carbonate reservoir inferred from hydraulic and mechanical measurements. *International Journal of Rock Mechanics and Mining Sciences* 42, 287–306.
- Chai, J.-C., Shen, S.-L., Zhu, H.-H., Zhang, X.-L., 2004. Land subsidence due to groundwater drawdown in Shanghai. *Geotechnique* 54–2, 143–147.
- Chang, H.-C., Lin, C.-W., Chen, M.-M., Lu, S.-T., 1998. An Introduction to the Active Faults of Taiwan, Explanatory Text of the Active Fault Map of Taiwan (in Chinese with English abstract). Special Publication of Central Geological Survey, vol. 10. Central Geological Survey, Ministry Economical Affairs, Taipei, Taiwan, R.O.C. 103 pp.
- Chen, C.-H., Lee, C.-Y., Lin, S.-B., 1995. The eruption age of volcanic ashes in the Wuku Well, Taipei Basin: constraints on mineral chemistry and $^{40}\text{Ar}/^{39}\text{Ar}$ dating. *Journal of Geological Society of China* 38, 371–382.
- Chen, C.-T., Lee, J.-C., Hu, J.-C., Chan, Y.-C., Lu, C.-Y., 2006. The active Shanchiao Fault in the Metropolitan Taipei Area, Northern Taiwan: geomorphic and geodetic analyses. *Eos Trans. AGU* 87–52, Fall Meeting Supplement, T33D–0543. Abstract.
- Chen, W.-F., Teng, L.S., 1990. Depositional environment of Quaternary deposits of the Linkou Tableland, northwestern Taiwan. Proceedings of the Geological Society of China 33, 39–63.
- Chia, Y.-P., Chang, M.-H., Liu, W.-I., Lai, T.-C., 1999. Hydrogeologic characterization of Taipei Basin (in Chinese with English abstract). Central Geological Survey Special Publication 11, 393–406.
- Chiu, H.T., 1968. The Hsinchuang Fault in the Taoyuan area, northern Taiwan. Proceedings of Geological Society of China 11, 60–73.
- Cho W.-C., 2006. Groundwater level change and elevation fluctuation of the Taipei Basin. Master thesis, National Taiwan University, Taipei, 73 pp.
- Dokka, R.K., 2006. Modern-day tectonic subsidence in coastal Louisiana. *Geology* 34, 281–284.
- Gambolati, G., Teatini, P., 1998. Natural land subsidence due to compaction of the upper Adriatic Sea Basin. *IGEA* 11, 29–40.
- Gambolati, G., Teatini, P., Tomasi, L., Gonella, M., 1999. Coastline regression of the Romagna region, Italy, due to natural and anthropogenic land subsidence and sea level rise. *Water Resources Research* 35-1, 163–184.
- Gatto, P., Carbognin, L., 1981. The Lagoon of Venice: natural environmental trend and man-induced modification. *Hydrological Sciences-Bulletin* 26 (4), 379–391.
- Ho, C.-S., 1975. An Introduction to the Geology of Taiwan. Ministry of Economic Affairs, Republic of China. 143 pp.
- Holzer, T.L., 1984. Ground failure induced by groundwater withdrawal from unconsolidated sediments. *Reviews in Engineering Geology* 6, 67–105.
- Hsieh, C.-H., Chang, Y.-F., Sun, R.-H., 1992. Seismic investigate Hsin-Chuan fault on the west of Taipei Basin (in Chinese with English abstract). *Ti-Chih* 12 (1), 13–26.
- Hu, J.-C., Yu, S.-B., Chu, H.-T., Angelier, J., 2002. Transition tectonics of northern Taiwan induced by convergence and trench retreat. *Geological Society of America Special Paper* 358, 149–162.
- Hu, J.-C., Chu, H.-T., Hou, C.-S., Lai, T.-H., Chen, R.-F., Nien, P.-F., 2006. The contribution to tectonic subsidence by groundwater abstraction in the Pingtung area, southwestern Taiwan as determined by GPS measurements. *Quaternary International* 147, 62–69.
- Huang, S.-Y., Rubin, C.M., Chen, Y.-G., Liu, H.-C., 2007. Prehistoric earthquakes along the Shanchiao Fault, Taipei Basin, Northern Taiwan. *Journal of Asian Earth Sciences*. doi:10.1016/j.jseas.2006.07.025.
- Hwang, J.-M., Wu, C.-M., 1969. Land subsidence problems in Taipei Basin. Proceedings of the Tokyo Symposium on Land Subsidence 1, 21–34, International Association of Scientific Hydrology and UNESCO, September 1969, Tokyo.
- Jelgersma, S., 1996. Land subsidence in coastal lowlands. In: Milliman, J.D., Haq, B.U. (Eds.), *Sea-Level Rise and Coastal Subsidence*, pp. 47–62.
- Kao, H., Shen, S.J., Ma, K.-F., 1998. Transition from oblique subduction to collision: earthquakes in the southernmost Ryukyu arc-Taiwan region. *Journal of Geophysical Research* 103, 7211–7229.
- Karig, D.E., Hou, G., 1992. High-stress consolidation experiments and their geologic implications. *Journal of Geophysical Research* 97 (B1), 289–300.
- Lee, C.-T., Wang, Y., 1988. Quaternary stress changes in northern Taiwan and their tectonic implication. Proceedings of the Geological Society of China 31 (1), 154–168.
- Lin, C.-W., Chang, H.-C., Lu, S.-T., Shih, T.-S., Huang, W.-J., 2000. An introduction to the active faults of Taiwan, Explanatory Text of the Active Fault Map of Taiwan (in Chinese with English abstract), 2nd ed. Special Publication of Central Geological Survey, vol. 13. Central Geological Survey, Ministry Economical Affairs, Taipei, Taiwan, R.O.C. 122 pp.
- Lin, M.-L., Huang, T.-H., Hung, J.-J., Chi, C.-C., 1999. A study on in situ measurement of ground subsidence of Taipei Basin (in Chinese with English abstract). Central Geological Survey Special Publication 11, 317–344.
- Lu, C.-Y., Angelier, J., Chu, H.-T., Lee, J.-C., 1995. Contractional, transcurrent, rotational and extensional tectonics: examples from Northern Taiwan. *Tectonophysics* 246, 129–146.
- Meckel, T.A., ten Brink, U.S., Williams, S.J., 2006. Current subsidence rates due to compaction of Holocene sediments in southern Louisiana. *Geophysical Research Letters* 33, L11403. doi:10.1029/2006GL026300.
- Oliver, M.A., Webster, R., 1990. Kriging: a method of interpolation for geographical information system. *International Journal of Geographical Information Systems* 4 (3), 313–332.
- Phien-wej, N., Giao, P.H., Nutalaya, P., 2006. Land subsidence in Bangkok, Thailand. *Engineering Geology* 82, 187–201.
- Shyu, J.B.H., Sieh, K., Chen, Y.-G., Liu, C.-S., 2005. Neotectonic architecture of Taiwan and its implications for future large earthquakes. *Journal of Geophysical Research* 110, B08402. doi:10.1029/2004JB003251.
- Suppe, J., 1981. Mechanics of mountain building and metamorphism in Taiwan. *Memoir of the Geological Society of China* 4, 67–89.

- Teatini, P., Ferronato, M., Gambolati, G., Bertoni, W., Gonella, M., 2005. A century of land subsidence in Ravenna, Italy. *Environmental Geology* 47, 831–846.
- Terzaghi, K.T., 1925. *Erdbaumechanik auf Bodenphysikalischer Grundlage*. Wien, Deuticke. 399 pp.
- Teng, L.S., 1990. Late Cenozoic arc-continent collision in Taiwan. *Tectonophysics* 183, 57–76.
- Teng, L.S., Yuan, P.B., Chen, P.-Y., Peng, C.-H., Lai, T.-C., Fei, L.-Y., Liu, H.-C., 1999. Lithostratigraphy of Taipei Basin deposits (in Chinese with English abstract). *Central Geological Survey Special Publication* 11, 41–66.
- Teng, L.S., Lee, C.-T., Tsai, Y.-B., Hsiao, L.-Y., 2000. Slab breakoff as a mechanism for flipping of subduction polarity in Taiwan. *Geology* 28, 155–158.
- Teng, L.S., Lee, C.-T., Peng, C.-H., Chen, W.-F., Chu, C.-J., 2001. Origin and geological evolution of the Taipei Basin, Northern Taiwan. *Western Pacific Earth Sciences* 1–2, 115–142.
- Waltham, T., 2002. Sinking cities—feature. *Geology Today* 18 (3), 95–100.
- Wang, C.-Y., Sun, C.-T., 1999. Interpretation of seismic stratigraphy in the Taipei Basin (in Chinese with English abstract). *Central Geological Survey Special Publication* 11, 273–292.
- Wang-Lee, C.-M., Cheng, Y.-M., Wang, Y., 1978. Geology of the Taipei Basin (in Chinese). *Taiwan Mining Industry* 30 (4), 350–380.
- Wei, K., Chen, Y.-G., Liu, T.-K., 1998. Sedimentary history of the Taipei Basin with constraints from thermoluminescence dates. *Journal of Geological Society of China* 41, 109–125.
- Wu, C.-M., 1987. Reviews on the land subsidence of the Taipei Basin (in Chinese). *Sino-Geotechnics* 20, 34–49.
- Yeh, Y.-H., Barrier, E., Lin, C.-H., Angelier, J., 1991. Stress tensor analysis in the Taiwan area from focal mechanisms of earthquakes. *Tectonophysics* 200, 267–280.
- Yu, S.-B., Chen, H.-Y., Kou, L.-C., Hou, C.-S., Lee, C.-F., 1999a. A study on the fault activities of the Taipei Basin (in Chinese with English abstract). *Central Geological Survey Special Publication* 11, 227–251.
- Yu, S.-B., Kuo, L.-C., Punongbayan, R.S., Ramos, E.G., 1999b. GPS observation of crustal deformation in the Taiwan–Luzon region. *Geophysical Research Letters* 26 (7), 923–926.
- Zang, S.X., Chen, Q.Y., Ning, J.Y., Zheng, K.S., Liu, Y.G., 2002. Motion of the Philippine Sea plate consistent with the NUVEL-1A model. *Geophysical Journal International* 150, 809–819.



A2. Note on Chapter 3

The content of Chapter 3 is a published manuscript with detailed citation below:

Chen, C.-T., Lee, J.-C., Chan, Y.-C., Lu, C.-Y., 2010a. Growth normal faulting at the western edge of the Metropolitan Taipei Basin since the Last Glacial Maximum, northern Taiwan. *Terrestrial, Atmospheric and Oceanic Sciences* 21-3, 409-428.



Growth Normal Faulting at the Western Edge of the Metropolitan Taipei Basin since the Last Glacial Maximum, Northern Taiwan

Chih-Tung Chen¹, Jian-Cheng Lee^{2,*}, Yu-Chang Chan², and Chia-Yu Lu¹

¹Department of Geosciences, National Taiwan University, Taipei 106, Taiwan, ROC

²Institute of Earth Sciences, Academia Sinica, Taipei 115, Taiwan, ROC

Received 25 April 2008, accepted 13 November 2009

ABSTRACT

Growth strata analysis is an useful tool in understanding kinematics and the evolution of active faults as well as the close relationship between sedimentation and tectonics. Here we present the Shanchiao Fault as a case study which is an active normal fault responsible for the formation of the 700-m-thick late Quaternary deposits in Taipei Basin at the northern tip of the Taiwan mountain belt. We compiled a sedimentary record, particularly the depositional facies and their dated ages, at three boreholes (SCF-1, SCF-2 and WK-1, from west to east) along the Wuku Profile that traverses the Shanchiao Fault at its central segment. By incorporating the global sea level change curve, we find that thickness changes of sediments and changes of depositional environments in the Wuku area are in a good agreement with a rapid sea level rise since the Last Glacial Maximum (LGM) of about 23 ka. Combining depositional facies changes and their ages with their thickness, we are able to introduce a simple back-stripping method to reconstruct the evolution of growing strata across the Shanchiao Fault since the LGM. We then estimate the vertical tectonic slip rate since 23 ka, which exhibits 2.2 mm yr⁻¹ between SCF-2 and WK-1 and 1.1 mm yr⁻¹ between SCF-1 and SCF-2. We also obtain the Holocene tectonic subsidence rate of 2.3 mm yr⁻¹ at WK-1 and 0.9 mm yr⁻¹ at SCF-2 since 8.4 ka. We thus conclude that the fault zone consists of a high-angle main fault to the east between SCF-2 and WK-1 and a western lower-angle branch fault between SCF-1 and SCF-2, resembling a tulip structure developed under sinistral transtensional tectonism. We find that a short period of 600-yr time span in 9 - 8.4 ka shows important tectonic subsidence of 7.4 and 3.3 m for the main and branch fault, respectively, consistent with possible earthquake events proposed by previous studies during that time. A correlation between geomorphology and subsurface geology in the Shanchiao Fault zone shows that an array of subtle geomorphic scarps corresponds to the branch fault, however, that the surface trace of the main fault seems to be completely erased by the surface force of erosion and sedimentation. We recommend that analysis in the light of growth-faulting scheme should be conducted in a more systematic way for earthquake geology study in other portions of the Shanchiao Fault within the Taipei Basin, as well as other areas worldwide currently under extensional deformation.

Key words: Growth faulting, the Shanchiao Fault, Tectonic subsidence, Active fault, Taiwan

Citation: Chen, C. T., J. C. Lee, Y. C. Chan, and C. Y. Lu, 2010: Growth normal faulting at the western edge of the Metropolitan Taipei Basin since the last glacial maximum, northern Taiwan. *Terr. Atmos. Ocean. Sci.*, 21, 409-428, doi: 10.3319/TAO.2009.11.13.01(TH)

1. INTRODUCTION

History of fault development is often tape-recorded in syn-tectonic sediments associated with the fault motion. Such growth faulting scheme has been invoked to interpret fault slip accumulation over time and variation of strata across and along strike, leading to models describing fault evolution and kinematics (e.g., Childs et al. 2003; Bull et al.

2006). Much attention has been paid to growth strata genesis in compressional tectonic environments, such as foreland settings in determining fault-fold kinematics (Vergés et al. 2002; Hubert-Ferrari et al. 2007). Growth faulting along with sequence analyses were successfully applied to understand basin formation and petroleum systems in the northern Gulf of Mexico where deltaic shelf sediment infills are modulated by gravity-driven normal faulting and eustatic sea level change (Brown et al. 2004). Growth faulting may form at low elevations in the vicinity influ-

* Corresponding author
E-mail: jclee@earth.sinica.edu.tw

enced by recent sea level rise, and thus serve to be a potential tool for neotectonic investigations on seismogenic normal faults.

Normal fault system is one of the important sources of earthquake hazard in continental extensional provinces, where large plains, and therefore urban development and heavy populations, are often present. Examples of paleoseismology and earthquake geology studies in such setting include the Tyrnavos Basin in the Aegeon region (Caputo et al. 2004), the Wasatch Fault Zone in central Utah, United States (Machette et al. 1991; McCalpin and Nishenko 1996), and the upper Rhine Graben near Basel, northern Switzerland (Meghraoui et al. 2001). The Taipei metropolitan, the capital of Taiwan where several million people reside, is unfortunately also under seismic threat from the active Shanchiao normal fault (Fig. 1; Chang et al. 1998; Lin et al. 2000). Since pioneering studies of the Shanchiao Fault (e.g.,

Lin 1957; Wu 1965), the geological characteristics of this fault have remained relatively poorly understood though they bear important information on hazard mitigation and regional geodynamics. Properties of the activity of the fault such as its long-term Quaternary slip rate are mostly inferred from geologic data in the Taipei Basin (Teng et al. 2001) and are therefore crude in nature. Recently, Huang et al. (2007) correlated the sediments of three borehole sets across the deduced fault surface trace (Lin 2001) and proposed three paleoseismic events during the Holocene; the validity of their analysis is doubtful as the borehole sets may have covered only part of the Shanchiao Fault zone when considering the geometry of the basin basement. In this study, we re-compiled their borehole set in the central part of the Shanchiao Fault to form the Wuku Profile (Fig. 2a). The stratigraphy of the three wells in the Wuku Profile is correlated and a geologic cross-section is thus revealed.

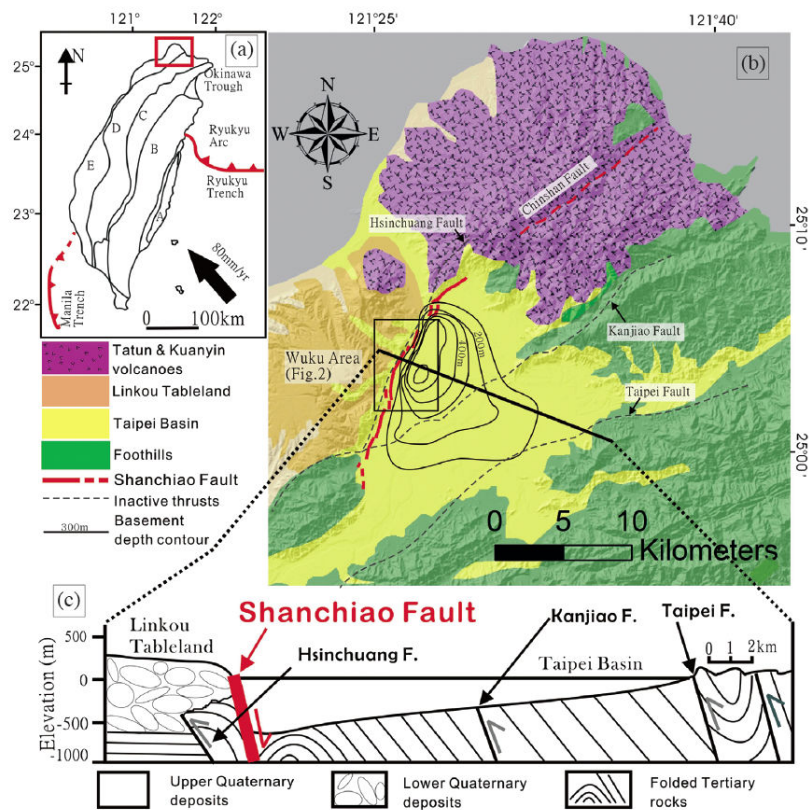


Fig. 1. (a) General tectonic framework of Taiwan. A: Coastal Range; B: Backbone Range; C: Hsueshan Range; D: Western Foothills; E: western Coastal Plain. (b) Simplified geology of the Taipei area. Four geological domains are defined in the Taipei area as indicated by different colors shown in the legend. The thick red lines are the Shanchiao Fault traces (Chen et al. 2006). Thin black lines within the Taipei Basin are the basement depth contour of 100 m interval (adapted from Teng et al. 2001). (c) Geological cross section of the Taipei Basin (modified from Teng et al. 1999).

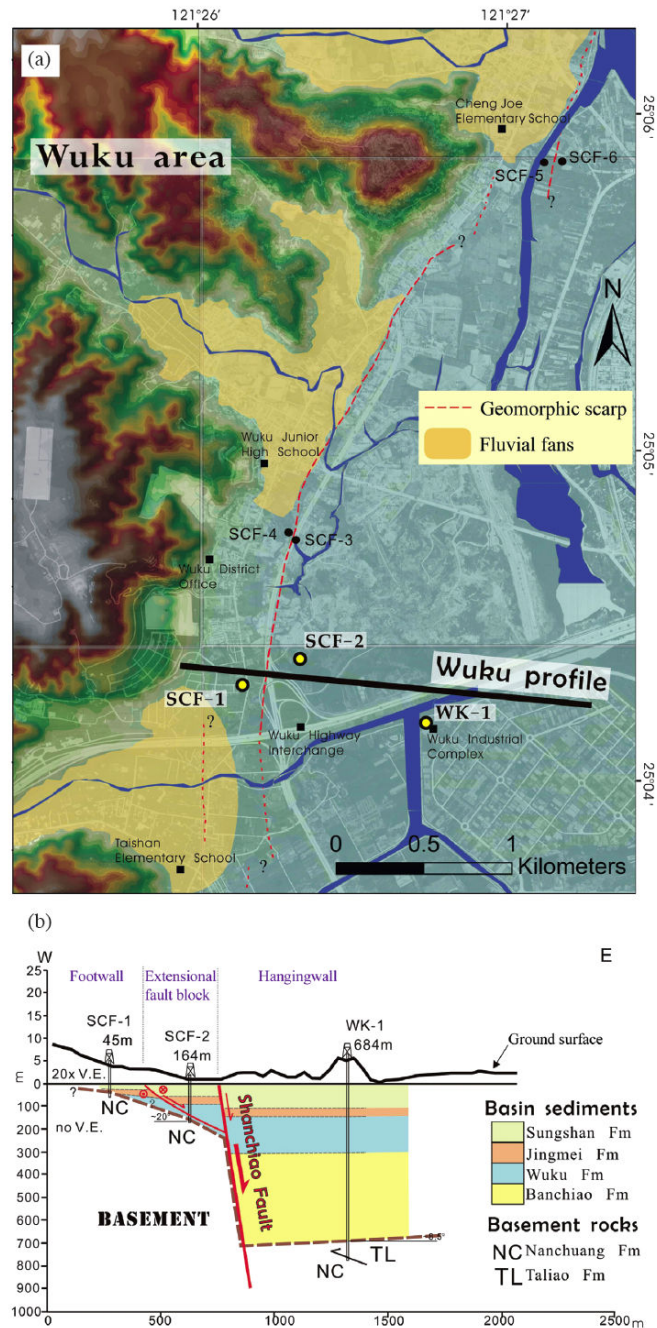


Fig. 2. (a) Map of the Wuku area, showing locations of the three boreholes used in this study, the Shanchiao Fault trace (dashed lines), and geomorphic features. (b) Interpreted Wuku geological profile. We interpret the Shanchiao fault as a combination of a main fault between SCF-2 and WK-1 to the east and the branch fault between the SCF-1 and SCF-2 to the west. Note that there is no vertical exaggeration beneath the sea level, and 20 times vertical exaggeration for surface topography.

In this paper, we document a valuable example of subaerial growth faulting case in the central portion of the Shanchiao Fault where growth strata provide a clear distinction on the sedimentation rate and throw rate across the fault on the thousand-year scale. A detailed growth faulting history is constructed over a time span since the Last Glacial Maximum revealing close coupling between sedimentation, tectonic process, drainage system changes, and eustatic sea level rise. Fault zone location and its deformation structure within unconsolidated basin sediment can therefore be better defined. Vertical slip rates on main and branch faults starting from 23 ka are constrained, implying an approximately 2 mm yr^{-1} averaged tectonic subsidence rate across the Shanchiao fault zone for the last 8400 years.

2. GEOLOGICAL SETTING

Taiwan is situated on the plate boundary of active convergence between the Eurasian and Philippine Sea plates since around 5 Ma (Suppe 1981; Ho 1986; Teng 1990; Wu et al. 1997) with a rapid convergence rate of about 82 mm yr^{-1} in the NW direction (Seno 1977; Yu et al. 1997; Lin et al. 2010; Fig. 1a). This oblique convergence leads to the southward-propagation of the Taiwan orogeny (Suppe 1981). Unlike regions of central and southern Taiwan presently in a state of full and mature collision (Angelier et al. 1986; Yu et al. 1997; Shyu et al. 2005), the northern part of the mountain belt, including the Taipei region, is now in a state of post-collision with an extensional or transtensional tectonic setting rather than a compressional one (Teng 1996), as evidenced by the presence of Quaternary extensional structures (Lee and Wang 1988; Lee 1989; Lu et al. 1995), extensional earthquake focal mechanisms (Yeh et al. 1991; Kao et al. 1998), and GPS displacement fields (Yu et al. 1997; Rau et al. 2008). The Taipei half-graben of Quaternary deposits is therefore formed in a close association with down-dip slips on the Shanchiao Fault, which is considered to be the major neotectonic structure responsible for the tectonic inversion from compression to extension across the Taipei region (Teng et al. 2001; Fig. 1).

The flat low-lying Taipei Basin, a triangular-shaped half-graben filled with late-Quaternary fluvial deposits since c. 400 ka (Wei et al. 1998; Teng et al. 2001), developed on top of the folded Oligo-Mio-Pliocene shallow marine strata, as a fold-and-thrust belt during earlier stage of mountain building. The late Quaternary terrestrial deposits in the Taipei basin form an asymmetric sedimentary wedge: reaching a maximum depth of about 700 m near the western margin and becoming thinner rather drastically toward the east and south (Fig. 1c). These unconsolidated deposits are divided into four major lithostratigraphic units (Teng et al. 1999). From bottom to top (Fig. 2b), they are: (1) the *Banchiao Formation*: consisting of intercalated fluvial sand, mud and conglomerate, with occasional pyroclastics and topped by

thick laminated mud, with a maximum thickness of 380 m with ages ranging from 250 to 400 ka; (2) the *Wuku Formation*: consisting of fluvial sands and conglomerates, with minor mud and lateritic conglomerates, reaching a maximum thickness of c. 160 m with ages ranging from 80 to 250 ka; (3) the *Jingmei Formation*: comprising lateritic fluvial (alluvial-fan) conglomerates with an utmost thickness of 50 m. These particular conglomerate layers are interpreted as products when the Tahan River was captured and flowing into the Taipei basin about 25 to 23 ka (Teng et al. 2004a); (4) the *Sungshan Formation*: composed of estuarine interbedded sand-mud deposits, with a thickness of 50 - 100 m. The basin deposits are marked by prominent lateral facies changes with frequent pinch-outs. However, the widespread lateritic gravels of the Jingmei Formation and the laminated mud in the upper Banchiao Formation (Teng et al. 2004b) usually serve as basin-wide marker beds (Teng et al. 1999).

Geological evolution of the Taipei Basin was proposed by Teng et al. (2001), based on interpretation of regional geology. While the Plio-Pleistocene orogeny of mountain building reached its climax in northern Taiwan in Quaternary, the Paleo-Tanshui River, the major river in the Taipei Basin, began to provide sediments to produce the Linkou fan-delta around the ancient mountain front (Chen and Teng 1990). Accompanying the waning of compressive stress in the northernmost Taiwan island during the middle to late Quaternary (Lee and Wang 1988) is the vigorous eruptions of the Tatan volcanoes to the north of the Taipei Basin (Wang and Chen 1990; Song et al. 2000), probably reflecting the onset of regional extension. Subsidence along western margin of the Taipei basin, as evidenced by several hundred meters of thick fluvial deposits, is interpreted as a result from repeated normal faulting (the Shanchiao Fault) as inverted from the Hsinchuang fault, an ancient frontal thrust in northern Taiwan (Chiu 1968; Hsieh et al. 1992). The extension tectonics gradually transformed the Taipei area from rugged mountains into a sediment-receiving basin. The accumulation of fluvial and lacustrine sediments started at about 0.4 Ma (Wei et al. 1998; Teng et al. 2001). Since then the Taipei Basin has kept expanding due to erosion and continual asymmetric subsidence along the Shanchiao Fault in the western edge of the basin. Under the combining influences of sea level fluctuations, volcanic activities, drainage system changes, and tectonic processes, the basin was infilled with various types of sediments, including alluvial, lacustrine, marine and pyroclastic deposits, up to 700 m thick as mentioned above.

3. THE ACTIVE SHANCHIAO FAULT

The Shanchiao Fault was mapped (Lin 2001; Chen et al. 2004, 2006; Huang et al. 2007; Figs. 1b and 2a) along the topographic boundary between the Linkou Tableland and the Taipei Basin, sub-parallel to the Hsinchuang Fault (Lin

2001; Teng et al. 2001). There are features which indicate that the steeper Shanchiao normal fault may merge into the Hsinchuang thrust fault at depth (e.g., Hsieh et al. 1992). Following the late-Quaternary tectonic inversion, tectonic subsidence from down-dip slips on the Shanchiao Fault led to formation and development of the Taipei Basin. Left-lateral transcurrent motion together with clockwise block rotation is also expected to occur along the Shanchiao Fault, based on studies on regional structural geology, paleomagnetism, and GPS measurements (Lu et al. 1995; Lee et al. 1999; Rau et al. 2008).

Much effort has been made to characterize this active fault. Shallow reflection seismic profiling across the Shanchiao Fault imaged vertical offsets of Holocene sediments at shallow depths, although the location of the main fault remains questionable (Wang and Sun 1999; Shih et al. 2004). GPS surveys of the Taipei area showed WNW-ESE extension with a slow rate of $0.08 \mu\text{strain yr}^{-1}$ across the fault (Yu et al. 1999). Asymmetric tectonic subsidence related to the Shanchiao Fault across the basin was illuminated through recent study on 30-year-long levelling data (Chen et al. 2007). Huang et al. (2007) correlated stratigraphy of three sets of boreholes, and proposed three paleoseismic events during the Holocene (i.e., at 8500, 9200, and 11100 years b.p., respectively). Geomorphology analysis also reveals a series of scarps closely related to the development of the Shanchiao Fault (Chen et al. 2006; Fig. 2a). Radon and helium anomalies in soil-gas along the fault zone were documented (Walia et al. 2005) indicating the presence of possible active faults and a deep fracture-advection system. The Shanchiao Fault is therefore considered currently active (Chang et al. 1998; Lin et al. 2000). Subsurface geology of the fault zone, by contrast, has not been fully explored.

4. RECONSTRUCTION OF GEOLOGICAL PROFILE ACROSS THE SHANCHIAO FAULT

In recent years, the Central Geological Survey of Taiwan carried out a number of drillings in the Taipei Basin in order to better understand its subsurface geology and engineering environment (e.g., Lin et al. 1999). Among them three boreholes in the Wuku area, SCF-1, 2, and WK-1, have been selected for the present analysis due to their optimal locations associated with the Shanchiao fault (Fig. 2a) and data quality. All three wells are situated in a flat marshy lowland in the Wuku area on the western edge of the basin. Drill hole WK-1 reaches the deepest known depth of the late Quaternary basin deposits at 679 m. Many radiocarbon dates have been acquired (Lin et al. 1999) which are crucial for a successful stratigraphic correlation. At SCF-1 and SCF-2 boreholes, the Sungshan Formation in the upper part was studied by Huang et al. (2007) whose classification of strata serves as a basis for this study. The main stratigraphic system of the complete basin deposit is adapted

from Teng et al. (1999), as discussed above. Through stratigraphic analysis of the three boreholes by incorporating the growth faulting scheme, we reconstruct the Wuku geological profile to reveal the present configuration of fault zone stratigraphy and structure in the central part of the Shanchiao Fault.

4.1 Stratigraphic Correlation between the Boreholes

First, we carried out analysis and correlation of stratigraphic units between the three boreholes, SCF-1, SCF-2 and WK-1, based on lithology and radiocarbon dates. We reprocessed all available raw radiocarbon dates previously published (Lin et al. 1999; Huang et al. 2007) by calibrating these radiocarbon dates to calendar years before present (cal. yr BP) using the model curve of Fairbanks et al. (2005). Table 1 shows details of the results. Note that a few calibrated radiocarbon dates reveal a reversed stratigraphic order (i.e., older ages on top of younger ones), implying that they might be reworked samples. Thermoluminescence ages acquired in WK-1 (Lin et al. 1999) are summarized in Table 2. We thus reconstructed a detailed correlation of lithostratigraphic units of the three boreholes (Fig. 3) and the unit descriptions are listed in Table 3. Comparing the strata in three boreholes (SCF-1, SCF-2, and WK-1), one finds that the thickness of all the four formations increases dramatically toward the east. Hereafter we describe how we correlated the lithofacies units between these three boreholes (Fig. 3).

For the uppermost Sungshan Formation at SCF-1 and SCF-2, Huang et al. (2007) divided this formation into three units as C1, C2, and C3. We find that such division also applies to the Sungshan Formation at WK-1 (Fig. 3 and Table 3). The C1 unit is comprised of mainly sandy layers with mollusk shells at bottom whose onset of deposition is around 8400 years B.P. (8.4 ka) and is of alluvial facies (Huang et al. 2007). At SCF-1 this unit extends from land surface to a depth of 14.5 m (where the shells occur) and is filled with fine to medium sand with occasional thin silts at 2 - 3 and 8 m depths. At SCF-2 this unit is composed of fine sands with one thin mud and silt layer and ends at the shell lag of 22.3 m in depth. Collectively, we find that the C1 unit shows a prograde depositional character in both SCF-1 and SCF-2. At WK-1 the shell layer is found at 33.6 m with an age ~8.4 ka, which lies under interlayers of fine to medium sands and muddy-silts; these sediments of floodplain facies in a prograding fashion (Teng et al. 2000) are therefore considered to be correlative to the C1 unit.

Underneath the C1 unit which was deposited from ~9 to 8.4 ka is predominantly clayey and rich in peat and charcoal as defined at SCF-1 and SCF-2 (Huang et al. 2007). The upper part of C2 at SCF-1 is filled with muddy silts and the lower part with mud to a depth of 21.3 m. At SCF-2 the C2 unit consists of mud in the upper section

Table 1. Radiocarbon age data of the three boreholes along the Wuku Profile.

Borehole	Data source*	¹⁴ C age (yr B.P. ± 1σ)	Calendar year range** (cal. yr B.P.)	Depth (m)	Unit
SCF-1	(1)	5730 ± 40	6457 - 6567	5.35	C1
	(1)	5697 ± 46	6418 - 6528	9.40	C1
	(1)	7590 ± 130	8280 - 8506	16.12	C2
	(1)	7923 ± 58	8618 - 8868	22.80	C3
	(1)	8450 ± 120	9345 - 9563	32.30	C3
	(1)	8620 ± 60	9517 - 9611	34.99	C3
SCF-2	(1)	5625 ± 49	6348 - 6450	10.40 - 10.50	C1
	(1)	7635 ± 55	8381 - 8463	19.20 - 19.30	C1
	(1)	8018 ± 54	8834 - 9032	22.55	C2
	(1)	7790 ± 50	8518 - 8612	30.40	C2
	(1)	8200 ± 56	9057 - 9239	36.70	C3
	(1)	8400 ± 160	9223 - 9567	49.00	C3
	(1)	9064 ± 67	11176 - 11270	55.50	C3
	(1)	34060 ± 600	38824 - 40038	87.52	Jingmei
	(1)	> 50000	N/A	102.20	Wuku
(1)	> 47100	N/A	138.18	Wuku	
WK-1	(2)	7160 ± 70	7917 - 8037	24.80	C1
	(2)	7560 ± 70	8321 - 8425	36.55	C2
	(2)	7930 ± 60	8628 - 8888	42.2 - 42.6	C2
	(2)	9010 ± 110	10035 - 10301	49.4 - 50.2	C2
	(2)	8660 ± 80	9515 - 9705	50.2 - 50.4	C2
	(2)	9090 ± 60	10196 - 10280	54.7 - 55.05	C3
	(2)	10180 ± 150	11549 - 12151	63.4 - 63.8	C3
	(2)	9530 ± 60	10687 - 10967	67.6 - 67.7	C3
	(2)	10080 ± 60	11493 - 11805	68.6 - 68.7	C3
	(2)	9810 ± 80	11159 - 11285	74.1 - 74.7	C3
	(2)	18950 ± 540	21914 - 23228	89.3 - 89.5	C3
	(2)	21300 ± 160	25287 - 25777	94.0 - 94.1	C3
	(2)	> 42000	N/A	183.6	Wuku
	(2)	> 50000	N/A	219.3	Wuku

* Raw radiocarbon ages: (1) Huang et al. 2007 and (2) Lin et al. 1999; ** Calibration with Fairbanks 0107 calibration curve (Fairbanks et al. 2005); N/A = not available.

Table 2. Thermal luminescence (TL) ages. Data from Lin et al. 1999.

Borehole	TL age	Depth (m)	Unit
WK-1	80 - 120 ka	155.9	Wuku
	83 - 113 ka	177	Wuku
	73 - 99 ka	234.2	Wuku
	164 - 264 ka	251	Wuku
	169 - 227 ka	328	Banchiao
	192 - 288 ka	351.5	Banchiao

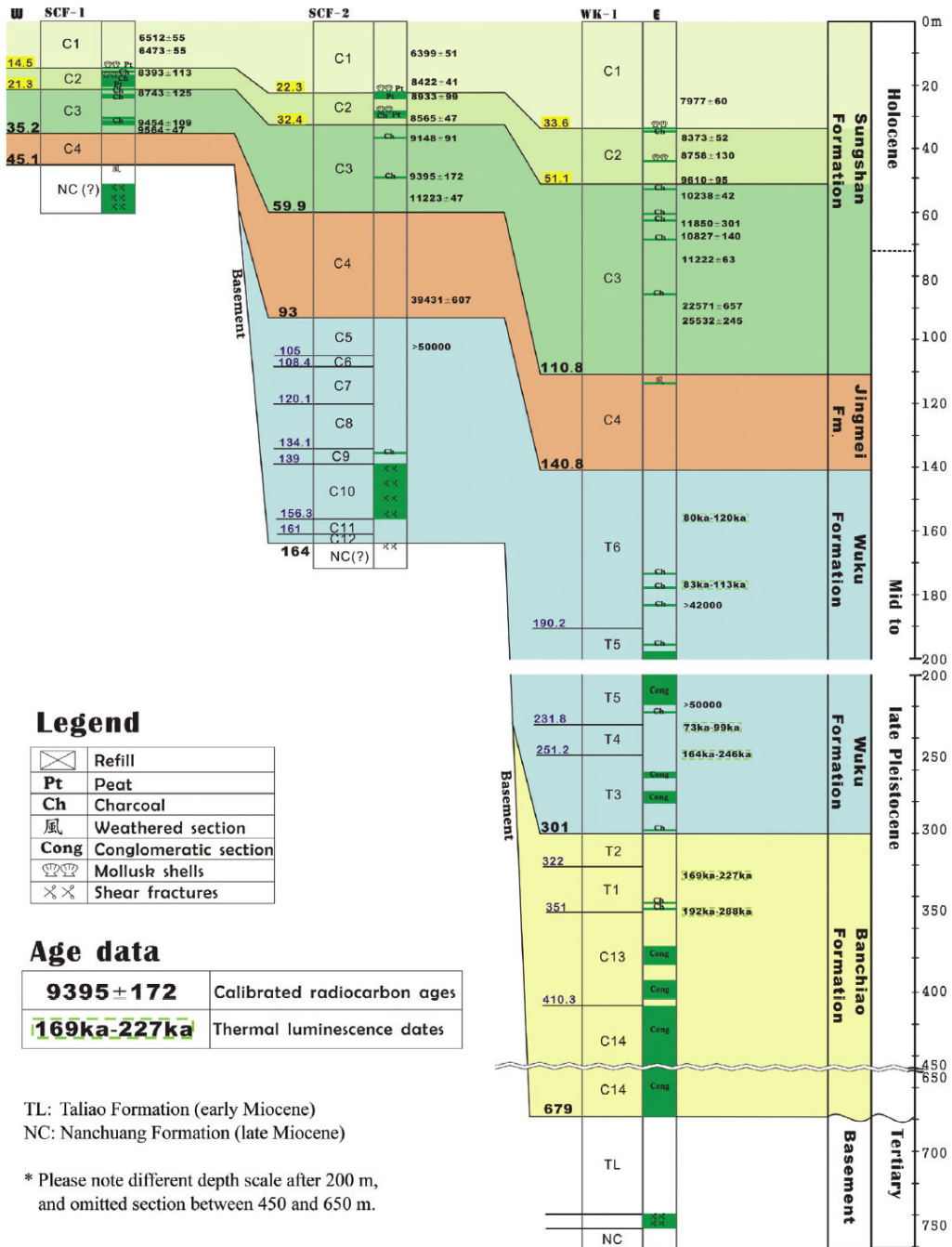


Fig. 3. Stratigraphic correlation between boreholes (SCF-1, SCF-2, and WK-1) of the Wuku profile. Location of the boreholes is indicated in Fig. 2. Four major geological formations consist of the late Quaternary deposits of the Taipei basin: from top to bottom, the Sungshan, Jingmei, Wuku, and Banchiao Formations. Each formation has been divided into several stratigraphic units. See details in the text. Please note different depth scales between 0 - 200 and 200 - 750 m, and omitted section between 450 and 650 m.

Table 3. Lithofacies of the Wuku Profile.

Unit	Description	Thickness (m)			Stratigraphy*	Reference**
		SCF-1	SCF-2	WK-1		
C1	Mainly sandy layers, parallel lamination in clayey layers, mollusk shells at bottom	14.5	22.3	33.6	Sungshan	a
C2	Mainly clay layers, occurrences of mollusk shells, peat in top section, paleosol and peat in middle section, charcoal-rich bottom section	6.8	10.1	17.5	Sungshan	a
C3	Sand within thin charcoal-rich clay layers, occurrences of paleosols	13.9	27.5	59.7	Sungshan	a
C4	Lateritic conglomerates with minor grey gravels	9.9	33.1	30	Jingmei	b
C5	Brown-grey silty sand	-	12	-	Wuku	This study
C6	Conglomerate with grey silt	-	3.4	-	Wuku	This study
C7	Brown silt	-	11.7	-	Wuku	This study
C8	Conglomerate with brown clay	-	14	-	Wuku	This study
C9	Charcoal-rich silt	-	4.9	-	Wuku	This study
C10	Sand-silt thin interlayers (containing several sheared sections localized in silt layers)	-	17.3	-	Wuku	This study
C11	(Tuffaceous?) silt	-	4.7	-	Wuku	This study
C12	Conglomerate with yellow-brown clay	-	3	-	Wuku	This study
T6	Clay within thin silt/sand	-	-	49.4	Wuku	c
T5	Conglomerate bounded by sand	-	-	41.6	Wuku	c
T4	Non-stratified clay with sand of parallel and cross lamina	-	-	19.4	Wuku	c
T3	Two conglomeratic layers in sands	-	-	49.8	Wuku	c
T2	Varve with rare thin silt/sand	-	-	21	Banchiao	c
T1	Non-stratified clay containing vivianite concretions, cross-laminated sand at bottom section	-	-	29	Banchiao	c
C13	Silt-clay with thin conglomerates	-	-	59.3	Banchiao	This study
C14	Conglomerate with rare thin sand/silt	-	-	268.7	Banchiao	This study

* Defined in Teng et al. (1999); ** Reference for unit definitions: a: Huang (2003) and Huang et al. (2007); b: Teng et al. (1999); c: Teng et al. (1993).

and silts near the bottom at 32.4 m. At WK-1 a thick muddy-silt layer of estuarine environment (Teng et al. 2000) extending to 51.1 m is found corresponding to the C2 unit with analogous sediments. In fact, the radiocarbon ages also support this correlation of stratigraphy. The sediments of the C2 unit are distinctively finer-grained than those above (C1 unit) or beneath (C3 unit), making it much easier to recognize. Abundant detrital charcoal chips and mollusk shells are present in C2 unit at all three boreholes.

The C3 unit, the lowermost member in the Sungshan Formation, is made up of sandy layers with alternating thin charcoal-rich clay layers older than 9 ka at SCF-1 and SCF-2. At SCF-1, the C3 unit consists of silts and fine sands 13.9 m

thick wherein their accumulation started at ~10 ka. At SCF-2 the C3 unit is 27.5 m thick composed of interbedded fine sands and silts, and began sedimentation ~12 ka. Between 51.1 and 110.8 m depth at WK-1, alternating charcoal-rich layers of fine-medium sands and mud is found equivalent to the C3 unit described above, albeit of greater thickness and longer time span of deposition ranging from ~23 to ~9 ka. The C3 sediments in WK-1 exhibit an upward transition from alluvial fan to distal floodplain facies in a retrograde stacking pattern, without a break of sedimentation between C3 and underlying Jingmei Formation of C4 unit (Teng et al. 2000). By contrast, there appears a substantial hiatus at the same stratigraphic boundary between C3 and C4 units at

SCF-1 and SCF-2, according to the radiocarbon dates.

The Jingmei Formation (lateritic clast-supported conglomerate layer, C4 unit in Table 3) also appears to increase in thickness towards the east. At borehole SCF-1, it rests unconformably above weathered Tertiary basement rock and is 9.9 m thick. At SCF-2 it is 33.1 m thick (between 59.9 to 93 m), and at WK-1 it is 30 m (between 110.8 to 140.8 m), both lying on the Wuku Formation. The Jingmei Formation, a product from the diversion of the Tahan River into the Taipei Basin, was interpreted to be formed during 23 and 25 ka (Teng et al. 2004a). The only radiocarbon date of 38 - 40 ka in the lower part of the Jingmei Formation at SCF-2 is presumably acquired from reworked material.

The remaining lower part of SCF-2 of about 71 m thick (93 - 164 m), below the Jingmei Formation, is composed of silts in combination of sands, with three conglomeratic units, and is defined as the upper part of the Wuku Formation (C5 - C12 units), which lies unconformably upon the folded Miocene basement rocks. At borehole WK-1, below the Jingmei Formation, two late Quaternary formations lying unconformably above the Tertiary basement rocks can be observed: (a) the Wuku Formation lies in between 140.8 to 301 m (about 140 m thick) and (b) the underlying Banchiao Formation extends from 301 to 679 m (378 m thick). The uppermost Wuku Formation was dated to be far older than 50 ka, implying a large gap of sedimentation before the onset of depositing the overlying Jingmei conglomerates. The oldest dated age for the Wuku Formation is about 200 ka at WK-1 borehole. The Banchiao Formation constitutes the lower half of the WK-1 borehole. Existing thermoluminescence ages imply that the age for the Banchiao Formation is no younger than 150 ka (Table 2) and might be no older than 400 ka (Wei et al. 1998; Teng et al. 2001).

All three boreholes penetrated to the Tertiary basement rocks which are known exposed surrounding the Taipei Basin as the rugged foothills. Basement rocks reached at SCF-1 and 2 are probably the late-Miocene Nanchuang Formation, with weathered top basement rock in SCF-1. Rocks retrieved from WK-1 in 679 to 741 m belong to the early Miocene Taliao Formation, which is thrust over the Nanchuang Formation at 750 - 760 m depth by a shear zone containing fault breccias (Lin 2005). Note the dramatic increase of basement depth between SCF-2 and WK-1 boreholes compared to a relatively mild one between SCF-1 and SCF-2 boreholes (Fig. 2b), implying the location of the main Shanchiao Fault between the SCF-2 and WK-1 and will be discussed later in more detail.

Through lithologic correlation in aid of radiocarbon ages, the Sungshan and Jingmei formations are present across the entire profile, while the Wuku Formation is only found at SCF-2 and WK-1, and the Banchiao Formation is restricted to WK-1. The Sungshan Formation (and units within), the Jingmei Formation, and the Wuku Formation all thicken toward the east, and the stratigraphic horizons

deepen eastward. The sedimentation rate appears to vary both temporally and spatially. We found two major hiatus: one between the deposition of Wuku and Jingmei sediments and the other between the deposition of the Jingmei and Sungshan sediments at SCF-1 and 2. Sediments within the Sungshan and Jingmei formations are quite similar between the boreholes, indicating the sediment source was generally the same and was presumably basin wide, as from the Tahan - Tanshui river system (sediment transporting direction normal to the profile and rather homogeneous). Tributaries drained from the Linkou Tableland to the east didn't seem to assert significant contribution to the deposits since no alluvial-fan conglomerates are found beyond the deposition of the Jingmei gravels in these boreholes suggesting little local sediment transport.

4.2 Stratigraphic Architecture of the Shanchiao Fault Zone

In active extensional settings, such as the Shanchiao fault area, the rate of increase of accommodation space is enhanced on the hanging-wall due to subsidence caused by normal faulting. Hereafter we briefly describe the theory of reconstructing the growth strata across an active normal fault we apply in this study. On a relatively flat depositional surface, sediments deposited within a given time span (growth strata) will be thicker on the hanging wall than those in the footwall if the normal fault is active, and uniform if there's quiescence in tectonic activity. The top of such layers will be even when deposition smooth out the fault scarp (if there is any), mimicking the regional topography. Subsequent layers will continue to form above the newly-formed horizon and repeat the geometric pattern governed by fault activity should there be room for sedimentation. Existing growth strata will be displaced downward at the same time and record all successive deformations. The entire package of syn-tectonic sediments may therefore yield information on fault location and structure, faulting history, and kinematics of fault-related folding (e.g., Sharp et al. 2000).

Based upon the above established stratigraphic correlation, the growth normal faulting scheme within shallow sediments are illuminated. First, architecture of the latest Sungshan Formation is most useful for its completeness and synchronicity of sedimentary facies within the Holocene time. Between the SCF-1 and SCF-2, the units within the Sungshan Formation are indeed down-thrown and thicken eastward, representing effects of normal faulting, as Huang et al. (2007) previously proposed, at the same site of mapped fault-related scarp by Chen et al. (2004). However, these effects on growth strata appear to be much more pronounced between boreholes WK-1 and SCF-2. We thus estimate the accumulation (sedimentation) rates at each drilling hole for the Sungshan Formation, including the C1, C2, and C3 units. By adopting the dated ages and the thickness of the units in

each hole with simple mathematics, we obtain a variation of thickness for each unit across the three holes (Fig. 4). It reveals that the thickness shows an eastward increasing trend for each unit, in particular across the SCF-2 and the WK-1 holes. As a result, the variations indicate the presence of a likely normal fault between SCF-1 and SCF-2 and a more significant vertical offset of normal faulting between SCF-2 and WK-1. We therefore intend to map two fault zones in the shallow sediments of the Wuku profile, with the eastern one as the main fault zone (Fig. 2b).

Because the interface between unconsolidated basin sediments and the Tertiary basement rocks dramatically deepens between boreholes SCF-2 and WK-1 to be at least 34° dip angle (Fig. 2b), we tend to interpret the main fault zone in further depth to follow this interface. The secondary fault zone between SCF-1 and 2 is supported by a shear zone near the bottom of the basin sediments at SCF-2 within the C10 unit, which contains several sheared intervals with striations denoting oblique sinistral-normal faulting and frequent centimeter-scale growth normal faults (Lee et al. 1999). This secondary fault may merge with the main fault zone at where the basement floor abruptly steepened. The secondary fault is therefore regarded as a branch fault, which develops within the basin sediments. We interpret the region between the branch and main fault zones as an 'extensional fault block.' The Wuku formation is much thinner in the extensional fault block than in the actual hanging wall east of the main fault zone, and probably a slim sheet of it remains west of the branch fault but is terminated east of SCF-1. The Banchiao formation is exclusively confined in the hanging wall in greater depth.

Figure 2b shows the proposed fault zone structure in the late-Quaternary basin sediments consisting of a high-angle main fault and a western lower-angle branch fault. Seismic profiling about 1.5 km south of the studied boreholes (Wang and Sun 1999) reveals similar two-fault setting in the Shanchiao Fault zone. Minor sinistral slip component is present on the branch fault according to oblique fault striations documented by Lee et al. (1999), and such fault zone configuration may genetically bear resemblance to a negative flower structure or tulip structure (Woodcock and Schubert 1994) as unveiled in a shallow seismic survey along the fault zone in the northern corner of the Taipei Basin (Shih et al. 2004).

We can not rule out the possibility that the branch fault zone between SCF-1 and 2 may extend down into the basement other than lying entirely within loose sediments. The extensional fault block may include the basement rock, producing staircase-shaped basement floor geometry in imbricate listric normal faulting (e.g., Wernicke and Burchfiel 1982). It is also possible that the area between SCF-1 and WK-1 rests above an extensional fault-propagation fold (e.g., Gawthorpe and Hardy 2002) with the two fault zones as trishear zone boundaries where shearing is concentrated.

These options, though cannot be excluded, are not incorporated in the present study due to lack of evidence, and will not lead to momentous defects in the following presentation.

5. RECONSTRUCTION OF GROWTH FAULTING HISTORY

5.1 Sea Level Fluctuation and Sedimentation in the Taipei Basin

Sedimentary processes in coastal areas and their vicinities are sensitive to base level changes (van Wagoner et al. 1988), so are in the Taipei Basin. Teng et al. (2000) noted two erosion surfaces below lowstand systems tracts in the basin deposits. Sedimentary facies of the basin deposits include estuary and lake, distal to proximal floodplain, braid plain, and alluvial fan facies (Peng et al. 1999; Teng et al. 2000). Given that the present sits at the highstand of the eustatic sea level cycle since around 20 ka of the Last Glacial Maximum (LGM)(Fig. 5), the youngest basin deposits of the Sungshan Formation (10 - 23 ka to present) were accumulated during the recent sea level rise. Before the Jingmei conglomerates deposited at about 25 ka when the Tahan River was captured, the basin (by then covered by the Wuku Formation) was in a stage of erosion with deeply-incised valleys (Teng et al. 2000, 2004a) during the period of LGM. The restored geometry of the top of the Wuku formation represents the paleogeography of the Taipei Basin in LGM. Subsequent stacking of Jingmei and Sungshan deposits, belonging to the most recent sequence, can be discerned by linking rates and facies of sedimentation to accommodation provided by base level rise and tectonic subsidence.

Under the basin-wide deposition scheme described above, the geological history of the sediments in association with the activity of the Shanchiao Fault since the LGM can be illuminated through sedimentary records recovered from the investigated boreholes. A series of retro-deformed cross-sections can therefore be established since LGM of about 25 ka. In the following two sections, we first present the criteria for generating the restored cross-sections by a back-stripping method and the resultant profiles, and then illustrate the geological evolution of the Shanchiao Fault zone starting from 25 ka through semi-quantitative sections under the same scheme. Compaction of loose sediments is negligible because of the young ages and shallow depths of the units (Chen et al. 2007; Taylor et al. 2008).

5.2 Restoration by a Simple Back-Stripping Method

As mentioned above, the basin-wide sedimentation process in late Quaternary was governed by sea level fluctuations along with changes of drainage system, so did the accumulation of Sungshan and Jingmei Formations in the Wuku Profile since local influences other than tectonics

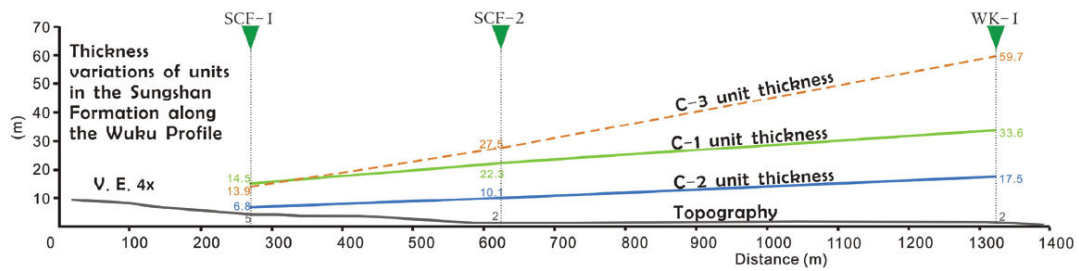


Fig. 4. Thickness variations of units in the Sungshan Formation along the Wuku Profile. Three units all show an increase of thickness toward the east, strongly suggesting growth faulting in-between the drilling holes. By comparing the present topography, the thickness variations clearly exceed differences of local topography and therefore advocate syn-sedimentation normal faulting.

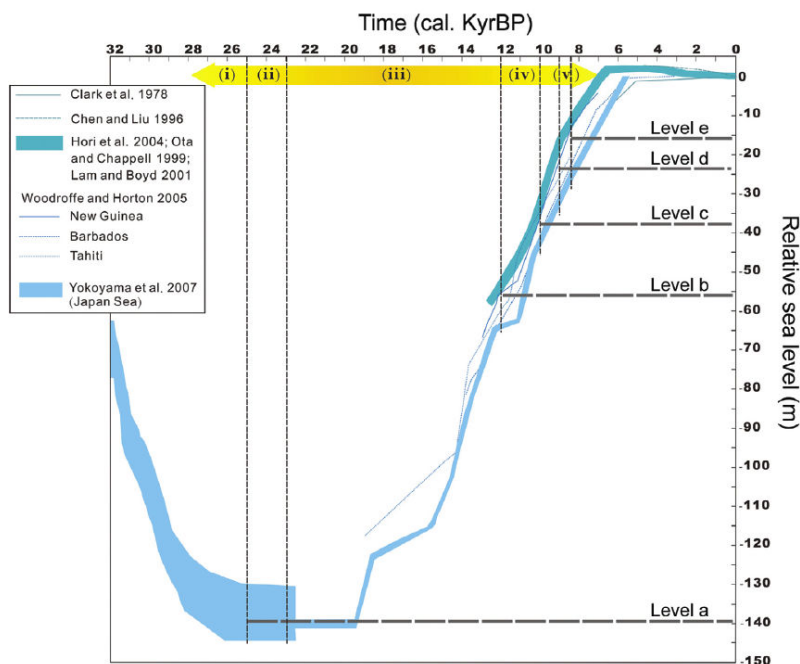


Fig. 5. Eustatic sea level changes since 30 ka. Levels are compiled from Clark et al. 1978; Chen and Liu 1996; Ota and Chappell 1999; Lam and Boyd 2001; Hori et al. 2004; Woodroffe and Horton 2005; and Yokoyama et al. 2007. In addition to the present-day sea level, five paleo-levels (Level a - e) were selected as the sea levels corresponding to specific ages with significant geological processes. See details in the text.

are not observed in sediment records. When the sea level reached similar elevation to that of the Taipei Basin plain (resembling the present configuration) since the recent major marine incursion in the basin at 10 - 9 ka (Teng et al. 2000), sediments piled up across the entire profile, including the footwall, hanging wall and extensional fault block areas. Given the high rate of erosion and hence rapid sediment accumulation of the Taiwan Island in the present day (Dadson et al. 2003), the room of sedimentation created by

rising eustacy is considered to be filled up contemporaneously, therefore producing flat topography similar to the modern one.

Under this assumption, the topography at beginning of the deposition for the C1 unit of the Sungshan Formation would be approximately flat. Because the C1 unit of SCF-1 lies in the footwall area, hence it would not involve significant vertical motion of the faulting. Referring to the growth normal faulting scheme, the bases of C1 units in the hang-

ing wall side would be expected to be consequently downward displaced by dip-slips of the Shanchiao Fault which provided additional sedimentation rooms resulting in lateral thickening of the units. The elevation differences between the base of C1 unit at SCF-2 and SCF-1 (7.8 m), and SCF-2 and WK-1 (11.3 m) thus are interpreted to represent cumulative vertical displacements on the branch and main faults, respectively, from 8.4 ka till present (Fig. 6a). Furthermore, we can observe that the height of sea level e (around -16 m) at the onset of the C1 (~ 8.4 ka) is close to the depth of the base of the C1 unit (-14.5 m) in the footwall area (SCF-1).
 Back to 8.4 ka, because that the top of the basin depos-

its (C2 unit) in the footwall appears to be near the sea level (level e), therefore the height of the top of the estuarine deposits of the C2 unit across the profile would be considered to be very much flat. Under this assumption, the fault zone stratigraphic configuration by then can be approximated by removing the C1 unit above and re-leveling the C2 unit tops in WK-1 (hanging-wall region) and SCF-2 (extension fault block) to the one at SCF-1 (footwall region) as restoration by 'back-stripping' (Fig. 6b). We calculate the remaining vertical differences of the depths of C2 unit between three holes as mentioned above. We then obtain 3.3 and 7.4 m, which hence denote to be cumulative vertical offsets on the

Evolution model for the Shanchiao Fault zone along Wuku profile since 23000 yrBP (Assuming negligible sediment compaction)

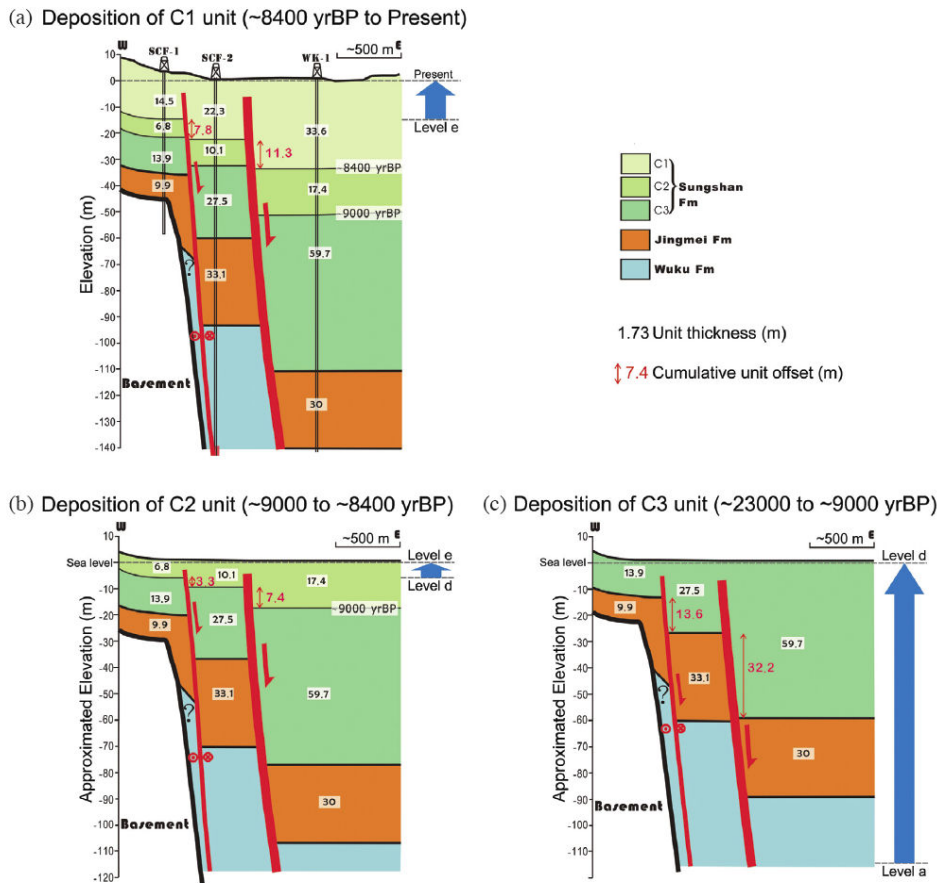


Fig. 6. Back-stripping method and reconstruction of cumulative deformation on the Shanchiao Fault since the LGM of about 23 ka. Three periods of 8.4 ka - present (a), 9 - 8.4 ka (b), and 23 - 9 ka (c), which correspond to depositional ages of Units C1, C2, and C3, respectively, are adopted for explaining the evolution of the growth faulting of the Shanchiao Fault. Numbers in black color: thickness of stratigraphic units. Numbers in red: vertical differences of thickness for each stratigraphic unit between drilling holes. Levels a to e are paleo-sea levels through time, which are denoted in Fig. 5.

branch and main faults respectively during the 9 to 8.4 ka period (Fig. 6b). These relatively large amounts of vertical offset in a short time span of 600 years appear to be consistent with two possible earthquake events occurred during this period inferred by previous study (Huang et al. 2007). We will discuss it in more detail in the later section.

The above approach became much difficult to apply to deeper sediments of the Sungshan Formation because the 10 ka datum is obscure at SCF-2 and WK-1, and synchronicity of sedimentation along the Wuku profile was absent during 23 to 10 ka. However, the Jingmei Formation alluvial fan deposits of 25 - 23 ka resulted in a relatively flat topography at the end of the river-capture event. Provided the comparable thicknesses of the Jingmei conglomerates (C4 unit) at SCF-2 and WK-1, the ancient topography of the Wuku profile is considered to be roughly even at around 23 ka, therefore permitting the 'back-stripping' of C3 unit and evaluation of fault vertical displacements during the deposition of the C3 unit. Under this assumption, we then obtain that the Shanchiao branch fault slipped 13.6 m vertically and the main fault 32.2 m during ~23 ka to 9 ka according to constraints from top horizons of the C3 unit and the Jingmei Formation (Fig. 6c).

Details of sediment accumulation and fault throws between ~23 to 9 ka cannot be accurately resolved, while the stacking pattern of the deposits does show westward onlapping of layers which is closely tied to tectonic modification on local geomorphology and base level changes controlled by eustasy. Regional sedimentation rate (modulated by tectonic movements) was zero at the LGM as the sea level (level a) was low at about -140 m compared to the present day level. Since LGM the sedimentation rate is expected to be rapidly increasing in pace with the rising sea level, and again dropped to trivial numbers when eustasy stabilized to elevations similar to that of today at ~6 ka (Fig. 5).

In summary, the total vertical offset across the Shanchiao fault zones since 23 ka can be yielded by summing the above results during different periods, as shown in Fig. 6. We thus obtain a total vertical offset of 75.6 m, with 24.7 and 50.9 m for the branch fault and the main fault, respectively, since the LGM of 23 ka. It can translate to an average vertical fault slip rate of 3.3 mm yr⁻¹ across the Shanchiao fault zone in Wuku profile, with 1.1 mm yr⁻¹ for the branch fault and 2.2 mm yr⁻¹ for the main fault, since 23 ka.

5.3 Evolution of Sedimentation vs. Growth Faulting

Combining information on stratigraphic architecture and knowledge on sea level changes since the LGM, the fault zone evolution is depicted in six scenes shown in Fig. 7.

(1) Shortly before 25 ka (Fig. 7a)

Global and East Asian eustatic sea level plunged to more than 100 m below the present level since 30 ka, as the

LGM began (Yokoyama et al. 2007). The sea level around Taiwan stabilized at approximately -140 m (level a) from about 28 ka compared to the present day. The 25-ka paleotopography as top of the Wuku formation can be estimated by adding the present day -140.8 m deep with 75.6 m of total vertical subsidence due to faulting with our back-stripping method, as described above. We obtain a depth roughly at -65 m for the top of Wuku formation along the Wuku profile (Fig. 7a). It means that the Wuku formation was about 75 m high above the sea level at that time. As a result, sediments of the Wuku formation were subject to strong erosion by drainage system in the Taipei basin.

The relatively high local topography 75 m above sea level indicates that no major channels, neither the Tanshui River nor the creeks originated from the Linkou Tableland in the west, existed in the investigated profile, which would form gorge-like incised valleys. The shallow basement at SCF-1 was exposed without cover of late-Quaternary deposits and thus was subject to be weathered (Fig. 7a). Surface scarps resulted from slips on the Shanchiao Fault were likely to be rapidly erased or retreated westward on topography by intense erosion, obscuring attempts to estimate fault activity during this period.

(2) 25 to 23 ka (Fig. 7b)

The Jingmei sediments were interpreted to be quickly deposited when the Tahan River was captured into the Taipei Basin during 25 - 23 ka (Teng et al. 2004a). These alluvial fan conglomerates accumulated within a time span of 2000 year and attained ~30 m thick in the Wuku region. The top of the Jingmei conglomerates should be rather flat by the time deposition ceased in the Wuku Profile because sediment transport was normal to the profile towards the north and no major channels were present. The gravel bed of the Jingmei Formation is 10 m thick onlapping onto the weathered Mio-Pliocene basement at SCF-1, implying an ancient topographic scarp located between SCF-1 and SCF-2. However, we interpret that the Shanchiao Fault was inactive during this 2000-year-long period because the Jingmei Formation is of uniform thicknesses (i.e., 30 - 33 m) across the main fault between SCF-2 and WK-1.

On the other hand, during 25 to 23 ka, the sea level did not change significantly and remained about -140 m compared to the present level. So that the top of the Jingmei formation lies about -35 m compared to the present, that is, about 105 m high above the sea level.

(3) 23 to ~12 ka (Fig. 7c)

We anticipate that the Taipei basin started to subside along the Shanchiao Fault after completion of the Jingmei conglomerate with probably both the hanging-wall block and the extensional fault block displaced downward. However, braid plain to floodplain sediments of 23-12 ka (lower part of C3 Unit of the Sungshan Formation) exist only at

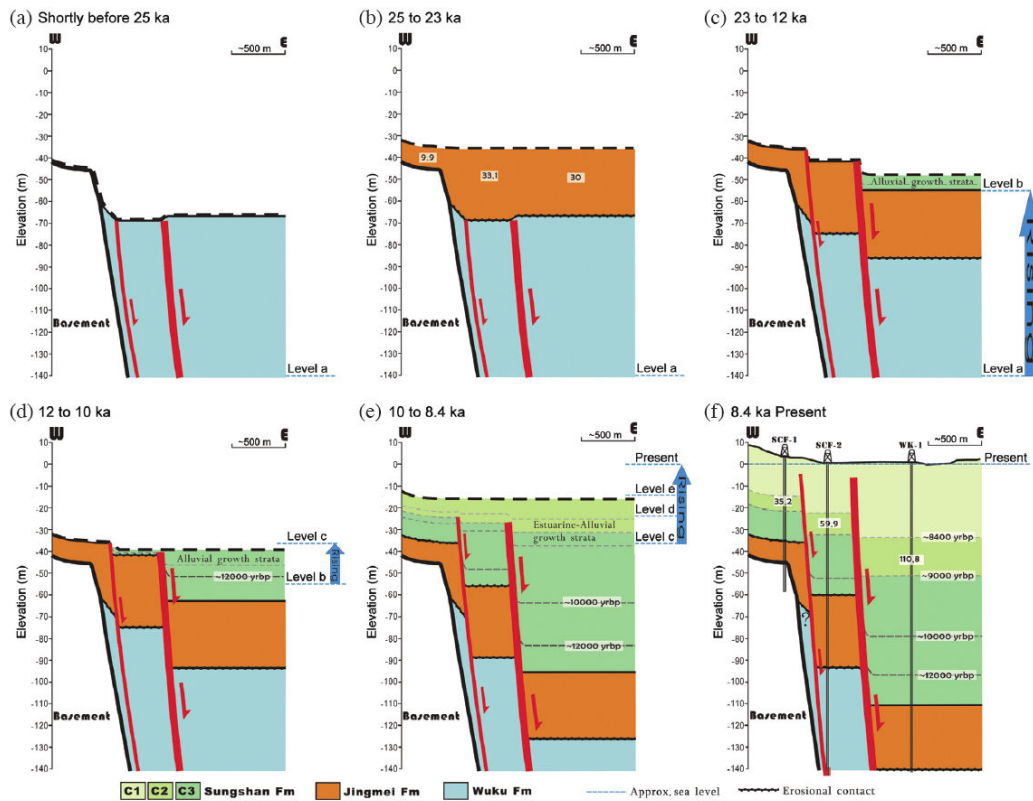


Fig. 7. Interpreted sedimentation and growth faulting and post-LGM development history of the Shanchiao Fault zone in the Wuku profile. Several geological events with confident age control were adopted to divide the period into six stages: (a) shortly before the deposition of the Jingmei formation (25 ka), (b) deposition of the Jingmei conglomerates (25 - 23 ka), (c) shortly before the sea level rising to reach the basin ground level (23 - 12 ka), (d) the sea level beginning to surpass the basin ground level (12 - 10 ka), (e) basin-wide sedimentation containing a 600-year time span with possible earthquake events coupled with rapid sedimentation (9 - 8.4 ka), and (f) the latest stage of the sedimentation and growth faulting with gradual sea level rise and stabilized (8.4 - 0 ka). Levels a to e are denoted in Fig. 5.

WK-1. It implies that during this 10000-year-long period the hanging wall had subsided enough to accumulate braid plain and flood plain fluvial growth sediments of while the Jingmei gravel would be exposed in the footwall and the extensional fault block region. In the meantime, sea level rose rapidly from -140 m (level a) to -55 m (level b) from ~18 to 12 ka (Fig. 5) during this period. So the elevation of the basin floor decreased drastically from 105 to 10 - 20 m high above the sea level from 23 to 12 ka.

(4) ~12 to 10 ka (Fig. 7d)

The situation over the next 2000 years in 12 - 10 ka was similar to the previous period as the sea level rose rapidly, except that the growth strata of fluvial deposits (middle part of Unit C3 of the Sungshan Formation) started to lap on

to the area of the extensional fault block between the main and branch faults. This suggests that the subsidence in the extensional fault block region allowed fluvial sediments to accumulate. Sea level rose from -55 m (level b) to about -37 m (level c) during this period, while it still kept slightly lower than the basin ground.

(5) 10 to 8.4 ka (Fig. 7e)

The beginning of this period marked the onset of major marine incursions in the basin (Teng et al. 2000) as the sea level gradually rose from -37 m (level c) to -16 m (level e) from 10 to 8.4 ka. Sediments began to pile up across the entire section, and the accommodation space was filled contemporaneously with the rising sea level. Since then the regional topography should be very similar to the flat one

today, with less than 5 meters of difference in elevation between the borehole sites. The top horizons of C3 and C2 units, the estuarine deposits during that time, are therefore assumed to be similar in elevation along the Wuku profile in the three boreholes at around 9 and 8.4 ka, respectively. Accordingly, while the sea level continued to rise from level d to level e from 9 to 8.4 ka (Fig. 7e), we estimate that an extraordinarily rapid sedimentation of Unit C2 with 6.8, 10.1, and 17.4 m thickness at SCF-1, SCF-2, and WK-1, respectively. In the meantime, the Shanchiao Fault slipped vertically 3.3 m on the branch fault and 7.4 m on the main fault during the 600-year interval when C2 rapidly deposited in a relative deep, lower estuarine environment.

(6) 8.4 ka to present (Fig. 7f)

From 8.4 ka till present, as the sea level continued to rise from level e (-16 m) to present level and coupled with tectonic fault movement, the estuarine deposits of the C1 unit piled up and completed the uppermost sediments of the Taipei basin in the Wuku profile. The extensional fault block has been observed to subside (relative to the footwall) 7.8 meters and additional 11.3 meters for the hanging wall of the main fault.

6. DISCUSSION

6.1 Tectonic Loading Rates and Earthquake Events

Given that the rate of sediment supply and the rate of increasing accommodation space from rising sea level and tectonic subsidence are at balance, the sedimentation rate provides a direct way to estimate the effects of these components through time. When this is the case, sedimentation rate of growth strata across the fault offers explicit evaluation of both regional deposition rate and additional contribution from tectonic subsidence, with that obtained on the footwall containing only the former one.

Sedimentation rate investigation as described above is conducted on the C1 and C2 units of the Sungshan forma-

tion in the Wuku Profile, that is from 9 ka to present. The reason why constraining to the Holocene time is mainly because of the synchronicity of deposition and quality of age controls. We obtain the Holocene sedimentation rates (dividing the unit thickness by the time span of deposition) for three blocks: (a) derived from units on the footwall at SCF-1 block stand for the regional deposition rate, while (b) derived on the extensional fault block at SCF-2 and (c) the hanging wall block at WK-1 include excess rates representing tectonic subsidence. The estimations are presented in Table 4 and Fig. 8a. The yielded sedimentation rates are 1.7, 2.7, and 4.0 mm yr⁻¹ for footwall, extensional fault block, and hanging wall, respectively, during 8.4 ka - present (C1 unit). However, we obtain a much higher sedimentation rate of 11.3, 16.8, and 29.2 mm yr⁻¹ for footwall, extensional fault block, and hanging wall, respectively, during 9 - 8.4 ka (C2 unit). Note that difference in compaction rate of these Holocene units between the boreholes (i.e., different parts across the fault) would be well lower than 1 mm yr⁻¹ (Meckel et al. 2006) and is thus ignored in the evaluation. By incorporating sea level rise, we obtain rate excess which we interpreted as tectonic subsidence rate (Table 4; Fig. 8a): 0.9 and 2.3 mm yr⁻¹ for branch fault and main fault, respectively during 8.4 ka - present (C1 unit) and 5.5 and 17.8 mm yr⁻¹ for branch fault and main fault, respectively during 9 - 8.4 ka (C2 unit).

Base on the above results, the period of 9 - 8.4 ka when C2 was laid is characterized by both rapid base level rise and high tectonic subsidence rate. Two paleo-earthquake events documented on the branch fault zone by Huang et al. (2007) coinciding the start and end of C2 deposition may lead to the much enhanced sedimentation rate and tectonic rate calculated. The total vertical tectonic subsidence of 3.3 and 7.4 m for branch and main fault during this period of 9 - 8.4 ka would mainly be subject to these two possible earthquake events. The rates derived from the C1 unit, embodying averages for a longer time period of 8.4 - 0 ka, are considered to better represent the Holocene and late Quaternary

Table 4. Sedimentation rate and inferred tectonic subsidence rate of the Shanchiao Fault zone in the Wuku Profile since ~9 ka (assuming negligible differences in compaction rates).

		Footwall (SCF-1)	Extensional fault block (SCF-1)	Hanging wall (WK-1)
C1 (~8.4 ka - present)	Thickness (m)	14.5	22.3	33.6
	Sedimentation rate (mm yr ⁻¹)	1.7	2.7	4
	Tectonic subsidence rate (mm yr ⁻¹)	-	0.9	2.3
C2 (~9 - ~8.4 ka)	Thickness (m)	6.8	10.1	17.5
	Sedimentation rate (mm yr ⁻¹)	11.3	16.8	29.2
	Tectonic subsidence rate (mm yr ⁻¹)	-	5.5	17.8

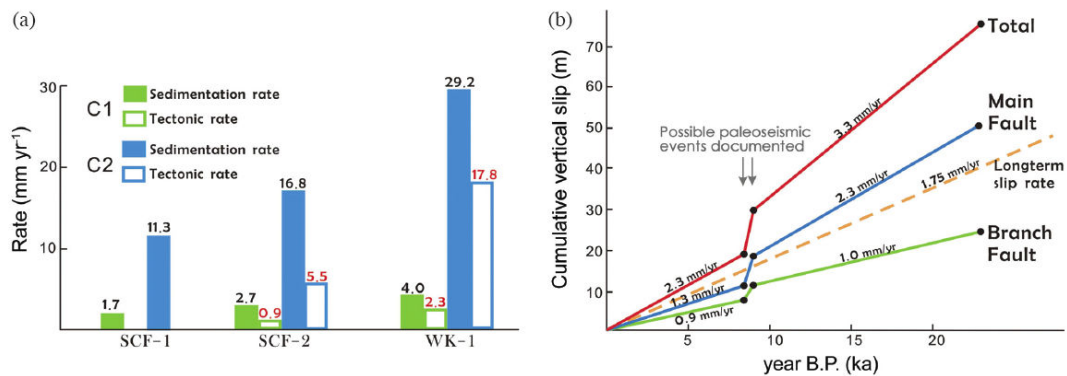


Fig. 8. (a) Sedimentation rate and tectonic subsidence rate of the C1 and C2 units at the Wuku boreholes. (b) Accumulative vertical slips for the Shanchiao fault since the LGM documented in the Wuku Profile.

long-term tectonic subsidence rate of the Shanchiao Fault which is 2.3 mm yr^{-1} on the hanging wall and 0.9 mm yr^{-1} on the extensional fault block, with a regional sedimentation rate of 1.73 mm yr^{-1} , and yield a rather high growth index (defined as fault throw rate divided by footwall sedimentation rate; Childs et al. 2003) of 1.3.

Tectonic subsidence rates of the Shanchiao Fault since 23 ka can also be inferred from vertical offsets of the horizons (Fig. 8b). Differences to the top depths of the Jingmei Formation (Unit C4) encompass the total vertical offsets of the Shanchiao Fault system since 23 ka, indicating the average vertical slip rates of 3.3 mm yr^{-1} with 1.1 mm yr^{-1} on the branch fault and 2.2 mm yr^{-1} on the main fault since the LGM. We also obtain about 1.0 and 2.3 mm yr^{-1} of averaged vertical slip rates on the branch and main faults, respectively, during 23 - 9 ka. The faulting rates obtained from various time periods and criteria are quite consistent with the exception of those from C2 unit. We can also conclude that the hanging wall down-throw rates were higher than the regional sedimentation rates since at least 9 ka.

Comparing to the long-term tectonic subsidence rate of the Shanchiao Fault, which was estimated to be 1.75 mm yr^{-1} since 0.4 Ma (Chen et al. 2007), the results of short-term rate of 3.3 mm yr^{-1} since 23 ka appears to be significantly higher (Fig. 8b). Although it is possible that the Shanchiao Fault has been more rigorous during the last tens of thousands of years, however, without study to complete the gap between 0.4 Ma and 23 ka, it is too early to draw a conclusion right now.

6.2 Correlation between Surface Topography and Sub-surface Geology

Previous study of topographic mapping aiming at characterizing Shanchiao Fault zone geomorphology has identified a series of fault-related scarps arranged in an en-

echelon array (Chen et al. 2006), which are present along the western edge of the Taipei Basin (Fig. 2a). The locations of fault-related scarps are generally in good agreement with existing borehole analyses which placed the surface trace of the Shanchiao Fault between borehole pairs including SCF-1 and 2, SCF-5 and 6, SCF-3 and 4 (Fig. 2a; Lin 2001; Huang et al. 2007). In the Wuku Profile, however, these traces and geomorphic features actually correspond to the branch fault zone; the main fault zone of the Shanchiao Fault may reach land surface east of SCF-2 where ground elevation is close to zero. We speculate that any topographic depressions caused by activities on the main fault zone would be readily erased since such troughs below the sea level tend to be rapidly filled by sediments given frequent typhoons and floods of Taiwan. This demonstrates that young faults without clear geomorphic evidence do not preclude the possibility of their recent activities, and hence the potential seismic threats.

Figure 9 shows a 3-D block diagram summarizing structural and geomorphic characteristics of the Shanchiao Fault zone. Structures of faulted and tilted strata within the basement rocks mainly reflect deformation features occurred in the mountain-building stage in the Taipei region consisting of thrust sheets, as the Hsinchuang Fault and the one seen in WK-1. The Hsinchuang Fault, by then the mountain frontal thrust some 2 Ma, only broke in the lower part of the Linkou Formation, and the basement rocks are buried within the fan-delta Linkou conglomerates (Teng et al. 2001). The uplift of the Linkou Tableland on the footwall block may be closely associated with the development of the normal faulting of the Shanchiao fault. The eastern border of the tableland, consisting of steep cliffs bearing some triangular facets and generally two threads of terraces (Chen et al. 2006), is composed of colluvial deposits with local outcrops of basement rocks (Teng et al. 2001). Geomorphic scarps bordering these terraces of uncertain origin might be related to past earthquake events as retreated fault scarps enhanced

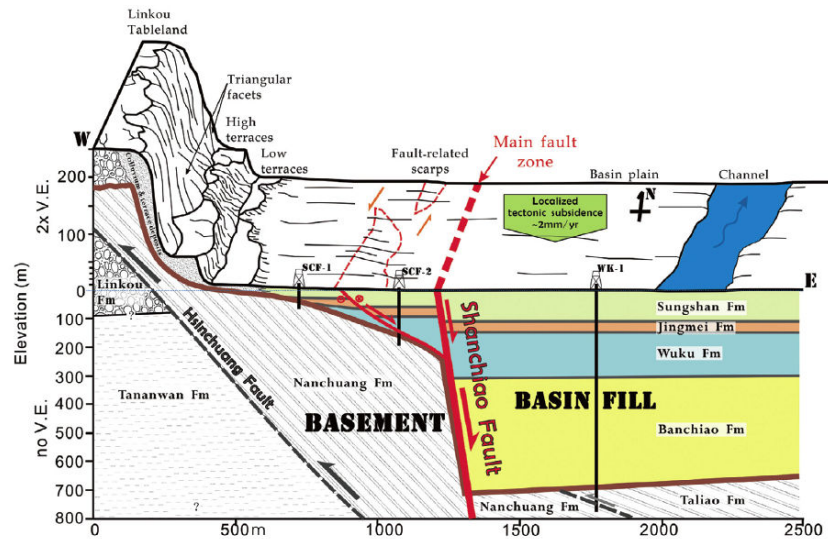


Fig. 9. Schematic 3-D diagram of the fault zone in the Wuku area, central portion of the Shanchiao Fault, displaying regional subsurface geology and its relation to surface topographic features.

by fluvial processes. The only in situ fault-related scarps are associated with the branch fault, and exhibit right-stepping segmentation which denotes sinistral transcurrent tectonic environment, in line with the fault striation recovered in the drilling hole (SCF-2; Lee et al. 1999) and with the regional GPS measurements (Rau et al. 2008).

7. CONCLUDING REMARKS

The Shanchiao Fault zone is interpreted to be composed of a main fault zone and a westerly shallower branch fault zone, with an extensional fault block in between. Left-lateral transcurrent motion in addition to normal faulting is present at least on the branch fault. The Shanchiao Fault has been highly active by almost incessant faulting since the Last Glacial Maximum of 23 ka. By comparing stratigraphy and its age, we are able to correlate stratigraphic units in a great detail across the three drilling holes along the Wuku profile. Under the assumption that the rapid rise of the sea level since the LGM would provide immense sediments to keep the topography flat in Taipei basin, we reconstructed the history of growth strata, which shows sedimentation significantly reflecting a combination effect of sea level rise and tectonic subsidence across the Shanchiao Fault since 23 ka. Furthermore, we calculated averaged vertical throw rates of about 2.2 and 1.1 mm yr⁻¹ on the main and branch faults, respectively. The branch fault, corresponding to the major fault designated in previous documentations, made up about a third of total vertical displacement on the

entire Shanchiao Fault zone since around 23 ka. Holocene tectonic subsidence rate of the fault appears to be similar and is constrained to be 2.3 mm yr⁻¹ in the near-fault part of the hanging wall block, and 0.9 mm yr⁻¹ in the extensional fault block area during 8.4 - 0 ka. However, an episode with possible two earthquake events revealed substantial tectonic subsidence of 7.4 and 3.3 m in the main fault and the branch fault, respectively, during a 600-yr time span of 9 - 8.4 ka. Presently, only the branch fault has geomorphic expressions; any topographic depressions caused by faulting on the main fault seem to be quickly filled. This has important implication for neotectonic investigations that faults of suspected status may still be active even though no clear direct geomorphic evidence can be found.

Acknowledgements This study was supported by the National Science Council of Taiwan (grant NSC 98-2116-M-001-011), Academia Sinica, and National Taiwan University. Special thanks to Louis S. Teng for very stimulating and knowledgeable discussions and comments. We are grateful to Yue-Gau Chen and Jyr-Ching Hu for their valuable comments and supports. Constructive reviews by Hao-Tsu Chu and Andrew T. Lin, which improved greatly the manuscript, are deeply appreciated. This is a contribution of the Institute of Earth Sciences, Academia Sinica, IESAS 1397.

REFERENCES

Angelier, J., E. Barrier, and H. T. Chu, 1986: Plate collision

- and paleostress trajectories in a fold-thrust belt: The foothills of Taiwan. *Tectonophysics*, **125**, 161-178, doi: 10.1016/0040-1951(86)90012-0. [[Link](#)]
- Brown, L. F., R. G. Loucks, R. H. Treviño, and U. Hammes, 2004: Understanding growth-faulted, intraslope sub-basins by applying sequence-stratigraphic principles: Examples from the south Texas Oligocene Frio Formation. *AAPG Bull.*, **88**, 1501-1523, doi: 10.1306/07010404023. [[Link](#)]
- Bull, J. M., P. M. Barnes, G. Lamarche, D. J. Sanderson, P. A. Cowie, S. K. Taylor, and J. K. Dix, 2006: High-resolution record of displacement accumulation on an active normal fault: Implications for models of slip accumulation during repeated earthquakes. *J. Struct. Geol.*, **28**, 1146-1166, doi: 10.1016/j.jsg.2006.03.006. [[Link](#)]
- Caputo, R., B. Helly, S. Pavlides, and G. Papadopoulos, 2004: Palaeoseismological investigation of the Tyrnavos Fault (Thessaly, Central Greece). *Tectonophysics*, **394**, 1-20, doi: 10.1016/j.tecto.2004.07.047. [[Link](#)]
- Chang, H. C., C. W. Lin, M. M. Chen, and S. T. Lu, 1998: An introduction to the active Faults of Taiwan, explanatory text of the active fault map of Taiwan. *Spec. Publ. Cent. Geol. Surv.*, **10**, 103 pp. (in Chinese)
- Chen, C. T., K. H. Lin, Y. W. Jen, J. C. Lee, and Y. C. Chan, 2004 : Geomorphic studies of the Shanchiao Fault in the Taipei Basin, Xth Symposium on Quaternary of Taiwan, Taipei, Taiwan, 151-154.
- Chen, C. T., J. C. Lee, J. C. Hu, Y. C. Chan, and C. Y. Lu, 2006: The active Shanchiao Fault in the Metropolitan Taipei area, Northern Taiwan: Geomorphic and geodetic analyses. *Eos, Trans., AGU*, **87-52**, Fall Meeting Supplement, Abstract T33D-0543.
- Chen, C. T., J. C. Hu, C. Y. Lu, J. C. Lee, and Y. C. Chan, 2007: Thirty-year land elevation change from subsidence to uplift following the termination of groundwater pumping and its geological implications in the Metropolitan Taipei Basin, Northern Taiwan. *Eng. Geol.*, **95**, 30-47, doi: 10.1016/j.enggeo.2007.09.001. [[Link](#)]
- Chen, W. F. and L. S. Teng, 1990: Depositional environment of Quaternary deposits of the Linkou Tableland, north-western Taiwan. *Proc. Geol. Soc. China*, **33**, 39-63.
- Chen, Y. G. and T. K. Liu, 1996: Sea level changes in the last several thousand years, Penghu Islands, Taiwan Strait. *Quat. Res.*, **45**, 254-262, doi: 10.1006/qres.1996.0026. [[Link](#)]
- Childs, C., A. Nicol, J. J. Walsh, and J. Watterson, 2003: The growth and propagation of synsedimentary faults. *J. Struct. Geol.*, **25**, 633-648, doi: 10.1016/S0191-8141(02)00054-8. [[Link](#)]
- Chiu, H. T., 1968: The Hsinchuang Fault in the Taoyuan area, northern Taiwan. *Proc. Geol. Soc. China*, **11**, 60-73.
- Clark, J. A., W. E. Farrelle, and W. R. Peltier, 1978: Global changes in postglacial sea level: A numerical calculation. *Quat. Res.*, **9**, 265-287, doi: 10.1016/0033-5894(78)90033-9. [[Link](#)]
- Dadson, S. J., N. Hovius, H. Chen, W. B. Dade, M. L. Hsieh, S. D. Willett, J. C. Hu, M. J. Horng, M. C. Chen, C. P. Stark, D. Lague, and J. C. Lin, 2003: Links between erosion, runoff variability and seismicity in the Taiwan orogen. *Nature*, **426**, 648-651, doi: 10.1038/nature02150. [[Link](#)]
- Fairbanks, R. G., R. A. Mortlock, T. C. Chiu, L. Cao, A. Kaplan, T. P. Guilderson, T. W. Fairbanks, A. L. Bloom, P. M. Grootes, and M.-J. Nadeau, 2005: Radiocarbon calibration curve spanning 0 to 50000 years B.P. based on paired ²³⁰Th/²³⁴U/²³⁸U and ¹⁴C dates on pristine corals. *Quat. Sci. Rev.*, **24**, 1781-1796, doi: 10.1016/j.quascirev.2005.04.007. [[Link](#)]
- Gawthorpe, R. and S. Hardy, 2002: Extensional fault-propagation folding and base-level change as controls on growth-strata geometries. *Sediment. Geol.*, **146**, 47-56, doi: 10.1016/S0037-0738(01)00165-8. [[Link](#)]
- Ho, C. S., 1986: A synthesis of the geologic evolution of Taiwan. *Tectonophysics*, **125**, 1-16, doi: 10.1016/0040-1951(86)90004-1. [[Link](#)]
- Hori, K., S. Tanabe, Y. Saito, S. Haruyama, V. Nguyen, and A. Kitamura, 2004: Delta initiation and Holocene sea-level change: Example from the Song Hong (Red River) delta, Vietnam. *Sediment. Geol.*, **164**, 237-249, doi: 10.1016/j.sedgeo.2003.10.008. [[Link](#)]
- Hsieh, C. H., Y. F. Chang, and R. H. Sun, 1992: Seismic investigation of the Hsin-Chuan fault on the west of Taipei Basin. *Ti-Chih*, **12**, 13-26. (in Chinese)
- Huang, S. Y., 2003: Prehistoric earthquakes along the Shanchiao Fault, Taipei Basin, Northern Taiwan. Master Thesis, Central Washington University, Washington, USA, 83 pp.
- Huang, S. Y., C. M. Rubin, Y. G. Chen, and H. C. Liu, 2007: Prehistoric earthquakes along the Shanchiao fault, Taipei Basin, northern Taiwan. *J. Asian Earth Sci.*, **31**, 265-276, doi: 10.1016/j.jseaes.2006.07.025. [[Link](#)]
- Hubert-Ferrari, A., J. Suppe, R. Gonzalez-Mieres, and X. Wang, 2007: Mechanisms of active folding of the landscape (southern Tian Shan, China). *J. Geophys. Res.*, **112**, B03S09, doi: 10.1029/2006JB004362. [[Link](#)]
- Kao, H., S. S. J. Shen, and K. F. Ma, 1998: Transition from oblique subduction to collision: Earthquakes in the southernmost Ryukyu arc-Taiwan region. *J. Geophys. Res.*, **103**, 7211-7229, doi: 10.1029/97JB03510. [[Link](#)]
- Lam, D. D. and W. E. Boyd, 2001: Some facts of sea-level fluctuation during the late Pleistocene-Holocene in Ha Long Bay and Ninh Binh area. *J. Sci. Earth*, **23**, 86-91.
- Lee C. T. and Y. Wang, 1988: Quaternary stress changes in northern Taiwan and their tectonic implication, *Proc. Geol. Soc. China*, **31**, 154-168.

- Lee, J. C., 1989: Neotectonics of northern Taiwan based on the faults and paleostress analyses. Master Thesis, National Taiwan University, Taipei, Taiwan, ROC, 128 pp. (in Chinese)
- Lee, J. F., C. Z. Lin, D. C. Lai, T. W. Su, Z. L. Chiu, and C. J. Zeng, 1999: The study on the formation of Taipei Basin. *Spec. Publ. Cent. Geol. Surv.*, **11**, 207-226. (in Chinese)
- Lin, C. C., 1957: Geomorphology of Taiwan. Taiwan Province Literature Communication, Taipei, 424 pp. (in Chinese)
- Lin, C. W., H. C. Chang, S. T. Lu, T. S. Shih, and W. J. Huang, 2000: An Introduction to the Active Faults of Taiwan, 2nd Ed., Explanatory Text of the Active Fault Map of Taiwan. *Spec. Publ. Cent. Geol. Surv.*, **13**, 122 pp. (in Chinese)
- Lin, C. Z., 2001: Geologic environment of the Taipei metropolis. Symposium on Geological Hazards in the Taipei Metropolis, 1-19. (in Chinese)
- Lin, C. Z., 2005: Shanchiao Fault and the geological structures along the western margin of the Taipei Basin. Symposium on Volcanic Activities and the Shanchiao Fault in the Taipei Metropolis, 191-198. (in Chinese)
- Lin, C. Z., T. C. Lai, L. Y. Fei, H. C. Liu, C. C. Chi, and T. W. Su, 1999: Results of deep borehole investigations in the Taipei Basin between 1992 to 1996. *Spec. Publ. Cent. Geol. Surv.*, **11**, 7-39. (in Chinese)
- Lin, K. C., J. C. Hu, K. E. Ching, J. Angelier, R. J. Rau, S. B. Yu, C. H. Tsai, T. C. Shin, and M. H. Huang, 2010: GPS crustal deformation, strain rate, and seismic activity after the 1999 Chi-Chi earthquake in Taiwan. *J. Geophys. Res.*, doi: 10.1029/2009JB006417, in press.
- Lu, C. Y., J. Angelier, H. T. Chu, and J. C. Lee, 1995: Contractional, transcurrent, rotational and extensional tectonics: Examples from Northern Taiwan. *Tectonophysics*, **246**, 129-146, doi: 10.1016/0040-1951(94)00252-5. [[Link](#)]
- Machette, M. N., S. F. Personius, A. R. Nelson, D. P. Schwartz, and W. R. Lund, 1991: The Wasatch fault zone, Utah - Segmentation and history of Holocene earthquakes. In: Hancock, P. L., R. S. Yeats, and D. J. Sanderson (Eds.), Characteristics of Active Faults. *J. Struct. Geol.*, **13**, 137-149, doi: 10.1016/0191-8141(91)90062-N. [[Link](#)]
- McCalpin, J. P. and S. P. Nishenko, 1996: Holocene paleoseismicity, temporal clustering, and probabilities of future large ($M > 7$) earthquakes on the Wasatch fault zone, Utah. *J. Geophys. Res.*, **101**, 6233-6253, doi: 10.1029/95JB02851. [[Link](#)]
- Meckel, T. A., U. S. ten Brink, and S. J. Williams, 2006: Current subsidence rates due to compaction of Holocene sediments in southern Louisiana. *Geophys. Res. Lett.*, **33**, L11403, doi: 10.1029/2006GL026300. [[Link](#)]
- Meghraoui, M., B. Delouis, M. Ferry, D. Giardini, P. Huggenberger, I. Spotke, and M. Granet, 2001: Active normal faulting in the upper Rhine Graben and paleoseismic identification of the 1356 Basel earthquake. *Science*, **293**, 2070-2073, doi: 10.1126/science.1010618. [[Link](#)]
- Ota, Y. and J. Chappell, 1999: Holocene sea-level rise and coral reef growth on a tectonically rising coast, Huon Peninsula, Papua New Guinea. *Quat. Int.*, **55**, 51-59, doi: 10.1016/S1040-6182(98)00024-X. [[Link](#)]
- Peng, C. H., L. S. Teng, and P. B. Yuan, 1999: Facies characteristics of Taipei Basin deposits. *Spec. Publ. Cent. Geol. Surv.*, **11**, 67-99.
- Rau, R. J., K. E. Ching, J. C. Hu, and J. C. Lee, 2008: Crustal deformation and block kinematics in transition from collision to subduction: Global positioning system measurements in northern Taiwan, 1995-2005. *J. Geophys. Res.*, **113**, B09404, doi: 10.1029/2007JB005414. [[Link](#)]
- Seno, T., 1977: The instantaneous rotation vector of the Philippine Sea Plate relative to the Eurasian Plate. *Tectonophysics*, **42**, 209-226, doi: 10.1016/0040-1951(77)90168-8. [[Link](#)]
- Sharp, I. R., R. L. Gawthorpe, J. R. Underhill, and S. Gupta, 2000: Fault-propagation folding in extensional settings: Examples of structural style and synrift sedimentary response from the Suez rift, Sinai, Egypt. *Geol. Soc. Am. Bull.*, **112**, 1877-1899, doi: 10.1130/0016-7606(2000)112<1877:FPFIES>2.0.CO;2. [[Link](#)]
- Shih, R. C., Y. H. Chan, and H. C. Liu, 2004: Shallow seismic reflection surveys of the Shanchiao Fault in the Guandu Plain. *Spec. Publ. Cent. Geol. Surv.*, **15**, 1-11. (in Chinese)
- Shyu, J. B. H., K. Sieh, Y. G. Chen, and C. S. Liu, 2005: Neotectonic architecture of Taiwan and its implications for future large earthquakes. *J. Geophys. Res.*, **110**, B08402, 33 pp, doi: 10.1029/2004JB003251. [[Link](#)]
- Song, S. R., S. J. Tsao, and H. L. Lo, 2000: Characteristics of the Tatun volcanic eruptions, north Taiwan: Implications for a cauldron formation and volcanic evolution. *J. Geol. Soc. China*, **43**, 361-378.
- Suppe, J., 1981: Mechanics of mountain building and metamorphism in Taiwan. *Mem. Geol. Soc. China*, **4**, 67-89.
- Taylor, S. K., A. Nicol, and J. J. Walsh, 2008: Displacement loss on growth faults due to sediment compaction. *J. Struct. Geol.*, **30**, 394-405, doi: 10.1016/j.jsg.2007.11.006. [[Link](#)]
- Teng, L. S., 1990: Geotectonic evolution of late Cenozoic arc-continent collision in Taiwan. *Tectonophysics*, **183**, 57-76, doi: 10.1016/0040-1951(90)90188-E. [[Link](#)]
- Teng, L. S., 1996: Extensional collapse of the northern Taiwan mountain belt. *Geology*, **24**, 949-952, doi: 10.1130/0091-7613(1996)024<0949:ECOTNT>2.3.CO;2. [[Link](#)]
- Teng, L. S., P. B. Yuan, and P. Y. Chen, 1993: Study on

- stratigraphy and sedimentary environment. Report on Taipei Basin Subsurface Geology and Engineering Environment Research Project 1992, Central Geological Survey, MOEA, Taipei, Taiwan, ROC.
- Teng, L. S., P. B. Yuan, P. Y. Chen, C. H. Peng, T. C. Lai, F. Y. Fei, and H. C. Liu, 1999: Lithostratigraphy of the Taipei Basin deposits. *Spec. Publ. Cent. Geol. Surv.*, **11**, 41-66.
- Teng, L. S., P. B. Yuan, N. T. Yu, and C. H. Peng, 2000: Sequence stratigraphy of the Taipei Basin deposits: A preliminary study. *J. Geol. Soc. China*, **43**, 497-520.
- Teng, L. S., C. T. Lee, C. H. Peng, W. F. Chen, and C. J. Chu, 2001: Origin and geological evolution of the Taipei Basin, Northern Taiwan. *West. Pac. Earth Sci.*, **1**, 115-142.
- Teng, L. S., T. K. Liu, Y. G. Chen, P. M. Liew, C. T. Lee, H. C. Liu, and C. H. Peng, 2004a: Influence of Tahan River capture over the Taipei Basin. *Geogr. Res.*, **41**, 61-78. (in Chinese)
- Teng, L. S., C. T. Lee, P. M. Liew, S. R. Song, S. J. Tsao, H. C. Liu, and C. H. Peng, 2004b: On the Taipei dammed lake. *Geogr. Res.*, **36**, 77-100. (in Chinese)
- van Wagoner, J. C., H. W. Posamentier, R. M. Mitchem, P. R. Vail, J. F. Sarg, T. S. Loutit, and J. Hardenbol, 1988: An overview of the fundamentals of sequence stratigraphy and key definitions. In: Wilgus, C. K., H. W. Posamentier, C. A. Ross, and C. G. St. C. Kendall (Eds.), *Sea-Level Changes: An Integrated Approach*, Society of Economic Paleontologists and Mineralogists Special Publication, **42**, 39-45.
- Vergés, J., M. Marzo, and J. A. Muñoz, 2002: Growth strata in foreland settings. *Sediment. Geol.*, **146**, 1-9, doi: 10.1016/S0037-0738(01)00162-2. [[Link](#)]
- Walia, V., T. C. Su, C. C. Fu, and T. F. Yang, 2005: Spatial variations of radon and helium concentrations in soil-gas across the Shan-Chiao fault, Northern Taiwan. *Radiat. Meas.*, **40**, 513-516, doi: 10.1016/j.radmeas.2005.04.011. [[Link](#)]
- Wang, C. Y. and C. T. Sun, 1999: Interpretation of seismic stratigraphy in the Taipei Basin. *Spec. Publ. Cent. Geol. Surv.*, **11**, 273-292. (in Chinese)
- Wang, W. S. and C. H. Chen, 1990: The volcanology and fission track age dating of pyroclastic deposits in Tatun volcano group, northern Taiwan. *Acta Geol. Taiwan.*, **28**, 1-40.
- Wei, K., Y. G. Chen, and T. K. Liu, 1998: Sedimentary history of the Taipei Basin with constraints from thermoluminescence dates. *J. Geol. Soc. China*, **41**, 109-125.
- Wernicke, B. and B. C. Burchfiel, 1982: Modes of extensional tectonics. *J. Struct. Geol.*, **4**, 105-115, doi: 10.1016/0191-8141(82)90021-9. [[Link](#)]
- Woodcock, N. H. and C. Schubert, 1994: Continental strike-slip tectonics. In: Hancock, P. L. (Ed.), *Continental Deformation*, Pergamon Press, New York, 251-263.
- Woodroffe, S. A. and B. P. Horton, 2005: Holocene sea-level change in the Indo-Pacific. *J. Asian Earth Sci.*, **25**, 29-43, doi: 10.1016/j.jseae.2004.01.009. [[Link](#)]
- Wu, F. T., 1965: Subsurface geology of the Hsinchuang structure in the Taipei Basin. *Petrol. Geol. Taiwan*, **4**, 271-282.
- Wu, F. T., R. J. Rau, and D. Salzberg, 1997: Taiwan orogeny: Thin-skinned or lithospheric collision? *Tectonophysics*, **274**, 191-220, doi: 10.1016/S0040-1951(96)0304-6. [[Link](#)]
- Yeh, Y. H., E. Barrier, C. H. Lin, and J. Angelier, 1991: Stress tensor analysis in the Taiwan area from focal mechanisms of earthquakes. *Tectonophysics*, **200**, 267-280, doi: 10.1016/0040-1951(91)90019-O. [[Link](#)]
- Yokoyama, Y., Y. Kido, R. Tada, I. Minami, R. C. Finkel, and H. Matsuzaki, 2007: Japan Sea oxygen isotope stratigraphy and global sea-level changes for the last 50000 years recorded in sediment cores from the Oki Ridge. *Palaeogeogr. Palaeoclimatol. Palaeoecol.*, **247**, 5-17, doi: 10.1016/j.palaeo.2006.11.018. [[Link](#)]
- Yu, S. B., H. Y. Chen, and L. C. Kuo, 1997: Velocity field of GPS stations in the Taiwan area. *Tectonophysics*, **274**, 41-59, doi: 10.1016/S0040-1951(96)00297-1. [[Link](#)]
- Yu, S. B., H. Y. Chen, L. C. Kou, C. S. Hou, and C. F. Lee, 1999: A study on the fault activities of the Taipei Basin. *Spec. Publ. Cent. Geol. Surv.*, **11**, 227-251.

A3. Note on other published manuscript (Chen et al., 2011, Terra Nova)

Chen, C.-T., Chan, Y.-C., Lu, C.-Y., Simoes, M., Beysac, O., 2011. Nappe structure revealed by thermal constraints in the Taiwan metamorphic belt. *Terra Nova* 23, 85-91.



Nappe structure revealed by thermal constraints in the Taiwan metamorphic belt

Chih-Tung Chen,¹ Yu-Chang Chan,² Chia-Yu Lu,¹ Martine Simoes³ and Olivier Beyssac⁴

¹Department of Geosciences, National Taiwan University, Taipei, Taiwan; ²Institute of Earth Sciences, Academia Sinica, Taipei, Taiwan;

³Institut de Physique du Globe de Paris, Sorbonne Paris Cité, UMR 7154 CNRS, F-75005, Paris, France; ⁴Institut de Minéralogie et de Physique des Milieux Condensés, Université Pierre et Marie Curie, CNRS UMR7590, Paris, France

ABSTRACT

Vitrinite reflectance and Raman spectroscopy of carbonaceous material data are used to better resolve the thermal history of the Hsuehshan Range, which is accreted between the foreland fold-thrust belt and bulldozer hinterland units in the Taiwan mountain belt. The observed thermal data indicate that the strata in the northern Hsuehshan Range underwent dynamic metamorphism during the Neogene orogeny, while the strata in the southern Hsuehshan Range may have predominantly experienced burial metamorphism during Palaeogene sedimenta-

tion. Based on the thermal constraints, the Hsuehshan Range is interpreted to consist of nappe stacks, originating from the rifted Eurasian continental margin. This interpretation is consistent with well-documented cases in the European Alps and the Himalayas and is also shown in physical modelling and thermo-kinematic studies invoking underplating and erosion processes.

Terra Nova, 23, 85–91, 2011

Introduction

The island of Taiwan was created by active convergence between the Luzon arc of the Philippine Sea Plate and the Eurasian continental margin in the late Miocene and early Pliocene (Suppe, 1981; Teng, 1990). In the Taiwanese mountains, underplating (i.e. basal accretion) has been proposed to contribute <25% (e.g. Dahlen and Barr, 1989), approximately 50% (Fuller *et al.*, 2006) or more than 90% (Simoes *et al.*, 2007) of the influx of material into the orogenic wedge. The underplating process substantially compensates for materials removed by surface erosion based on previous studies on the central part of Taiwan (Fuller *et al.*, 2006; Simoes and Avouac, 2006; Simoes *et al.*, 2007, and references therein). However, little attention has been paid to the northern part of the island, where the collision process is waning, if not at a total halt. As the northern part records a longer history of mountain growth, it provides better opportunities for studying the *P–T* paths and dynamic processes during the Neogene orogeny.

In this article, the thermal metamorphism of the Hsuehshan Range in Taiwan is investigated through a new

compilation of vitrinite reflectance (VR) data (Chiu and Chou, 1988; Lin and Kuo, 1996; Lin *et al.*, 2001) and the published Raman spectroscopy of carbonaceous materials (RSCM) measurements of Beyssac *et al.* (2007). The Hsuehshan Range is a prominent physiogeographic division accreted between the foreland fold-thrust belt and hinterland units in the Taiwan mountain belt (Lu and Hsu, 1992; Clark *et al.*, 1993; Chan *et al.*, 2005; Shyu *et al.*, 2005). The pattern of observed peak metamorphic temperatures provides new perspectives on the structural evolution of the Hsuehshan Range and, at the same time, highlights the important roles of underplating and surface erosion on the present mountain structure, as also shown in recent physical modelling and thermo-kinematic studies (Bonnet *et al.*, 2007; Simoes *et al.*, 2007; Malavieille, 2010).

Regional background

The Hsuehshan Range, bounded by the Chuchih Fault and the Lishan Fault (Lee *et al.*, 1997), is composed of metamorphosed and exhumed continental margin sediments, which were deposited in then-subsiding grabens related to the Palaeogene opening of the South China Sea (Teng, 1992) (Fig. 1). The meta-sediments in the northern Hsuehshan Range are divided into the following stratigraphic units: the Eocene Hsitsun Formation, the Oligo-Eocene Szeleng Sandstone, the Oligocene Kankou Formation, the

Oligocene Tsuku Sandstone, the late-Oligocene Tatungshan Formation and the early–middle Miocene Sule Formation. In the eastern part of the northern Hsuehshan Range, the Tatungshan, Tsuku and Kankou Formations become indistinguishable and are pooled into the Paling Formation

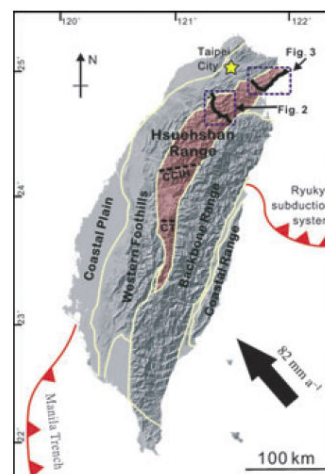


Fig. 1 Simplified geologic divisions of Taiwan with the Hsuehshan Range highlighted. The region along the Northern Cross-Island Highway is presented in Fig. 2, and the region along the Taipei-Ilan Highway and the North Coast Highway is presented in Fig. 3. CCIH, Central Cross-Island Highway; CT, Choshui Transect. Plate convergence rate and direction are from Yu *et al.* (1997).

Correspondence: Dr Yu-Chang Chan, Institute of Earth Sciences, Academia Sinica, 128 Sec. II Academia Road, Nankang, Taipei 115, Taiwan. Tel.: +886 2 27839910; fax: +886 2 27839871; e-mail: yuchang@earth.sinica.edu.tw

(Fig. 2). In contrast, the central and southern Hsuehshan Range is composed of another set of stratigraphic units: the Eocene Tachien Sandstone, the Oligocene Paileng Formation, the Oligocene Chiayang Formation and the late-Oligocene Shuichangliu Formation. All of the formations were deformed during the Neogene orogeny and have traditionally been assigned to the prehnite-pumpellyite

metamorphic facies with a core of lower greenschist facies in the eastern part of the range (Chen and Wang, 1995; Beyssac *et al.*, 2007).

Metamorphic temperature constraints from RSCM data

The RSCM method, a novel geothermometer recording the maximum metamorphic temperature of carbona-

ceous materials (Beyssac *et al.*, 2002), was applied to the slates in the Hsuehshan Range on the Central Cross-Island Highway (CCIH) and the Choshui Transect (CT) (Fig. 1). The RSCM temperatures range from 350 to 475 °C along the CCIH in the Chiayang Formation, exhibiting a reasonable geothermal gradient of ~30 °C km⁻¹. The RSCM temperatures are below 330 °C in the Paileng

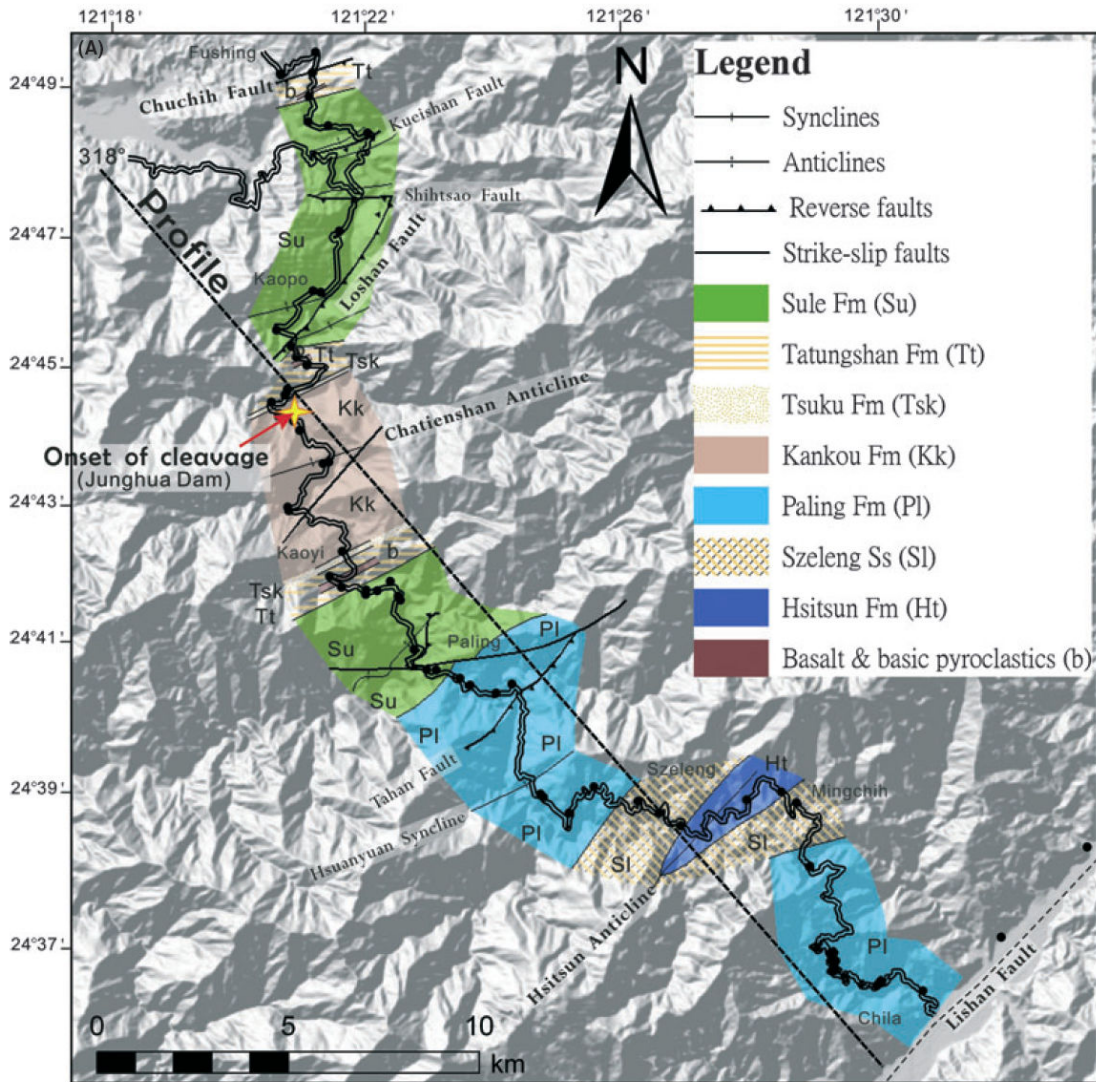


Fig. 2 (A) Geologic strip map of the Northern Cross-Island Highway transect. Vitrinite reflectance sampling sites from Lin and Kuo (1996) and Chiu and Chou (1988) are marked as black dots. (B) Sketch of the geologic structures along the transect shown in (A), with projected sampling sites of vitrinite reflectance measurements. (C) The profile of vitrinite reflectance values along the transect. (D) Derived maximum temperature profile of the transect.

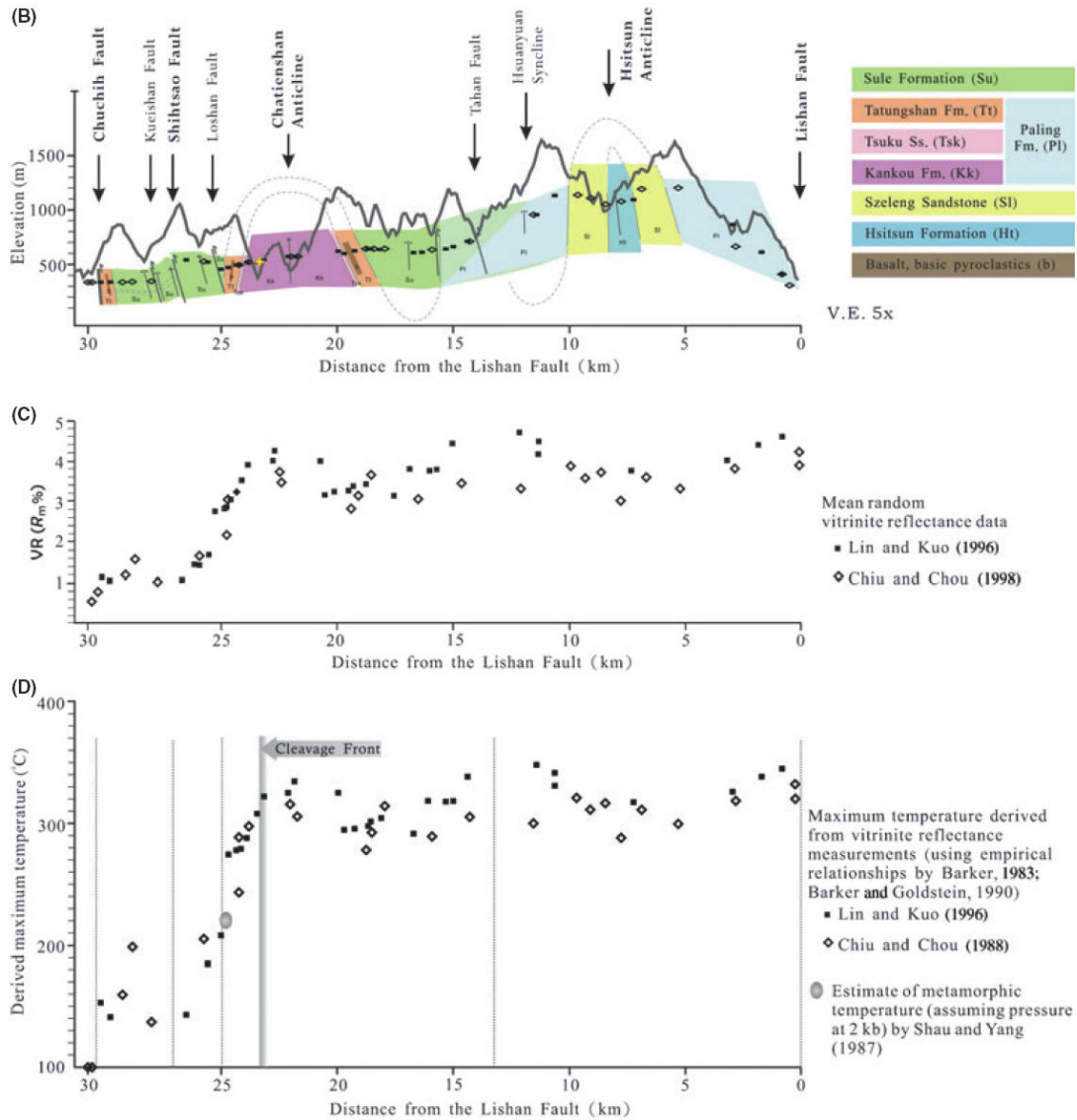


Fig. 2 Continued

Formation. Thermochronological data including zircon fission track and (U–Th)/He and apatite fission track dating are totally reset to Plio-Pleistocene ages in the Chiayang Formation/Tachien Sandstone and partially reset in the Paileng Formation (Liu *et al.*, 2001; Fuller *et al.*, 2006; Beysac *et al.*, 2007). Along the CT transect, the RSCM temperatures remain between 345 and 375 °C in the Chiayang Formation and below 330 °C in the Paileng Formation, while the Tachien

Sandstone is thermochronologically reset (Beysac *et al.*, 2007).

Since all the rocks were deposited during the Palaeogene, post-dating the previous Cretaceous orogeny (Yui *et al.*, 1988), the observed metamorphic records are all associated with the Cenozoic sedimentation and orogenic processes. Three lines of evidence indicate that the metamorphism of the central–southern part of the Hsuehsan Range is predominantly static or burial metamorphism. First,

the uppermost Paileng Formation is associated with low temperatures (below 330 °C), and zircon fission track and (U–Th)/He dates are not reset or partially reset; secondly, the Chiayang Formation is associated with higher temperatures (from 330 to 475 °C) down-section and eastward, i.e. deeper in the half-graben deposition basin; and, thirdly, the lowermost Tachien Sandstone is thermochronologically reset, as shown by existing zircon fission track and (U–Th)/He

dates. The meta-sediments were then heated in the basins on the rifted Eurasian continental margin, which can be over 10 km deep (Lin *et al.*, 2003), and subsequently transported to the surface during the Neogene orogeny (Beysac *et al.*, 2007; Simoes *et al.*, 2007).

Metamorphic temperature constraints from VR data

Vitrinite reflectance measures irreversible coalification, which sensitively reflects the diagenesis and metamorphic conditions of the host rock (Teichmüller, 1987). Its value is affected by several kinetic factors, but for heating durations over 10 000 years the maximum temperature is the major control (Barker, 1983). Therefore, VR is considered a reliable geothermometer in diagenetic to lower greenschist facies rocks for

peak temperatures not exceeding 400 °C (Barker and Goldstein, 1990). The mean random VR as a percentage (R_m) and the maximum temperature (T_M) have an empirical logarithmic relation:

$$T_M = \frac{\ln(R_m) + 0.832}{0.00683} \text{ (Barker, 1983)}$$

$$T_M = \frac{\ln(R_m) + 1.26}{0.00811} \text{ (Barker and Goldstein, 1990)}$$

The rocks of the Hsuehshan Range contain abundant organic material and have been heated during deep burial and/or metamorphism over million-year time-scales. They are thus suitable for VR studies. Here, we integrate VR measurements along the Northern Cross-Island Highway (NCIH) (Chiu and Chou, 1988; Lin and Kuo, 1996), the Ilan-Taipei Highway and the North Coast Highway (Lin *et al.*, 2001) in northern Taiwan. The VR data are

converted to peak metamorphic temperatures using the empirical equations above. We then mapped the derived temperatures to reveal the pattern and spatial variation of metamorphism.

VR results in the north-central part of the range

A geologic map and the distribution of maximum metamorphic temperatures along the NCIH are presented in Fig. 2. The area comprises a series of NNE-trending folds and reverse faults, with depositional ages spanning from late Eocene to middle Miocene (Fig. 2A,B). The combined VR datasets from Chiu and Chou (1988) and Lin and Kuo (1996) provide exceptionally detailed sampling, with 58 measurements along the 30 km long transect. The VR values (Fig. 2C) and the derived peak tem-

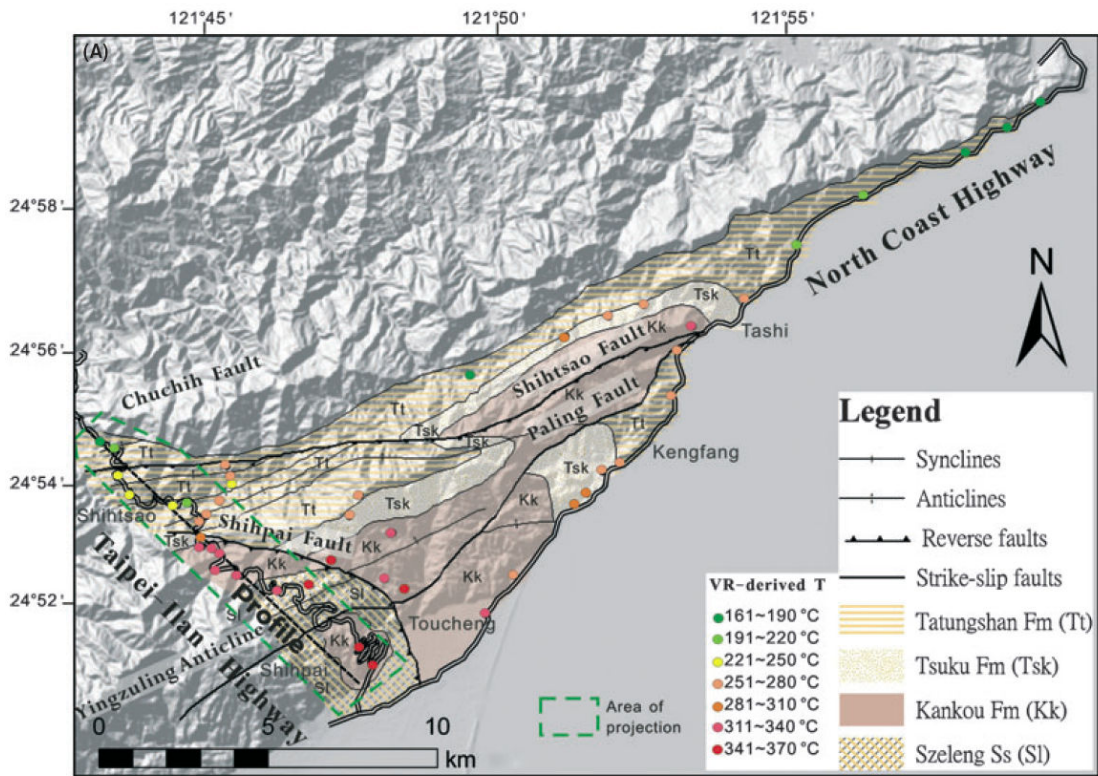


Fig. 3 (A) Geology of the northernmost part of the Hsuehshan Range. Vitrinite reflectance sampling sites and the maximum temperatures derived from vitrinite reflectance data from Lin *et al.* (2001) are marked by coloured dots. Data and area incorporated into the Taipei-Ilan Highway transect are indicated. (B) Geologic structures along the Taipei-Ilan Highway transect with projected sampling sites of vitrinite reflectance measurements. (C) Derived maximum temperature profile along the transect.

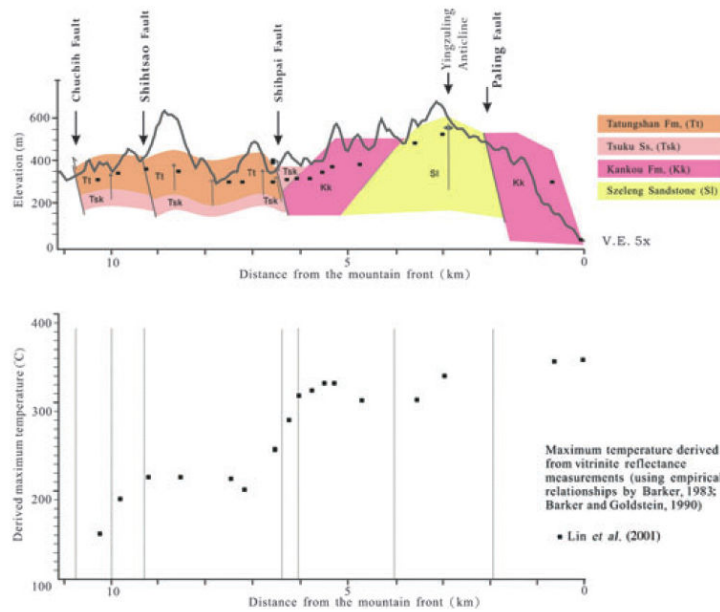


Fig. 3 Continued

peratures (Fig. 2D) exhibit a relatively simple pattern. Across the Chuchih Fault the VR value increases abruptly and the T_M ascends above 100 °C from the Western Foothills to the Hsuehshan Range. The T_M remains stable at around 150 °C between the Chuchih and Shihtsao Faults. Southeastward from the Shihtsao Fault, the T_M rises rather linearly from 150 °C to over 300 °C at the core of the Chatienshan Anticline. The pattern of derived temperatures agrees with the petrology of meta-basalts proposed by Shau and Yang (1987).

For the rest of the NCIH transect, starting at the Junghua Dam, where slaty cleavage becomes visible, the T_M values cluster mostly between 300 and 350 °C without significant variation and are almost totally unrelated to the stratigraphic position and structures. The VR data indicate that the Eocene to Miocene rocks between the Chatienshan Anticline and the Lishan Fault have been subjected to similar peak metamorphic temperatures, equivalent to 10–20 km depth assuming a geothermal gradient of 15–30 °C km⁻¹. The fact that the VR-derived temperatures do not correlate with stratigraphy suggests that dynamic metamorphism overprinted the original burial metamorphism along the NCIH transect.

VR results in the northern-most part of the range

At the northern tip of the Hsuehshan Range, Oligocene meta-sediments of the Szeleng, Kankou, Tsuku and Tatungshan Formations crop out and are deformed into a series of NE-trending folds and reverse faults (Fig. 3A). By plotting the VR data of Lin *et al.* (2001) and their derived T_M values (Fig. 3A), two different patterns of metamorphic grade can be observed. In the southern part of the area, along the Taipei-Ilan Highway, the documented metamorphic temperatures are clearly decoupled from stratigraphy, as observed along the NCIH. Figure 3B shows the geologic cross-section of the Taipei-Ilan Highway transect, where the Chuchih, Shihtsao and Shihpai Faults seem to affect the R_m and derived T_M values (Fig. 3C). Between the Shihtsao and Shihpai Faults, despite the presence of several mappable folds and possible Miocene strata, peak metamorphic temperatures are almost constant at 230–240 °C.

At the Shihpai Fault the T_M profile exhibits a remarkably steep and continuous rise within the area of the Tsuku Sandstone, reaching about

330 °C, resembling what is observed on the western limb of the Chatienshan Anticline in the NCIH transect. At the southeastern end of the profile lies a major south-dipping normal fault bounding the Ilan Plain. The Ilan Plain is connected to the actively rifting Okinawa Trough and may have enhanced exhumation of the Hsuehshan Range rocks (Clift *et al.*, 2008). In the rest of the region, particularly north of the Shihpai Fault, R_m and T_M are closely associated with stratigraphy: 130–230 °C for the Tatungshan Formation, 230–300 °C for the Tsuku Formation and 300–330 °C for the Kankou Formation.

Discussion

According to the thermal data from VR and RSCM measurements, three distinct metamorphic regimes can be distinguished in the Hsuehshan Range (Fig. 4). (1) In the central to southern part of the range (viewed as an upper nappe unit) peak temperatures correspond to 20 km deep stratigraphic levels in the original sedimentary basin settings with a reasonable geothermal gradient (Beysac *et al.*, 2007) and an eastward deepening of sedimentary levels matching the half-graben structures during the Eo-Oligocene opening of the South China Sea (Teng, 1992). (2) In the internal portion of the northern part of the range (viewed as a lower nappe unit), located east of the Shihtsao Fault along the NCIH and south of the Shihpai Fault on the Taipei-Ilan Highway, meta-sediments have lost their burial diagenetic signatures and are dynamically metamorphosed. (3) In the external portion of the northern part of the range (viewed as a shallow duplex unit), the strata preserve their rather high and SE-increasing diagenetic temperatures, with closely spaced fold-and-thrust structures.

We propose that the upper nappe unit and the shallow duplex unit acquired their peak metamorphism during the Palaeogene as a result of diagenesis and that they were later transported upward and deformed at lower temperatures during the Neogene orogeny (Simoes *et al.*, 2007) without prograde metamorphic overprinting. In contrast, the lower nappe unit was tectonically buried to levels

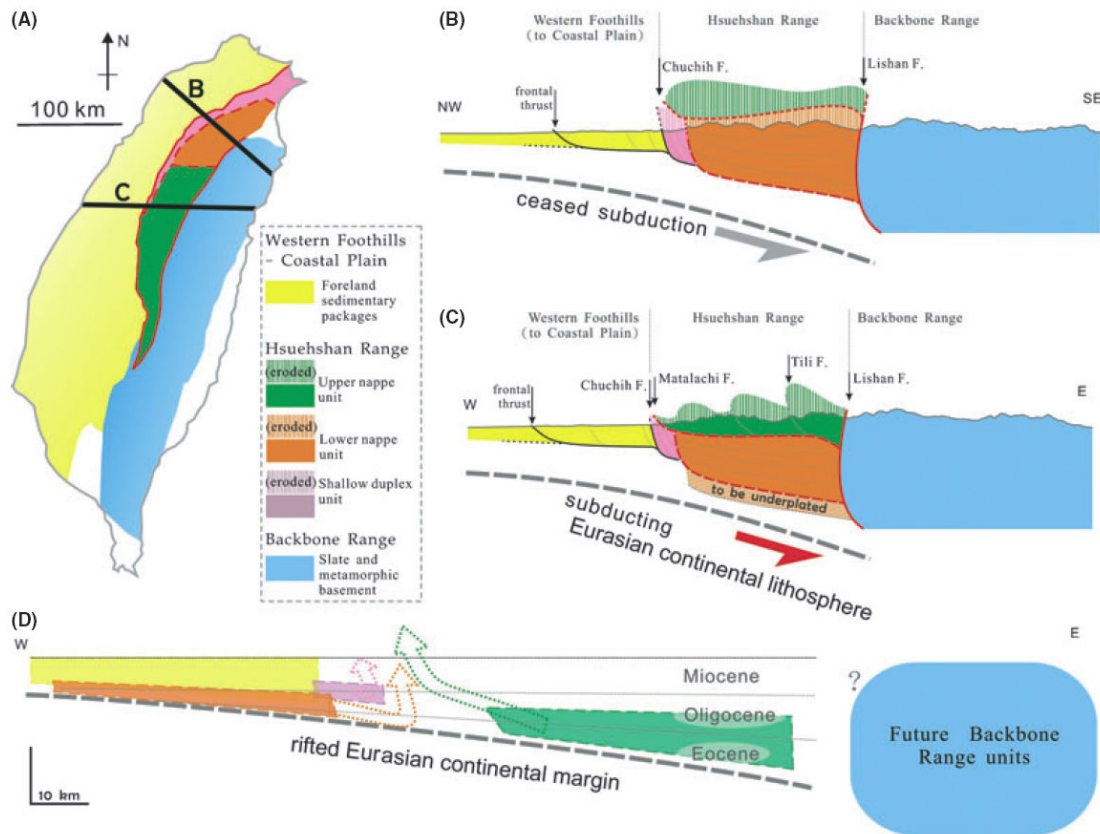


Fig. 4 Proposed tectonic model of the Hsuehshan Range with nappe structures. (A) Simplified geologic map and the studied transects. (B) Structural profile across the northern part of the range, where underplated lower nappes are exposed. (C) Structural profile across the central part of the range, where the upper nappe unit is above the Matalachi Fault. (D) Depositional configurations on the original rifted Eurasian continental margin and inferred transport paths of the depositional units (after Lin *et al.*, 2003; Simoes *et al.*, 2007).

deeper than the previously deposited levels and thermally overprinted during the Neogene orogeny. The observed thermal data suggest that the lower nappes were first subducted and then underplated into the orogenic wedge, probably at 10–20 km depth assuming a 15–30 °C km⁻¹ geothermal gradient. The peak temperatures experienced by the lower nappes, ranging from about 300 to 350 °C, can be interpreted as temperatures at the detachment level during underplating of the lower nappes. This interpretation was similarly stated in the wedge kinematics as modelled by Simoes *et al.* (2007) where the underplating mechanism was mentioned.

To bring together the above observations and arguments, a tentative

tectonic model of the Hsuehshan Range is proposed (Fig. 4). Along the profile of the CCIH (Fig. 4C), the continental margin sediments were accreted into the orogenic wedge, driven by the bulldozer of the Backbone Range (Lu and Hsu, 1992; Shyu *et al.*, 2005). The accretion process formed a thin-skinned fold-and-thrust belt, i.e. the Western Foothills, and the complex Hsuehshan Range capped by the upper nappe unit, which was uplifted by underplating. Nappe stacks resulting from underplating are commonly observed in orogenic belts. Underplating may occur simultaneously with frontal accretion, exerting significant controls on wedge development (Fuller *et al.*, 2006; Simoes and Avouac, 2006; Beyssac *et al.*, 2007; Bonnet *et al.*,

2007; Simoes *et al.*, 2007; Malavielle, 2010). Further north along the NCIH (Fig. 4B), the upper nappe unit has been eroded in windows that expose the underplated lower nappes. The Matalachi Fault, a formerly well-recognized boundary fault in the Hsuehshan Range (Biq, 1989), is considered to be the main detachment between the upper and lower nappes. The original sedimentary configuration of the Eurasian continental margin before the Neogene orogeny is schematically reconstructed in Fig. 4D. The figure shows that the Eo-Oligocene sedimentary boundary is tilted, reflecting the Palaeogene rifting, and the tectonic transport paths for the upper and lower nappes and shallow duplex unit.

Conclusion

We interpret the southern Hsuehshan Range in Taiwan as a detached nappe originating from the deep portion of the rifted Eurasian continental margin, based on the observed thermal data. The Eo-Oligocene nappe strata were transported in the foreland direction and subsequently uplifted by the stacking of underplated materials during the Neogene orogeny. A portion of the allochthonous nappe has been eroded, exposing the underplated nappes in the northern Hsuehshan Range. The interpreted nappe stack in Taiwan further supports the essential processes, such as basal accretion and surface erosion (e.g. Simoes and Avouac, 2006; Simoes *et al.*, 2007; Malavieille, 2010), simultaneously acting upon the Taiwan accretionary orogen.

Acknowledgements

This study was supported by Taiwan National Science Council grants NSC99-2116-M-001-014 and NSC98-2628-M-001-015 to Y.-C. Chan and is a contribution of the Institute of Earth Sciences, Academia Sinica. It was also partly funded by the Agence Nationale de la Recherche through the ACTS Taiwan project (PI S. Lallemand). We thank Jacques Malavieille, Timothy Byrne, Louis S. Teng, Hao-Tsu Chu, Jian-Cheng Lee and Yue-Gau Chen for their insightful discussions. Helpful and constructive comments by Sean Willett, Ching-Hua Lo and Associate Editor Igor M. Villa are gratefully appreciated.

References

- Barker, C.E., 1983. Influence of time on metamorphism of sedimentary organic matter in liquid-dominated geothermal systems, western North America. *Geology*, **11**, 384–388.
- Barker, C.E. and Goldstein, R.H., 1990. Fluid-inclusion technique for determining maximum temperature in calcite and its comparison to the vitrinite reflectance geothermometer. *Geology*, **18**, 1003–1006.
- Beysac, O., Goffe, B., Chopin, C. and Rouzaud, J.N., 2002. Raman spectra of carbonaceous material in metasediments: a new geothermometer. *J. Metamorph. Geol.*, **20**, 859–871.
- Beysac, O., Simoes, M., Avouac, J.-P., Farley, K.A., Chen, Y.-G., Chan, Y.-C. and Goffe, B., 2007. Late Cenozoic metamorphic evolution and exhumation of Taiwan. *Tectonics*, **26**, TC6001.
- Biq, C., 1989. The Yushan-Hsuehshan megashear zone in Taiwan. *Proc. Geol. Soc. China*, **32**, 7–20.
- Bonnet, C., Malavieille, J. and Mosar, J., 2007. Interactions between tectonics, erosion, and sedimentation during the recent evolution of the Alpine orogen: analogue modeling insights. *Tectonics*, **26**, TC6016.
- Chan, Y.-C., Okamoto, K., Yui, T.-F., Iizuka, Y. and Chu, H.-T., 2005. Fossil fluid reservoir beneath a duplex fault structure within the Central Range of Taiwan: implication for fluid leakage and lubrication during earthquake rupturing process. *Terra Nova*, **17**, 493–499.
- Chen, C.-H. and Wang, C.-H., 1995. *Explanatory Notes for the Metamorphic Facies Map of Taiwan*, 2nd edn. *Special Report of Central Geological Survey* **2**, 51pp. Central Geological Survey, Taipei, Taiwan.
- Chiu, H.-T. and Chou, T.-H., 1988. Petroleum geochemical studies of the slate formation in northern Taiwan. *Petrol. Geol. Taiwan*, **24**, 1–17.
- Clark, M.B., Fisher, D.M., Lu, C.-Y. and Chen, C.-H., 1993. Kinematic analyses of the Hsuehshan Range, Taiwan: a large-scale pop-up structure. *Tectonics*, **12**, 205–217.
- Clift, P.D., Lin, A.T.-S., Carter, A., Wu, F., Draut, A.E., Lai, T.-H., Fey, L.-Y., Schouten, H. and Teng, L.S., 2008. Post-collisional collapse in the wake of migrating arc-continent collision in the Ilan Basin, Taiwan. *Geol. Soc. Am. Spec. Pap.*, **436**, 257–278.
- Dahlen, F.A. and Barr, T.D., 1989. Brittle frictional mountain building I. Deformation and mechanical energy budget. *J. Geophys. Res.*, **94**, 3906–3922.
- Fuller, C.W., Willett, S.D., Fisher, D. and Lu, C.-Y., 2006. A thermomechanical wedge model of Taiwan constrained by fission-track thermochronometry. *Tectonophysics*, **425**, 1–24.
- Lee, J.-C., Angelier, J. and Chu, H.-T., 1997. Polyphase history and kinematics of a complex major fault zone in the northern Taiwan mountain belt: the Lishan Fault. *Tectonophysics*, **274**, 97–115.
- Lin, M.-L. and Kuo, Y.-C., 1996. Degrees of metamorphism in the northern Hsuehshan Range: a study of vitrinite reflectance in metapelites along the Northern Taiwan East-west Cross-Island Highway. *J. Geol. Soc. China*, **39-3**, 355–372.
- Lin, M.-L., Lin, C.-K. and You, M.-J., 2001. Vitrinite reflectance as a possible indicator of metamorphic grade and stratigraphic position of formations: a study of Oligocene metapelites in NE Taiwan. *J. Asian Earth Sci.*, **19**, 223–232.
- Lin, A.T., Watts, A.B. and Hesselbo, S.P., 2003. Cenozoic stratigraphy and subsidence history of the South China Sea margin in the Taiwan region. *Basin Res.*, **15**, 453–478.
- Liu, T.-K., Hsieh, S., Chen, Y.-G. and Chen, W.-S., 2001. Thermo-kinematic evolution of the Taiwan oblique-collision mountain belt as revealed by zircon fission track dating. *Earth Planet. Sci. Lett.*, **186**, 45–56.
- Lu, C.-Y. and Hsu, K.J., 1992. Tectonic evolution of the Taiwan mountain belt. *Petrol. Geol. Taiwan*, **27**, 21–46.
- Malavieille, J., 2010. Impact of erosion, sedimentation, and structural heritage on the structure and kinematics of orogenic wedges: analog models and case studies. *GSA Today*, **20**, 4–10.
- Shau, Y.-H. and Yang, H.-Y., 1987. Petrology of basaltic rocks from Jung-hua, Taoyuanhsien, northern Taiwan. *Proc. Geol. Soc. China*, **30**, 58–82.
- Shyu, J.B.H., Sieh, K. and Chen, Y.-G., 2005. Tandem suturing and disarticulation of the Taiwan orogen revealed by its neotectonic elements. *Earth Planet. Sci. Lett.*, **233**, 167–177.
- Simoes, M. and Avouac, J. P., 2006. Investigating the kinematics of mountain building in Taiwan from the spatio-temporal evolution of the foreland basin and western foothills. *J. Geophys. Res.*, **111**, B10401.
- Simoes, M., Avouac, J.P., Beyssac, O., Goffe, B., Farley, K.A. and Chen, Y.-G., 2007. Mountain building in Taiwan: a thermokinematic model. *J. Geophys. Res.*, **112**, B11405.
- Suppe, J., 1981. Mechanics of mountain building and metamorphism in Taiwan. *Mem. Geol. Soc. China*, **4**, 67–89.
- Teichmüller, M., 1987. Organic material and very low-grade metamorphism. In: *Low Temperature Metamorphism* (M. Frey, ed.), pp. 114–161. Blackie & Son, London.
- Teng, L.S., 1990. Geotectonic evolution of late Cenozoic arc-continent collision in Taiwan. *Tectonophysics*, **183**, 57–76.
- Teng, L.S., 1992. Geotectonic evolution of Tertiary continental margin basins of Taiwan. *Petrol. Geol. Taiwan*, **27**, 1–19.
- Yu, S.-B., Chen, H.-Y. and Kuo, L.-C., 1997. Velocity field of GPS stations in the Taiwan area. *Tectonophysics*, **274**, 41–59.
- Yui, T.-F., Lu, C.-Y. and Lo, C.-H., 1988. A speculative tectonic history of the Tananao Schist of Taiwan. *Proc. Geol. Soc. China*, **31-2**, 7–18.

Received 23 April 2010; revised version accepted 11 January 2011